3D-Printed Interaction

Digital Fabrication of Touch, Deformation, and Environmental Sensing

Second Edition

Vom Fachbereich Informatik der Technische Universität Darmstadt genehmigte

Dissertation

zur Erlangung des akademischen Grades eines **Doktor rerum naturalium (Dr. rer. nat.)**.

Eingereicht von

Martin Schmitz, M.Sc.

Erstreferent:	Prof. Dr. Max Mühlhäuser (Technische Universität Darmstadt)
Korreferent:	Prof. Dr. Jürgen Steimle (Universität des Saarlandes)

Tag der Einreichung: 22.10.2018

Tag der Disputation: 03.12.2018

Fachgebiet Telekooperation
Fachbereich Informatik
Technische Universität Darmstadt
Hochschulkennziffer D 17

Darmstadt 2018 – 2020

ABSTRACT

The progressing digitalization increases the demand for interactive devices that bridge the physical and digital world. While there is great potential for customized interactive devices tailored to specific applications or users, until recently, integrating interactivity in custom devices required pre-defined components (e.g., rectangular buttons or flat touchscreens) that constrains the shape of the device. A more flexible alternative has opened up with the advent of 3D printing which empowers companies, developers, and end users to design and fabricate custom-shaped individual objects on demand with relatively low effort. Even though recognized as revolutionizing the manufacturing process, the 3D printing of custom-made interactive devices still requires novel sensor concepts, that operate on complex geometries, and significant design or assembly effort.

This thesis concerns the 3D printing of interactive input devices that respond to a variety of external stimuli and are printed in a single pass without requiring significant assembly steps. It consists of the following five major contributions: The first contribution is a fabrication pipeline to design and 3D print custom-shaped touch sensors on complex 3D objects. Then, the second contribution extends the first pipeline to detect hovering, touching, or pressing of a finger on a 3D-printed object. The third contribution continues to explore deformation-aware 3D-printed objects that detect pressure, squeeze, and bending in combination with a capacitive touchscreen. The fourth contribution adds liquid to 3D-printed objects to detect tilting and motion interactions. Based on these liquid-filled objects, the fifth contribution is an alternative sensing approach that does not require powered electronics during the interaction. Instead, each sensor concept memorizes the effect of a pre-defined external stimulus by changes in its internal structure. These changes can be read-out at a later time through a capacitive touchscreen. A series of evaluations and applications show the feasibility and broad applicability of all contributions for 3D printing of custom-made interactive devices.

ZUSAMMENFASSUNG

Die fortschreitende Digitalisierung erhöht die Nachfrage nach interaktiven Geräten, die die physische und digitale Welt verbinden. Während es ein großes Potenzial für maßgeschneiderte interaktive Geräte gibt, die auf bestimmte Anwendungen oder Benutzer zugeschnitten sind, erforderte die Integration von Interaktivität in Geräte bislang vorgefertigte Komponenten (z.B. eckige Tasten oder flache Touchscreens), die die Geräteform einschränken. Mit dem Aufkommen des 3D-Drucks hat sich eine flexiblere Alternative eröffnet, die es Unternehmen, Entwicklern und Endanwendern ermöglicht, mit geringerem Aufwand spezifisch geformte, individualisierte Objekte nach Bedarf zu entwerfen und herzustellen. Auch wenn der 3D-Druck als Revolution traditioneller Fertigungsprozesse anerkannt ist, erfordert die Herstellung maßgeschneiderter interaktiver Geräte neue Sensorkonzepte für komplexe Geometrien und bisher erheblichen Design- oder Montageaufwand.

Diese Arbeit befasst sich mit dem 3D-Druck von interaktiven Eingabegeräten, die auf eine Vielzahl von äußeren Reizen reagieren und in einem einzigen Durchgang gedruckt werden, ohne dass wesentliche Montageschritte erforderlich sind. Es besteht aus den folgenden fünf Hauptbeiträgen: Der erste Beitrag ist eine Fertigungspipeline zum Design und 3D-Druck von individuellen Berührungssensoren auf komplexen 3D-Objekten. Der zweite Beitrag erweitert diese Fertigungspipeline zur Erkennung von Schweben, Berühren und Druck eines Fingers über oder auf einem Objekt. Der dritte Beitrag befasst sich mit Sensorkonzepten, die Druck, Quetschen oder Biegen auf kapazitiven Touchscreens detektieren. Der vierte Beitrag fügt Flüssigkeiten zu 3D-gedruckten Objekten hinzu, um Kippen und Bewegung zu erkennen. Basierend auf diesen flüssigkeitsgefüllten Objekten, erforscht der fünfte Beitrag einen alternativen Messansatz, der während der Interaktion keine Elektronik und keinen Strom erfordert. Stattdessen speichert jedes Sensorkonzept den Einfluss eines vordefinierten externen Stimulus durch Änderungen in seiner internen Struktur. Diese Änderungen können zu einem späteren Zeitpunkt über einen kapazitiven Touchscreen ausgelesen werden. Eine Reihe von Studien und Anwendungen zeigen die Machbarkeit und Anwendbarkeit aller Beiträge für den 3D-Druck von maßgeschneiderten interaktiven Geräten.

ACKNOWLEDGMENTS

CONTENTS

Part I

INTRODUCTION & BACKGROUND

INTRODUCTION

> *Despite our fascination with screens, we still live in the real world. It's the food we eat, our homes, the clothes we wear, and the cars we drive. Our cities and gardens; our offices and our backyards. That's all atoms, not bits.*
>
> Chris Anderson, 2012 [And12]

With these words, Chris Anderson characterizes the ongoing and inevitable need for **atoms**, i.e., "the real world of places and stuff," despite the trend towards an increasingly digitized world consisting of **bits**, i.e., the "elemental units of the digital world" [And12, p. 8]. Since decades information technology aims at increasing digitization by converting previously analogous tasks (such as paperwork or communication) to the digital world. While this conversion is often beneficial, it frequently neglects more subtle information (such as the feel of a book or the non-verbal cues in face-to-face communication), awakening the desire to increase the fusion of digital and real world. This desire manifests in the trends of **ubiquitous computing** in which digital technology distributes and blends into the real world [Wei91], and **tangible interaction** in which the physical world provides the means to interact with the digital world [IU97]. However, the interaction with ubiquitous or tangible devices often does not meet the custom requirements of users or application scenarios. One enabling technology to realize this fusion and at the same time maintain the need for customized interactive devices is 3D printing.

1.1.1 *Atoms: The Emergence of 3D Printing*

3D printing is considered to have the potential to trigger a new industrial revolution [And12]. It is intended to enable broad masses of creative developers, communities, or companies to invent new or improved individualized

products and to produce them on demand in one step at low cost, even in small series, and, if necessary, to distribute them themselves. Affordable special requirements and individual products as well as a democratization of production offer opposition to uniform mass products of large companies. In the course of this development, open workshops, called fab labs or maker spaces, with access to 3D printers form worldwide. Even if no industrial revolution will take place, it is mainly undisputed that traditional industrial production will continue to develop in the direction of faster development of prototypes and customized products due to 3D printing.

1.1.2   *Bits: The Need for Custom-Made Interactive Devices*

Parallel to the development of 3D printing, the demand for **custom-made interactive devices** is continuously increasing in the field of human-computer interaction: information technologies support more and more everyday products and require more product-specific interaction technologies (e.g., touch-sensitive desk lamps or smart kitchen appliances). This development shows that for specialized tasks or user groups customized interactive devices can offer an improved user experience compared to standard techniques [IU97]. For instance, more precise [Han+06] or faster [Wei+09] data entry is possible with a tangible device instead of a touch-based interface. However, designing and manufacturing product-, task-, or user-specific interactions have so far been very time-consuming and costly. Therefore, custom-made interactive devices remain limited to expensive specialized systems or research prototypes.

1.1.3   *The Gap between Atoms and Bits*

Apparently, **3D printing for custom-made interactive devices** can profitably combine both motivating trends. From the perspective of 3D printing, this means that **interactive** devices could now be individually designed and produced in small quantities. From the perspective of custom-made interactive devices, there is the opportunity to benefit from the cost and effort reducing effects of 3D printing.

To beneficially combine both trends, it must be possible to **3D print interaction**. That is, a digital blueprint of an interactive device is specifically generated according to custom requirements and automatically fabricated us-

ing 3D printing. For example, this combination may enable custom-shaped touch-sensitive surfaces or optical elements that exactly fit the needs of users or application scenarios. Research is currently making significant progress in these directions (cf. [SZH12; Wil+12; OWS14]).

Custom-made interactive devices can massively change the market if people, research groups, independent designers or companies are enabled to design, print, and use interactive devices specifically made for their use case with minimal effort. However, considerable progress is still required before the benefits of 3D printing apply to custom-made interactive devices. This progress includes improvements concerning a more user-friendly design, interactive structures that apply to a wide range of 3D geometries, and algorithms that generate and precisely fit such structures in 3D geometries.

1.2 TOWARDS 3D-PRINTED CUSTOM-MADE INTERACTIVE DEVICES

The vision of creating 3D-printed custom-made interactive devices is as follows: Like today's desktop 2D printers, 3D printers will be fast, cheap, reliable, and widely available in almost every home or professional 3D printing shops. Instead of mass production, users fabricate many objects on-demand in varying shapes, colors, and materials without the need for excessive post-processing. Inspired by this general vision of 3D printing, this thesis envisions a potential future **fabrication environment for interactive devices** that enables researchers, application developers, and also end user without skills in computer-aided design to equip a selected 3D object with user-defined interactivity. As illustrated in Figure 1.1, this environment builds upon tangible interaction concepts (A), such as touching or moving an object. Users express their ideas in a digital design phase by adding various interactive
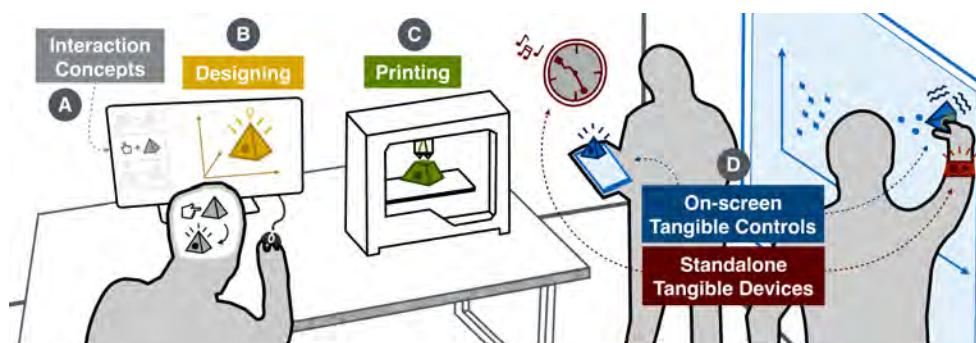
Figure 1.1: The envisioned fabrication environment to create custom-made interactive devices.

structures to a 3D object (B). They can then fine-tune properties such as the desired size or resolution of interactive structures. Users then (possibly repeatedly) 3D print their custom-made interactive object at home or a 3D printing shop (C) and use it (D) either as a tangible **stand-alone device** (red) or **on-screen control** (blue) that interacts with an interactive surface (e.g., a tablet or a wall-sized display).

This fabrication environment should be as natural and automatic as today's creation of paper documents using word-processing software and a 2D desktop printer. For instance, end users combine it with 3D scanning to adjust wearable devices to their body dimensions, to design entirely new interactive devices on top of existing objects, or to customize home appliances pre-designed by a company to their needs.

1.2.1 *Addressing the Challenges*

Towards this vision of easy and automatic fabrication environments, numerous challenges still need to be resolved: One research challenge concerns the exploration of interaction concepts and primitives for custom-shaped interactive structures, specifically tailored for the complex geometries of 3D-printable objects. Another research challenge involves algorithms that generate such structures on or in the 3D object since manual design today is lavish, requires considerable expertise, and is prone to errors. Moreover, the design of interactivity and the 3D geometry of the object are separated, i.e., fixed-form standard components (e.g., a flat display panel) are attached to or embedded into non-functional, passive 3D objects that have been mass-produced. Therefore, another research challenge is the investigation of novel design concepts that enable users to embed interactive free-form 3D structures at the design phase.

This thesis focuses on 3D-printed interactive devices that respond to a variety of external stimuli and are printed in a single pass without requiring significant assembly steps. As illustrated in Table 1.1, it addresses the challenges mentioned above as follows: By exploring different composites of 3D printing materials (e.g., a deformable object containing conductive material), each chapter contributes a set of concepts and approaches that allow sensing touch, deformation, and environmental interactions performed with a 3D-printed object. These stimuli are detected either stand-alone via a microcontroller or on-screen via a capacitive touchscreen (see Figure 1.1).

	Enabling Touch	Adding Deformation		Adding Environment	
	CAPRICATE (Chapter 3)	TRILATERATE (Chapter 4)	FLEXIBLES (Chapter 5)	LIQUIDO (Chapter 6)	OFF-LINE (Chapter 7)
Material Composite					
Solid					
Deformable					
Conductive					
Liquid					
Touch Interaction					
Hover	✓ (< 10 mm)	✓			
Contact	✓	✓	✓		
Multi-Touch	✓	✓ (distinct sides)			
Deformation Interaction					
Bend			✓		
Press		✓	✓		
Squeeze			✓		✓
Environmental Interaction					
2D Pose			✓		
Tilt				✓	✓
Flip				✓	✓
Accelerate				✓	✓
Cool					✓
Heat					✓
Read-Out Scheme					
Stand-Alone	✓	✓		✓	
On-Screen	✓		✓		✓

Table 1.1: Each chapter of this thesis explores a unique composition of 3D printing materials in order to detect different interactions either stand-alone with a microcontroller or on-screen with a capacitive touchscreen.

1.2.2 *Contributions of this Thesis*

The main contributions of this thesis are as follows:

Based on a design space for 3D-printed custom-made interactive devices, the first contribution is CAPRICATE, a fabrication pipeline that enables users to easily design and 3D print customizable touch-sensitive objects based on capacitive sensing. Objects are composed of solid and conductive material and are printed in a single pass using a commodity multi-material 3D printer. By exploring 3D-printed capacitive sensing, it provides the conceptual and technological basis for all subsequent contributions.

TRILATERATE extends the 3D-printed capacitive sensing approach to also allow for pressure interactions. It contributes a fabrication pipeline to 3D-print interactive structures that are composed of solid, deformable, and conductive materials. Electrodes placed in the object capacitively trilaterate the 3D position of a finger, which is used to classify the type of interaction as hover, touch, or press.

FLEXIBLES continues to explore deformation input. It focuses on on-screen read-out and contributes sensor concepts to capture pressing, squeezing, or bending input with multiple levels of intensities based on different types of deformation mapping. Objects are composed of deformable and conductive material.

While the last three contributions focused on hover, touch, and deformation interactions, LIQUIDO proposes to embed liquids into 3D-printed objects to detect interactions based on movement. By utilizing readily available liquids, it is a low-cost and easy-to-apply approach that also reduces the assembly effort.

Based on embedded liquids explored in the previous contribution, OFF-LINE SENSING contributes passive 3D-printed sensors that detect one-time interactions, such as accelerating or flipping. These sensors are composed of deformable, solid, conductive, and liquid materials and do not require active electronics nor power at the time of the interaction.

All major parts of this thesis have been published at international peer-reviewed conferences, such as the ACM User Interface Software and Technology Symposium (UIST) or the ACM SIGCHI Conference on Human Factors in Computing Systems (CHI). Chapter 3 builds upon the paper "CAPRICATE: A Fabrication Pipeline to Design and 3D Print Capacitive Touch Sensors for Interactive Objects" (UIST 2015) [Sch+15a]. Chapter 4 builds upon the paper "./TRILATERATE: A Fabrication Pipeline to Design and 3D Print Hover-, Touch-, and Force-Sensitive Objects" (CHI 2019) [Sch+19]. Chapter 5 builds upon the paper "FLEXIBLES: Deformation-Aware 3D-Printed Tangibles for Capacitive Touchscreens" (CHI 2017) [Sch+17]. Chapter 6 builds upon the paper "LIQUIDO: Embedding Liquids into 3D Printed Objects to Sense Tilting and Motion" (CHI EA 2016) [Sch+16]. Chapter 7 builds upon the paper "OFF-LINE SENSING: Memorizing Interactions in Passive 3D-printed Objects" (CHI 2018 with an Honorable Mention Award) [Sch+18].

1.3   STRUCTURE OF THIS THESIS

This thesis is structured as follows:

- Chapter 2 discusses conceptually different approaches to create interactive objects and establishes fundamentals regarding digital fabrication. Moreover, it presents a design space for 3D-printed custom-made interactive objects.

- Chapter 3 contributes CAPRICATE, a fabrication pipeline to 3D-print objects with embedded capacitive **touch** input.

- Chapter 4 proposes TRILATERATE, an extended fabrication pipeline and a method to trilaterate a finger in 3D space to infer **hover**, **touch**, and **pressure**.

- Chapter 5 then adds FLEXIBLES, enabling sensing of deformations via **pressure**, **squeezing**, and **bending**. It also presents a method to sense the **2D posture** and **id** of 3D-printed objects on a capacitive touchscreen.

- Chapter 6 proposes LIQUIDO, an approach to embed liquids into 3D-printed objects to infer **tilt** and **acceleration**.

- Chapter 7 extends upon the previous chapter by proposing OFF-LINE SENSING, a set of liquid-based sensors that memorize **tilt**, **acceleration**, **pressure**, **squeeze**, **flip**, **heat**, and **cooling** without requiring any power supply during the interaction.

- Chapter 8 integrates the contributions of this thesis and gives an outlook on possible future work directions.

CREATING INTERACTIVE OBJECTS

Different streams of research in Human-Computer Interaction (HCI) pursue the goal of enabling the creation of interactive objects. As depicted in Figure 2.1, they fundamentally differ with respect to automation and the complexity of object shapes they support: Some research is investigating how to **externally** augment objects through sensors or output structures placed in the environment. Other research is considering methods to **craft** interactivity, i.e., by attaching sensors or actuators to an object's surface or embedding them in the object itself. A recent stream of research is studying how to **print** interactivity directly into or onto the objects without the need for further (in-object) assembly or external sensors.
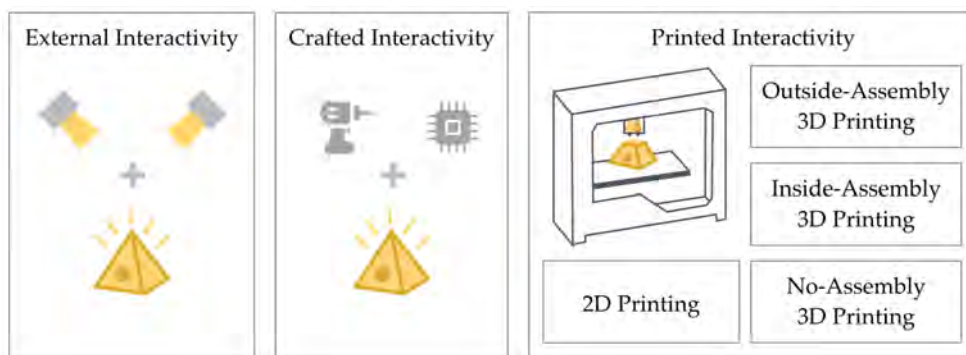
Figure 2.1: An interactive object may be created (1) using external sensors and output in the environment, (2) by crafting the object and embedding electronics, or (3) via 2D or 3D printing the desired interactions at the same time as the object.

Section 2.1 presents and discusses related research. Then, Section 2.2 introduces the basics of digital fabrication, including a discussion about printing technologies and materials. This chapter concludes by presenting the generally used 3D printing pipeline in Section 2.3, that is used to digitally fabricate an object.

2.1   RELATED WORK

This section discusses three different streams of research that aim to create an interactive object via (1) external, (2) crafted, and (3) printed interactivity.

2.1.1   *External Interactivity*

One common approach to adding interactive capabilities to an otherwise inactive object is to deploy input and output components **externally** in the environment of the object. While these approaches enable fast creation of interactive objects with complex geometries, external sensors need to be attached to the user or placed in the environment. This stream of research has explored a variety of interactions, ranging from input based on **touch**, **deformation**, or **tangibles** to **visual output**. In the following, research is discussed grouped by interaction (see Figure 2.2).

The **detection of touch and gestures** on object surfaces is one of the most common input modalities that external methods have been exploring. Standard color or infrared cameras are often used to sense hand gestures in 3D space [MM09; MMC09]. More recently, depth cameras are utilized to detect the touch of a finger on a surface for tabletop setting [Wil10] or attached to a user [HBW11]. While these approaches allow previously inactive objects to be made interactive quickly and easily, they still require the instrumentalization of users or the environment and require precise calibration or markers to operate. Moreover, the detection of touches or gestures on sides of an object that are not oriented towards the camera remains challenging.

Similarly, research has investigated the **detection of deformation** of an object for interaction. By utilizing optical tracking systems [Kha+11; Kha+12; RSL14] or depth cameras [SJM13; Tan+15] in the environment, deformations such as bending [SJM13], folding [Kha+12; RSL14; Tan+15], or rolling [Kha+11] can be sensed. While, in principle, capable of sensing complex deformations, these techniques currently only detect simple deformations (e.g., bending or folds) or are limited to simpler object geometries (e.g., a 2D sheet of paper).

Moreover, the **detection of tangible input** has been a broad stream of research in the last decades. More recently in this stream, color, infrared, or depth cameras are used to detect the usage of an object [WSM13; Cor+13;
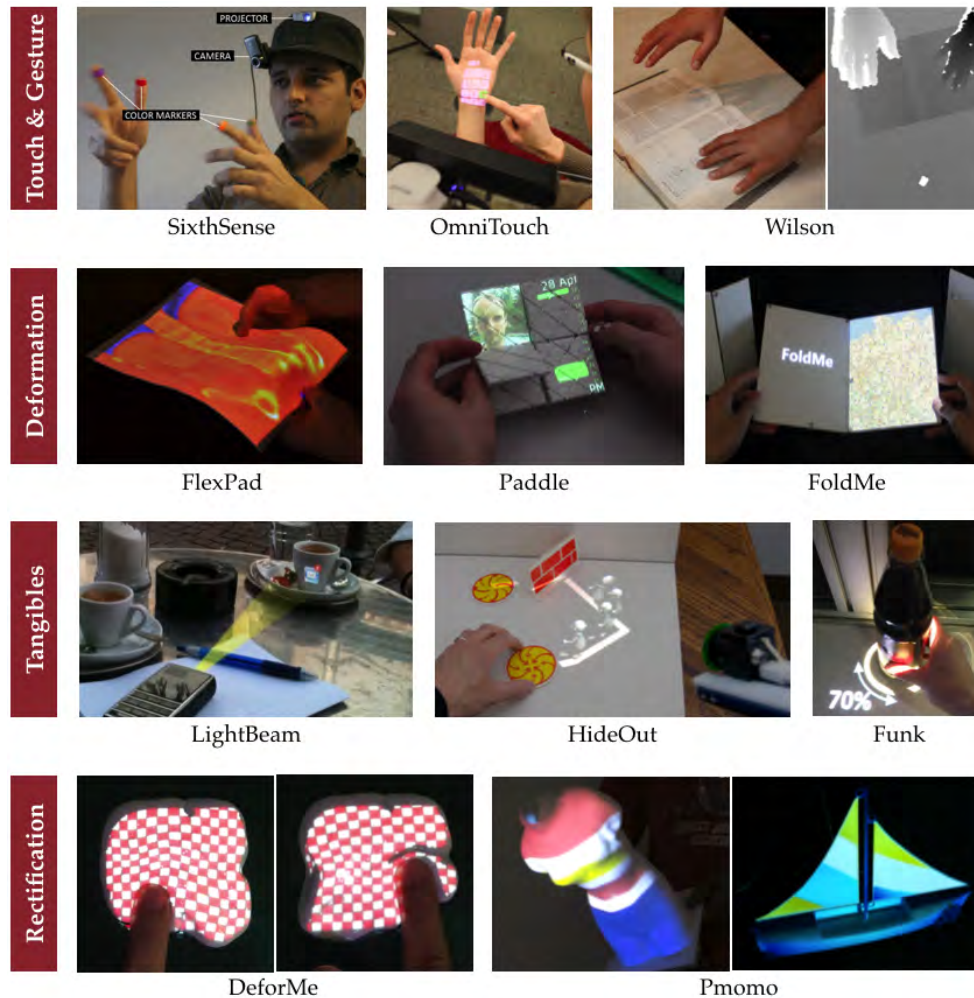
Figure 2.2: Examples of external input using gestures [MMC09], touch [HBW11], deformation [SJM13; RSL14; Kha+12], or tangibles [Hub+12; WSM13] and projected external output, also used for rectification on deformed surfaces [PIS13; PIS15; Zho+16].

FKS14; Ben+01; Rie+18], moving paper or displays in space [Hub+12; Spi+13]. Research also utilizes optical tracking or motion capture systems to sense the movement of paper [Lis+12] or 3D objects in space [SBS06].

Concerning output, a stream of research has investigated how to **project visual content** on objects. That is, they display visual content on objects via projectors mounted in the environment. Thus, they allow displaying visual content directly on the surface of an object. This technique is widely used to augment objects in space, such as tangible paper displays [Lis+12; Spi+13], deformable displays [Kha+11; Kha+12; SJM13; RSL14], flat surfaces [WPS11; Wil+11b; FKS14] or 3D objects [AGV10; Hub+12; MGF13]. Moreover, HCI research explores methods to rectify visual content on deformed surfaces, i.e., they perspectively correct the visual output according to the deformation,

using infrared cameras [PIS13; PIS15] or depth cameras [Zho+16]. While practical and widely used to investigate interaction with high-resolution visual output, these approaches are susceptible to occlusion and often require expensive tracking systems installed separately in the environment to determine the position of the projection area. Moreover, the quality of the projection depends on the color of the object.

In conclusion, approaches utilizing external interactivity enable to use a wide range of complexly-shaped objects for interaction. By combining input sensing with a visual output, they are, in general, powerful approaches to create interactive objects. However, they require separate hardware, for instance, a depth camera installed in the room or carried as a wearable device. These approaches often result in complex and stationary setups that are subject to occlusion effects and, thus, restrain the interactive capabilities on the backside of an object. As a consequence, this thesis investigates methods to 3D print complex interactive functionality directly into the objects without requiring input or output capabilities in the environment. In contrast, printed interactivity facilitates the production of complex-shaped interactive objects tailored to each user, without instrumentalizing users or the environment. Moreover, the digital description of the form and interactive design of an object also facilitates its replication and modification.

2.1.2   *Crafted Interactivity*

Another approach is to **craft** a non-interactive object together with electrical components. That is, the components used for input or output are manually embedded inside the object or attached to its surface. This stream of research has been widely explored for **rapid prototyping** and **paper electronics**, a set of crafting techniques used to create electrical devices on or with paper utilizing conductive inks and electrical components. Regarding input sensing, many approaches have been proposed that detect **deformations**, or **touch (gestures)**. Approaches that focus on these aspects are discussed in the following (see Figure 2.3).

Various **rapid prototyping** frameworks and hardware platforms have been proposed to ease the assembly and use of varying electrical components for HCI researchers. Among others [San+09; Ull+08], some of the most prominent platforms are Arduino [MI07], Phidgets [GF01], and .NET Gadgeteer [VSH11; Hod+13]. Moreover, low-cost sensor platforms emerged that allow using electrical components on tape [DKP15; GWP12] or provide means to

Figure 2.3: Examples of assembled interactivity in the areas of rapid prototyping [VSH11; MI07; DKP15; GWP12], paper electronics [Kar+13; Mel+13; QB10], touch sensing [SPH12; OST13], and deformation sensing [Chi+15; SPH11; Ren+14; HV11].

sketch [OM11] or construct [HM06] physical user interfaces rapidly with low-cost materials.

While hardware platforms and frameworks ease the use of the electrical component, they often restrict the shape of an object. Therefore, research has proposed **paper electronics**, a set of crafting techniques that use omnipresent paper to create interactive objects. Paper electronics accelerate prototyping and also enable to explore new forms of interaction. Around this principle, researchers have proposed to prototype tangible interfaces with a combination of paper and Anoto pens [SN07], electronic tags [Kle+04], or RFID tags [Li+16]. Also, research has explored methods to craft circuits with tape [QB10; QB14] or conductive ink [Mel+13; SRM14; NHK15; Wie+12]. Such augmented paper may be further used to harvest energy by touching, rubbing, and sliding [Kar+13], to animate it with shape memory alloys [QB12],

or to sense touch input via metalized paper [Maz+12]. Although users need to create objects manually, these works intentionally proposed paper electronics as a mean to facilitate the rapid crafting of interactive systems. Following this principle, research in the field of printed interactivity (see Section 2.1.3) aims at combining the benefits of paper electronics with the advantages of digital fabrication.

Furthermore, research has proposed sensing techniques for a wide range of **touch and deformation interaction** performed with objects. By attaching sensors to a non-interactive object, touch, force, and hand gestures can be sensed capacitively [SPH12], acoustically [OST13; OST15], or using tape [HV11]. Further, research has explored sensing of complex bending deformations using tape [Bal+99; WB11], plastic [Chi+15], silicone [SPH11; Sly12; Yoo+18], or foils [Ren+12; Ren+14]. Also, Parzer et al. have investigated touch and deformation on flexible textiles [Par+16; Par+17]. Moreover, research has explored other types of deformation, such as stretching [SII12; Yoo+17], squeezing [Van+13; Wan+11], pressing [MN94], and varying shape flexibility [KTI13; Yao+13].

While allowing for a wide variety of interactions, standard electrical components often restrict the design of 3D objects due to their pre-defined form factor or involve many manual assembly steps. Moreover, foil-based approaches are not meaningfully applicable on object geometries with higher complexity. Research in printed interactivity aims at combining the individuality of crafted interactive objects with low assembly effort. As printing requires a digital description of the interactive object, it further facilitates, in contrast to crafting, an easier copy and distribution of interactive objects. Therefore, this thesis investigates how to use digital fabrication to print freeform sensing structures that detect various interactions with lower assembly effort.

2.1.3   *Printed Interactivity*

A recent field of research investigates how to **print** interactive objects using digital fabrication. It aims at a (semi-)automatic creation of individualized, single-copy interactive objects that, due to the required digital specification, can be easily copied, modified, and printed on demand, and at the same time require less assembly and setup effort than previous approaches. Moreover, this research aims to mitigate the drawbacks of external approaches, that require instrumentalization of users or the environment, and crafted

approaches, that are time-consuming and restricted by pre-defined form factors. That is, it beneficially combines the following advantages of previous approaches:

1. They go beyond pre-defined form factors by digitally printing customizable, single-copy interactive objects.
2. They do not require external sensors in the environment of the object.

In order to achieve these goals, various streams of research have been established that concern:

1. **2D printing** in combination with conductive inks,
2. **inside-assembly 3D printing** that requires additional assembly steps in the interior of an object,
3. **outside-assembly 3D printing** that only requires to bring the object in loose or electrical contact with a sensor unit, and
4. **no-assembly 3D printing** that encodes self-contained interactive functionality in the object without further assembly steps.

Each stream of research is discussed based on the following requirements.

REQUIREMENTS

The following requirements are established to classify existing research streams that focus on printed interactivity:

R1 & R2: Minimize Monetary and Time Costs. Research in the field of printed interactivity often focuses on more cost-effective and time-effective production of single-copy, custom-made objects. This aspect is covered by minimizing monetary costs (R1), i.e., the costs to fabricate an object with the given approach, and time costs (R2), i.e., the time it takes to create the object.

R3, R4, & R5: Minimize Effort to Design, Print, and Assemble. Moreover, the effort to create the object all the way to its use should be minimized. Compared to R2, the effort describes the ease of use and the expertise required to create an object. The requirements distinguish the effort necessary to execute the following three steps during creation: First, a user needs to **design** the object (R3), i.e., she creates a digital representation. Second, the object is constructed by a specific **printing** process (R4), which may range from the manual application of various print layers to the fully automatic production of the object. Third, many approaches require manual **assembly** steps after printing (R5). That is, electrical components need to be attached or embedded, and wires need to be routed manually inside or outside the object.

R6 & R7: Maximize Customizability of Object and IO Geometry. This requirement targets the rising complexity of supported object geometries (R6). Approaches apply to a particular set of geometries, ranging from simple, developable to more complex, non-developable surfaces. Based on [Sny87], **developable surfaces** are defined as follows:

Definition 1 *A developable surface is one that can be transformed into a plane without distortion.*

That is, developable surfaces can be constructed from a plane without stretching or compressing only through transformations such as folding, bending, rolling, or cutting. Two of the most common examples of developable surfaces are cylinders and cones.

In contrast, **non-developable surfaces** require stretching or compressing to be transformed into a plane. Such surfaces are often also referred to as being doubly-curved or having double curvature. A simple example of a non-developable surface is a sphere. Also, many real-world objects (e.g., office equipment or appliances) are non-developable.

The requirements explicitly differentiate between the customization of the enclosing object (R6) from the possible complexity and customizability of the input sensing and output structures (R7). That is, R7 covers the degree of customization a user may apply to the input and output structures. For instance, an approach may allow for custom sensing structures (R7) but may be limited to developable surfaces (R6).

R8: Maximize Resolution of In- and Output. The maximal resolution of input capturing and output capabilities is also an essential property to classify printing approaches. For input sensing, the resolution can range from a binary decision to a determination of several or continuous levels of interaction.

2D PRINTING

A recent stream of research uses 2D printing technologies, such as inkjet printers or vinyl cutters, to create interactive objects. This stream builds upon research in material science that concerns 2D-printed paper electronics [TÖ11; vOsc+08] and aims at rapid prototyping of circuits and interactions with low assembly effort. The resulting 2D structures are often custom-shaped. They may be embedded into or wrapped around non-interactive objects.

Figure 2.4: Examples of 2D-printed interactivity in the areas of paper electronics [Kaw+13; RTL15; CW15], touch [Olb+13; SZH12; Gon+14], deformation [Olb+15; VS17], and visual or haptic output [OWS14; WGS18; GS18].

Rapid prototyping of circuits often requires extensive wiring of multiple components. Therefore, research has explored **2D-printed paper electronics**, a set of methods to automatically create schematics and wirings using an automated conductive pen [Wan+18b] or conventional inkjet printers equipped with a cartridge filled with conductive ink [GHP11; KLT12; Kaw+13; RTL15; CW15]. Moreover, Nagels et al. [Nag+18] proposed a fabrication workflow for embedding electronics on highly stretchable substrates.

Various approaches for **2D-printed multi-touch sensing** have been proposed with fixed [Zir+11; KM14] or custom-shaped sensors, that utilize vinyl cut-

ters [SZH12], inkjet printing [Olb+13; DKA14; KG15; Nit+18] or screen printing [GS18; Nit+18].

Moreover, research has investigated various **deformation-based methods**, such as folding [Gon+14; Olb+15], shearing [Olb+15], pressure [Gon+14; Wei+15], squeezing [Wei+17], bending [VS17], or self-folding [Sun+15].

Also, 2D printing has been utilized to create **visual or tactile output**. Research has explored custom-shaped displays using electrochromic [Col+99] or electroluminescent [OWS14]. Based on these, research has contributed screen- or hydro-print displays on stretchable substrates [WTM16; GS18] that allow covering non-developable geometries but result in distortions of sensing structures that designers need to consider. Moreover, research has investigated 2D-printed feel-through tactile output [WGS18] that is very thin and applicable to non-developable geometries on the body.

The concept of automatically fabricating custom-shaped and individualized sensors significantly inspired this thesis: 2D printing approaches automate the process of designing (R3) and printing (R4) custom-shaped 2D sensors (R7), which are often low-cost (R1). They speed up the general creation process significantly (R2) and allow for medium- or high-resolution input and output (R8).

On the contrary, approaches still often require manual assembly steps to connect wires or auxiliary electrical components (R5). Compared to 3D printing approaches, the set of applicable geometries is limited to developable surfaces (R6). That is, 2D-printed substrates need to be wrapped around or embedded into 3D objects which again results in considerable assembly effort or is not possible in principle for non-developable surfaces without distortion. While promising research can be applied to more complex geometries (cf. [GS18]), distortions must be compensated during the design phase. Therefore, this thesis aims at closing the gap between high-res custom-shaped sensors and complex geometries by contributing concepts for 3D sensor geometries, generation algorithms, and practical guidelines to fabricate interactive 3D objects using commercially available printers and materials.

INSIDE-ASSEMBLY 3D PRINTING

To mitigate the drawback of 2D printing regarding assembly steps and object complexity, a recent stream of research (cf. [BGL18]) uses 3D printing to
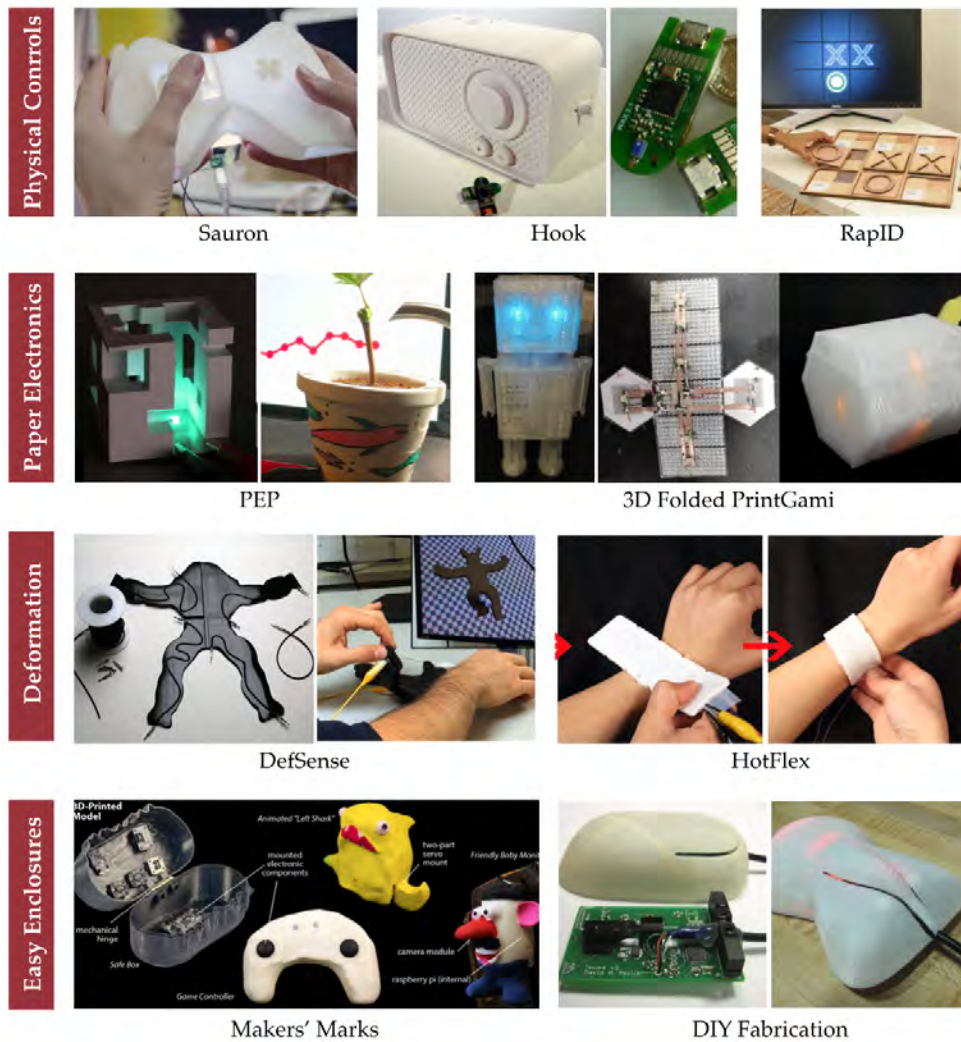
Figure 2.5: Examples of 3D-printed objects requiring inside-assembly in the areas of physical controls [SCH13; Hoo+14; Spi+16], paper electronics [Oh+18; DKY16], deformation [Bäc+16; GCS16], and enclosures [Sav+15; Mel14].

create interactive objects[1]. This research also often utilizes the 3D capabilities of 3D printing to explore new types of input or output geometries.

This section discusses 3D printing approaches that require **inside-assembly**. That is, they use 3D printing to create customized objects, but require additional assembly steps during or after printing that need to be executed in the interior of the object (see Figure 2.5).

Human input on **physical controls** (e.g., sliders or buttons) can be sensed in 3D-printed objects by embedding cameras [SCH13], wireless accelerometers [Hoo+14], mobile devices [Led+17], or RFID tags [Spi+16].

---

1 see Section 2.2 for an introduction to 3D printing technologies

Research has further proposed to generate **pipes inside 3D-printed objects** filled after printing with various media (e.g., to detect touch or provide sound, light, or air feedback) [Sav+14] or are equipped with resistive wires to reconstruct complex deformations [Bäc+16]. Gröger et al. have proposed to embed heating elements in 3D-printed objects to allow for post-print customization of the shape of an object [GCS16].

Moreover, researchers have contributed methods to more efficiently generate **3D enclosures** that house electrical components [Mur+08; SH12; WLG13; Mel14; Sav+15; DMC18] or paper electronics containing functional layers of paper [Oh+18] or functional origamis [DKY16].

Even though these approaches require only a few components and ease the process of designing (R3) and printing (R4) at low-cost (R1), they still require manual assembly steps inside the object to place and connect electrical components (R5). Standard components still restrict the design of 3D objects due to their pre-defined form factor, but custom-shaped sensors are possible due to the combination with more complex enclosing 3D geometries than for 2D printing (R7). In contrast to 2D printing, these approaches significantly extend the field as they apply to non-developable objects (R6). While the interactive object still often needs to be hollow, opened or assembled after printing, the use of standard components often enables high-resolution input and output (R8).

This research inspired this thesis regarding the possible complexity of 3D printing objects and the associated possibilities for sensor geometries. In combination with multi-material printing, objects can contain interactive structures that go beyond existing fixed-form components and simultaneously reduce assembly effort.

OUTSIDE-ASSEMBLY 3D PRINTING

This section discusses 3D printing approaches that require **outside-assembly**. That is, they use 3D printing to create customized objects that already contain input and output structure in the interior of the object. They only require additional assembly steps after printing at the outside of the object. The combination of a 3D-printed object and a component of an electronic device (e.g., a capacitive touchscreen of a smartphone) are defined as a necessary assembly step because the object itself only becomes interactive together with the additional electronics inside the device.

Figure 2.6: Examples of 3D-printed objects requiring outside-assembly in the areas of output feedback [Wil+12; Váz+15; IP14; Sun+17b], deformation [He+17; HPS16; Kim+17; Guo+17], touch [ZLH17; HIS17; Bur+15], and physical controls [UKM16; Lap+15; GS16].

3D printing of conductive materials has been investigated in Material Science utilizing conductive wires [Esp+14], silicone [PML07], sprays [Sar+12; IP14], carbon-filled plastic [Lei+12], inks [Ahm13], tapes [US16], or threads [Hud14]. In this field, research has contributed methods to combine 3D objects with electronic components during printing [LMW12; She+13; Esp+14]. While the 3D printing of first conductive materials is already at consumer-level, the automatic integration and connection of electrical components with highly conductive materials still requires specialized printers at a research level. As a consequence, HCI research often investigates methods to integrate interactive capabilities (e.g., complex sensor geometries or pipes) into an object but assemble the electrical components at the outside of the object.

Some approaches utilize **3D-printed pipes** for pneumatic feedback [Váz+15] or to interact via touch, mechanical movement, or internal illumination

[Wil+12; BPH13; PRM14]. Also, Ou et al. have investigated micro-pillars for actuation and surface textures [Ou+16].

Ishiguro and Poupyrev [IP14] further demonstrate how to 3D print interactive speakers using conductive spray. Also, research investigates actuation via self-folding [Sun+17b], liquid-based movement [Mac+15], or grasping [Tru+18], and sensing of stacking [YST15] and physical controls [Lap+15].

Furthermore, research has explored **deformation sensing** that only requires outside assembly for interaction such as squeezing [He+17], bending [Tru+18], pressing [HPS16; Kim+17], or stretching [Guo+17].

A larger body of research has contributed touch sensing on 3D-printed objects via conductive plastic [KM16; UKM16; Lei+12; Bur+15], or fabric [Pen+15; Hud14], also considering generation and placement of touch electrode on 3D surfaces [GA16; HIS17] and markers for tangible objects on capacitive touchscreens [GS16]. Moreover, Zhang et al. have contributed a promising approach using electric field tomography that also operates on fully-conductive 3D-printed objects [ZLH17].

These approaches improve over **inside-assembly** as they allow for custom-shaped complex sensor geometries (R7) inside non-developable objects (R6). Also, they reduce the assembly effort (R5) after easy printing (R4) but often require expensive printers (R1) and manual design effort (R3) that can be laborious (R2). While already allowing for complex 3D input sensing, often with medium or high resolution (R8), many types on input modalities (e.g., many deformations or tilting) has not been explored by research so far.

In conclusion, **outside-assembly 3D printing** is a promising research direction as it can beneficially minimize costs and effort, and at the same time allows for non-developable IO structures and objects. As discussed, research has started to explore important properties of interactive systems, such as printed visual output [Wil+12] or physical input [Lap+15]. Inspired by this research, this thesis contributes additional sensing concepts, such as for deformation or touch detection, that also targets an automatic generation of 3D structures and less complex assembly.

no-assembly 3d printing

Recently, a stream of research emerged in HCI that does not require any assembly at all after printing. The interactive functionality of an object is encoded inside their geometrical structure during the design phase (see Fig-
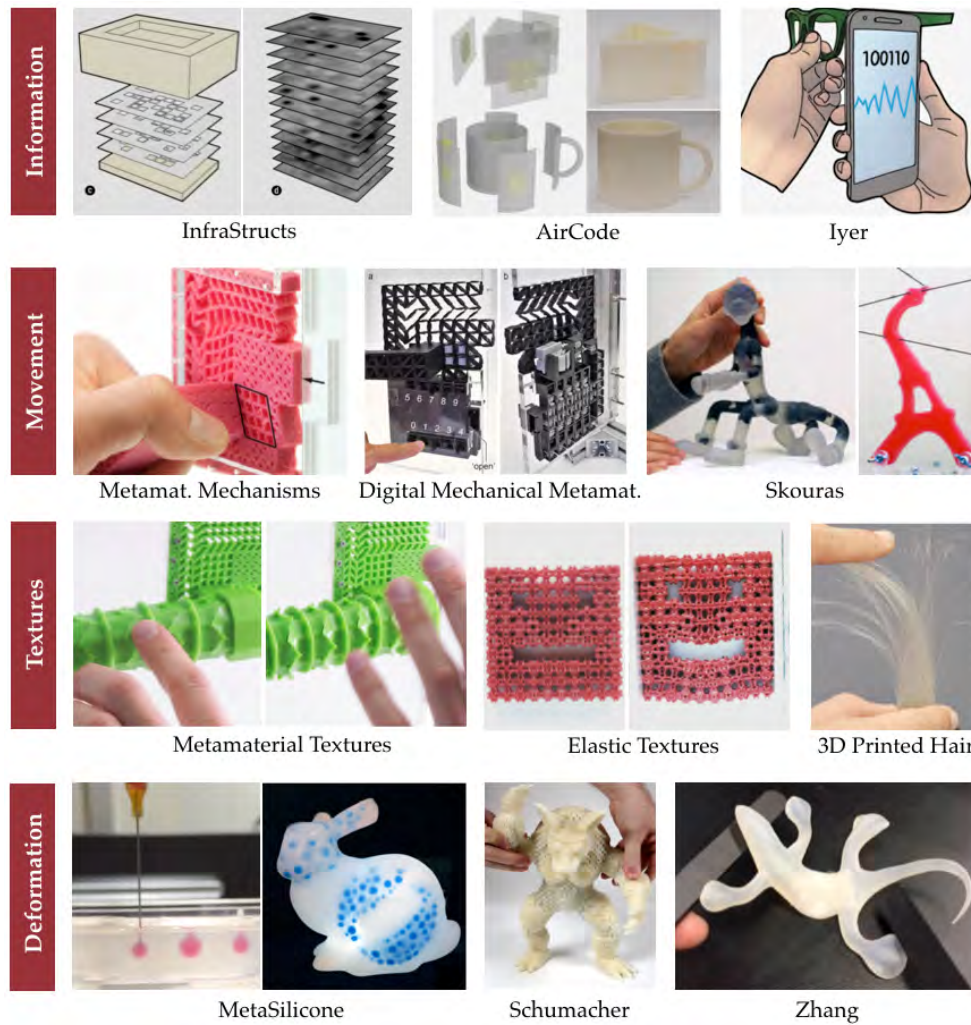
Figure 2.7: Examples of 3D-printed objects requiring no assembly in the areas of encoding information [WW13; Li+17; ICG17], movement [Ion+16; Ion+17; Sko+13], textures [Ion+18; Pan+15; LCH15], and deformation behavior [Zeh+17; Sch+15b; Zha+16].

ure 2.7). These interactive structures are coined as **metamaterials**, i.e., structures engineered to yield new functional properties.

Promising first steps towards digitally fabricated objects containing metamaterials were made by research in the last years. Such metamaterials convey **digital information** using terahertz imaging [WSM13], magnetic storage [ICG17], or air pockets [Li+17]. Moreover, they are used for fabricating the desired **movement** of mechanics [Ion+16], logical operations [Ion+17], character actuation [Sko+13], self-folding [An+18; Wan+18a].

Related research has also investigated controlling computational material design. That is, the 3D model is altered or generated to convey global prop-

erties, such as the **texture** of an object. This research includes 3D printing of haptic feel aesthetics [Tor+15], multi-color textures [Zha+11], or hair structures [LCH15]. Also, research has investigated how to print dynamically changing textures [Ion+18] or divide objects so that the parts interlock [Son+15]. It, further, explored the generation of perforations that encode a projective image [Zha+15] or the printing human-scale dynamic inflatable objects [Sar+17].

Furthermore, a multitude of research has also explored to generate specific **deformation** behavior by controlling stiffness [Zeh+17], elasticity [Sch+15b; Pan+15; Zha+16], and bending [Bic+10; Pér+15; Xu+15].

While significantly reducing the time costs (R2), as well as the design (R3), print (R4), and assembly (R5) effort, the set and resolution of intrinsically encodable interactions that do not require electronics is limited (R7, R8). More importantly, objects encode their functionality intrinsically without any connection to the outside, i.e., they either operate without any greater interactive systems or need to be read-out using external sensors (see Section 2.1.1). These approaches inspire this thesis in two aspects: First, they explore complex 3D-printed structures that encode functionality and change due to external stimuli. Second, they contribute to the concept of extracting information out of a 3D-printed object using an external sensor unit (e.g., a smartphone).

2.1.4   *Conclusion for this Thesis*

There are three fundamentally different approaches to create an interactive object: (1) external approaches, providing input and output through the environment, (2) crafted approaches, creating objects with traditional tools and materials, and (3) printed approaches, utilizing digital fabrication technologies to automatically create an object according to a digital description.

As illustrated in Figure 2.8, all approaches differ in the degree of automation to fabricate the object and also in their possible geometric object complexity (cf. [Sch16]): Whereas **crafted** interactivity allows using a large set of standard components, the supported object geometries are often limited to developable surfaces and the creation is in many cases laborious. In contrast, **external** approaches allow adding interactivity to a broad spectrum of objects. However, the creation of objects (e.g., they need to be equipped with markers) is often time-consuming and prone to errors. Therefore, **printed**
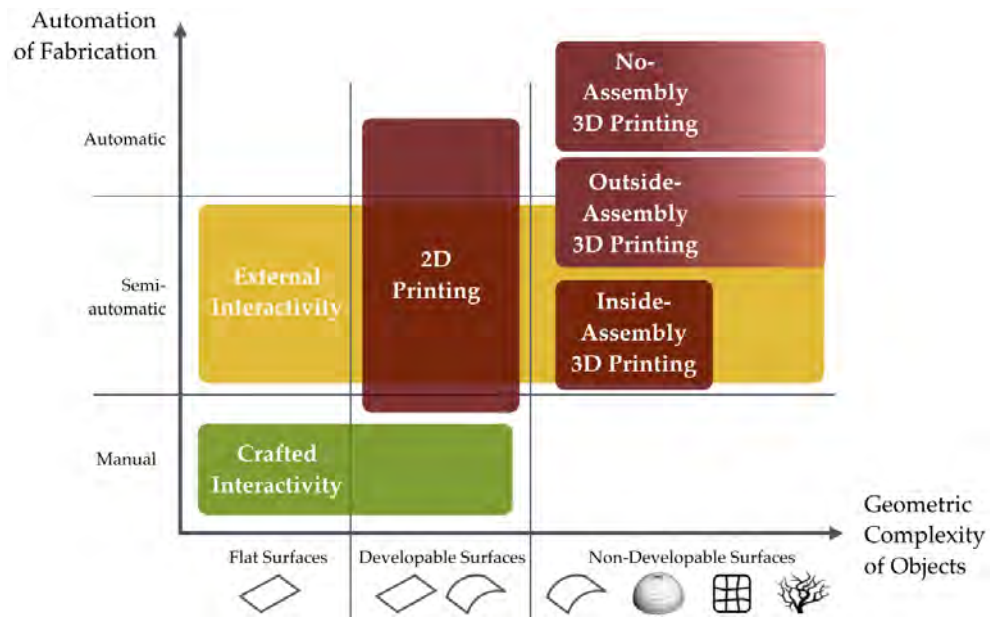
Figure 2.8: Classification of related work based on the geometric complexity of the object to be made interactive and the automation of fabrication.

interactivity strives at beneficially combining object complexity and automation of fabrication.

PRINTED INTERACTIVITY

As discussed, approaches in the field of printed interactivity may be grouped into 2D printing, as well as inside-assembly, outside-assembly, and no-assembly 3D printing. Table 2.1 compares selected relevant research in each group concerning the previously established requirements. While 2D printing approaches take a significant step forward regarding supported interactivity and ease of fabrication, they are in principle limited to developable surfaces. 3D printing aims at solving these problems, but is challenging with regard to 3D geometries and materials: Existing approaches may be grouped into inside-assembly, where objects are 3D-printed with internal structures but need to be equipped after printing with additional materials or hardware, still requiring manual work and, hence, reducing their automation. Therefore, research has emerged that only requires assembly steps at the outside of a 3D-printed object, reducing the amount of manual assembly, but still allowing for complex, non-developable object geometries. This research has been complemented by work that encodes interactive functionality in their internal structure and, hence, does not require any assembly at all. While practical for many use cases, objects do not interchange any data with an outside system, i.e., they are not able to communicate with soft-

	R1, R2 (Costs)		R3, R4, R5 (Effort)			R6, R7 (Custom.)		R8
	Monetary	Time	Design	Print	Assemble	Object	IO-Structure	Resolution
2D Printing								
Instant Inkjet Circuits [Kaw+13]	●	○	○	◑	◑	◑	●	◑
Cuttable Multi-Touch [Olb+13]	●	◑	◑	●	◑	◑	●	●
PrintSense [Gon+14]	●	◑	◑	●	◑	◑	●	●
Printing Multi-Key Touch [KG15]	●	◑	◑	●	◑	◑	●	◑
ObjectSkin [GS18]	◑	○	◑	◑	○	●	●	●
Inside-Assembly 3D Printing								
Wireless Accelerometers [Hoo+14]	○	◑	○	●	○	●	○	●
A Series of Tubes [Sav+14]	◑	◑	●	●	○	●	●	◑
DefSense [Bäc+16]	◑	◑	◑	●	◑	●	●	●
PEP [Oh+18]	◑	◑	●	●	○	●	◑	◑
Outside-Assembly 3D Printing								
Printed Optics [Wil+12]	○	○	○	●	●	●	●	●
Acoustruments [Lap+15]	○	○	○	●	◑	●	●	●
PrintPut [Bur+15]	●	○	○	●	●	●	●	◑
SqueezaPulse [He+17]	○	○	○	●	◑	●	●	◑
No-Assembly 3D Printing								
Metamaterial Mechanisms [Ion+16]	●	○	○	○	●	●	◑	◑
MetaSilicone [Zeh+17]	○	◑	●	○	●	●	◑	◑
Metamaterial Textures [Ion+18]	●	○	○	○	●	●	◑	◑

Table 2.1: Comparison of related research regarding the previously defined requirements. ○, ◑, and ● indicate a low, medium, or high approval of a requirement. That is, the more costs and effort are minimized, the better. The higher the customizability and resolution, the better.

ware. In other words, the interaction is limited to the object itself and is not embedded in a more complex interactive system.

This thesis contributes to the category of outside-assembly as it explores new types of input modalities and 3D sensor geometries for touch, deformation, and environmental interactions that only require assembling objects and electronics, either in the form of a microcontroller or a capacitive touchscreen.

The following sections provide the fundamentals of technologies and materials for digital fabrication (see Section 2.2) and the processing steps involved in the 3D printing pipeline (see Section 2.3).

HCI research employs digital fabrication technologies to rapidly prototype novel user interfaces. In the past years, an emerging stream of research adds to this by providing approaches to create interactive objects that are customized to user needs or an application scenario, or use the powerfulness of this technology to investigate novel input and output modalities in three dimensions.

In general, **Digital Fabrication** describes a myriad of different technologies to manufacture 3D objects based on a digital model (i.e., a digital blueprint describing the geometry, color, or other properties of an object). This thesis defines the term as follows:

Definition 2 *Digital Fabrication is a production process that creates three-dimensional objects based on a digital model.*

Digital Fabrication technologies can be grouped into two main approaches (see Figure 2.9). There are Additive Manufacturing processes that build up an object from a material layer by layer. In contrast, Subtractive Manufacturing processes decompose an existing block of material so that the object to be produced remains. That is, objects created using Subtractive Manufacturing consist only of a single material. This thesis contributes approaches that require hybrid objects, consisting of multiple materials with diverse properties (such as conductivity or flexibility), to support interactivity. Therefore, this section focuses on Additive Manufacturing.

The remainder of this section is structured as follows: First, Section 2.2.1 establishes **technology requirements** that were used to select an appropriate 3D printing process suitable for this research. Second, Section 2.2.2 presents various **3D printing technologies** and classify each one according to the requirements. Third, Section 2.2.3 discusses a **classification of 3D printing materials**. Finally, Section 2.2.4 details on **functional 3D printing materials**.

2.2.1   *Technology Requirements*

The following set of requirements is essential for 3D printing interactive objects. **R1: Conductive Printing Material.** As electrodes and wires used for sensing and electronics need to be conductive, one essential requirement is a
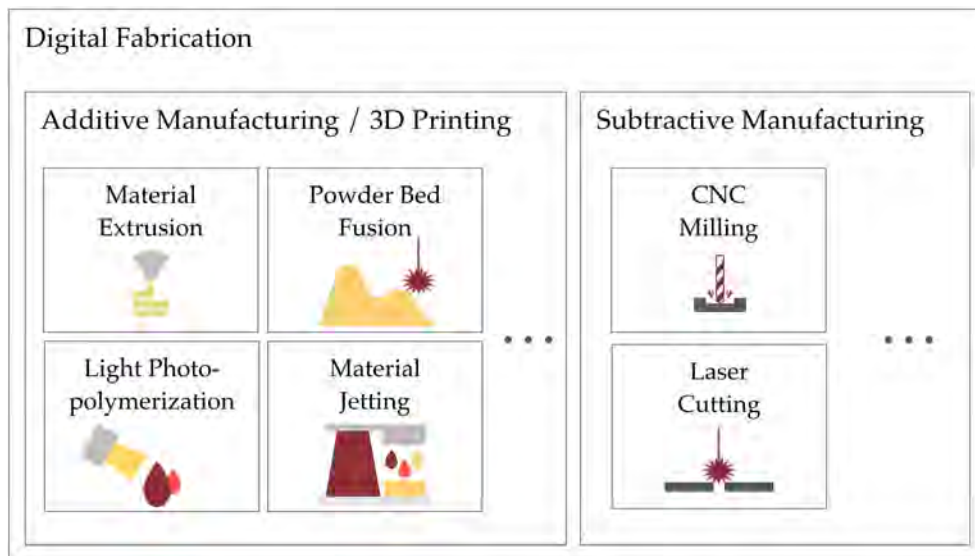
Figure 2.9: Classification of digital fabrication technologies.

conductive printing material. For the connection of complex electronics, this material should have the lowest possible resistance with good printability at the same time.

R2: Multi-Material Fabrication. While some parts of the object are required to be conductive to implement electrical structures for sensing, the remaining part of the object cannot be implemented with a conductive material as well, as this would result in electrical shorts. To that end, at least one insulating material is required in conjunction with a conductive material. Hence, a 3D printing process should be able to print at least two materials simultaneously.

R3: Off-The-Shelf Hardware. The presented approaches should be accessible to a broad community of researchers and developers to facilitate practicability in the field of HCI. To that end, the required hardware and the printing materials to implement the proposed sensing techniques should be readily available off-the-shelf at low-cost as possible.

2.2.2   *3D Printing Technologies*

Based on [Geb16], the following section discusses 3D printing technologies according to the previously established requirements. This thesis focuses on 3D printing technologies that are already available at a consumer-level to foster practicability for HCI researchers.
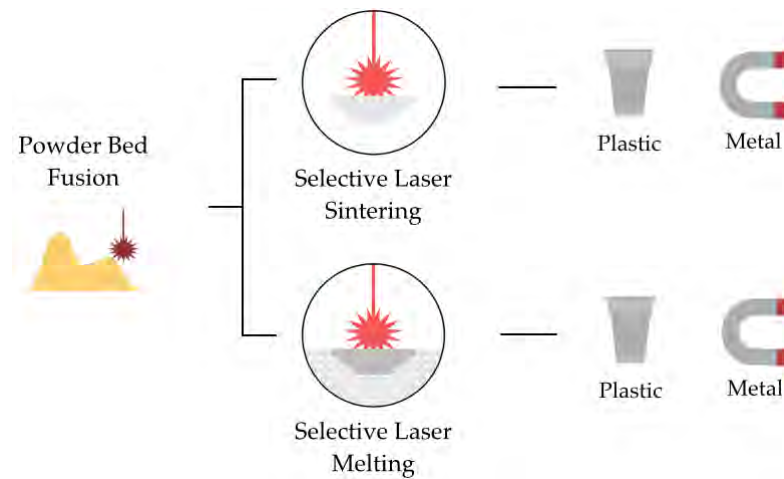
Figure 2.10: Printing technology using Powder Bed Fusion (based on [3DH18a]).

POWDER BED FUSION

As illustrated in Figure 2.10, approaches to 3D printing based on powder bed fusion can be grouped into Selective Laser Sintering and Selective Laser Melting.

Selective Laser Sintering (SLS) sinters a 3D object layer by layer using a moving laser beam. That is, a thermoplastic or metallic powder is heated and fused below the melting temperature. After completion of a single layer, the printing platform is lowered, and new powder is applied to print the next layer. When finished, the resulting object is completely covered in unsintered powder which needs to be removed.

Selective Laser Melting (SLM) operates very similar to SLS, but, in contrast, actually melts a powdery printing material using a moving high-energy laser beam (for example in the infrared range). However, compared to Selective Laser Sintering, Selective Laser Melting often requires support structures due to high residual stresses [3DH18a].

SLS and SLM both allow thin layer thicknesses of up to 0.08 mm. The powder used for SLS and SLM is often based on polymers or conductive metals (R1). However, printing can only use a single material (R2). Due to costs for lasers, this technology is currently more expensive than other technologies (R3).
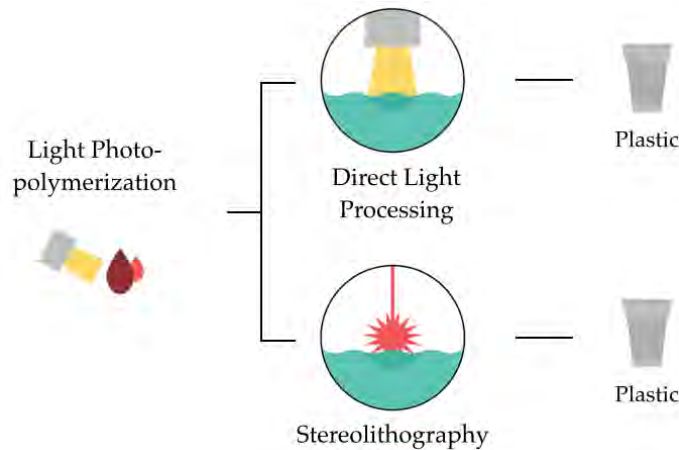
Figure 2.11: Printing technology using Light photopolymerization (based on [3DH18a]).

LIGHT PHOTOPOLYMERIZATION

As illustrated in Figure 2.11, approaches to 3D printing based on Light Photopolymerization, i.e., a liquid material is solidified via a light source, can be grouped into Stereolithography or Digital Light Processing.

Stereolithography (SLA) builds upon the principle of Photopolymerisation: A basin is filled with liquid monomers (such as Acrylate or Epoxid). At first, the printing platform rests at the top of the basin such that only a single layer of fluid material covers it. Then, a single layer is cured by moving a single-point light source. After completion of a single layer, the printing platform is slightly lowered. As a result, new fluid material flows over the incomplete print in order to print a new layer.

Digital Light Processing (DLP) printers use the same principle but, in contrast, cure a whole layer simultaneously by projecting a 2D image onto the basin instead of moving a single-point light source. As a consequence, the speed up the printing process significantly.

Stereolithography and Digital Light Processing both allow thin layer thicknesses of up to 0.025 mm. With cheap projectors and hardware, this technology is already available off-the-shelf at a consumer level (R3). However, there are currently no conductive printing materials commercially available (R1), and printing can only use a single material (R2).
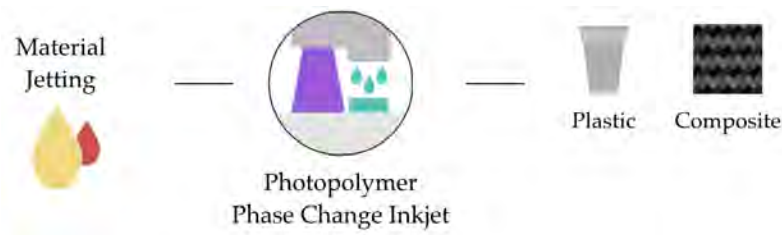
Figure 2.12: Printing technology using Material Jetting (based on [3DH18a]).

MATERIAL JETTING

Material Jetting is a 3D printing technology that also utilizes Photopolymerization. However, the material is applied differently compared to the previous approaches. The following discussion focuses on a technology called **Photopolymer Phase Change Inkjet** (PolyJet) as it is the most widely used kind (see Figure 2.12).

Similar to 2D inkjet printers, PolyJet printers utilize a print head that can deposit small droplets of photopolymer material simultaneously. For a single layer, this print head moves across the build platform to deposit material. At the same time, an attached UV light is used to cure the deposited material. For the next layer, the build platform is slightly lowered.

PolyJet allows for thin layer thicknesses of up to 0.016 mm. While being able to print multiple materials simultaneously (R2), there are currently no conductive printing materials commercially available (R1). This technology is currently costly (R3).

Relevant for this thesis is also promising concurrent research by Sundaram et al. [Sun+17a]. They propose a process called **drop-on-demand multi-material printing** that operates similar to PolyJet but is also able to print conductive and liquid materials.

MATERIAL EXTRUSION

As illustrated in Figure 2.13, approaches to 3D printing based on material extrusion mainly utilize Fused Deposition Modeling (FDM)[2].

In general, FDM operates as follows (see Figure 2.14): The printing material is available in the form of the **filament**, i.e., a strand of material with a uniform diameter.

---

2 FDM is sometimes referred to as Fused Filament Fabrication.
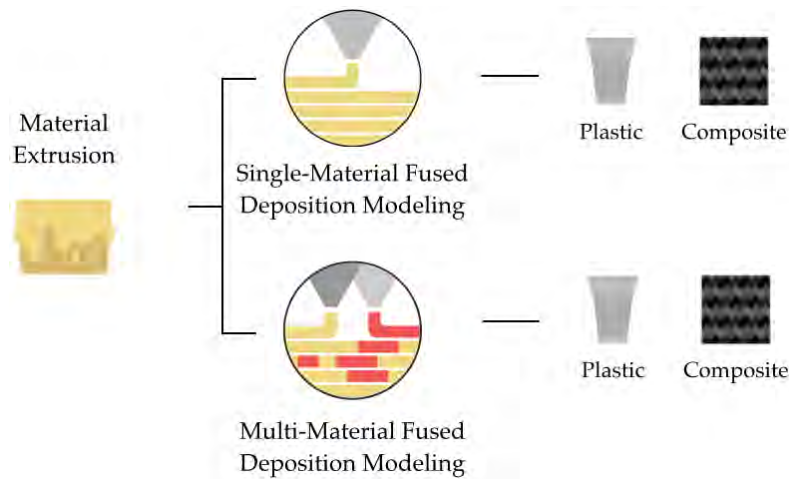
Figure 2.13: Printing technology using Material Extrusion (based on [3DH18a]).

FDM printers consist of two main parts: First, the build platform where the object is printed on. It moves in z-direction after a layer is finished. Second, the print head, where the material is extruded. It moves in x- and y-direction to form a single layer of material. The filament is pulled into the print head by a **stepper motor**. The stepper motor is either mounted directly on the print head, which is called **direct drive**. While this allows for more precise control of the movement of the filament, it makes the print head heavier and less movable. Another variant is to mount the stepper motor externally and to guide the filament through a Bowden tube into the print head. This variant, called **Bowden drive**, significantly reduces the weight of the print head. However, deformable filaments are challenging to print with a Bowden drive, because the material might be compressed in the tube, which complicates precise material extrusion.

Then, the **heater**, a component that is heatable to a precise temperature, melts the pulled filament. In the heater, the filament is squeezed throughout the **nozzle**, a conical tapering with a fixed diameter (called **nozzle diameter**), onto the object layered up on the build platform. The **layer height** may be adjusted by varying the amount of extruded filament or the nozzle diameter, resulting in more coarse or fine-grained printing quality. Currently, printers can print layers down to 0.05 mm (most common 0.2 mm). Moreover, the object is partitioned into the **perimeter**, the outer shell of an object, and the **infill**. As objects are usually not filled with the material, objects are build up in the inside with a structure called **infill pattern**. There exist various infill patterns each with specific properties, such as to improve loading capacity or material consumption. By controlling the **infill density**, the amount of ma-
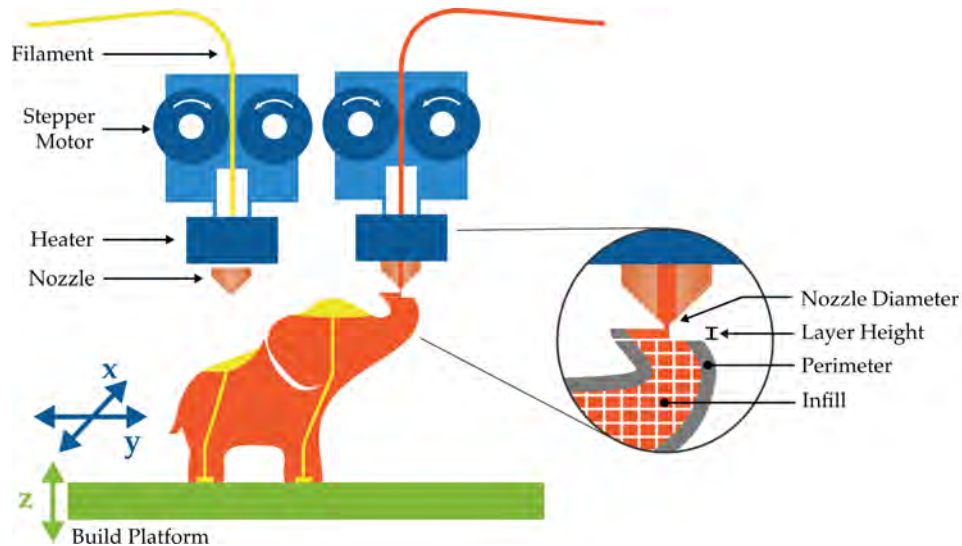
Figure 2.14: The principle of multi-material material extrusion (based on [Kho15])

terial used to create the pattern compared to 100% filling can be controlled further.

Printers following the principle of Fused Deposition Modeling can be further grouped into single- and multi-material variants. Single-material printers (abbreviated 1-FDM) utilize a single printhead and are bound to a single material (R2). Building a multi-material FDM printer (abbreviated n-FDM) which can print more than one material simultaneously is challenging: First, multiple print heads need to be mounted next to each other without interference. Second, while one material is printed, the other materials should stay inside the nozzle. Leaking material without intention, called **oozing**, should be prevented, especially when printing conductive structures. While many multi-material printers utilize print heads that all operate according to the FDM principle, printers have been proposed that combine a standard print head and a pneumatic syringe print head, that can extrude pastelike materials, such as conductive silver inks (cf. [16]).

A variety of different filaments for FDM exist. Among other functional materials such as deformable or magnetic filaments, there are a few conductive printing materials commercially available (R1). Most recently, filament splicers (cf. [Man18]) for up to four and also multi-material printers for up to five materials (cf. [Pru18]) were presented at low-cost (R2, R3). While opening up whole new possibilities in the combination of functional materials, only dual-material printers (2-FDM) were available in the consumer segment during this research.

	Requirements			Resolution	
	Conductive Material (R1)	Multi-Material (R2)	Consumer-Level (R3)	Z (mm)	X/Y (mm)
Powder Bed Fusion (SLS, SLM)	✓	✗	✗	0.08 mm	0.3 mm
Light Photopoly- merization (SLA, DLP)	✗	✗	✓	0.025 mm	0.01 mm
Material Jetting (PolyJet, Drop-on-demand)	✓	✓	✗	0.016 mm	0.05 mm
Material Extrusion (1-FDM, n-FDM)	✓	✓	✓	0.05 mm	0.2 mm

Table 2.2: Comparison of different digital fabrication technologies regarding the previously established technical requirements.

CONCLUSION FOR THIS THESIS

While allowing for precise prints with up to 0.025 mm layer height, both Powder Bed Fusion and Light Photopolymerization cannot print multiple materials simultaneously (see Table 2.2). Also, Light Photopolymerization is becoming more available in the consumer segment, but it can not compete regarding price and versatility with available printers that utilize Material Extrusion. While Material Jetting is a promising technology that enables printing of high-resolution multi-material objects, it is currently either still at a research level or very expensive. In conclusion, Material Extrusion is currently the only digital fabrication technology that can print multiple conductive and insulating materials simultaneously while being readily available to consumers.

In the remainder of this thesis, 3D printing refers to printers and materials using FDM.

2.2.3 *Classification of 3D Printing Materials*

3D printing materials for FDM are discussed in the following. This thesis focuses on readily available materials that are extrudable using FDM.

As FDM is based on melting, many thermoplastics are well suited for printing. The most common thermoplastics used in FDM are Polylactic Acid (PLA), Acrylonitrile Butadiene Styrene (ABS) or Thermoplastic Polyurethane (TPU).

METHODOLOGY

In order to classify the most important printing materials for FDM, this section defines a set of mechanical, visual, and process properties (based on [3DH18b]).

Ease of Printing. This property describes the printability of a material. It is a combination of multiple factors such as maximal printing speed, flow accuracy, or the ratio of failed to successful prints.

Visual Quality. The visual quality is defined as the combination of geometrical accuracy and the ability to recreate detail and texture (cf. [3D-18]): Geometrical accuracy characterizes the ability to recreate various spatial properties such as correct size, angles, curvature, deposition accuracy, or amount of smearing. Details and texture focus on the ability to fabricate fine-grained structures (e.g., thin ridges) and the smoothness of the surface (e.g., textures).

Maximum Stress. The maximum stress is defined as the maximal force an object can be exposed to before breakage if slowly pulled.

Elongation at Break. The elongation at break is defined as the maximum length the object was stretched before breaking.

Impact Resistance. The impact resistance is defined as the energy required to break an object with a sudden impact.

Layer Adhesion. The layer adhesion is defined as the amount of adhesion between the material layers.

Heat Resistance. The heat resistance is defined as the maximum temperature the object can withstand before softening or deforming.

CONCLUSION FOR THIS THESIS

As illustrated in Figure 2.15, this section classifies the most important FDM printing materials (ABS, PLA, and, TPU) according to the previously defined properties.

While ABS is slightly more impact resistant than PLA, both are, not surprisingly, outperformed by TPU regarding impact resistance and elongation at break due to the elasticity of TPU.
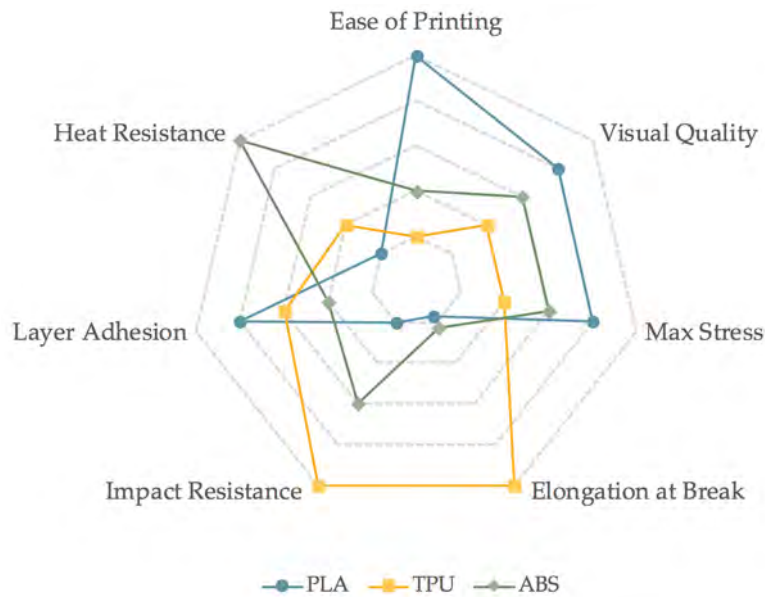
Figure 2.15: Comparison of material properties of ABS, PLA, and TPU on a 5-point scale from low (center) to high (exterior) (based on [3DH18b]).

While PLA is not as heat-resistant as ABS, it improves over ABS and TPU in terms of ease of printing, maximal stress, layer adhesion and visual quality of 3D objects.

In conclusion, TPU is well suited if elasticity is required but hard to print. If an object should be solid but easy to print, PLA should be used. For more durable solid objects, ABS is suited.

2.2.4   *Functional 3D Printing Materials*

In order to achieve functional properties ranging from simple colorization to conductive or magnetic properties, the previously discussed thermoplastics are combined as a **matrix material** with different **functional reinforcements**. Inspired by [Sav16], this section presents a set of commercially-available functional 3D printing materials, that can be processed with FDM (see Figure 2.16).

COLOR-CHANGING

By using color-changing particles as functional reinforcement, a few filaments are commercially available that changes its color as a response to
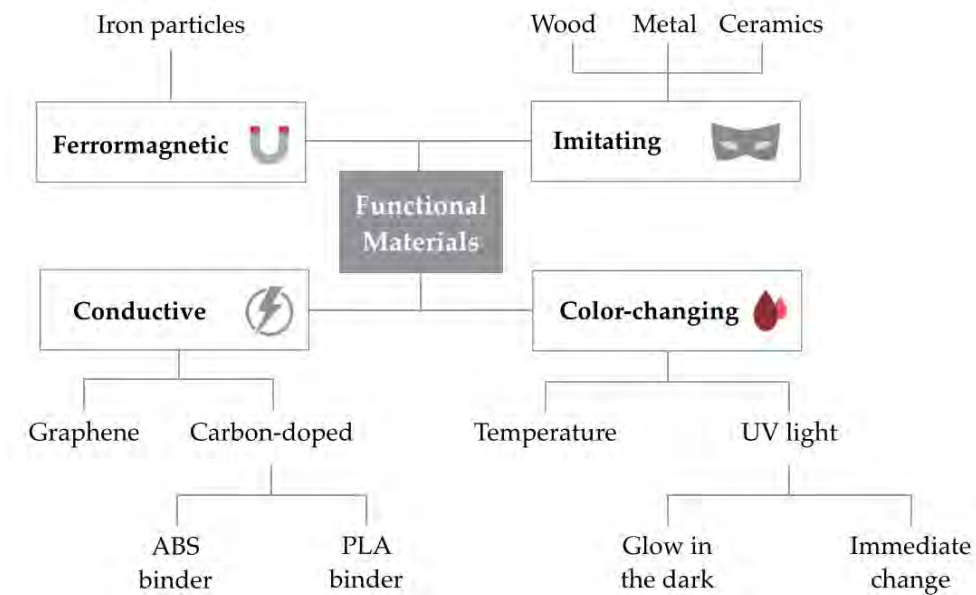
Figure 2.16: A set of commercially-available functional material for FDM.

(1) a temperature change, (2) direct exposure to Ultraviolet light, (3) after exposure to Ultraviolet light, but only in the dark.

IMITATING

Moreover, many filaments aim at imitating existing materials, such as wood, ceramics, or metal by adding the respective material in the form of powder to the matrix material.

FERROMAGNETIC

By adding iron particles as functional reinforcement, plastic filament exists that acts as a ferromagnetic material. That is, magnets attracted the material, but the material itself does not attract other ferromagnetic material.

CONDUCTIVE

Moreover, matrix materials can be functionally reinforced with conductive particles, such as carbon, to produce conductive plastic filament. For instance, they allow novel conductive structures and schematics that cannot be realized with traditional materials.

CONCLUSION FOR THIS THESIS

This thesis contributes approaches that combine different materials to sense interactions. Since sensing often requires electrical components, conductive materials are the most crucial. There is a small set of materials commercially available with different matrix materials and functional reinforcements:

1. **Conductive Graphene PLA**, a composite material consisting of conventional PLA and graphene. Its volume resistivity[3] is approximately $0.6\,\Omega * \mathrm{cm}$. While commercially available, the filament is very expensive, hard to process, and only available in filament diameters that are not compatible with the 3D printers used in this thesis.

2. **Conductive ABS** (cABS), a composite material consisting of ABS and carbon particles. This filament is used in this thesis for CAPRICATE (see Chapter 3) and challenging to print due to the properties of ABS. Its volume resistivity is approximately $900\,\Omega * \mathrm{cm}$.

3. **Conductive PLA** (cPLA), a composite material consisting of PLA and carbon particles. cPLA came onto the market in the course of this thesis. Except for CAPRICATE, cPLA was used in this thesis, as it features a better printability and conductivity than cABS. Its volume resistivity is approximately $15\,\Omega * \mathrm{cm}$.

2.3   3D PRINTING PIPELINE

Several steps need to be performed to 3D print a digital model (see Figure 2.17): A digital model of the object is transformed into a machine-readable list of instructions that are then executed by a 3D printer. After 3D printing, the object is often post-processed.

Modeling
Create a 3D model manually or automatically.

Slicing
Convert the 3D model into printable G-code.

Printing
Execute the printable G-code on a 3D printer.

Finishing
Post-process the printed object with craft tools.

Figure 2.17: Overview of the 3D printing pipeline.

---

3 The **resistivity** is an electrical property of a material and defined as $\rho = R\frac{A}{l}$ where R is conventional electrical resistance, A the cross-sectional area of the material, and l the length of the material. It is often expressed using the unit $\Omega * cm$.

2.3.1 *Modeling*

3D printing of an object requires a **digital model** of its geometry. This model is not necessarily created manually with CAD software but can also be generated by algorithms or via 3D scanning.

POLYGON MESHES

Digital models can be represented in various ways such as point cloud or meshes. This thesis focuses on **polygon meshes**, as the most common formats for 3D printing use this representation or a variant thereof. Therefore, this thesis uses the following definitions:

Definition 3 *A **vertex** is a point in three-dimensional space.*

Definition 4 *An **edge** is a connection between two vertices.*

Definition 5 *A **face** (or triangle) is an ordered and closed set of edges and a normal vector indicating its direction.*

Definition 6 *A **polygon** is a coplanar set of faces. That is, all faces of a polygon are in a single geometric plane.*

Definition 7 *A **mesh** is a set of polygons.*

Definition 8 *In this thesis, a **Dirichlet tessellation** of a set of 3D points is defined as the partition of a mesh such that each vertex is mapped to the point with minimal Euclidean distance.*

ALGORITHMIC CREATION OF A MESH

Meshes can be created using algorithms that output a generalized data representation of a mesh.

One possible data representation often used in the context of 3D printing, is the Standard Tessellation Language or STereoLithography (STL) format. STL is a simple format with an ASCII and binary version. It may contain
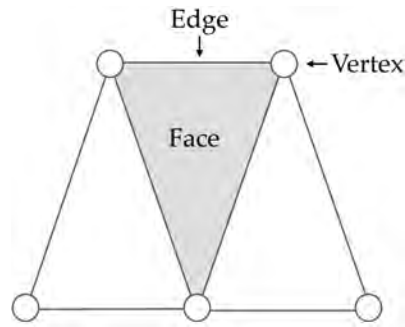
Figure 2.18: An example of a triangle mesh with three faces, five vertices, and seven edges.

any number of solids (Listing 2.1 shows a simple example). A solid may contain any number of faces. Three vertices, ordered by the right-hand rule, and a normal represent each face.

```
solid name
  facet normal  0 0 1
     outer loop
        vertex 0 0 0
        vertex 0 1 0
        vertex 1 0 0
     endloop
  endfacet
endsolid name
```

Listing 2.1: A short STL example with a single triangle face illustrating its syntax.

STL itself does not specify unit information. In the context of 3D printing, the unit is often assumed to be millimeter.

MANUAL MODELING OF A MESH

Since the algorithmic creation of meshes is cumbersome and a considerable effort for large and complex objects, manual modeling supported by software is usually applied for the creation of 3D objects. There are two approaches to model a 3D object manually:

Explicit Modeling. Similar to a 2D drawing tool, objects are created and modified through a series of primitive operations such as add, cut or deform. Designers directly modify the mesh step-by-step. Hence, changes immediately affect the geometry. This approach is comparatively easy-to-use

and suited for the creation of highly individualized, single-copy objects Popular software for this type of modeling are Blender[4] or AutoCAD[5].

Parametric Modeling. A common form of parametric modeling is Constructive Solid Geometry (CSG). It proposes a set of primitive objects, Boolean operators, and geometric transformations. Complex models are constructed by combining multiple primitive objects or the result of a previous operation with an operator. Typical primitive objects are simple geometric shapes, such as cuboids, spheres, cones, or pyramids. Besides geometric transformations (e.g., rotation or translation), three Boolean operators are provided:

1. union (i.e., merging two objects)
2. difference (i.e., subtracting one object from another)
3. intersection (i.e., the combined volume of both objects)

One implementation of CSG is OpenSCAD[6] which provides a scripting language to create models. As illustrated in Listing 2.2, it may, for instance, be used to subtract a primitive cylinder with diameter 10 from a primitive cube of size 15 and translate it in x direction:

```
translate([1,0,0]) {
   difference() {
      cube(size = 15, center=true);
      cylinder(h = 7.5, r = 5);
   }
}
```
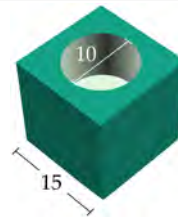

Listing 2.2: A short CSG example of a cylinder that is removed from a cube.

Furthermore, OpenSCAD allows importing and modifying existing meshes and provides means for modules, functions, and variables.

In contrast to explicit modeling, parametric modeling enables users to numerically adjust one or more primitives (e.g., their dimensions) and generate the model again. For instance, the radius of the cylinder (see Listing 2.2) may be changed after the first draft. In parametric modeling, the designer adjusts the textual description of the model accordingly and regenerates the object. However, in explicit modeling, all operations have to be performed again after the initial cube was created. Although this would be quite simple for this example, it is a considerable disadvantage for more complex objects.

---

4 http://blender.org
5 http://autocad.com
6 http://openscad.org

2.3.2 *Slicing*

In the slicing phase, the 3D model is converted into a layered 3D-printable representation. This process is usually performed by software called **slicer**. The slicer cuts the 3D model into distinct layers. The contour of each layer is analyzed and used to plan a travel path for the print head. Depending on the settings, the slicer creates an infill pattern inside the object or support structures for overhanging parts. The latter are manually removed after printing. For multi-material prints, the slicer handles the switching between extruders.

The slicer produces G-code, a machine-readable file format with primitive operations (e.g., move the print head to X or activate the extruder). Listing 2.3 shows a short example of a G-code.

Commonly used slicers are Slic3r, Cura or Simplify3D, each with a different set of features and supported 3D printers.

2.3.3 *Printing*

A 3D printer usually executes the G-code created by the slicer via a serial USB connection, wirelessly, or from an SD card. While in general, 3D printers operate automatically without user intervention, multi-material 3D prints often need supervision and on-demand fine-tuning of properties such as printing speed.

```
G28                              ; move all axes to 0 (X, Y, and Z)

M109 S190 T0                     ; wait until extruder T0 is heated to 190°C
M109 S200 T1                     ; wait until extruder T1 is heated to 200°C

T0                               ; use extruder T0
G90                              ; use absolute positioning for the XYZ axes
G1 X10 Y20 F2400                 ; move to (10,20) at 2400 mm/min
G1 E10 F800                      ; extrude 10mm of filament

T1                               ; use extruder T1
G1 X30 E10 F1800                 ; push 10mm into nozzle while moving to X=30
```

Listing 2.3: A short G-code example illustrating the syntax and most basic commands relevant for multi-material 3D printing.

2.3.4 *Finishing*

3D-printed objects may be post-processed to remove support material or to improve their look and feel. For instance, visible layer lines are often removed via grinding and then painted or sprayed. In the context of interactive objects, post-processing often also concerns connecting wires to the objects.

2.3.5 *Conclusion for this Thesis*

This thesis focuses on the **modeling** and **printing** steps. It explores design concepts, 3D sensor geometries, and practical printing guidelines for multi-material 3D printing. This thesis aims to contribute towards the vision of a (semi-)automatically fabrication of individualized, interactive 3D objects that sense a variety of different input.

2.4 A DESIGN SPACE FOR 3D-PRINTED INTERACTIVE OBJECTS

3D printing of custom-made interactive objects opens up a wide range of new degrees of freedom. This section presents a six-dimensional design space which forms the basis of the 3D-printed interactions explored in this thesis. The design space is illustrated in Figure 2.19.

2.4.1 *Materials*

Multi-material 3D printing (see Section 2.2.2) allows the combination of many materials with different properties in one object. Therefore, this thesis distinguishes between two conceptual types of material:

- The **structure material** is insulating and may be **solid** or **deformable**. It is the shaping material of an object and gives it its appearance.

- The **sensor material** is conductive and may be **solid**, **deformable** or **liquidly**. It is required for various concepts of input sensors.

As discussed in Section 2.2.3 and Section 2.2.4, 3D-printable materials exist that are solid, deformable, and conductive. Throughout this thesis, each chapter explores a different kind of **material composite**, i.e., a unique com-
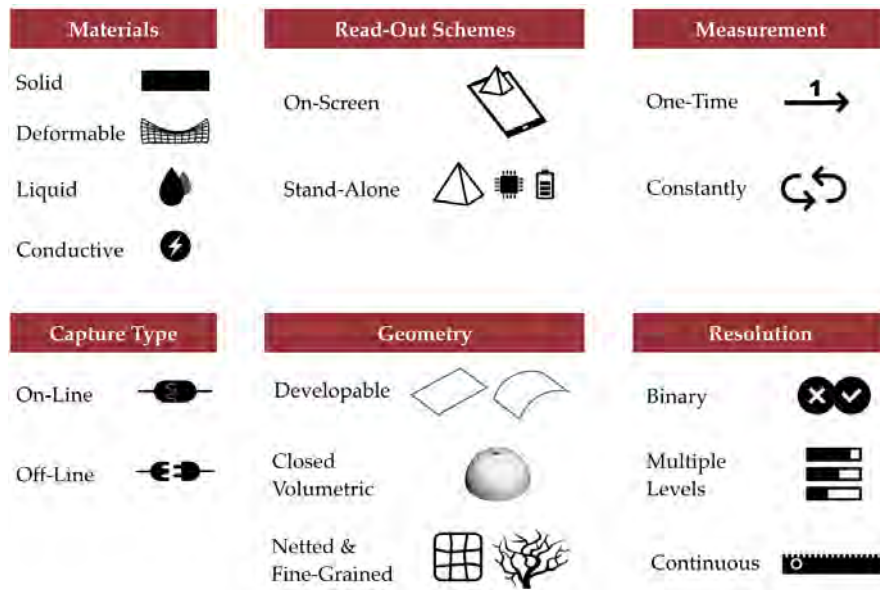
Figure 2.19: A design space for 3D-printed custom-made interactive objects.

bination of structure and sensor materials. A composite may also consist of multiple kinds of structure or sensor material combined in a single object. For instance, an object may consist of both solid and liquidly sensor materials, and a deformable structure material.

2.4.2 *Read-Out Scheme*

Electronics is usually required in order to read-out the interactions performed with an object. This thesis distinguishes between two conceptual schemes to read-out interactions performed with an object:

- The **stand-alone read-out** scheme requires a micro-controller that is physically tethered to the object via an electrical connection. While objects using this read-out may word as a stand-alone device, they also require a micro-controller and a power supply and possibly additional wiring or a wireless data connection.

- The **on-screen read-out** scheme operates together with an interactive surface, such as a smartphone, tablet or wall-sized display. Objects are not electrically connected to the interactive surface (i.e., without a direct conducting path). Instead, the sensing hardware built into the surface couples itself to the object using an electric field.

Both schemes are also illustrated in Figure 1.1. Throughout this thesis, each chapter contributes approaches that operate with one or both schemes. Approaches that support the on-screen read-out schema can usually also be used in the stand-alone read-out schema. However, this does not always apply in the opposite direction without restriction.

2.4.3 *Capture Type*

The aim of sensing is usually real-time processing of measurements. While often practical and useful, it requires a constant power supply. However, there are cases in which it can be beneficial to sense an interaction without power and read it out at a later point in time. Therefore, this thesis distinguishes between two conceptual types of capturing an interaction:

- During **on-line capture**, measurements are directly and constantly processed to detect an interaction.

- During **off-line capture**, a specially designed object detects the interaction without requiring a power supply and memorizes it for later read-out.

The approaches presented in this thesis mainly focus on on-line capture as it allows for real-time interaction with 3D-printed objects. However, Chapter 7 focuses explicitly on off-line capture.

2.4.4 *Geometry*

While 3D printing can create complex geometries, traditional sensing approaches are often limited to standard components of fixed form or flat rectangular shapes. Therefore, this thesis explores how to sense interactions on objects with more complex surface geometries. This thesis distinguishes between the following types of geometries:

- A **developable geometry** consists of objects that are either flat or can be transformed into a 2D plane without distortion (see Definition 1). Cones, cubes, cylinders, or a bent sheet of paper are examples of developable geometries.

- A **closed-volumetric geometry** is an arbitrarily complex, non-developable geometries but with a closed volume. That is, the

surface of the geometry does not contain holes, and its volume allows the creation of internal structures. A sphere is an example of a closed-volumetric geometry.

- In contrast, a **netted or fine-grained geometry** consists of holes or small and thin structures that do not allow the creation of additional internal structures.

This thesis mainly focuses on closed-volumetric geometry, as sensing structures need to be generated inside the volume of an object. However, Chapter 4 also supports netted or fine-grained geometries.

2.4.5   *Measurement*

This thesis distinguishes between the following types of measurement:

- A **one-time measurement** is performed only once.

- A **constant measurement** is performed as long as a sensing system is operational.

While this thesis explores both types of measurements, Chapter 7 focuses explicitly on one-time measurements.

2.4.6   *Resolution*

An interaction may be detected with a different resolution, for instance depending on the sensing principle. Hence, this thesis distinguishes between the following kinds of resolution of an interaction:

- A **binary resolution** can only detect the presence of one specific interaction (e.g., touch vs. no touch).

- A **multi-level resolution** can detect the presence of multiple levels of an interaction (e.g., no pressure, slight pressure, strong pressure).

- A **continuous resolution** can detect an interaction on a continuous scale (e.g., a bending angle).

This thesis proposes a variety of sensing concepts to detect interactions, that each sense with one of kind of resolution.

2.4.7   *Conclusion for this Thesis*

Each of the following chapters contributes an instance of the design space that can be used to detect a variety of interactions. That is, the approaches and concepts proposed in the following chapters each provide different resolution, allow for one-time or constant measurement, operate on varying complex geometries, and capture the interaction either directly on-line or off-line at a later stage.

Regarding 3D printing, each chapter investigates a different composition of materials: Based on an exploration of solid and conductive composites in Chapter 3, Chapter 4 adds deformable materials to the composite. Chapter 5 continues to investigate the composition of deformable and conductive materials. Based on Chapter 6 that adds liquid to previously explored solid and conductive composites, Chapter 7 explores the combination of solid, deformable, conductive, and liquid materials.

Subsequently, Chapter 8 wraps up and integrates the contributions concerning the design space.

Part II

ENABLING TOUCH INTERACTION

CAPRICATE: 3D-PRINTED MULTI-TOUCH SENSING

The last chapter discussed approaches to create interactive objects and analyzed how digital fabrication technologies (e.g., 3D printing) transform this process so that users can customize not only the shape and appearance of an object but also its response to external stimuli, such as **touching** an object. Moreover, the last chapter identified shortcomings in existing sensing approaches, that are often restricted to developable surfaces[1] of rectangular shape (cf. [Olb+13; Gon+14; DKA14]), require to instrumentalize the environment with sensors (cf. [Wil10; HBW11]) or need additional assembly steps (cf. [SCH13; Hoo+14]). As most real-world objects (e.g., office equipment or appliances) are non-developable, providing the means to embed touch sensing capabilities into such surfaces is a vital research question. Therefore, this chapter contributes CAPRICATE, a fabrication pipeline to rapidly design and 3D print interactive objects with embedded capacitive multi-touch sensors.

The remainder of this chapter is structured as follows. Section 3.1 discusses related work. Section 3.2 introduces the **fabrication and sensing approach** underlying CAPRICATE. Section 3.3 then details on the **design** of touch-sensitive areas on 3D objects that can have custom 3D shape, size, and orientation. Following this, Section 3.4 presents two **touch sensing techniques** that automatically generate touch buttons and grids in such areas and operate on developable and non-developable surfaces. Section 3.5 then details on the **3D printing process** for touchsensitive objects in a single print pass using commodity multi-material 3D printers and on the sensing using either standard capacitive touch sensing controllers (e.g., an Arduino) or capacitive multi-touch surfaces (e.g., a tablet). Section 3.6 presents a set of example applications. Section 3.7 reports on a technical evaluation regarding the possible accuracy depending on various surface geometries and reports on empirical observations regarding multi-material 3D printing with carbon-based conductive materials and derives practical guidelines. To conclude, Section 3.8 discusses the limitations of CAPRICATE.

---

1 That is, a surface that can be transformed into a plane without distortion (see Definition 1).

Contribution Statement: This chapter is based on [Sch+15a]. I led the conceptual design, the 3D printing, the implementation, and the evaluation. The master student Matthias Balwierz modeled, printed and implemented the algorithms and example applications under my supervision. The master student Stefan Just implemented the design tool. The student assistant Jalal Khademi implemented the smart glass example application. The student assistant Andreas Leister supported the 3D printing. My supervisors Jürgen Steimle and Max Mühlhäuser advised me on the conceptual design and contributed to writing the paper.

3.1 RELATED WORK

The following section shortly presents relevant research in the context of printed capacitive touch sensing and compares them to CAPRICATE. Section 2.1.3 discusses the majority of related work.

3.1.1 *Fabricating Custom Capacitive Sensors*

Midas [SZH12] contributes a digital design approach based on a vinyl cutter and conductive sheets. Other approaches utilize inkjet-printing [Kaw+13; Olb+13; Gon+14], hydro-printing [GS18], screen-printing [WTM16], or laser-patterning [Wei+15] to fabricate thin and deformable capacitive touch sensors of custom 2D shape that can be embedded into or wrapped around objects to cover a 3D surface. While widely used and practical, they require additional assembly effort, are only applicable for developable surfaces without distortion of the sensing structures.

Also, researchers propose different techniques that integrate electrical components directly into 3D-printed objects through conductive wires [Esp+14], silicone [PML07], sprays [Sar+12], inks [Ahm13], or threads [Hud14]. Lopes et al. suggest a hybrid approach that combines 3D printing with electronic components [LMW12]. However, they do not discuss capacitive touch sensing. Research in material science demonstrates the feasibility of capacitive sensing with low-conductive 3D-printed conductors [Lei+12; She+13]. Their proof-of-concept prototypes use all-flat and manually designed touch electrodes for sensing of simple touch buttons (one point of contact). CAPRICATE allows realizing touch grids (multiple points of contact) on non-developable surfaces.

3.2 FABRICATION AND SENSING APPROACH

This section introduces the sensing principle that underlies CAPRICATE and presents the overall fabrication approach.

As depicted in Figure 3.1, users obtain a 3D-printable object (1) via a standard 3D modeling environment, (2) by 3D scanning, or (3) by downloading a model from the Internet. Touch-sensitive areas are then added to an
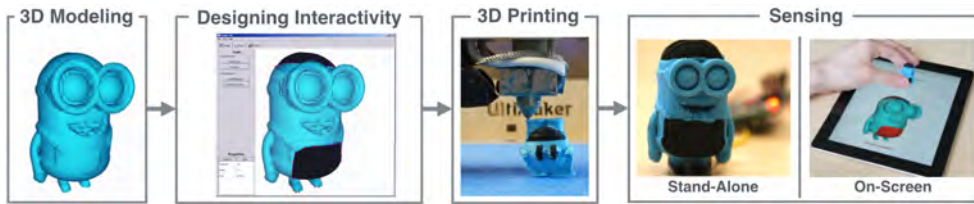
Figure 3.1: Fabrication Pipeline in CAPRICATE.

object using an easy-to-use graphical design tool. After export, objects are printed in a single pass and are then either tethered to a microcontroller or coupled with a touchscreen. To sense multiple touches, CAPRICATE supports capacitive sensing in the read-out schemes **stand-alone** or **on-screen** (see Section 2.4.2).

3.3 DESIGN

While the emergence of digital fabrication technologies allows users to **print** custom 3D objects rapidly, the **design** of touch electrodes is still a tedious task and often requires expert knowledge in CAD. Although advances in 3D scanning mitigate this to some extent, the problem persists when designing touch electrodes that should be well-integrated in the model. For instance, custom-shaped areas on a 3D surface need to be selected, extruded and fused manually with the original model. Also, when designing complex touch grids, a multitude of touch electrodes need to be designed and wired by hand and possibly have to be mapped onto a non-developable surface. Adding capacitive touch sensing to such surfaces is one of the main challenges addressed in CAPRICATE.

To mitigate these difficulties, CAPRICATE provides a design tool that allows users to intuitively (1) **create** custom-shaped touch sensors on complex 3D surfaces, (2) automatically **wire** these to pre-designed or custom-shaped endpoints, and (3) **generate** fabrication files to 3D print the object. Figure 3.2 illustrates this process.

3.3.1 *Designing Touch Sensors*

After a user loads a 3D-printable model into the design tool, a conventional 3D view, that can be navigated as such (i.e., zooming or rotating the 3D
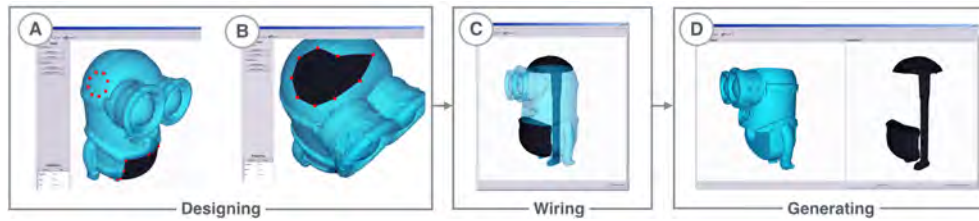
Figure 3.2: Designing with CAPRICATE: A user (a) chooses a sensor type, selects an approximate location on the surface, and (b) fine-tunes the selection. The tool (c) automatically wires the sensors to endpoints, and (d) generates the files for 3D printing.

model using the mouse), displays the model. By selecting the respective item in a sidebar, users are then able to either create touch-sensitive electrodes or endpoints.

ADDING TOUCH-SENSITIVE ELECTRODES

Users can design custom-shaped touch areas on any part of the 3D model by using a two-step interaction technique:

1. To create a touch-sensitive area, users select the general type of touch element (e.g., a touch button or grid) that should be created via a tool-bar. Then, they indicate the rough location and the approximate size of the sensor on the 3D surface. The tool supports the users via a 3D visu-alization that closely follows the 3D surface as the mouse cursor hovers over a part of the object (see Figure 3.2A). This visualization indicates the possible placement of the sensor. The size of the selection can be adjusted using the mouse wheel. By clicking, the user applies the touch sensor to the desired location, but its shape remains customizable.

2. Similar to adjusting free-form paths in 2D drawing applications, the user can fine-tune the shape and size of the initial selection by drag-ging existing edge points or by adding new edge points between two lines (see Figure 3.2B). In the case of a touch sensor grid, the user can freely define the number of electrodes it shall contain. The model au-tomatically reflects each change of the selection.

ADDING ENDPOINTS

To allow users to define a target area for automatic routing, users can cre-ate and place custom- or pre-defined endpoints using the design tool. Users

can place and customize endpoints using the same two-step interaction technique as described for the creation of touch-sensitive areas. Alternatively, the design tool allows creating and placing standard connector formats (e.g., banana connectors).

3.3.2 *Wiring Electrodes*

After users have finalized their custom touch sensors, the design tool supports to automatically connect electrodes and endpoints without the need for schematics or any further user input (see Figure 3.2C).

3.3.3 *Generating 3D-Printable Models*

Multi-material printing requires distinct 3D models per material that do not overlap each other. As a result, objects in the fabrication pipeline consist of 3D models for conductive and insulating parts (see Figure 3.2D). The design tool supports to export both 3D models into a 3D-printable file format after wiring.

Moreover, a machine-readable description is generated to ease the mapping of a stand-alone or on-screen touch event to the respective 3D touch electrode. To that end, electrodes are named according to the user-defined settings to ease mapping of touch events in an interactive program.

3.4   TOUCH GRIDS ON NON-DEVELOPABLE SURFACES

Capacitive touch grids on developable surfaces (e.g., a cube or cylinder) can be effectively implemented with standard rectangular lattices [SZH12; Kaw+13; Olb+13; Gon+14]. However, rectangular lattices produce significant distortions when mapped on non-developable surfaces, resulting in non-uniformly distributed touch points [BPH13]. Although promising topologies for spherical surfaces have been proposed [BPH13], touch sensing on more complex non-developable surfaces remains a challenge.

CAPRICATE addresses this challenge by contributing two techniques for touch sensing grids on custom-shaped areas of developable and especially non-developable surfaces. The first technique consists of **curved surface touch**

Figure 3.3: Cross-section of the Himalaya mountains model showing touch sensing with (a) curved electrodes on the surface, and (b) flat electrodes in the subsurface (black parts are touch-sensitive).

electrodes, which closely follow the curvature (see Figure 3.3A). To significantly speed up the fabrication process, the second technique utilizes **flat subsurface touch electrodes** and an automatic sensor calibration to account for the variance in the overlying non-conductive material (see Figure 3.3B).

3.4.1 *Curved Surface Touch Grids*

Electrodes follow the exact geometry of a non-developable surface of an object with this technique (see Figure 3.3A). In order to achieve reliable capacitive touch sensing with the same resolution within a touch-sensitive area, touch electrodes need to be evenly distributed on the selected area.

This technique addresses this primary challenge in two steps: First, touch points are **uniformly distributed** in the selected area using a graph optimization mechanism. Second, **touch electrodes are generated** directly on the surface of the object, using a region growing approach, forming a touch grid consisting of multiple touch electrodes.

RELAX ALGORITHM: UNIFORM TOUCH POINT DISTRIBUTION

While rectangular and Fibonacci lattices can be used for developable and spherical surfaces [BPH13], it is challenging to uniformly distribute touch points on (1) custom-shaped areas of non-developable surfaces (see Figure 3.4), as they are arbitrarily curved, defying a deterministic optimization.

Therefore, this chapter proposes an iterative graph optimization, called relax algorithm, to create touch grids with *n* uniformly distributed touch points on a closed custom-shaped 3D surface selection. That is, the objective of the optimization is an increasing uniformity of the touch points' distribution within the selected surface.
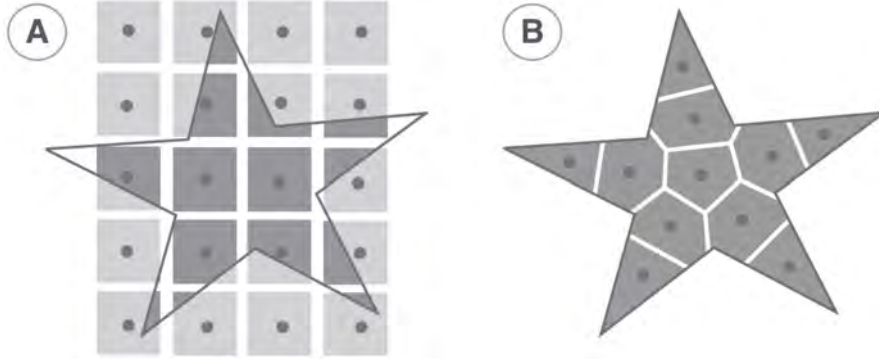
Figure 3.4: Comparing the distribution of touch points (gray circles) on a custom
            shape in 2D: (a) a standard touch grid, (b) a curved surface touch grid
            proposed by CAPRICATE.

The concept of the relax algorithm for the simplified one-dimensional case
is the following: On an axis, n points are randomly distributed. To yield
a uniform distribution (i.e., the axis is covered with points equidistantly)
each point should be iteratively moved slightly towards the neighbor far-
thest away until the points' positions converge. In the following, these slight
movements are called **repulsion**.

For the one-dimensional case, there are at most two neighbors per point,
and the distance between them is easily computed. However, for the three-
dimensional case, the number of neighbors increases and at the same time
distance measurements are ambiguous and tend to be complex to compute
along heavily curved surfaces. In order to avoid calculating the neighbor-
hood for each point, each point is repulsed by every other point. The sum
of distance reciprocals is used to ease distance measurements on the 3D sur-
face. To that end, a repulsion force f_r is evaluated iteratively for each point
v, called vertex in the following, and the set of all neighboring vertices W by
summing up all distance reciprocals:

$$f_r(\vec{v}) = \sum_{\vec{v} \neq \vec{w}_i, \vec{w}_i \in W} \frac{1}{|\vec{v} - \vec{w}_i| + c}$$

where c is a constant to avoid division by zero. To enforce an even distribu-
tion inside the shape instead of at the edges, W also contains virtual vertices
at the edges of the custom shape.

In the context of the relax algorithm, the 3D mesh is considered a graph con-
sisting of vertices and edges. Each touch point is occupying a single vertex.
Per iteration, a point may only be moved one edge to the next vertex.

After randomly distributing n points inside the 3D surface selection, the relax algorithm executes the following iterative steps:

1. Dijkstra-based region growing is performed to compute the distance field for each point $v \in W$.

2. The repulsion force f_r is evaluated iteratively for each point v.

3. Each point is moved one edge towards the adjacent vertex with the lowest repulsion.

Algorithm 1 illustrates the pseudocode. The complexity of the relax algorithm is $O(n^3)$ because the distances $|\vec{v} - \vec{w}_i|$ in the repulsion force are computed in every iteration for each point.

---

procedure RELAX(n, M, s)
    $T \leftarrow$ randomly distribute n touch points on mesh M
    for s steps **do**
        for $t \in T$ **do**
            $v \leftarrow$ corresponding vertex of t in mesh M
            $N \leftarrow$ neighbors of v in mesh M
            $D \leftarrow$ distance field of v to N
            $F_r \leftarrow f_r(v, d)$ for all neighbors in D
            move t to vertex with minimal f_r
        end for
    end for
    return T
end procedure

Algorithm 1: The relax algorithm evenly distributes n touch points on a custom-shaped area of a mesh M. It returns an evenly distributed set of touch points T on the mesh.

TOUCH ELECTRODE GENERATION

Based on the uniformly distributed touch points, n electrodes are generated using a Dijkstra-based region growing approach, which results in a Dirichlet tessellation (see Definition 8) of the surface as described in Algorithm 2. Since faces, where vertices belong to different electrodes, are not assigned to a touch electrode, they form a gap in-between and thus avoid accidental interconnections.

---

procedure ELECTRODEGENERATION(T, M)

    $A \leftarrow$ map of a single $t \in T$ to a set of faces $f \in$ mesh M

    for face $f \in M$ **do**

        if all verticies of f are nearest to a single $t \in T$ **then**

            $A[t] \leftarrow$ add face f

        end if

    end for

    return A

end procedure

Algorithm 2: The electrode generation algorithm partitions a mesh M such that each face is assigned to the touch point of the set T with minimal euclidian distance. It returns a mapping A of each touch point to a set of faces.

After generation, the electrodes, i.e., sets of faces, are extruded along the normal directions and can, optionally, be submerged under the surface. In order to maintain a 3D-printable model, the 3D model of the object needs to be adjusted. That is, the volume occupied by the computed electrodes is removed using boolean subtraction. Figure 3.5 depicts example objects with non-developable surfaces.

3.4.2 *Flat Subsurface Touch Grids*

Instead of printing surface touch grids, a second touch sensing technique consists of printing flat touch electrodes, which sense touch through the overlying non-conductive material (see Figure 3.3B). While the touch electrodes are flat, the overlying geometry can be non-developable. This technique can significantly speed up the fabrication process due to less switching between materials because switching is time-consuming. In contrast to the previous technique, which may span many printing layers, flat electrodes can be printed on just a few layers, although they may be slanted.

Capacitive sensing is capable of capturing touch through non-conductive materials. However, sensor readings are affected by the **overlay thickness**, i.e., the distance between a finger and a touch electrode. As the overlay thickness might be different for each touch electrode, it is essential to separately calibrate each one to be able to classify touch precisely. Given the significant differences in overlay thickness, using the same threshold for all electrodes would be unreliable.

This section addresses this challenge by an auto-calibration technique which calibrates each touch electrode independently. It does not require any manual interaction, as it makes use of the geometric information available in the 3D model. For each touch electrode, the average thickness t_{avg} of material that overlays it in normal direction can be calculated from the 3D model (for varying overlay thicknesses above one touch electrode, the average gives a good approximation even if a finger would approach it inclined). Moreover, a **material function** is defined as:

$$f(t) = \Delta C = |C_{touch} - C_{noTouch}|$$

It relates a change in capacitance ΔC to different overlay thicknesses t. An approximation of this function can predict a specific capacitive change for each overlay thickness computed from the 3D model. Using ΔC the specific threshold thr for a touch electrode can be computed as a percentage of the capacitance change to expect. The function needs to be empirically measured for varying overlay materials. For example, for 90% the threshold would be set to $thr = 0.9 \cdot \Delta C = 0.9 \cdot f(t_{avg})$. The technique weighs the ΔC from an activated electrode and all adjacent electrodes by thickness to interpolate the x-y-position and then compute the z-position from the 3D model.

By using the results for commonly used PLA (see Section 3.7), a non-linear least squares model and the capacitance formula $C = \epsilon_r \epsilon_0 \frac{A}{t}$, an approximation of the material function $f_{PLA}(t) = a \cdot t^b$ with a = 0.80096 ($\sigma = 0.04231$) and b = -0.64139 ($\sigma = 0.0456$) with a residual standard error of 0.0753 (df = 4) is computed.

The auto-calibration resolves false-positive cases where an electrode is activated that is not directly below the finger. In contrast to a simple binary threshold, the technique uses the continuous values from an electrode and its neighboring electrodes (regardless of whether their threshold is met) to first interpolate the x-y-position and then compute the z-position from the 3D model. The x-y-position is calculated by weighting the delta per neighbor since the influence of the overlay thickness on capacitance is known.

3.4.3 *Automatic Routing of Wires*

In order to connect touch sensors and endpoint with wires, a dynamic routing approach based on A* [HNR68] is used (as in [Sav+14]). It operates on a

---

procedure PATHFINDING(*G*, *E*, *P*)
    for electrode $e \in E$ **do**
        endpoint $p \leftarrow$ get and remove one element from *P*
        $p \leftarrow$ shortest path from *e* to *p* in graph *G*
        $R \leftarrow$ add path *p* to routes
        $G \leftarrow$ graph *G* without path *p*
    end for
    return *R*
end procedure

Algorithm 3: The path finding algorithm routes wires between a set of electrodes *E* to a set of endpoints *P* on a graph *G* that is based on a voxelized 3D model. It returns a set of routes *R*.

graph consisting of a regularly-spaced volumetric 3D grid created inside the 3D model.

VOXELIZING

Voxelizing a polygon mesh into a volumetric grid is a common problem in computer graphics (cf. [Hua+98]). First, a bounding box is created that covers the whole 3D model. Then, the bounding box is subdivided into a regularly-spaced grid of voxels. To check, whether a voxel is inside or outside of the 3D model, a particle system is used that emits particles on each 3D grid point inside of the 3D model. GPU acceleration or parallelization may further improve the performance of this process.

PATHFINDING

Pathfinding requires knowledge about the neighborhood of each voxel. As such, the voxelized 3D model needs to be transformed into a traversable graph structure. A node represents a voxel. An edge connects two nodes whose voxels are neighbors. The pathfinding ignores all voxels at the surface of an object.

Based on this graph structure, the pathfinding employs common shortest path algorithms, such as A* [HNR68], to route wires for all sensors. Algorithm 3 describes the steps performed for pathfinding.

IMPORTANT FACTORS

The following factors may be modified to adjust the properties of the algorithm:

Wire Thickness. Depending on the printing properties, the size of the 3D-printed object, and the electrical properties of the sensing mode, the wire thickness may be adjusted.

Step Size. As described, the routing employs a volumetric grid created in the 3D model. As such, the step size defines the volume of each voxel. Decreasing the step size increases the precision and resolution of wires. However, at the cost of increased computation time and aliasing artifacts, possibly preventing the algorithm to find suitable routes.

3.5 IMPLEMENTATION

Multi-material 3D printing with carbon-based materials implies practical challenges that stem from using multiple materials in a single print pass. To successfully 3D print objects with integrated conductive parts, this section describes the reference apparatus used for the evaluation of CAPRICATE and proposes several practical guidelines for multi-material 3D printing. They are applicable for any 3D printer using FDM and are implemented by injecting custom G-Code into existing slicing routines.

3.5.1 *Sensing*

The reference apparatus used to evaluate CAPRICATE is as follows: The controller board consists of an Arduino Micro (tethered to a PC) and an MPR121 capacitive sensor (12 sensing pins at a frame rate of 29 Hz). The sensing pins and the printed object were connected with crocodile clips or banana connectors. CAPRICATE uses either WebSockets or direct touch input to send touch events to an application. The controller could be easily scaled down by using a smaller Arduino or a custom-designed board. The connection could be made wireless, such that the controller could be directly integrated into an object. The number of sensing pins could be increased by using multiplexers.

3.5.2   *Fabrication*

CAPRICATE requires a multi-material 3D printer and a conductive material. It was evaluated using an Ultimaker Original 3D printer with Dual Extrusion Kit (ca. $1500) and a commercially available conductive ABS material (cABS) with 5-8% carbon by Torwell Technologies (approx. 44 €/kg), which has an average resistivity of $8\,\Omega * mm$. The optimal extrusion temperature for the apparatus was 230 °C (nozzle diameter 0.8 mm) with the cooling fan turned off.

GUIDELINES FOR MULTI-MATERIAL PRINTING

Residuals. In order to prevent residuals at the time of switching materials, the previously used material should be retracted by 1 mm. While the print head moves more than 1 cm without extruding, lift the z-axis by 1 mm and lower it before continuing extrusion.

Since carbon particles reduce the viscosity of the ABS material, the likelihood that the nozzle gets clogged is considerably increased. Clogging may occur as soon as the extruder has been inactive for about a few minutes and often results in failed prints.

Clogging. In order to prevent clogging, the previously used extruder should be cooled down to the non-flowing state (to 150 °C for conductive and 100 °C for non-conductive material). Then, extrude the next material on a garbage stack located at the printing origin (10 mm for conductive and 6 mm for non-conductive). This procedure prevented the nozzle from clogging for the reference apparatus independent of the time the extruder remained unused. This modification takes 40 seconds per material switch and costs less than 1 cent of material.

Disconnected Wires. In order to prevent disconnection in wires, a wire diameter should be used that is a multiple of the nozzle diameter (at least 4 x 0.8 mm for the reference apparatus). Therefore, the maximum density of wires is for the reference apparatus four wires per cm^2 (with 3 mm wire spacing). It also defines the maximum density of touch electrodes.

3.6 EXAMPLE APPLICATIONS

In order to show the practical applicability of CAPRICATE, this section presents example applications in three contexts: rapid prototyping of physical input, wearable computing, and tangible user interfaces.

3.6.1 Rapid Prototyping of Physical Input Devices

Several physical input devices were printed using CAPRICATE (see Figure 3.5A):

- First, a **hemispherical input device** with which users may navigate in a hierarchy by rotating fingers around the hemisphere and select an item by pressing the touch area on top.

- Second, printed mechanical structures to sense **physical manipulations**. The push-button includes a spring mechanism such that pushing of the button is capacitively sensed using a touch electrode connected to the controller and a forwarding electrode without any connection. The design principle of the physical slider consists of a series of rectangular-shaped touch electrodes that are linearly arranged and a conductive sliding knob. Both designs can distinguish between touching and physically manipulating.

- Third, an on-screen **directional pad**. Untethered touch electrodes are printed on its four ends. These forward a touch onto a capacitive surface when pressed by a user.

3.6.2 Wearable Computing Devices

With CAPRICATE users can rapidly design and 3D print **highly individualized** wearables (e.g., an interactive ring or wristband) or accessories for existing wearable devices (e.g., a touch-sensitive frame for Google Glass with more touch sensing possibilities). As proof of concept, CAPRICATE was used to print a bracelet that features an embedded non-developable slider and an interactive glasses frame that can recognize touch-gestures on its front and left side (see Figure 3.5B).
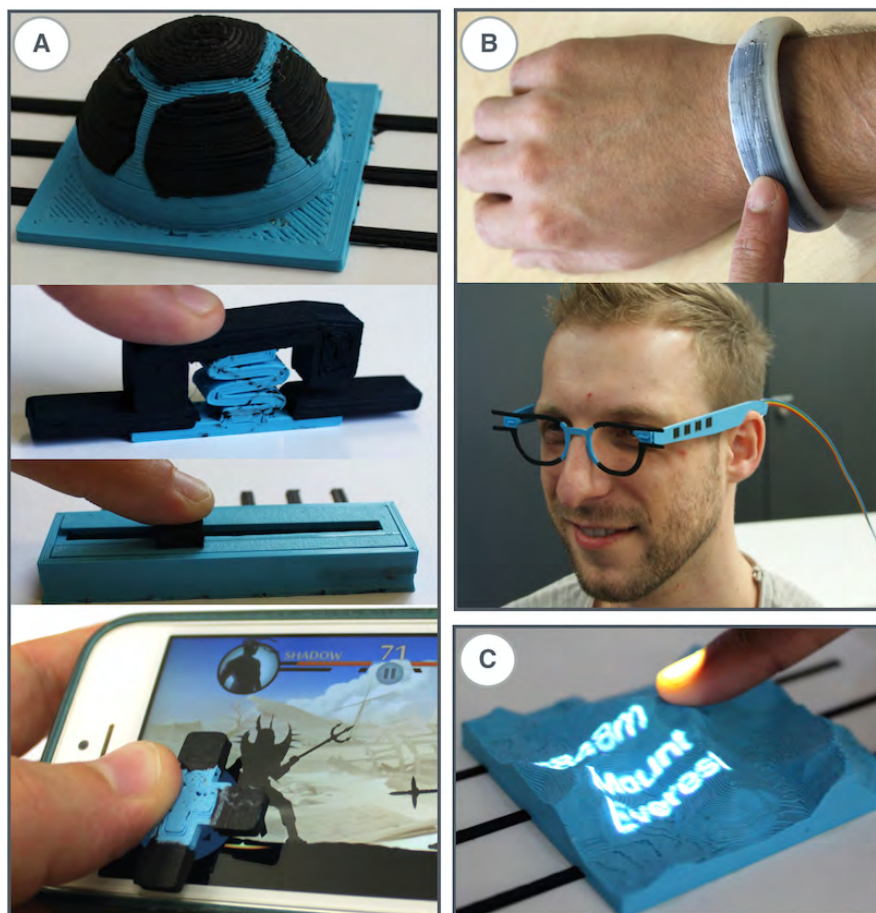
Figure 3.5: A series of example objects for (a) physical input prototyping, (b) wearable computing, and (c) tangible user interfaces.

3.6.3 *Printed Tangible User Interfaces*

Designers of tangible user interfaces may use CAPRICATE to create tangible controls that represent a specific form and also have interactive behavior (cf. [Gün+17]). For example, CAPRICATE was used to fabricate an interactive model of the Himalayas mountains with six embedded touch electrodes to facilitate the exploration of related information (see Figure 3.5C). Names and heights of the Himalayas mountains are top-projected when the user is touching on the respective location on the object. This application can be extended to distinguish touch on toy characters (see Figure 3.1), separate letters, number, icons, or Braille, thus allowing for haptic alphanumeric or iconic mapping to digital information.

This section evaluates the performance of 3D-printed touch sensors concerning their conductivity and dimension. Moreover, it examines the effect of differently thick overlays.

3.7.1 *Conductivity Depending on Printing Direction*

As the conductivity of the material influences the performance of capacitive sensing, this section evaluates the resistivity ρ of a conductor printed with cABS, which depends on several factors: the fill density, the printing pattern, and the direction of electrical flow. As the objective was maximal conductivity, only 100% infill density was used. The analysis revealed significant differences in resistivity ($t(12) = 5.927$, $p < .001$, 14 samples at size $100 \times 12 \times 1$ mm^3) depending on whether the printing pattern consists of horizontal traces that are aligned (ρ_{avg} = 4.382 $\Omega * $ mm, $\sigma = 1.285$) or perpendicular (ρ_{avg} = 8.171 $\Omega * $ mm, $\sigma = 0.658$) to the direction of electrical flow. In the vertical direction, the average resistivity was ρ_{avg} = 9.976 $\Omega * $ mm ($\sigma = 1.729$). The measurements show that the resistivity highly depends on the direction of electrical flow. Thus, conductive traces should be printed alongside the direction of electrical flow and adapt slicing algorithms accordingly.

3.7.2 *Dimensions of Touch Electrodes*

In order to examine the performance of capacitive sensing with cABS, this section compares different touch electrode dimensions with varying resistances of the connecting traces. To that end, the changes in capacitance (i.e., touched or not touched by a finger) were measured for varying electrode sizes (Ø = 5, 10, 15, 20 mm) and increasing resistors (with resistances of 20 to 120 kΩ, 10 kΩ intervals). The measurements show that the wire resistance should not exceed 30 kΩ. Otherwise, the signal-to-noise ratio (SNR) drops below 5:1, jeopardizing robust touch sensing.

Moreover, a minimum thickness of 0.2 mm for touch electrodes is required to measure a capacitance change reliably. The nozzle diameter (here 0.8 mm) defines the minimal touch electrode width and length. For most minimal traces with the size of a single nozzle diameter (0.8 mm, 0.2 mm layer height)

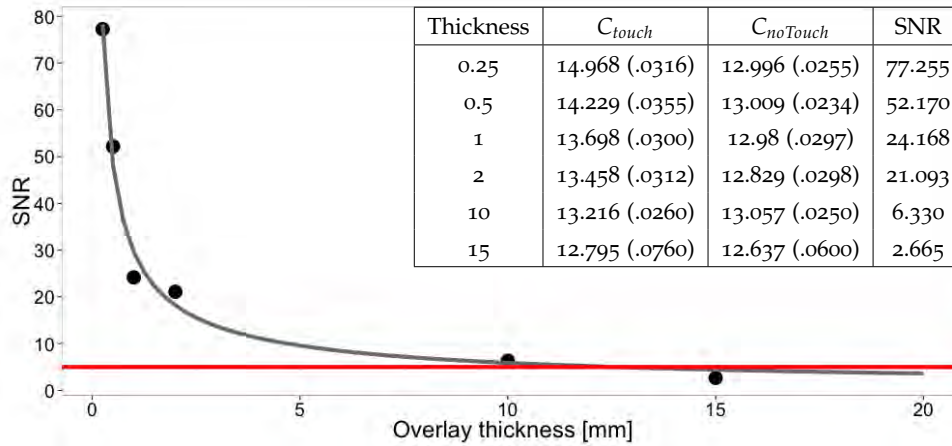| Thickness	C_{touch}	$C_{noTouch}$	SNR
0.25	14.968 (.0316)	12.996 (.0255)	77.255
0.5	14.229 (.0355)	13.009 (.0234)	52.170
1	13.698 (.0300)	12.98 (.0297)	24.168
2	13.458 (.0312)	12.829 (.0298)	21.093
10	13.216 (.0260)	13.057 (.0250)	6.330
15	12.795 (.0760)	12.637 (.0600)	2.665

Figure 3.6: Comparison of touch and no touch of a finger for varying overlay thicknesses of PLA. The red line marks a minimum SNR of five. The table shows the measured mean values with standard deviations.

a capacitance change up to 10 cm could be reliably sensed. The touch electrodes may be printed on the outermost layer or embedded inside the surface, allowing completely disguised touch sensing under any colorized material. In order to hide touch electrodes, the overlay should have at least the height of one printing layer (here 0.2 mm).

3.7.3   *Overlay Thickness*

To implement and test the flat subsurface touch electrodes technique, the effect of PLA overlays for different thicknesses onto sensing performance was evaluated by measuring capacitance in a 2-second interval either with or without touching (for circular electrodes of fingertip-size with Ø = 15 mm). The results show that for cABS the maximum overlay thickness is 10 mm. Figure 3.6 illustrates that the thickness greatly influences the sensing performance regarding the SNR. For 10 mm, the difference in capacitance is still robustly measurable with an SNR of 6.33 as shown by a t-test (t(3968.786) = 194.799, p < 0.001). For thicker overlays, the SNR falls below a minimum SNR of 5:1, which is generally considered as the lower bound for robust touch detection. Therefore, flat subsurface touch electrodes can be placed at most 10 mm underneath the outermost point on the surface. Further, the maximum height difference (along with the surface normal of the touch electrodes) between any two points on the surface cannot exceed 10 mm. If these requirements cannot be met, the sensor should be implemented using the curved surface touch electrodes technique.

3.8   DISCUSSION AND LIMITATIONS

CAPRICATE allows 3D printing of touch sensors. However, there are currently several limitations.

3.8.1   *Geometries*

While applicable for many non-developable surfaces, geometries consisting of small structures (<1 mm), high curvatures, or holes remain challenging.

3.8.2   *Resolution*

First, the number and density of touch electrodes in the example applications are rather low, particularly in touch grids. This limitation stems from the rather low resolution of the printer and the nozzle diameter. Future printers and materials that can be extruded with smaller nozzles are likely to alleviate this issue in the future.

Second, touch electrodes are currently distributed uniformly across the surface. While adequate for most cases, this may be inefficient for steep geometries. Future work should investigate adaptive layouts (e.g., adapt to local surface curvature).

Third, the number of input pins on the controller board is currently limited. A custom-designed board, multiplexers, or mutual capacitance controller boards can increase this number.

3.8.3   *Hovering*

Due to the high resistivity of cABS, the detection of other capacitive sensing modalities besides touch is very challenging. While hovering was successfully detected within small distances above the surface (<10 mm) of a fingertip-sized electrode (ø= 15mm), further distances cannot be reliably captured.

3.9   CONCLUSION

This chapter presented CAPRICATE, a fabrication pipeline to design and print capacitive touch sensors embedded in 3D-printed objects. In summary, the main contributions of this chapter are:

1. A consumer-level fabrication pipeline for 3D-printed touch-sensitive objects using commercially available printers and materials.

2. Two techniques for fabricating capacitive touch buttons and grids on developable and especially non-developable surfaces.

3. Practical guidelines for multi-material 3D printing with carbon-based conductive materials.

4. Example applications and technical experiments showing the accuracy and applicability.

CAPRICATE enables users to fabricate solid-conductive material composites using an easy-to-use design tool. As illustrated in Figure 3.7, objects created with CAPRICATE constantly measure binary touch and multi-level hover input on developable and non-developable, closed-volumetric geometries. This approach and its prototypical implementation open up a wide range of applications that use touch-sensitive objects either on capacitive touchscreens
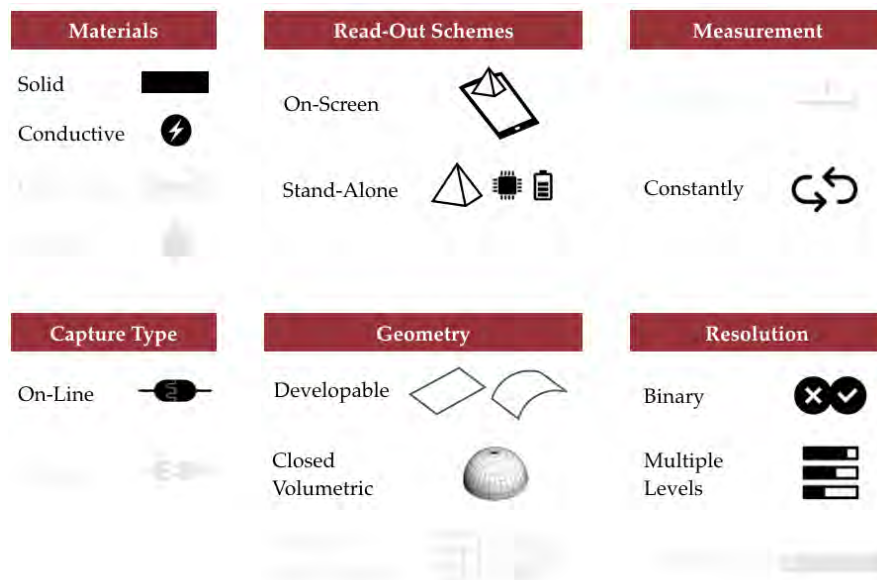

Figure 3.7: The classification of CAPRICATE regarding the design space of 3D-printed interaction.

or as stand-alone devices. However, netted and fine-grained geometries remain challenging. Therefore, the next chapter extends the capacitive sensing approach to support such structures and also to detect pressure input.

Part III

ADDING DEFORMATION INTERACTION

TRILATERATE: 3D-PRINTED HOVER, TOUCH, AND PRESSURE SENSING

The previous chapter introduced Capricate, a multi-material fabrication pipeline to create non-developable objects with embedded capacitive multi-touch sensing. While Capricate contributes 3D printing of complex touch sensors, it does not consider the pressure applied while touching as an additional input dimension. Therefore, this chapter contributes Trilaterate: a fabrication pipeline to create custom 3D-printed objects that recognize a continuous position of a finger hovering above, touching on or pressing inside them. Trilaterate does not require a distinct sensor for each interactive area but instead covers the whole surface and surrounding of the object by combining multiple capacitive measurements using trilateration.

The remainder of this chapter is structured as follows. Section 4.1 discusses related work. Section 4.2 introduces the sensing principle and fabrication pipeline. On this basis, Section 4.3 presents an algorithm to place and wire sensors inside the object, followed by the general printing setup and guidelines in Section 4.4. Following this, Section 4.5 describes how to compute a position estimate by combining multiple sensors. Then, Section 4.6 presents interactive example applications. Finally, Section 4.7 reports on the technical evaluation of Trilaterate and Section 4.8 discusses its limitations.

Contribution Statement: This chapter is based on [Sch+19]. I led the conceptual design, the 3D printing, the implementation, and the evaluation. The student assistant Andre Pfeifer, and the master students Martin Stitz and Carsten Englert were involved in modeling and 3D printing. The latter two have implemented the algorithms and the object generator application under my supervision. My supervisor Max Mühlhäuser advised me on the conceptual design and on writing the paper.

4.1   RELATED WORK ON PROXIMITY AND DEFORMATION INPUT

The following section shortly presents relevant research in the context of proximity and deformation input and discusses them regarding TRILATER-ATE. Section 2.1.3 discusses the majority of related work.

4.1.1   *Proximity Input*

An early stream of research has investigated the combination of multiple capacitive measurements for 3D proximity input. Fundamental works by Smith et al. and Zimmerman et al. allow sensing of hand geometry [Smi96], 3D finger position [Zim+95; Smi99], and hand gestures [Smi+98]. More recently, research has continued to explore capacitive near-field communication [Gro+14], and sensing of 3D gestures [AWB11; ESM11], objects [AWB12; Gro+13] or hand posture [LS04]. Such sensing is also combined with screens to detect gestures [Le +14], grasp [Cha+06], or fine-grained hovering [Hin+16]. While widely used, they utilize fixed-form sensors that need to be assembled to the objects or placed in the environment, which is time-consuming. Further, a broader variety of objects are supported by TRILATERATE as sensors are not of fixed form but are dynamically generated according to the geometry of the object.

4.1.2   *Deformation Input*

Prior works explore deformation-based input as a compelling and engaging input modality. Deformation sensing can be achieved by embedding sensors into objects [PCH14; Sug+11; TPH15; Van+13; Wan+11; WS17], by conductive foams [MN94; Nak+17; Ngu+15], or by using optical sensing [Go+12; HBB11; PIS15; SJM13; SII12; Wat+14]. Other approaches employ resistive [Bäc+16; Gon+14; SPH11], capacitive [Olb+15], or piezoelectric foils [Ren+12; Ren+14]. While many of these approaches capture deformations in high fidelity, they require additional assembly steps inside the object or on its surface or are only applicable on developable surfaces.

Regarding fabrication, Bächer et al. [Bäc+16] are probably most closely related to TRILATERATE. They contribute a computational approach to design and reconstruct complex deformations in 3D-printed objects by using resis-

tive sensing. However, objects must be manually equipped with wires which are not routed to the same location. Moreover, they focus entirely on global deformation sensing, i.e., the shape of an object is deformed at a global scale (e.g., bending an arm). In contrast, this chapter focuses on hover, touch, and local pressure sensing on the surface of an object without globally deforming it. Moreover, TRILATERATE objects are printed in a single pass and require further assembly only outside of the object.

4.2   FABRICATION AND SENSING APPROACH

This section introduces the sensing principle underlying TRILATERATE and describes the fabrication pipeline to create TRILATERATE objects using an existing 3D model.

4.2.1   *Sensing Principle*

A TRILATERATE object is defined as a 3D-printed material composite, which consists of three primary functional structures (see Figure 4.1A):

1. **Electrodes** and **traces**, i.e., conducting paths to electrodes, are fully 3D-printed in the object and used to detect interactions. They are printed using a conductive polymer and are connected to a capacitive sensor board.

2. **Shields** encapsulate all non-sensitive areas of electrodes and conducting traces. They are actively driven at the same potential as the electrodes to prevent the electrodes from being influenced by stray capacitance except in a predefined spherical segment of detection. The shields are printed with the same conductive polymer as electrodes and traces but are electrically separated from them with insulating padding.

3. All insulating parts of the object are defined as **Padding**, i.e., a dielectric structure that is made of either solid or deformable material. In the latter case, it allows the 3D-printed object to deform in order to detect pressure.
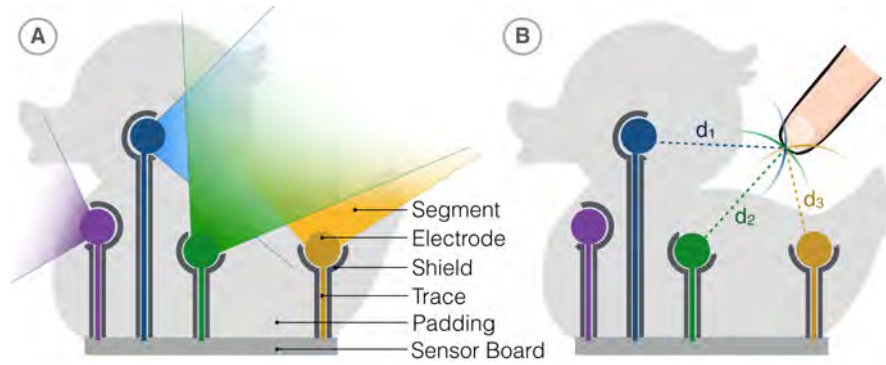
Figure 4.1: The principle of capacitive trilateration in 2D: The capacitance measured at a single electrode implies a finger on a circle in its segment with distance d_i (B). For 2D, at least three electrodes need to be combined to estimate the position of the finger at the intersection point of all circles.

As illustrated in Figure 4.1, the electrodes are distributed in the object so that the interaction of a finger can be detected. For each electrode, the capacitance is continuously measured for a predefined spherical segment, i.e., a conical portion of a sphere (see Figure 4.1A). The capacitance c_e measured at an electrode e equals a distance d_e in the spherical segment where a finger might be expected. Hence, the combined capacitances of multiple electrodes can be used to trilaterate the position of a finger at the intersection of the boundaries of all spherical segments (see Figure 4.1B).

As trilateration requires exact distance measurements, the traces are actively shielded to only be sensitive at the electrode itself. To that end, the shield is driven at the same voltage potential of the electrodes and traces. Hence, no capacitive coupling occurs between shield and trace. Further, any external interference is coupled to the shield with minimal interaction with the traces.

Of note is, that TRILATERATE supports sensing on thin and perforated surfaces as the trilateration principle, compared to prior approaches (cf. [Bur+15; ZLH17]), decouples the surface of the object from the electrodes. That is, the electrodes may also be placed below a fine-grained 3D-printed object. For the reference apparatus (see Section 4.5.4), such objects may have a size of up to $65 \times 56 \times 40$ mm^3. By varying the size of the electrodes or the sensitivity of the sensor board, this range may be further extended.
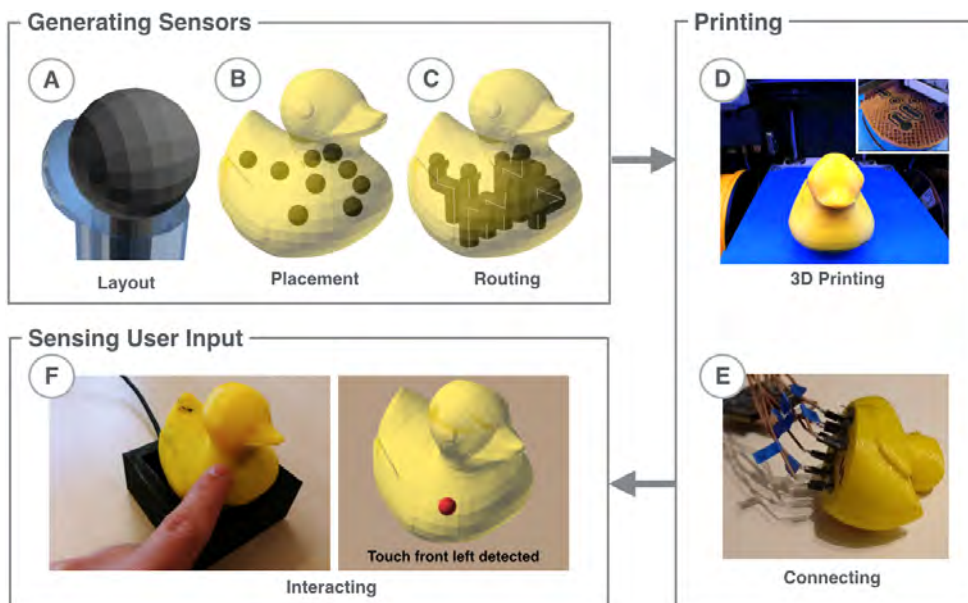
Figure 4.2: The TRILATERATE fabrication pipeline: Electrodes and conducting traces are created automatically in the 3D model using a graphical application. After 3D printing, the object is connected to the sensor board and can be used for interaction.

4.2.2 *Fabrication Pipeline*

As illustrated in Figure 4.2, the TRILATERATE fabrication pipeline consists of three steps to create an interactive object.

GENERATING SENSORS

First, a user loads a volumetric 3D model into the TRILATERATE object generator (see Figure 4.3). Second, the application automatically creates and places the required electrodes (see Figure 4.2B). Third, it routes all necessary traces and shields to the bottom of the object (specified by the user), so that no assembly inside the object is necessary (see Figure 4.2C). Users may specify individual properties (e.g., the sensor size or trace thickness) or direct the creation of the electrodes by selecting a subvolume of the object in the 3D view of the generator.

Figure 4.3: The TRILATERATE object generator: After loading a 3D model, trilateration sensors are generated (A). Users may inspect the expected accuracy (red equals high accuracy) using a heat map visualization (B).

PRINTING

The object generator can export printer-ready fabrication files for conductive structures and insulating padding. They are processed with the printer-specific slicing software and then 3D-printed (see Figure 4.2D).

To connect the object to the sensor board, the user attaches shielded wires to its bottom (see Figure 4.2E). If desired, the generator application supports ending all traces in a regularly-spaced grid (e.g., to connect standard pin headers).

SENSING USER INPUT

After a per-user calibration, the sensor board sends the capacitive measurement to a host computer. The measurements are then used to trilaterate the 3D position of the finger and to classify the interaction as hover, touch, or pressure (see Figure 4.2F).

4.3 GENERATING TRILATERATION SENSORS

TRILATERATE utilizes multiple capacitive electrodes to trilaterate a human finger. Applying this approach to complex 3D-printable models raises two main challenges: First, electrodes need to be distributed t such that interactions with the whole object can be sensed through trilateration. Second, the electrodes need to be connected through conducting traces to the sensor board without interfering with other electrodes or traces.

The following section contributes a spherical electrode layout and an algorithm to fully-automatically place electrodes for trilateration in volumetric 3D models. Further, it reports on the routing of traces from electrodes to the sensor board and the implementation details.

4.3.1   *Electrode Layout*

Capacitive electrodes are commonly implemented as planar plates of conductive material connected to a capacitive sensor through a thin trace. While plates are well suited when the sensing direction is known, the sensing direction for trilateration is unknown at the design time. As the electrodes need to be equally sensitive in all direction, TRILATERATE utilizes spherical electrodes (see the spheres in Figure 4.2A).

Since the whole conductive material connected to a sensor acts as a capacitive electrode to a varying degree, the traces are shielded actively to restrict the sensitive area to the electrodes. In order to direct the sensitivity of an electrode in a particular direction, it can also be partly shielded. As depicted in Figure 4.2A, the shield may be extended to cover a configurable spherical segment around the electrode (i.e., a user may vary the aperture angle of the spherical segment using the object generator). As a consequence, the electrode is only sensitive in directions without a shield. If a higher precision in an area is required, more electrodes can be placed and directed towards it by selecting a subvolume in the object generator.

4.3.2   *Electrode Placement*

Finding a suitable distribution of a limited set of electrodes inside the (sub) volume of the object is essential for assuring a uniform sensitivity across the whole object. Also, the distribution must ensure that each surface point of the object is as close as possible to at least four electrodes required for trilateration in 3D space. However, the volume of the object, wiring constraints, and the number of available sensor channels limit the number of electrodes that can be placed.

Therefore, this section proposes an algorithm called **Remove Least Utility**: It fills the volume of the object with electrodes and then iteratively removes all electrodes whose absence would degrade the expected sensing performance of the object the least for a given set of surface points S (see Figure 4.2B).

SURFACE POINTS

Since sensing should be uniform across the whole surface of the object, the set of surface points S is defined as follows: The object is partitioned into a set of uniformly sized voxels that resembles the volume of the object. All voxels intersecting with the surface of the object are marked as a surface point $s \in S$.

A naive approach would resemble surface points by vertices. However, this would prioritize higher tesselated regions of the object. Nevertheless, users may disable or prioritize sensing in some regions of the object by adjusting S or by changing the size of the voxel itself.

INITIAL ELECTRODE CONFIGURATION

As the algorithm builds upon iteratively removing electrode, an initial electrode configuration E_{init} needs to be generated in the 3D object. To that end, electrodes are created at each voxel that is not a surface point. In order to avoid unwanted electrical connections, an adjustable safety distance is kept between electrodes. That is, all voxels inside the safety distance of an already created electrode are blocked.

Also, voxels are excluded whose distance d_{max} from all surface points is greater than the maximum sensing distance (approx. 10 cm for the reference instrument). Moreover, electrodes too near beneath the surface of the object are avoided as they prevent the object to deform appropriately and, hence, interfere with pressure input. That is, electrodes that fall below a minimal distance d_{min} to any surface point are excluded as well. Both distances, d_{max} and d_{min}, are adjustable as they depend on the electrode dimensions and the required deformability.
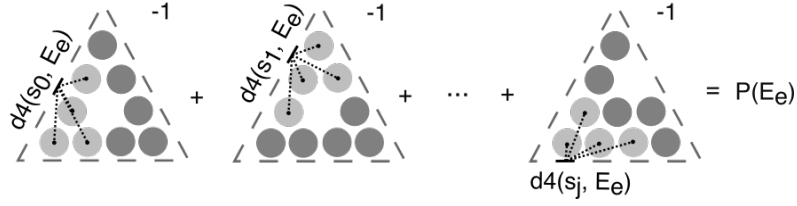
Figure 4.4: Electrodes E are distributed in a pyramid object with dashed surface points S. $|E|$ electrode configurations are computed, each time removing a single electrode e from the set. By comparing the performance $P(E_e)$ of each electrode configuration E_e, the electrode e whose removal still leads to the best overall performance is removed from the object.

PERFORMANCE HEURISTIC

In order to estimate the expected performance of an electrode configuration E, a heuristic concerning a set of surface points S is required. As trilateration in 3D requires at least four electrodes, TRILATERATE employs the sum of squared distances to the nearest four electrodes for a single surface point s:

$$d4_s(E) = \sum_{e \in E'} d(s,e)^2$$

where $E' = \{e | e \in E, e \text{ one of the four nearest points to } s\}$. This equation also takes into account that the nearest electrodes contribute the most sensitive measurements.

As illustrated in Figure 4.4, the performance $P(E)$ of an electrode configuration E is then defined as the sum of sums of all inverted squared distances for all surface points:

$$P(E) = \sum_{s \in S} \frac{1}{d4_s(E)}$$

That is, smaller distances result in higher sums, and, thus, a better configuration E results in a better performance $P(E)$.

CULLING

Let E be the set of all electrodes in an iteration. In order to determine which electrode to remove in each iteration, the algorithm proceeds as follows: For all electrodes in E the estimated performance $P(E_e)$ of the electrode configuration E_e without e, i.e., $E_e = E \backslash \{e\}$, is computed. That is, the algorithm creates a copy of the current set of electrodes with one electrode removed and calculates the expected performance.

Finally, the electrode e' whose absence still results in the best overall performance $P(E_{e'})$ is removed. That is, $E_{e'}$ is used as the set of electrodes for the next iteration. The algorithm may terminate when the number of electrodes equals the available input channels or when the expected overall performance $P(E_{e'})$ falls below a configurable threshold. Since the algorithm does not exclusively optimize the electrode positions but considers their effect on all surface points, it implicitly optimizes the spatial coverage of the surface with electrodes.

The complexity of the remove least utility algorithm is $O(n^2 \times s)$ where $n = |E_{init}|$, the number of initial electrodes, and $s = |S|$, the number of surface cells, because (1) the distances from all surface points S to all electrodes E_{init}, and (2) n estimated performances in n iterations need to be computed. For instance, a medium-sized object (approx. $10 \times 10 \times 10$ cm^3) with a resolution of one voxel per centimeter consists of 1000 voxels from which 271 ($= 10^3 - 9^3$), i.e., the outer surface of voxels, are classified as surface points. Without considering d_{min}, d_{max} or a safety distance between voxels, a pessimistic estimation of an initial electrode configuration consists of 729 electrodes. As a consequence, the algorithm needs to calculate $729 \times 271 = 197.559$ distances.

4.3.3 Routing of Traces

In order to connect the sensor board, traces and shields need to be routed to the bottom of the object (see Figure 4.2C). To that end, the voxelization of the object is transformed into a traversable graph structure where each voxel is represented as a node and two nodes whose voxels are neighbors are connected via an edge. Then, TRILATERATE finds the shortest routes for traces in this graph using the A* algorithm (cf. [Sav+14]) and the Manhattan distance as the heuristic to determine which voxel to expand next. A voxel is only used once by a single trace because all traces need to be electrically separated. As a result of the evaluation (see Section 4.7), voxels that are in line-of-sight between electrodes and surface points are downgraded for routing (but not forbidden to support narrow passages) to improve the coverage of surface points. Also, the sequence of routing traces is an essential factor for (1) trace length and (2) whether an electrode is connected at all. As all permutations cannot be reasonably tested, TRILATERATE employs the Lin-Kernighan heuristic to decide which electrode should be routed next.

If an electrode cannot be connected (e.g., due to lack of space), the user is asked to reduce the number of electrodes.

4.3.4   *Generating Printer-Ready Models*

As multi-material 3D printing requires distinct 3D models for insulating and conductive materials, all conductive structures are removed from the 3D model of the object by using boolean subtraction based on constructive solid geometry. Before printing, users may assess the expected accuracy, i.e., a surface point is colored red if more than four electrodes are in line-of-sight of it, in the 3D view of the generator. The positions of the electrodes inside the volume and the position of their respective trace ends are shown in the object generator and saved to a configuration file. After printing, the file is used in sensing to map each measurement to the position of an electrode.

4.3.5   *Implementation Details*

The object generator is written in Python and OpenSCAD. It calculates the distribution of electrodes inside the volume of the object selected by the user and routes the traces from those electrodes to interface points at the bottom of the object. The application uses a plugin mechanism to implement differ-ent distribution and routing strategies, which can be selected by the user at runtime. Also, users may optionally configure various properties (e.g., the size and thickness of electrodes, traces, shielding, or padding). These param-eters, the electrode positions, and the trace paths are automatically passed to OpenSCAD scripts inside the object generator to create the printer-ready files.

4.4   PRINTING

The following section details on the printing setup used in order to evaluate TRILATERATE. Moreover, it presents guidelines to 3D print objects using the generated printer-ready models.

4.4.1 *Setup*

TRILATERATE is implemented using consumer-level 3D printers and materials as this makes it accessible to a broader audience. It operates on standard multi-material 3D printers using FDM (BCN3D Sigma and Prusa MK3 MMU2) and commercially available printing materials. The conductive structures consist of carbon-doped Proto-pasta Conductive PLA (cPLA) with a volume resistivity of $30 - 115\,\Omega * \text{cm}$. Conductive and insulating materials are printed with a 0.4 mm thick nozzle at a temperature of 230 °C (enabled cooling fan) with a retraction of 5 mm (20 mm/s) and a heated bed (40 °C).

Depending on the use case, the padding can be printed either with solid PLA (only hover and touch) or deformable TPU (also pressure). TRILATERATE objects are printed with Verbatim PLA at 210 °C for solid objects and NinjaFlex TPU, a Polyurethane composition (material shore hardness 85A), at 230 °C for deformable objects. An infill density of 20%, i.e., a deformability of up to 1/5 of the original thickness, for the padding results in adequate sensing performance. The density may be adjusted to vary the deformability (e.g., to fit a use case).

4.4.2 *Guidelines for Generating & Printing*

The following practical properties should be considered when creating an object with TRILATERATE.

ELECTRODE TRACE RATIO

The most critical parameter apart from maximizing electrode size is the diameter of the traces of the electrode. As a general rule, these should be made as wide as possible without causing the entire trace to be thicker than the electrode itself. Having thicker traces lowers the chance of a printing artifact interrupting the electrical connection and reduces the electrical resistance, resulting in higher capacitive sensitivity. The voxels used for routing have an edge length of 11 mm.

SHIELD WIDTH

The width of the shielding is less critical because small holes in it do not affect the electric field between traces and shielding. The TRILATERATE objects utilize a shielding width of two nozzle widths (0.8 mm), which proved to provide sufficient shielding and conductivity. The shielding must be electrically separated from traces and electrodes.

SPACING BETWEEN MATERIALS

The conductive structures are generated based on the aforementioned parameters and are then subtracted from the model of the object. However, the conducted tests suggest that insulating and conductive material should be separated by a small margin to improve the printing quality. To that end, the object generator computes all conductive structures a second time with an increased thickness of 0.1 mm. The thickened model is used for subtraction while the original model is used for printing.

4.5   SENSING OF USER INPUT

Distances to the finger can be calculated using the capacitance measurements of all electrodes. Then, these distances are combined into a 3D position estimate using trilateration. By examining the relation of the 3D position estimate to the surface of the object, the interaction type (i.e., hover, touch, or pressure) is determined. This process requires the following three steps:

4.5.1   *Capacitance to Distance*

Using the capacitance c and the parallel plate model $c = \epsilon \frac{A}{d}$, the distance of a finger to each electrode can be estimated by $d = \epsilon \frac{A}{c}$. While A and ϵ are constant during sensing, the capacitance c measured by each electrode directly relates to the distance d. That is, the distance is inversely proportional to the capacitance between finger and electrode. Instead of the parallel plate model, other capacitor models can be employed to compute these distances.

As the measured capacitances differ in their magnitude due to variations in the environment, trace length, and print quality, a reference capacitance $c_r(e)$ with a known distance $d_r(e)$ is required for every electrode e to obtain abso-

lute distances. All reference measurements are recorded during a calibration: A user is instructed to touch randomly-distributed points on the surface that are highlighted on the 3D model of the object on a screen. All distances are computed relative to this reference.

Using the reference capacitance $c_r(e)$ and its distance $d_r(e)$ of an electrode e combined with the measured capacitance $c_m(e)$, the distance $d_m(e)$ is calculated as follows:

$$d_m(e) = d_r(e) * c_r(e) * \frac{1}{c_m(e)}$$

4.5.2   Distance to 3D Position

Once the distances of the finger to the electrodes are known, the 3D point of interaction can be calculated via trilateration. As the distance values are noisy and hence exhibit jitter, there does not exist a single position in space that has the exact distances to all electrodes. Therefore, an optimization algorithm needs to approximate this position. TRILATERATE employs a BFGS-based optimization algorithm that shifts a point p in 3D space such as to minimize the value of a loss function.

As the loss function L, TRILATERATE uses the mean squared differences between the Euclidean distance of the point p towards an electrode e and the measured distance $d_m(e)$:

$$L(p) = \frac{1}{|E|} * \sum_{e \in E}(||p - e|| - d_m(e))^2$$

That is, the algorithm shifts the point p in space in order to minimize the deviation between the model-based distance $||p - e||$ and its measured distance $d_m(e)$ for all electrodes $e \in E$. After convergence, the algorithm returns a 3D position p_i which represents the least deviation between actual and measured distances with respect to the loss function.

4.5.3   3D Position to Interaction Type

The type of interaction is obtained by determining the distance $||p_i - s||$ of the 3D position of interaction p_i towards the nearest point s on the surface of the object:

- If the position lies outside of the object, the interaction is classified as hover.

- If the position lies on the surface (within a narrow threshold), it is classified as touch.

- If the position lies within the object, it is classified as pressure.

For hover and pressure, the distance $||p_i - s||$ is also utilized as an intensity level of the particular interaction.

4.5.4 *Implementation Details*

The following section presents the reference apparatus in order to implement and evaluate TRILATERATE.

SENSOR BOARD

The 3D-printed object is connected to a sensor board. It receives the capacitance measurements of the electrodes and forwards them to a host computer. The developed sensor board consists of an Arduino Nano V3 used for the serial connection to the host computer, as well as multiple capacitive sensors. TRILATERATE employs single capacitance sensors (TI FDC1004 with active shielding) in loading mode [Gro+17], as this mode offers a more uniform sensitivity in all directions compared to the transmit-receive mode that measures between two points. To be able to control multiple FDC1004 chips on the same I2C bus, an I2C multiplexer (TI TCA9548A) is used. The sensor supports sample rates of up to 400Hz, with lower sampling rates offering higher sensitivity. As lower sampling rates offer higher sensitivity (i.e., increased accuracy over long distances), TRILATERATE operates at a sampling rate of 100Hz. Additionally, the Arduino applies a low pass filter to the sensor values to further increase accuracy.

All measurements of all channels of the connected FDC1004 sensors are triggered in series. As the sensor board currently uses a total of eight input channels, this results in a minimum refresh frequency of 12.5Hz ($\frac{1s}{100Hz} * 8$) and a maximal refresh frequency of 50 Hz ($\frac{1s}{400Hz} * 8$). The capacitance values are then forwarded to the interaction detector on the host PC.

INTERACTION DETECTION

The detector tool calculates the interaction position and type (i.e., hover, touch, or pressure) using the measurements. It is written in Python and provides all interaction events alongside with the 3D model and the 3D position to other application via an API. The detector tool displays the 3D model of the object. As soon as a finger is detected, a fingertip-sized red sphere visualizes the position of the finger (see Figure 4.2F). Further, the detector is used for calibration. To that end, it displays marking dots on the object model that need to be touched by the user (takes approx. 1.5 s per electrode). After calibration, the absolute 3D position of the finger is used together with the 3D model of the object to compute the interaction type (see Section 4.5.3).

4.6 EXAMPLE APPLICATIONS

The following five interactive example prototypes demonstrate the practical feasibility of TRILATERATE.

4.6.1 *Educational Aid*

3D objects are often useful to learn visual-spatial content. As an example, a prototype of the Matterhorn mountain (PLA padding) was 3D-printed that illustrates its geological 3D structure. Users can hover and touch different areas to obtain geographic information (see Figure 4.5). Further, a cubic platform was designed on which non-interactive single-material objects of any 3D-printable complexity can be placed (see Figure 4.6). By combining the 3D models of the platform and the object on it, interactions on the latter are also detected. As an example, a molecule learning environment was created that highlights atoms and displays their name when touched. In general, the platform could be reused for any cost-effective 3D-printable objects.

4.6.2 *PyARmid*

Augmented Reality is often criticized as lacking haptics and input richness [BP08]. Using TRILATERATE, haptic objects for Augmented Reality can be rapidly created. As illustrated in Figure 4.7, an exploration application of
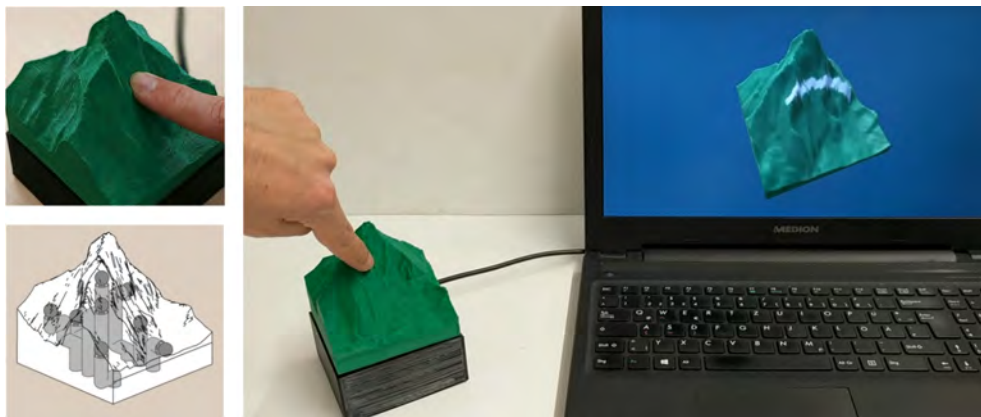
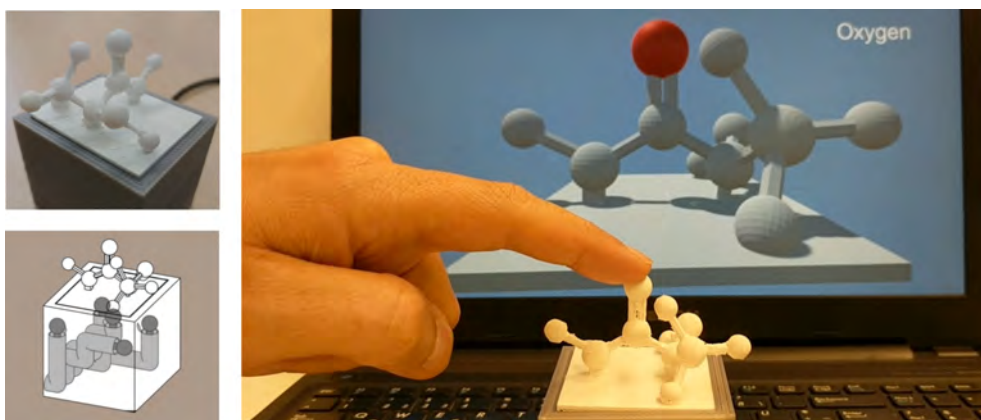Figure 4.5: A 3D-printed prototype of the Matterhorn used to explore geographic information.

Figure 4.6: A prototype of a 3D-printed molecule used to explore the chemical structure.

the Egyptian pyramids for the Microsoft HoloLens was implemented, that shows a textured overlay on top of a 3D-printed pyramid (TPU padding). By hovering, a virtual sun can be moved around the pyramid. The user can touch one side of the pyramid to take a look at its internal structure and press harder to see further into the pyramid.

4.6.3   *Making 3D Scans Interactive*

3D scanning allows easy digitization of the physical world. Even complex real-world objects can be made interactive using the previously described platform. As an example, a person was scanned and 3D-printed (PLA padding) as a tangible interactive avatar for friends or family that is highly per-
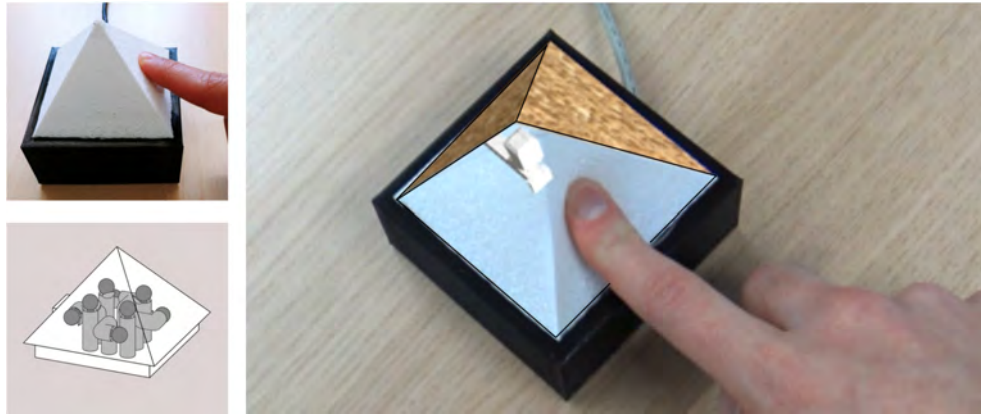
Figure 4.7: A 3D-printed prototype of a pyramid with an augmented reality overlay (the quality of the right image is due to the capture through HoloLens).

Figure 4.8: A 3D-printed prototype of a person, that is used to send a greeting notification to the corresponding person.

sonalized (see Figure 4.8). For instance, by touching the avatar of a person, a pre-defined greeting is sent to the mobile device of the person.

4.6.4 *Shut the Duck up*

In order to demonstrate the use of TRILATERATE for more meaningful touch interaction in everyday devices, an alarm clock was implemented (see Figure 4.9) that is shaped like a rubber duck (TPU padding). The duck is equipped with a speaker and allows listening to different alarm sounds by hovering around it. A touch selects the respective sound. An alarm is set by pressing the body of the duck until the desired alarm time is said via the speaker. Pressing harder changes the time faster. After an alarm has been set, the user can hover the duck for easily accessible, eyes-free function (e.g.,

Figure 4.9: A prototype of a 3D-printed duck that acts as an alarm clock.

to say the remaining time to sleep out loud). When the alarm goes off, a firm press deactivates the alarm.

4.7   EVALUATION

In order to evaluate TRILATERATE, quantitative evaluations on the sensing of 3D position and pressure were conducted. While research frequently utilizes mechanical apparatuses to evaluate capacitive sensing (cf. [Gro15; Zim+95]), this sections presents a user study with 12 participants (9m, 3f, mean age 27.3) to account for inter-individual differences in users' capacitive responses.

4.7.1   3D Position

Since a proper 3D position estimate is crucial for the quality of touch and hover input, both were evaluated in a single study. The effects of the following two factors on 3D-printed capacitive trilateration were investigated: (1) the **coverage**, i.e., the number of electrodes that cover a surface point without being shielded by another trace or shield, and (2) the **distance**, i.e., the mean distance of all electrodes to the respective surface point. To that end, a pyramid object (length 8 cm, height 6 cm, ground to earth) with eight electrodes was generated. Seven target positions on the surface (see Figure 4.10) were distributed such that they cover all combinations of the independent variables **coverage** (high vs. low) and **distance** (near vs. far): Positions 2, 3 and 4 are **near** electrodes (mean distance < 11.24 *mm*) and **highly** covered
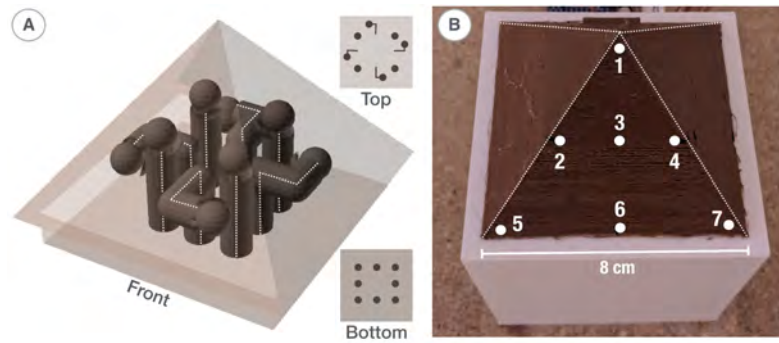
Figure 4.10: Distribution of eight electrodes inside the pyramid (A) and seven target positions, marked on the object (B).

(up to four electrodes). Position 1 is also **highly** covered, but the electrodes are **far** distant (mean distance 14.34 *mm*). Positions 5, 6, and 7 are **lowly** covered (only two to three electrodes) because the electrodes are partially blocked by traces and shields from the viewpoint of the position. In contrast to the positions 5 and 7, position 6 is **nearer** to the electrodes (mean distance 15.01 *mm* vs. 20 *mm*).

While the shape of the object is commonly an important factor for capacitive sensing, the trilateration approach is independent of the non-interactive, insulating surface that covers the electrodes, as the calibration accounts for differences in measurements. Since an informal test confirmed this assumption, the effect of object shape was not investigated further. As a consequence, a pyramid shape was used in order to make it easier for the participants to localize the target positions.

SETUP & TASK

To be able to perform tests with multiple participants in a repeatable and comparable way, the object was fixed on a wooden plate (see Figure 4.10B). Participants received an introduction to the system before exploring it freely until they felt comfortable. Then, they calibrated the system by touching predefined positions. Between tests performed by the same participant, the system was not recalibrated. Each participant was instructed to repeatedly touch the seven target positions ten times per position (counterbalanced using Balanced Latin Square), leading to a total of 840 samples. All target positions were marked on the object to give the participants an exact reference (see Figure 4.10B). Further, the position to be touched next was highlighted on a virtual model shown on screen. While touching the position, the participant triggered the data recording with a key press.
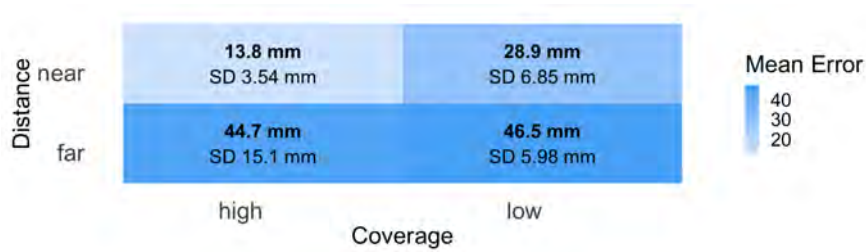
Figure 4.11: Mean position errors with standard deviations (SD) for all conditions.

RESULTS & DISCUSSION

As the dependent variable, measurement error, i.e., the euclidian distance between a target position and the measured 3D point reported by the system, was analyzed using a two-way repeated measures ANOVA. When significant effects were revealed, post-hoc analysis was performed using Bonferroni corrected pairwise t-tests. Also, the eta-squared η^2 as an estimate of the effect size as small, medium or large [Coh88] is reported.

The analysis revealed that the **distance** of electrodes had a highly significant ($F_{1,11} = 105.44$, $p < .001$, $\eta^2 = .587$) influence on the 3D position estimate with a large effect size. Post-hoc tests confirmed significantly smaller errors for the near distance conditions compared to the far conditions (see Figure 4.11). Moreover, the **coverage** of electrodes had a significant ($F_{1,11} = 11.23$, $p < .05$, $\eta^2 = .071$) influence on the 3D position estimate with a medium effect size. Post-hoc tests confirmed significantly smaller errors for the high coverage condition compared to the low coverage condition. Further, an interaction effect with a small effect size between the factors was found ($F_{1,11} = 7.4$, $p < .05$, $\eta^2 = .044$).

The analysis shows that electrodes should be placed as near as possible to the surface of the object. Also, coverage of at least four electrodes is crucial for a lower error. Hence, the routing algorithm should avoid voxels that are in line-of-sight between a surface point and other electrodes.

4.7.2 *Pressure*

The same participants continued the previous study to assess pressure accuracy (without recalibration).
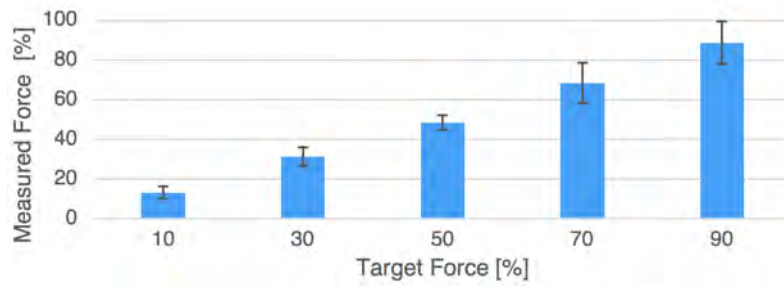
Figure 4.12: Mean pressure levels for a target pressure level across all participants. Error bars show the standard deviation.

SETUP & TASK

Since the evaluation of the pressure accuracy should not be affected by non-linear deformation effects of the padding, position 3 was used as the target point (see Figure 4.10B). The central location of this position allows the object to linearly and continuously deform.

The object allows for a maximal deformation at target position 3 of approx. 5 mm with moderate pressure. However, in contrast to the position tests, there is no fixed reference scale for the subjective pressure exerted by a participant. Each participant can differently perceive the applied pressure or is not at all able to exert the maximum pressure of another participant. Therefore, each participant sets an individual pressure scale by first applying a maximum and then a minimum pressure, confirming each by pressing a key. The test samples are then taken by asking the participant to set a specific target pressure level (10% to 90% in 20% steps) displayed on a screen and confirm it by pressing a key. The current pressure applied by the participant is displayed as a reference. Each participant was instructed to set a pressure level seven times.

RESULTS & DISCUSSION

The results of the pressure tests across all participants are depicted in Figure 4.12. For 10% target pressure, the system reported in average 13.12 % ($\sigma = 3.17$ %). The average for 30% target pressure was 31.25 % ($\sigma = 4.7$ %) and 48.41 % ($\sigma = 3.77$ %) for 50% target pressure. For higher target pressures of 70% and 90%, the system reported 68.36 % ($\sigma = 10.15$ %) and 88.61 % ($\sigma = 10.78$ %). Of note is, that the mean distance between target and measured pressure level is 1.8 % ($\sigma = 0.76$ %). That is, the participants hit the desired pressure level in average within 1.8%. On a scale of 5 mm (0% – 100%), 1.8% corresponds to a distance resolution of 0.09 mm (5 mm $* 0.018$).

In summary, the results show that for highly covered, near distance conditions, multiple 3D positions and levels of pressure applied by users can be reliably distinguished.

4.8 DISCUSSION AND LIMITATIONS

This chapter presents results on 3D-printed sensing on non-developable surfaces. However, it currently has limitations that must be considered during fabrication and sensing.

4.8.1 *Object Size & Geometry*

If not used with a sensing platform, an object must be able to accommodate at least four electrodes required for trilateration. Hence, a minimum of 4 cm³ closed volume is required (i.e., four electrodes sized Ø 9 mm at the edges of a rectangular cuboid with perpendicular traces). For slim objects, the thinnest section must at least fit as many voxels in the horizontal plane as electrodes as routing requires this space. Placement may not succeed for small structures (e.g., hairs). The number of electrodes supported by the sensor board and the sensing distance of an electrode (the maximum sensing distance is 10 cm for the current printing setup for a Ø 9 mm electrode) limit the maximal volume of an object to be covered. While the exact limits depend on the shape of the object, the maximum object size is approx. $10 \times 10 \times 10$ cm^3. However, multiple boards can be multiplexed for more channels.

Since distance and coverage are essential factors, they pose implications on suitable 3D models: (1) Objects with highly varying curvatures (e.g., a set of hairs) may result in too distant electrodes. (2) Objects whose parts are connected by a constriction (cf. an hourglass) are challenging for routing. As 3D printing advances, the resolution is likely to improve, enabling more accurate placement and routing.

4.8.2 *Distance Resolution & Accuracy*

For the current printing setup, the sensing resolution is 0.5 fF steps at -15 pF to +15 pF input range. The usable input range between the minimal self-

capacitance and the maximal capacitance of a direct touch for an electrode of Ø 9 mm is 12.84 fF (25670 steps). As this input range is not uniformly distributed across all distances due to the inversely proportional relation, the resolution for pressure, touch, and hover input varies. While a resolution of less than 1 mm for distances smaller than 5 cm was possible, the resolution decreases to 4 mm for a distance of 10 cm, which still can be considered sufficient for hovering.

The achievable accuracy may be further influenced by several factors: First, the choice of the capacitor model that transforms a capacitance to a distance. TRILATERATE employs the parallel plate model as each spherical electrode is actively shielded into a particular direction and a finger is commonly modeled as a plate (cf. [Gon+14; Gro15]) However, the sensing equations can be adapted to a more elaborate model for the electric field between a finger and a shielded spherical electrode.

Second, the relative permittivity of the dielectric between electrode and finger is often constant as only a single dielectric (e.g. air) is involved. In general, the relative permittivity is distance-dependent as with increasing distance, the ratio of printed TPU padding to air changes. While this effect was experienced to be negligible as the padding's infill density is only 20 % and, hence, consists of 80 % air, a more physically correct permittivity estimation that considers the air gap could result in more accurate position estimation.

4.8.3 *Scalability*

Traces should be printed with a width of at least 3 mm to guarantee proper conductivity (nozzle diameter 0.4 mm). In order to ensure proper shielding, the shield should be two times the nozzle width (0.8 mm for the current printing setup). Using a safety distance of 1.2 mm between shield and trace (filled with insulating material) and 0.6 mm to other traces at both sides, the minimal width of a trace including shield is for the current printing setup 8.2 mm. Currently, the routing requires an object with a flat bottom (min. size 3.5×3.5 cm^2). However, traces may be routed to multiple, non-flat locations.

In contrast to CAPRICATE, TRILATERATE uses a central sensing structure rather than placing sensors on the surface. As a result, it covers a larger sensing area with fewer electrodes. For instance, four half shielded TRILATERATE electrodes close to each other cover the whole surface of a hemisphere $H = r^2 * 2\pi$ with r = 70 mm (which is a pessimistic estimate concerning

the maximal sensing distance of 10 cm). To achieve a comparable accuracy (±13.8 mm), CAPRICATE needs electrodes sized $A = (2 * 13.8 \text{ mm})^2$. To cover the whole hemispherical surface H, this would require $\frac{H}{A} \approx 40$ distinct electrodes, implying 40 instead of just four traces. While CAPRICATE senses multiple touches simultaneously, these many traces imply not only a considerable routing effort in often limited object volumes but are also prone to stray capacitances without active shields.

4.8.4   *Environmental Noise, Multi-Finger & Multi-Pressure*

As discussed in detail in Section 4.7, TRILATERATE operates across varying users despite individual differences. If the coverage of a surface point with electrodes falls below the critical minimum of four electrodes required for trilateration, the accuracy of the 3D position is only suitable for coarser interactions (i.e., for low coverage, the position error was 37.7 mm, $\sigma = 6.4$ mm).

Moreover, environmental electromagnetic noise did not affect the sensing during testing and evaluating as the electrodes are shielded and also covered by insulating material. Distinguishing multiple hand posture or fingers is still challenging with TRILATERATE because a whole hand, differently-sized fingers (e.g., index vs. thumb), or multiple fingers next to each other have different capacitance, and, hence, can alter the measurements. That is, the same measurement could indicate a large capacitance further away or a small capacitance close-by. Nevertheless, multiple fingers may be tracked if a distinct set of electrodes handle a single finger. This aspect can be of use for more complex gestural interactions performed with an object (e.g., grasping an object from both sides). Also, while simultaneously sensing of pressure, touch, and hover input currently needs a stretched out finger pose, other finger poses are possible when hover input is not required.

Of note is, that the measured pressure does not equal the physical force, as the latter is dependent on the physical properties of the padding which this chapter does not focus. However, Hooke's law and the 3D structure of the padding may be combined in the future to map the position of a finger to a physical force.
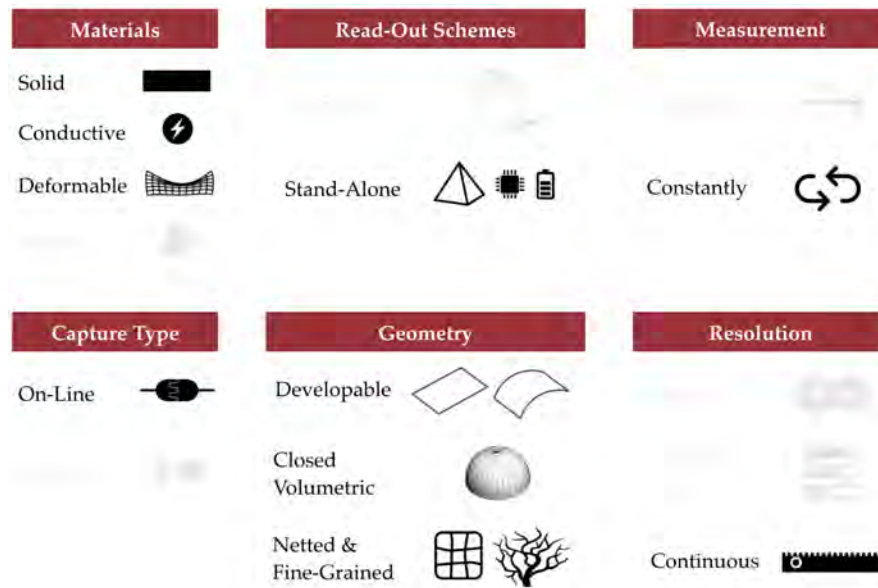
Figure 4.13: The classification of TRILATERATE regarding the design space of 3D-printed interaction.

4.9 CONCLUSION

This chapter presented TRILATERATE, a fabrication pipeline to create customizable 3D-printed objects that recognize the 3D position of a finger floating above, touching on or pressing in a 3D object. In summary, the main contributions of this chapter are:

1. A fabrication pipeline to autogenerate and print sensors in a single pass with off-the-shelf 3D printing.

2. A combination of 3D printing and capacitive trilateration to sense pressure, touch and hover with 3D objects.

3. An evaluation of the 3D position and pressure accuracy.

TRILATERATE enables users to fabricate solid conductive or deformable conductive material composites using an easy-to-use design tool. As illustrated in Figure 4.13, objects created with TRILATERATE constantly measure a 3D position and infer continuous hover, touch, and pressure input on developable, closed-volumetric, netted, and fine-grained geometries.

This approach and its prototypical implementation open up a wide range of applications for stand-alone devices that feature high precision input of a single finger. Moreover, it can be integrated with CAPRICATE, that, in contrast,

can infer multi-touch. By detecting pressure input, TRILATERATE already moved beyond simple touch input. However, there are many more kinds of deformation that may be performed with an object. Therefore, the next chapter investigates how to add more kinds of deformation to 3D-printed objects.

5

FLEXIBLES: 3D-PRINTED DEFORMATION SENSING

While the previous chapter focused on a fabrication pipeline to 3D print hover-, touch- and pressure-sensitive objects by attaching a capacitive sensor board, this chapter contributes FLEXIBLES that add *deformation-awareness* to passive objects on capacitive touchscreens. That is, FLEXIBLES enables a capacitive touchscreen to recognize pressing, squeezing, and bending of a 3D object[1]. As a consequence, FLEXIBLES add another haptic input dimension to touch interaction on smartphones, tablets, and tabletops, allowing for more physical control of digital content [Rek02; IU97].

The remainder of this chapter is structured as follows. Section 5.1 discusses related work. Section 5.2 introduces two principles for sensing deformations on capacitive touch sensors. On this basis, Section 5.3 details on the design of a FLEXIBLE and Section 5.4 presents a set of sensors for capturing various forms of pressing, squeezing, and bending input. Section 5.5 then presents the implementation of sensing and fabrication. Through three interactive example applications, Section 5.6 demonstrates the combination of multiple sensors in a single object. Section 5.7 reports on a technical evaluation to confirm changes in capacitance readings can be reliably mapped to deformations of varying intensities. To conclude, Section 5.8 discusses the limitations of FLEXIBLES.

---

1 In the remainder of this thesis, an object created with FLEXIBLES is called a FLEXIBLE.

Contribution Statement: This chapter is based on [Sch+17]. I led the conceptual design, the 3D printing, the implementation, and the evaluation. The bachelor students David Fischer, Max Stachalski, and Jens Krüger modeled, printed and implemented the sensors and algorithms under my supervision. The student assistants Alexander Hendrich and Daniel Kauth implemented the example applications. The student assistants Andre Pfeifer and Andreas Leister supported the 3D printing. My supervisors Jürgen Steimle and Max Mühlhäuser advised me on the conceptual design and contributed to writing the paper.

The following section shortly presents relevant research in the context of tangibles on interactive surfaces and discusses them regarding FLEXIBLES. Section 2.1.3 discusses the majority of related work.

5.1.1 *Tangibles On Interactive Surfaces*

A body of research has investigated how optical approaches can be used to detect tangible objects on a touchscreen [BBR10; Wil+11a]. More recent work is investigating how to detect tangibles using the now common capacitive touchscreens. Many works apply variations of capacitance tags [Rek02]. By embedding conductive material or by adding electronics to the tangible object, the capacitive touch sensor can detect presence and location of tangible objects [Yu+11; Voe+13; Voe+15], combinations of multiple objects [Cha+12], or forward touch on the object onto the touchscreen [Cha+12; KM15; KM16]. Other approaches utilize magnetic hall sensor grids to identify objects [Lia+14] and detect their posture above a screen [Lia+13].

While these approaches propose promising ways of interacting on capacitive touchscreens, they are, in contrast to FLEXIBLES, restricted to solid, nondeformable objects, and require additional hardware that needs to be assembled manually.

5.1.2 *Deformation Input*

As discussed in Section 4.1.2, research explores deformations as a powerful and engaging input modality. While many of these approaches capture deformations in high fidelity, they are either incompatible with conventional capacitive touchscreens or require built-in, tethered, or stationary hardware.

Probably most closely related to FLEXIBLES is work by Slyper et al. [SPH11] and more recently Bächer et al. [Bäc+16]. Slyper et al. embed wires inside manually fabricated soft silicone objects of various geometries to resistively or magnetically sense interactions, including pressing, twisting, bending, and stretching. Moreover, Bächer et al. contribute a computational approach to design and reconstruct complex deformations in 3D-printed objects by

using resistive sensing. For both, objects have to be equipped with wires, need to be actively powered and read out using a dedicated microcontroller to which the object needs to be permanently tethered. In contrast, the untethered and passive FLEXIBLES approach utilizes capacitive coupling to a standard multi-touch sensor, therefore demanding a different set of requirements.

Adding to this body of research, FLEXIBLES are 3D-printed in a single pass without any additional assembly and operate on commodity capacitive touch sensing hardware.

5.2 FABRICATION AND SENSING APPROACH

This section introduces the sensing principle that underlies FLEXIBLES and presents the overall fabrication approach.

5.2.1 *Sensing Principle*

Most commodity multi-touch controllers perform a variant of what is called **mutual capacitance sensing** [Zim+95]: A voltage is consecutively applied to unconnected rows and columns of a conductive grid, creating a uniform electric field at each intersection of the grid. When a conductor, such as a finger, gets close, it alters the electric field at the corresponding grid location. This effect can be measured as a change in capacitance.

Based on this general scheme, Rekimoto [Rek02] proposed capacitive tags as a means to detect tangible objects on capacitive touchscreens. The tangible object contains a conductor that reaches from the location where it is touched to the location where it is placed on the capacitive touchscreen. When the user touches the object, the conductor capacitively couples the finger to the touch sensor. This touch results in a detectable change in capacitance used to detect the presence and location of the object. That is, a touch on the object is "forwarded" to the location on the screen. Therefore, such a conductor is called a **forwarding conductor** (in short a **forwarder**) in the following. By using one or more forwarders in conjunction with specific 3D-printed geometries, this principle is extended to detect deformations with capacitive touchscreens.
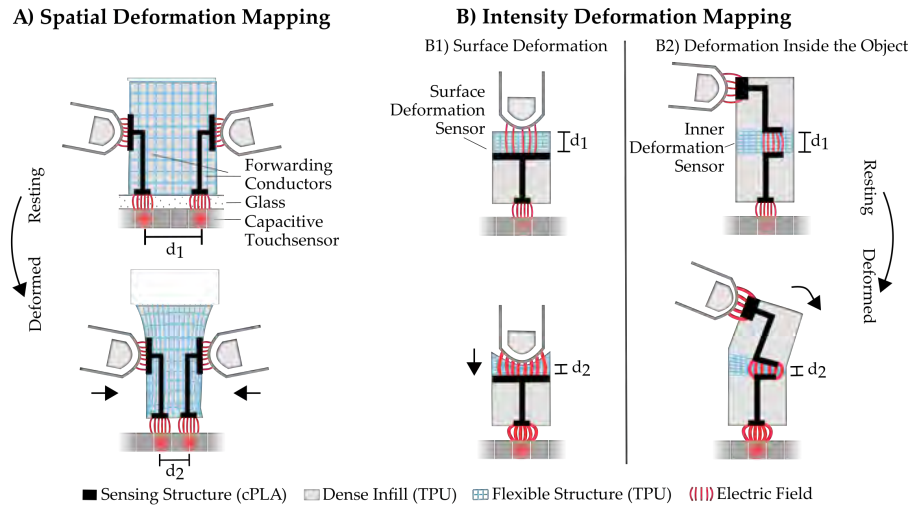
Figure 5.1: Detecting deformations of a FLEXIBLE on a capacitive touchscreen via spatial (A) or intensity (B) deformation mapping.

A FLEXIBLE is defined as a 3D-printed material composite, which consists of two primary functional structures (see Figure 5.1):

1. The **sensing structure** is embedded within the 3D-printed object and is used to recognize deformations by forwarding them onto the touchscreen. It is made of a conductive polymer.

2. The rest of the object consists of a **flexible structure** made of a deformable dielectric elastomer which allows the 3D-printed object to deform at specific locations. Its deformability can be variably adjusted.

Both structures can have a custom size and 3D shape. A 3D-printed object can embed multiple sensing and flexible structures. The remainder of the object is made of a denser deformable material with higher solidity.

This chapter proposes two principles to detect object deformations with a capacitive touchscreen: **spatial deformation mapping**, considering the spatial location of forwarders on the touchscreen, and **intensity deformation mapping**, considering the intensity of the capacitance.

5.2.2   *Spatial Deformation Mapping*

In spatial mapping, a deformation of the object is sensed by capturing the location of forwarders on the touchscreen (see Figure 5.1A). The 3D object is made of a flexible structure that allows it to deform in one or multiple

dimensions. At least two forwarders need to be embedded inside this flexible structure. When the object is deformed, they change their relative position on the sensor grid.

Using this technique, fine-grained deformations that are oriented parallel to the surface of the touchscreen can be detected, thanks to the high spatial resolution of the touchscreen. However, it is not directly applicable to out-of-plane deformations.

5.2.3 *Intensity Deformation Mapping*

In **intensity deformation mapping**, a deformation of the object is sensed by modifying the intensity of the capacitance reading depending on deformation (see Figure 5.1B).

SURFACE DEFORMATION

Deformations that occur at the surface of the object, where the user is touching it, can be captured with a structure called **surface deformation sensor** (illustrated in Figure 5.1B1): the forwarder is overlaid with a flexible structure that acts as a deformable dielectric. When a user applies force, the flexible structure is compressed, and the finger gets closer to the conductor.

Following the plate capacitor model [Bax96], a variation in distance d results in a change in capacitance, i.e., $C \propto A/d$ where A refers to the cross-sectional area of the capacitor plates. Based on the assumption that a distance variation relates to the amount of force exerted onto the flexible structure, deformations can be inferred from variations in capacitance that are captured by the touchscreen. As will be shown in the evaluation section below, this principle allows detecting multiple intensities for specific deformations using commodity capacitive touch sensing hardware.

DEFORMATION INSIDE THE OBJECT

Many deformations do not primarily occur at the surface location where the user is touching the object. In order to capture deformation at interior locations within a volumetric object, this section proposes a structure called **inner deformation sensor** (illustrated in Figure 5.1B2). At the interior location where a deformation shall be captured, the forwarder is interrupted by a

3D-printed capacitor. The capacitor consists of two parallel plates. A flexible dielectric in-between the plates deforms when the object is deformed. This deformation alters the distance or the angle between the plates of the capacitor and thereby modifies its capacitance, as well as the overall capacitance of the entire sensing structure.

5.3 DESIGN

Flexible and sensing structures are combined in sensors that allow detecting different types of deformations. Multiple of these sensors can be integrated into the 3D model of an object.

A FLEXIBLE can be designed using a similar graphical application and interaction techniques as described in Section 3.3. First, the user loads a volumetric 3D model that is shown in a 3D view of the application. Second, the user may add various deformation sensors to the model by using a two-step interaction technique:

1. The user selects a deformation sensor from a sidebar.

2. She adds the sensor to the object via dragging and dropping it onto a part of the 3D model.

After adding sensors, the application automatically creates required sensing structures and routes all necessary wires. Finally, the user can export printer-ready 3D models.
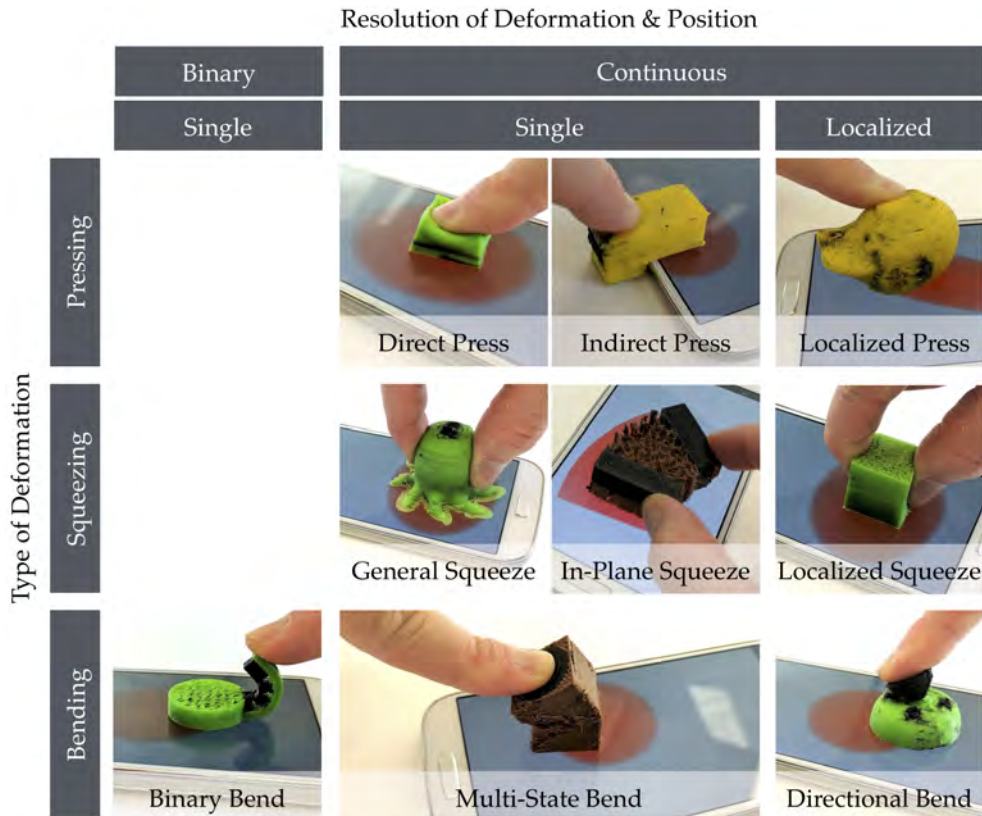
Figure 5.2: An overview of deformation-aware sensors that detect pressing, squeezing, and bending with multiple resolutions.

5.4   DEFORMATION-AWARE SENSORS

This section investigates **deformation-aware sensors** that build upon the concepts of spatial and intensity deformation mapping (see Section 5.2.1). These sensor concepts build upon a design space that consists of the following dimensions:

1. The **resolution of the intensity of deformation**, i.e., a binary (deformed vs. not deformed), multi-level, or continuous measurement of deformation.

2. The **resolution of the position of deformation**, i.e., whether only a single location or multiple locations or directions of deformation on the surface of the 3D object can be measured.

3. The **type of deformation**, i.e., a specific kind of deformation that is applied to a 3D object. In general, a deformation refers to any change in the shape or size of a 3D object.

As depicted in Figure 5.2, this section presents nine concepts for deformation sensor that cover press, squeeze, and bending deformations. These concepts are grouped by the type of deformation in the following. For each, a basic sensor is presented that capacitively senses the type of deformation either binary or with a continuous intensity. Then, the respective basic sensor is extended to additionally capture the on-object location where the force was applied or the direction of the deformation.

5.4.1 *Pressure Deformations*

This section investigates **pressure deformations** on the surface of an object. The concepts of the following sensors build upon intensity deformation mapping (see Section 5.2.3).

DIRECT PRESS SENSOR

The concept of a **direct press sensor** builds upon a surface deformation sensor that is placed inside an object. Its flexible structure allows the finger of the user to press into the object (see A and B in Figure 5.3).

The primary challenge is to find a suitable geometry for the conductor of the sensor and to preserve the deformability of the flexible structure at the same time. Hence, different types of geometries were explored by printing test objects with varying amount of infill density (10% to %80, 10% steps) and a conductor plane that was either flat or shaped like the out shape of the 3D object (see Section 5.5.2). As a result, the best strategy consists of 25% infill and designing the conductor in a 3D geometry that mimics the outer shape of the 3D object at the location where it is to be pressed. Similar to the original design of a plate capacitor, this geometry maximizes the cross-sectional area between the finger of the user and the conductor and also ensures a constant thickness of the flexible structure.

The designer defines this geometry by selecting an area of interest around an arbitrary location on the surface in the 3D CAD model. The selected area is downscaled by the required thickness of the flexible structure and translated in the normal direction to lie under the surface of the object. The volume between the surface of the object and the conductor is then filled with the flexible structure.
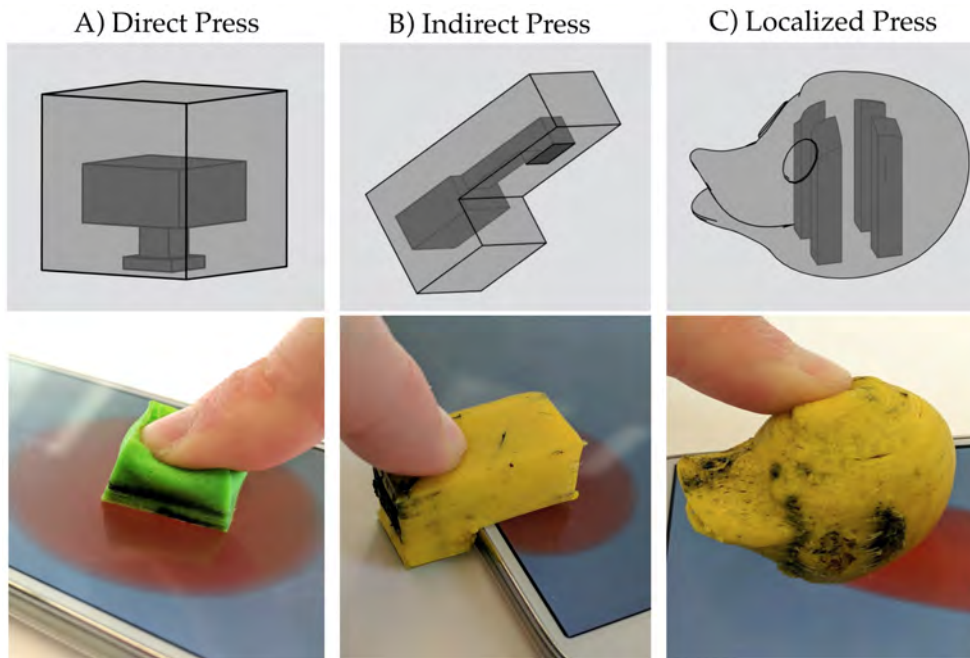
Figure 5.3: The pressure sensors illustrated as a rendering (top) and deformed by a user (bottom).

For the prototypes A and B (see Figure 5.3), both surface deformation sensors (cross-sectional size of 10×10 mm^2) are placed inside the object with 4 mm of flexible structure overlaid. Moreover, both are connected to the underside of the object using a forwarder with a size of 5×5 mm^2 at the contact face, such that the touchscreen can capture the capacitance.

INDIRECT PRESS SENSOR

While the connection can be direct, i.e., straight onto the touchscreen, it may also be **indirect**, i.e., does not have to be straight. A slightly modified conductor routing allows for forwarding press input to an arbitrary location on the touchscreen. This concept is called an **indirect press sensor**. For instance, this sensor allows capturing press input that occurs besides the touchscreen (see Figure 5.3B) or on objects with overhangs.

LOCALIZED PRESS SENSOR

The sensor for pressure input can be extended to not only capture a single pressure value but also to estimate the 1D or 2D location where the press occurs on the surface of the object. This concept is called a **localized press sensor**. It consists of a set of surface deformation sensors that are spatially

replicated into multiple distinct sensors, which each connects to a different area on the touchscreen. Hence, their capacitance values can be read out separately. This concept allows for simultaneously measuring pressure input on various distinct locations on the object. By using bilinear interpolation between all values, the location of the press on the surface can be estimated.

Figure 5.3C shows a prototype of a head of a duck that is equipped with four distinct surface deformation sensors. They are laid out in a 2×2 grid of 18×18 mm^2 (4×4 mm^2 per sensor) with 7 mm of a deformable overlay. By using bilinear interpolation, 3×3 locations can be robustly identified with this 2×2 grid.

5.4.2 *Squeeze Deformations*

This section investigates **squeezing deformations** on the surface of an object. In contrast to a press deformation, squeezing is characterized by a **bilateral** compression from two sides pointing inside the object. The concepts of the following sensors build upon spatial and intensity deformation mapping (see Section 5.2.2 and Section 5.2.3).

GENERAL SQUEEZE SENSOR

The concept of a **general squeeze sensor** builds upon a two-sided surface deformation sensor inside an object. Its flexible structure allows the finger of the user to squeeze from two sides into the object. An evaluation of varying infill densities and forms of sensors revealed that the most suitable geometry for this concept is a surface deformation sensor that mimics the outer shape of the object.

Figure 5.4A shows a prototype of an octopus object that is equipped with a surface deformation sensors (cross-sectional size of 10×10 mm^2) with 7 mm of an overlying flexible structure to both sides of the surface. The sensor is connected to the underside of the object using a forwarder with a size of 3×3 mm^2 at the contact face.

LOCALIZED SQUEEZE SENSOR

Besides the amount of squeezing, the location of the fingers on the surface can be of interest (e.g., distinguishing a squeeze from left-to-right or front-
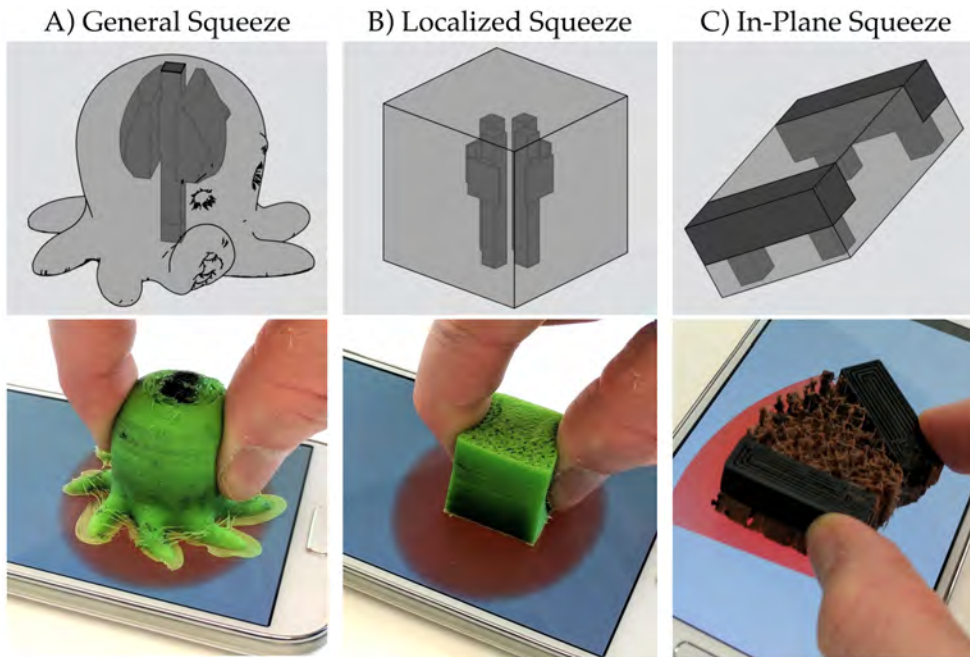
Figure 5.4: The squeeze sensors illustrated as a rendering (top) and deformed by a user (bottom).

to-rear). Therefore, the concept of the **localized squeeze sensor** build upon the general squeeze sensor as follows: Similar to the localized pressure sensor, the surface deformation sensor can be spatially replicated into multiple sensors, each facing a different direction. The rough squeeze input location is then identified from the pair of opposing sensors that have the highest value. The resolution improves further by using interpolation between adjacent sensors.

Figure 5.4B shows a prototype of a cube that is equipped with four distinct surface deformation sensors (cross-sectional size of 10×10 mm^2), aligned in 90° angles. The forwarder of each sensor connects to the touchscreen with a contact size of 3×3 mm^2. The sensors are placed at 7 mm distance from the respective faces of the cube.

IN-PLANE SQUEEZE SENSOR

Based upon spatial deformation mapping (see Section 5.2.2), the concept of an **in-plane squeeze sensor** is designed such as to detect squeeze deformations in a plane parallel to the touchscreen. For this sensor, four forwarders are placed at the outer edges on the underside of the object. Pairs of two forwarders are connected with the upper surface of the object, to ensure capacitive coupling between the finger of the user and the touchscreen. The

remainder of the object consists of a flexible structure to allows for squeezing.

When the object is deformed, the on-screen locations of the forwarders at the bottom change of the object. If a threshold for all four forwarders is exceeded, their respective distances on the screen are used to approximate a contour of the object, allowing to compute the intensity of the squeeze deformation.

Figure 5.4C illustrates a prototype of a cuboid that is equipped with four forwarders (contact size of 5×5 mm^2) of a conductor of size 30×10 mm^2 connects two of them. These conductors are separated by 30 mm of a flexible structure in-between.

This sensor concept employs the higher spatial resolution of the touchscreen to sense more fine-grained squeezing. However, it is limited to squeeze deformations that are performed in parallel to the touchscreen.

5.4.3 *Bend Deformation*

The following sensor concepts capture bending deformations inside an object based on intensity deformation mapping (see Section 5.2.3).

BINARY BEND SENSOR

The concept of a **binary bend sensor** is designed such as to detect a binary bend, i.e., whether an object is bent or not (see Figure 5.5A). Based on the concept of an intensity deformation mapping, it consists of one forwarder at the contact face of the object and a series of inner deformation sensors at its deformable tail. The user can grab the object at the outer end of its tail and deform the bendable structure. Multiple separate forwarders laid out at regular intervals on the bendable structure act as inner deformation sensors: they form a capacitive bridge that is closed as soon as the object is strongly bent. The concept builds upon an inner deformation sensor because a bend cannot be directly inferred from the distance of the finger of a user to a conductor.

One prototype, shown in Figure 5.5A, utilizes a circular forwarder on the touchscreen (diameter of 12 mm). The forwarder connects to two inner deformation sensors (each with a size of 4×2 mm^2), which end with a con-
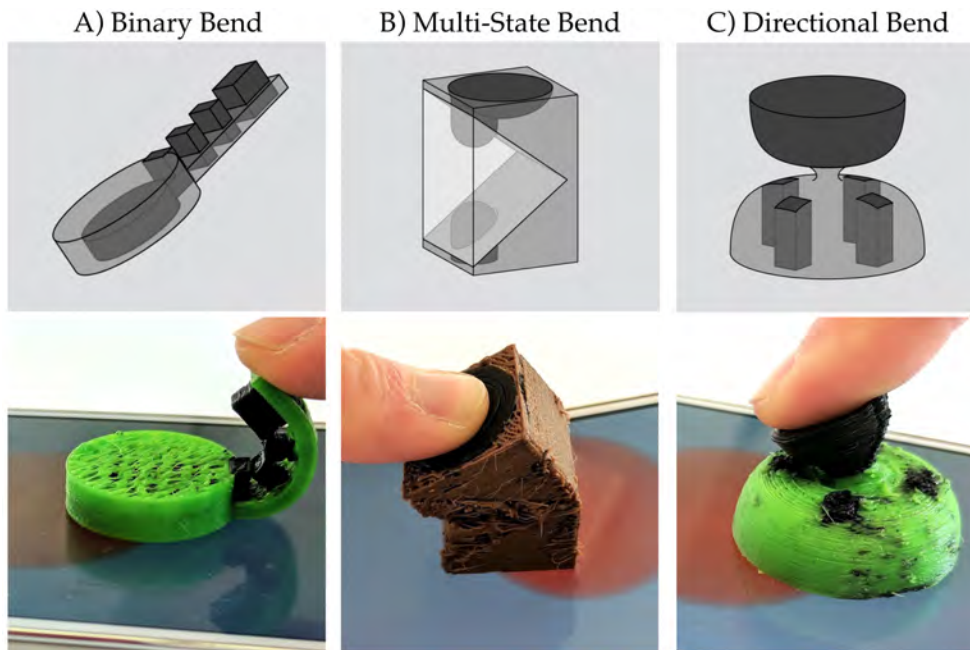
Figure 5.5: The bend input sensors illustrated as a rendering (top) and deformed by a user (bottom).

ductor for coupling with the finger of a user (size of 4×5 mm^2). Air is employed as the dielectric material in-between the inner deformation sensors (separated by 3 mm), which makes it easier to print. The capacitance significantly changes when all conductors are physically connected. Therefore, binary bends but not a bending angle can be reliably discerned using this sensor. In addition to bending, this concept can also be used to infer folding, since it can be printed in slim geometries.

MULTI-STATE BEND SENSOR

The concept of a **multi-state bend sensor** is designed such as to detect multiple bending states in a fixed direction, that is pre-defined by the designer. It builds upon the concept of an inner deformation sensor (see Section 5.2.1) that consists of multiple parts: The upper half of the sensor connects to the finger of a user through a forwarder. The lower half of the sensor connects to the touchscreen through a forwarder. By bending, the user reduces the distance between the upper and the lower forwarder. Hence, a capacitance change is induced on the screen. As will be shown in Section 5.7.3, four bending states can be reliably discerned using this concept.

Figure 5.5B shows a prototype. It utilizes a circular upper forwarder (diameter of 17 mm) combined with a circular lower forwarder (diameter of 5 mm) separated by 7 mm of a flexible structure in between.

DIRECTIONAL BEND SENSOR

The concept of a **directional bend sensor** can infer bendings in two dimensions of an object. It focuses on bending of two volumetric parts that are connected by a thinner structure (e.g., the head of a figurine is connected to its torso by a thinner neck, allowing the head to bend around two axes).

This sensor concept is based on an inner deformation sensor and extends the concept of a multi-state bend sensor as follows (see Figure 5.5C): The upper half of the sensor connects to the finger of a user through of a forwarder. The lower half of the sensor connects to the touchscreen through multiple distinct forwarders that are arranged circularly. Both parts are connected by a thin flexible structure, printed with high density to strengthen the connection.

When the object is bent in one direction, the forwarder of the upper half gets closer to one or two of the forwarders of the lower half, while it gets more distant from the remaining forwarders. This deformation results in capacitance change that can be measured by the touchscreen. A bending direction between 0° and 360° can be estimated with this concept by interpolating between the capacitance of adjacent lower forwarders.

Figure 5.5C illustrates the prototype. It utilizes a circular upper forwarder (diameter of 24 mm) mounted on a thin dielectric structure (diameter of 3 mm). The lower half consists of four distinct forwarders (contact size of 5×5 mm^2) connecting independently to the touchscreen. The sensor concept was successfully tested for up to eight forwarders placed at the lower half of the object.

5.4.4   *Touch Contact Input*

Of note is, that all these sensors are also suited to sense touch contact, i.e., when the finger of a user is touching the forwarder with minimal force. This touch results in a measurable increase of capacitance, which can be differentiated from no touch contact, but which is considerably weaker than when deformation occurs.

5.4.5   *Combining and Integrating Sensors*

While deformation-aware sensors by themselves already offer a rich expressiveness, they can also be combined and integrated into a single object. A combination results in various configurations that provide even more interaction possibilities because the combination enables parallel or sequential deformation interactions. As detailed in Section 5.6, this combination of sensors offers rich deformation interactions: The duck-shaped alarm clock (see Figure 5.9) illustrates two sensors in a single object routed onto the contact area to simultaneously sense press and squeeze input. The tree-shaped objects (see Figure 5.8) feature a combination of a squeeze and bend sensor to support different deformation interaction with the same object. While the independent usage of each sensor is supported, a combination of sensors also enables a variety of combined interaction: For instance, while an object is bent, an additional firm press initiates an action, or a squeeze is required after a bent to a certain degree.

In order to integrate multiple deformation-aware sensors in a 3D object, the forwarders that connect each sensor need to be routed to distinct locations at the underside of the object. As a consequence, the capacitance of each sensor can be read out independently and simultaneously by the touchscreen. While the routing process can be automatized (see Section 3.4), sufficient spacing between conductors is required. For the reference apparatus, a spacing of 5 mm between forwarders was satisfactory to ensure independent capacitance measurements of each sensor.

In conclusion, FLEXIBLES allows multiple sensors to be combined and integrated into a 3D object. Their measurements can be read out independently and simultaneously by the capacitive touchscreen.

5.4.6   *Calibration of Sensors*

A FLEXIBLE requires manual calibration once before use. To that end, the user places the object onto the touchscreen and holds it without deforming it. The system records a series of capacitance values and stores the mean as the value for minimal deformation. Then, the user deforms the object as much as possible. The system again records a series of values and stores the mean as the maximal deformation. With these values, the minimum and maximum of an empirically-derived mapping function are adjusted to take
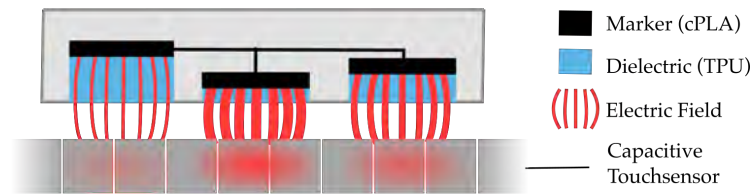
Figure 5.6: FLEXIBLES are identified and localized by varying the thickness of a dielectric between a marker and the touch sensor, resulting in a measurable difference in capacitance.

variations in printing quality and human capacitance into account. Details on such mapping functions are presented in Section 5.7.

5.4.7 *Identifying and Localizing Objects*

FLEXIBLES are identified and localized on the touchscreen via unique rotation-variant point patterns (cf. [Cha+12; Kra+11; Voe+15]). These patterns are made of conductive material and are directly 3D-printed into the contact area of the object. This concept improves over prior work by increasing the number of states that a single capacitive point can encode, leveraging the opportunities of 3D printing combined with capacitance measurements. By varying the amount of dielectric material that is printed between a capacitive point and the touchscreen, the intensity of the capacitance can be controlled (see Figure 5.6).

Informal tests revealed that three different states of a point could be reliably distinguished. In order to differentiate each FLEXIBLE, the relative strength of all points in the pattern to each other is considered. Once an object is recognized, the respective capacitive values inside the contact area (known from the 3D model) are used to recognize deformations. Android apps can use a library on a device that provides access to raw capacitances. The library sends events when a FLEXIBLE has been detected, its position or orientation changed, or deformation was detected.

5.4.8 *Conclusion*

As depicted in Table 5.1, the set of deformation-aware sensors each features an instance of the FLEXIBLES design space (see Section 5.2.1). While, in gen-

	Pressing		Squeezing			Bending		
	(In-)Direct	Localized	General	Localized	Inplane	Binary	Multi-State	Directional
Deformation Resolution	cont. (sigmoid)	cont. (sigmoid)	cont. (sigmoid)	cont. (sigmoid)	cont.	binary	4 levels	4 levels
Position Resolution	none	3 × 3 locations	none	2 directions	none	none	none	8 directions
Number of Forwarders	1	4	1	4	4	1	2	8
Deformation Mapping	intensity	spatial	intensity	intensity	intensity	intensity	intensity	intensity
Material Composite								

Table 5.1: Classification of each FLEXIBLES sensor regarding the design space.

eral, deforming a 3D object is a multi-faceted type of interaction, the presented set of sensor concepts focuses on pressing, squeezing, and bending.

Regarding deformation resolution, the evaluation in Section 5.7 shows that pressing and squeezing deformation can be continuously approximated with a Sigmoid function. Moreover, users can distinguish four levels of bending reliably. While practical in many cases, a more fine-grained resolution for bending could further improve the expressiveness of FLEXIBLES.

Regarding position resolution, localized press and squeeze were successfully tested with a 2 × 2 grid for the reference apparatus. Also, the directional bend sensor was successfully tested with eight circularly arranged forwarders. As the printing resolution increases, the sensor concepts scale to a more fine-grained position resolution.

The in-plane sensor concept builds upon spatial deformation mapping, i.e., it employs the higher spatial resolution of the touchscreen to sense more fine-grained squeezing. The prototype is illustrates squeeze deformations that are performed in parallel to the touchscreen. In principle, this concept can be used to sense more deformation (e.g., stretching) in high-resolution at object location further away from the touchscreen.

5.5 IMPLEMENTATION

The following section details on the reference apparatus used to validate FLEXIBLES.

5.5.1 *Sensing*

Capacitance raw data was obtained from a regular smartphone (Samsung Galaxy S4), and tablet (Samsung Galaxy Tab S2) equipped with a standard touch controller (Synaptics S5000B). By rooting the Android phone and activating Synaptics debug mode, raw capacitive values from the sensor as an 8-bit image with a resolution of 28x16 at 9 FPS are obtained. Up to 30 FPS are possible (cf. [HBK15]).

5.5.2 *Fabrication*

The reference apparatus for FLEXIBLES operates with a commonly available dual-extrusion 3D printer (Ultimaker Original with dual extrusion kit), as this makes the approach accessible to a wide audience. The prototypes were manually designed using Blender and reusable OpenSCAD scripts that allow generating sensing structures depending on adjustable parameters, such as the size or the thickness of conductors.

The sensing structure consists of carbon-doped Proto-pasta Conductive PLA (cPLA) with a volume resistivity of $30 - 115 \, \Omega * cm$. cPLA was printed with a 0.8 mm thick nozzle at a temperature of $220 \, °C$. The cooling fan and retraction of 5 mm (speed $20 \, mm/s$) were used.

The flexible structure is printed with NinjaFlex TPU, a Polyurethane composition (material shore hardness 85A), and a 0.4 mm thick nozzle at a temperature of $230 \, °C$ (retraction of 12 mm, the cooling fan turned off).

5.5.3 *Infill Pattern and Density*

The infill and density of the flexible structure are essential factors when fabricating deformation-aware objects because the composite of air chambers
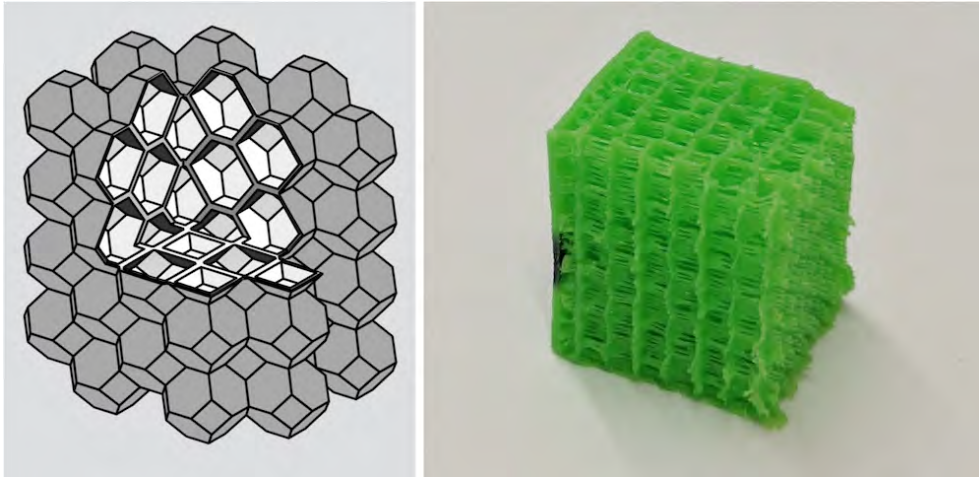
Figure 5.7: Illustration of the 3D Honeycomb infill pattern as a rendering (left) and as a 3D-printed deformable TPU cube (right).

and deformable material both affect the dielectric properties required for capacitive sensing and the deformability of the object. Common infill patterns, implemented in readily available slicing software, were tested in order to identify a suitable infill pattern for a FLEXIBLE. As a result, the 3D Honeycomb pattern was best suited because the inherent 3D structure of each honeycomb allows for equal deformations in each direction (see Figure 5.7). An infill density of 25%, i.e., deformability of up to 1/4 of the original length, resulted in adequate sensing performance. This density optimizes the deformability and dielectric constant of the flexible structure, i.e., the material between the sensing structure and the finger of the user.

Designers may want to reduce the density to increase the deformability. However, as shown by [Mos+16], a smaller infill density would reduce the overall dielectric constant of the flexible structure due to the dielectric constant of NinjaFlex TPU being twice as high compared to air. As a consequence, the sensitivity of the capacitive sensor would be reduced.

The infill density can be increased up to 100% to reduce the deformability. As the deformable material is very rigid at an infill density of 100%, designers may use this effect to adjust the haptic of the object or avoid unintentional deformations. Moreover, multiple infill densities for varying parts of the object can be achieved by splitting the 3D model of the object into multiple parts and assigning each a specific density.
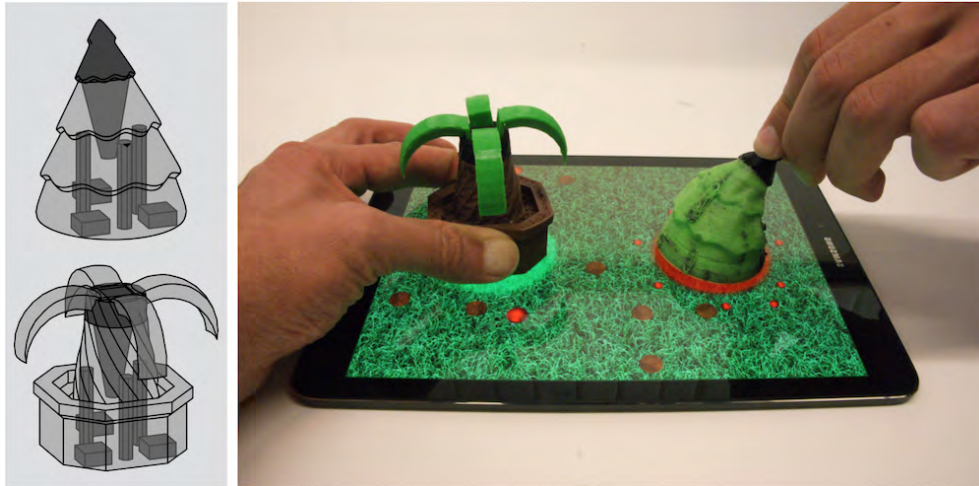
Figure 5.8: Interactive board game: two angry trees throw their fruits at each other.

5.6 EXAMPLE APPLICATIONS

Three interactive example applications were developed to demonstrate the practical feasibility and the potential of FLEXIBLES.

5.6.1 *Angry Trees*

The first example is a tangible game, inspired by Angry Birds (see Figure 5.8). Users can play against each other by using two FLEXIBLES: a palm tree and a Christmas tree. By bending and then releasing a tree, virtual fruits (either coconuts or Christmas balls) are thrown at the opponent. The on-screen trajectory of the fruits takes into account the current position and rotation of the tree on the screen. The amount of bending defines how far the fruits are thrown on the screen with simple physics simulation. By squeezing and releasing a tree, all fruits are thrown. If a tree has no fruits left, the fruits lying on the screen can be picked up again by squeezing.

5.6.2 *Alarm Duck*

To demonstrate the use of FLEXIBLES for interactive devices, a docking station, shaped like a rubber duck, was implemented that operates as an alarm clock (see Figure 5.9). It enhances a smartphone with deformation-aware controls. The system launches an alarm clock application when a user docks the
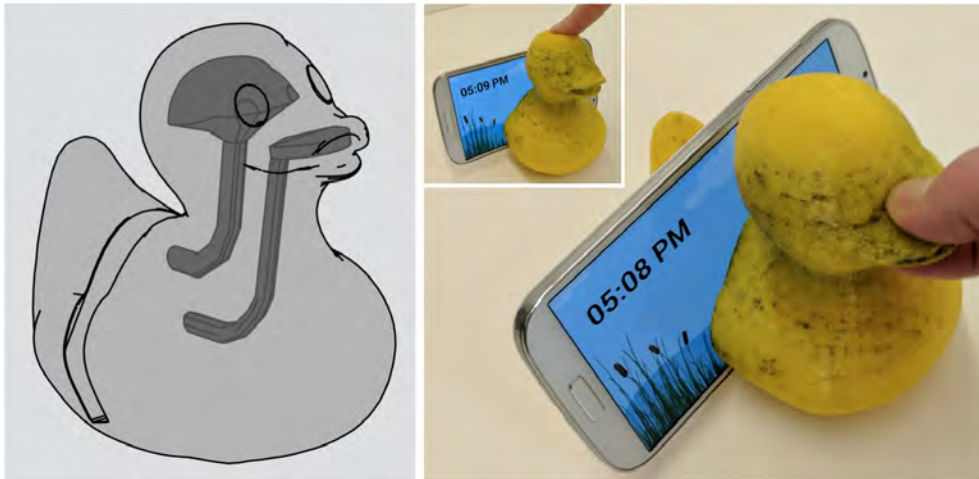
Figure 5.9: The alarm clock reacts to a squeeze or press (top left).

smartphone at the back of the duck. The user sets the alarm time by squeezing the beak of the duck until the desired wake-up time is displayed on the smartphone. By squeezing more firmly, the time on the display changes more quickly.

If an alarm is set, the user can press on the top of the duck for easy-to-reach functionality. A slight press shows the time left to sleep on the displays of the smartphone. A harder press lets the system read the time out loud. When the alarm goes off, the smartphone plays a chirping sound. The user can squeeze the beak to turn on snoozing. The length of the snoozing time depends on how firmly the user squeezes.

5.6.3 *Squeezy Tube*

In this example, a squeezable tube is used together with a touchscreen (see Figure 5.10). In analogy to a physical pipette, users can select primary colors by placing the tube onto a color on the display and then squeeze the tube. The color can then be dispensed by placing the tube on another screen location and squeezing it. Depending on the amount of squeezing, more or less color is dispensed, which allows mixing of colors. This interaction opens up a broad range of tangible applications in education (cf. [Sch+12]), for instance to more directly combine different amounts of virtual fluids.

In conclusion, FLEXIBLES can be used to enrich today's touch interaction via physical manipulation of digital content, for instance, to provide faster, more fine-grained, or eyes-free input control on capacitive touchscreens. They en-
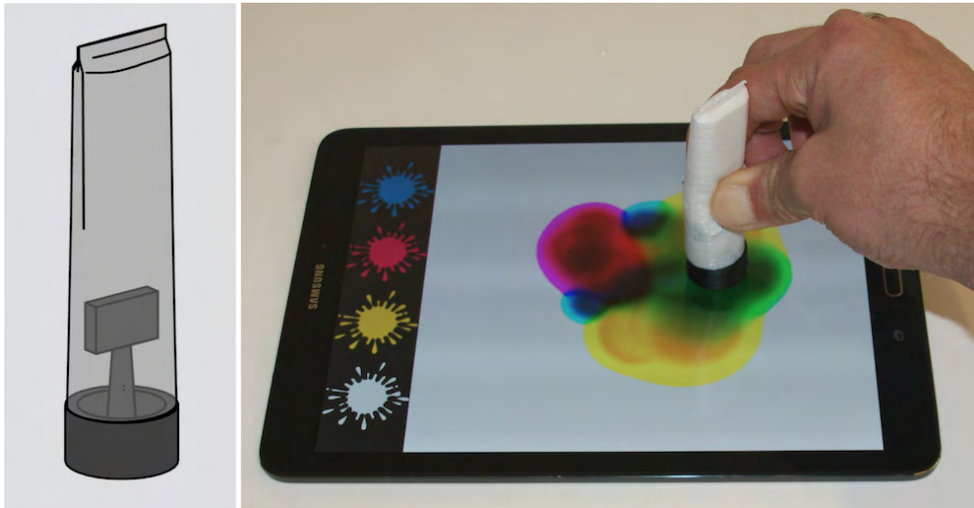
Figure 5.10: Mixing colors by squeezing them out of a deformable tube.

compass the benefits of tangibles but add the additional input dimension of precise eyes-free deformation input. Also, they enable engaging interactions with customized 3D-printed tangible objects that are controlled by a smartphone without any additional power supply.

5.7 EVALUATION

This section presents technical experiments that evaluate the accuracy of the press, squeeze and multi-state bend input sensors with users.

5.7.1 *Accuracy of Pressure Input*

The accuracy of the press sensor was assessed with the prototype shown in Figure 5.3B.

SETUP & TASK

The main objective of this evaluation was to compare the raw capacitance measured by the touchscreen with the actual force with which a user is pressing the object. To that end, a force sensing resistor (FSR) was mounted inside an object equipped with a direct press sensor. The FSR was placed in-between the flexible and the sensing structure. As the object was being pressed, a force was exerted onto both the FSR and the press sensor. The
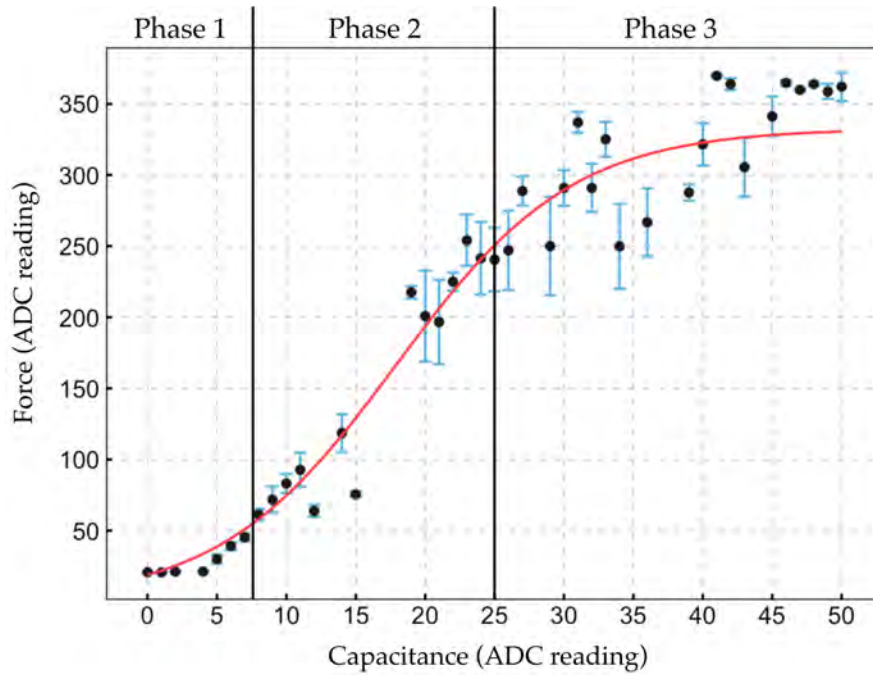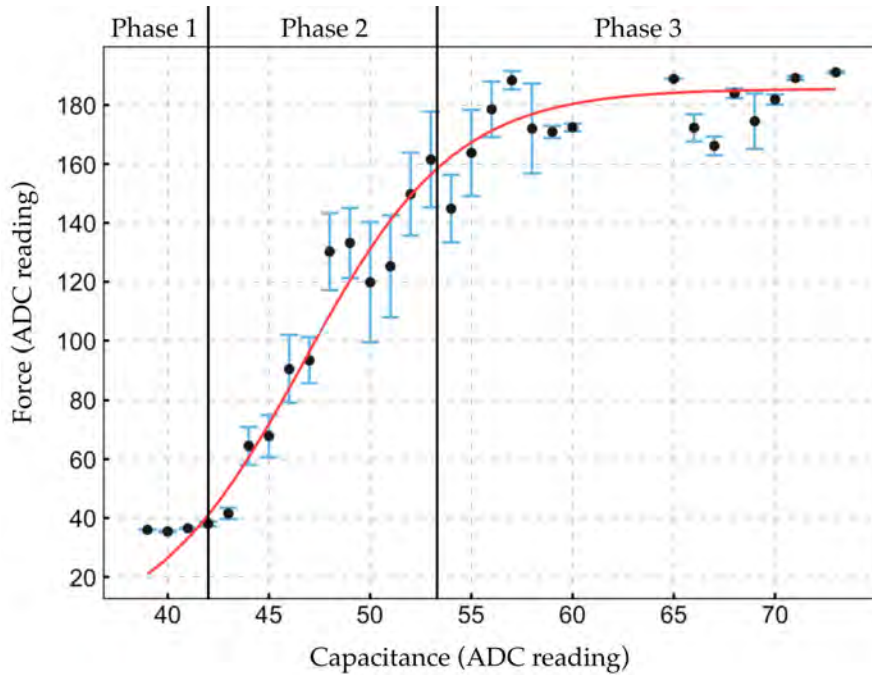
Figure 5.11: Mean forces (with standard deviations) for measured capacitances for press input. The mapping function is shown in red.

analog-to-digital (ADC) readings from the FSR and raw ADC readings from the capacitive touchscreen controller were measured and logged simultaneously by wiring them to the same computer.

Five participants had the task to each press onto the object with a continuously increasing normal force, ranging from no force to a firm press. This procedure generated 500 data points. By conducting the study with users instead of a mechanical apparatus, the setup accounts for the inter-individual differences in users' capacitive responses.

RESULTS & DISCUSSION

As shown in Figure 5.11, the press sensor is capable of sensing multiple intensities of pressure. The mapping between measured capacitance and force undergoes three phases: For small forces in phase 1 (<55), the capacitance increases without considerable effect on the measured force. In this phase, the finger slightly touches the object with an increasing contact surface. This phase is followed by phase 2 (between a force of 55 and 250) where the mapping between capacitance measurements and applied force is approximately linear. For large forces in phase 3 (>250), the flexible structure reaches its limits in elasticity, and the mapping is non-linear.

This behavior can be modeled with a non-linear least squares model based on a sigmoid. Using this model, a mapping function from capacitance C to force $f(C) = a/(1 + exp(-b * (C - c)))$ with a = 332.73 ($\sigma = 5.92$), b = 0.16 ($\sigma = 0.007$), and c = 17.89 ($\sigma = 0.50$) with a residual standard error of 43.8 can be computed.

The response of an object may differ due to variations in the printing process or individual properties of the user. As discussed, this needs to be compensated by adjusting the minimum and maximum of the mapping function via calibration. The mapping function is specific to the geometry of the sensor.

5.7.2 *Accuracy of Squeeze Input*

The accuracy of the squeeze sensor was assessed with the prototype shown in Figure 5.4A.

SETUP & TASK

This evaluation used the same setup and the same task as for the evaluation of pressure input. That is, 500 samples of squeezing (i.e., a set of capacitance and FSR readings belonging together) were collected with five study participants who had to squeeze an object with varying force.

RESULTS & DISCUSSION

Figure 5.12 illustrates that this sensor can measure multiple intensities of squeezing. The mapping between measured capacitance and force undergoes three phases: For small forces in phase 1 ($<$40), the capacitance increases without considerable effect on the measured force. In this phase, the finger slightly touches the object with an increasing contact surface. This phase is followed by phase 2 (between a force of 40 and 160) where the mapping between capacitance measurements and applied force is approximately linear. For large forces in phase 3 ($>$160), the flexible structure reaches its limits in elasticity, and the mapping is non-linear.

This behavior can be modeled with a non-linear least squares model based on a sigmoid. Using this model, a mapping function from capacitance C to force $f(C) = a/(1 + exp(-b * (C - c)))$ with a = 185.56 ($\sigma = 4.38$), b = 0.27

Figure 5.12: Mean forces (with standard deviations) for measured capacitances for squeeze input. The mapping function is shown in red.

($\sigma = 0.02$), and c = 46.71 ($\sigma = 0.32$) with a residual standard error of 42.1 can be computed.

Of note is, that the relation between measured capacitance and force is very similar for the press and squeeze sensor. As discussed, the data for pressure and squeeze deformations can be grouped into three phases: Phase 1, in which the finger slightly touches the object with an increasing contact surface. Followed by phase 2, in which the flexible structure is deformed approximately linearly with the distance to the sensing structure. Completed by phase 3, in which the flexible structure is nearly compressed to its maximum.

5.7.3 *Accuracy of Bend Input*

The accuracy of the multi-state bend sensor was assessed with the prototype shown in Figure 5.5B.
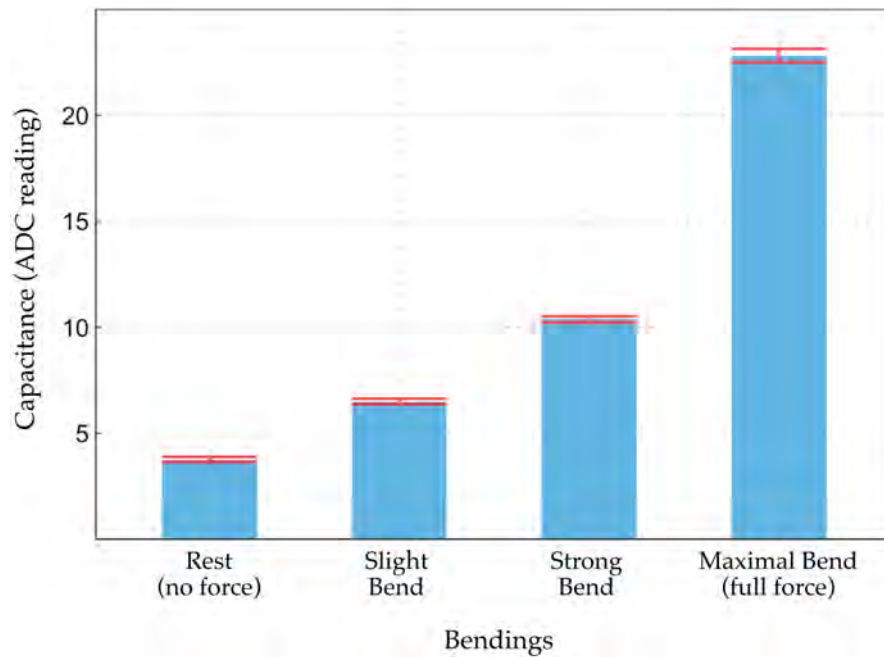
Figure 5.13: Mean capacitances (with standard deviations) for four pre-defined bend states.

SETUP & TASK

The raw capacitive ADC readings were recorded for four pre-defined bend states as users were not able to reliably replicate more than four levels of bending in an informal pre-study: rest state (with no force applied), slight bend, strong bend, maximal bend (with maximal force applied). Four bend states were tested as users were not able to reliably replicate more than four levels of bending in an informal pre study. Participants had to deform the object to match a given bend state. In each trial, a computer screen displayed an image that showed a photograph of the object in the target state. For each condition, capacitance data was recorded. In total, 1200 samples were collected (for five users).

RESULTS & DISCUSSION

Across all samples, the mean values were 3.77 ($\sigma = 2.1$) for rest state, 6.51 ($\sigma = 2.23$) for slight bend, 10.37 ($\sigma = 2.55$) for strong bends, and 22.81 ($\sigma = 5.5$) for maximal bends (see Figure 5.13). The results show that at least four different bend states can be reliably distinguished across different users.

5.8   DISCUSSION AND LIMITATIONS

This chapter presents first results on how to leverage capacitive coupling between a touchscreen and a 3D-printed object to sense specific pre-defined deformations. However, FLEXIBLES have limitations that must be considered during design, fabrication, and sensing.

5.8.1   *Set of Deformations and Resolution*

In general, a flexible object can be deformed in many complex ways. This chapter explores a basic and widely used set of deformations. More complex deformations (e.g., twisting) or continuous, high-resolution deformation input are not covered. The main reason is that the electrical properties of today's deformable conductive printing materials are interference-prone (see appendix of [Bäc+16]).

Despite these restrictions, FLEXIBLES allows capturing multiple intensity levels of pressing, squeezing and bending, alongside information about the location or direction of the deformation.

5.8.2   *Scalability and Geometries*

Scalability is an important issue, as the size of a FLEXIBLE and of the capacitive touchscreen may vary from small (e.g., smartphones) to very large (e.g., wall-sized displays). The sensors presented in this chapter use sensing structures that are optimized for the size of a fingertip (16-20mm [DRS03]). Hence, the results apply only to deformations that are performed with fingers. Also, the approach requires a volumetric object inside which conductors can be routed. Therefore, geometries with thin structures, high curvatures, or cavities remain challenging.

The rather low resolution and the high nozzle diameter of today's commodity 3D printers limit the minimal size of a sensor. Using the reference apparatus, the minimal cross-sectional size of a conductor is 3×3 mm^2. The second limit to miniaturizing sensors relates to the flexible structure. If shrunk, the sensing resolution will be reduced because the flexible structure is deformable to a lesser extent. For very thin objects (<4 mm), the sensors will

not function because there is no space for compressing the flexible structure. Future printers and materials, which can be extruded with smaller nozzles, are likely to alleviate these restrictions.

Designers may increase the cross-sectional size of a conductor to enhance its sensitivity or to better match a larger body part for interaction (e.g., hands). However, the maximum size of a sensing structure is not only limited by the print volume of the 3D printer (for the reference apparatus $21 \times 21 \times 20$ cm^3). It is also limited by the rather low conductivity of the conductive material and by environmental stray capacitance. Forwarders of length up to 15 cm were successfully tested without noticing an influence on sensing performance. However, designers should construct conductors only as large as necessary for their use case to minimize influences by stray capacitance. It is also possible to increase the thickness of the flexible structure, to enable greater deformations. However, an increased thickness of the flexible structure weakens the capacitive effect. Therefore, the size of the sensing structure should be increased accordingly. A thickness of 4 mm to 10 mm is a good trade-off between the sensitivity of the sensor and the deformability of the material.

5.8.3 *Material Fatigue and Latency*

No evidence of material fatigue was found after repeatedly deforming the objects (more than 500 times). This finding is in line with Ion et al. [Ion+16] who demonstrate that the same TPU material can be deformed 5000 times without noticeable degradation.

Also, the approach does not rely on deforming the conductive material; only non-conductive parts are deformed. This characteristic avoids latency known from deformable conductors, such as eTPU, whose resistance is dependent on both history and rate of deformations performed over time [Bäc+16].

5.8.4 *Movement of Objects*

Deformation sensing and object movement can occur in parallel. As the spatial resolution of touch grids is limited, the forwarders of a FLEXIBLE are not always perfectly aligned with one intersection point of the grid during object movement. In that case, the capacitance splits up into different intersection

points, which affects the sensor readings. This problem can be solved by using a specialized kernel with bilinear interpolation of readings from adjacent intersection points.

FLEXIBLES printed with TPU at their lowermost layer exhibit higher stiction and friction compared to PLA on touchscreen glass. Nevertheless, participants easily moved TPU objects. Depending on the application, designers may want to increase or decrease the stiction or friction of a FLEXIBLE by varying the ratio of PLA and TPU in the lowermost layer of the object. While the 3D printer used in the reference apparatus supports only two materials, this requires a 3D printer that can handle at least three materials (cPLA, TPU, and PLA). Throughout this thesis, 3D printers were released that support up to five different materials (cf. [Pru18]).

5.8.5   *Unintentional Input*

Capacitive measurements could be affected by capacitive effects when the user is unintentionally touching another location. Likewise, capacitive cross-talk between adjacent conductors could influence the sensor readings. To minimize these effects, designers should consider the following aspects:

1. The cross-sectional area of a surface deformation sensor should be much larger than of the remaining forwarders inside the object.

2. Any forwarder should be located preferably in the center of the object instead of close to its outer sides unless the forwarder is designed to be touched by users for capacitive coupling. A forwarder should be as thin as possible and distant from other forwarders. The specific dimensions depend on the resolution of the printer and the conductivity of the material. Adjacent forwarders should maintain a minimum distance of at least 5 mm.

3. The infill density at non-interactive locations should be increased to avoid accidental deformations.

Due to the rather low resolution of today's 3D printers, the larger cross-sectional area of wires is a reason for cross-talk between conductors that are routed in parallel. This issue is of note for objects with many spatially replicated forwarders or combined sensors, which require many forwarders. Future printers are likely to mitigate this issue due to increased resolution.

5.8.6 *Commodity Touch Sensing Hardware*

Despite using unmodified commodity touch sensing hardware, the approach uses a debug interface to capture raw capacitance data. Open access to such data would require a modified driver which could be supplied by OEMs.

5.9 CONCLUSION

This chapter presented FLEXIBLES, 3D-printed flexible tangibles that add deformation-awareness to passive tangibles on standard capacitive touch sensing hardware. In summary, the main contributions of this chapter are:

1. Two principles of mapping deformations in 3D-printed objects using commodity capacitive touch sensing hardware.

2. 3D-printable sensors to capacitively detect multiple levels of pressing, squeezing, and bending input on passive 3D objects. Mechanisms can be combined in an object.

3. Results from technical experiments investigating the accuracy of deformation sensing and example applications validating the practical feasibility of the approach.
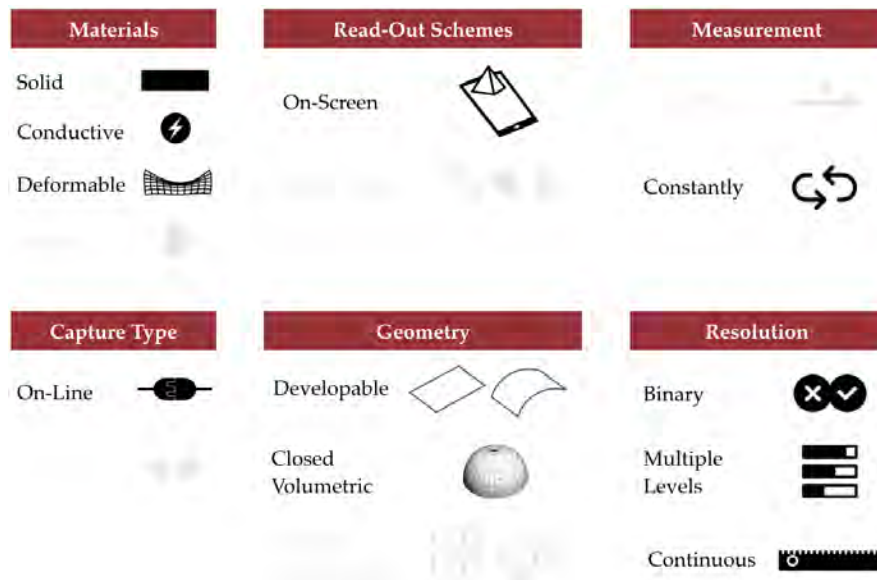
Figure 5.14: The classification of FLEXIBLES regarding the design space of 3D-printed interaction.

FLEXIBLES enable many new possibilities for the interaction with on-screen tangibles and cover a broad spectrum on the design space of 3D-printed interaction (see Figure 5.14). It consists of two deformation mapping principles and a set of 3D-printable sensors that constantly capture press, squeeze, and bend input on a variety of resolutions. They can be integrated within developable and closed-volumetric geometries. A FLEXIBLE itself consists of deformable and solid materials with embedded solid conductive sensing structures that can be 3D-printed in a single pass on a consumer-level 3D printer without further modifications.

The next part of this thesis adds **environmental interaction**, i.e., the detection of stimuli that occur due to the usage of a 3D-printed object. Therefore, the next chapter moves beyond the exploration of deformation-based input and investigates a liquid-based sensing approach that can infer tilting and motion interactions performed with a 3D-printed object.

Part IV

ADDING ENVIRONMENTAL
INTERACTION

6

LIQUIDO: 3D-PRINTED TILT AND MOTION SENSING

The last three chapters focused on hover, touch, and deformation interactions around, on, or inside 3D-printed objects. While these contributions already cover a broad range of interactive possibilities, they do not consider interactions based on **3D posture and movement** of an object in 3D space. Therefore, this chapter contributes Liquido, an approach to easily sensing a variety of tilting and motion interactions. By combining 3D-printed capacitive sensing, explored in the previous chapters, with embedded liquids, Liquido measures various liquid levels and infers tilting or motion.

The remainder of this chapter is structured as follows. Section 6.1 discusses related work. Section 6.2 introduces fabrication pipeline and the liquid-based capacitive sensing principle and Section 6.3 details on the generation and design of objects. On this basis, Section 6.4 presents a set of sensors for capturing various forms of tilting and motion input. This section is followed by Section 6.5 that presents the implementation of sensing and fabrication. Then, Section 6.6 demonstrates a set of interactive example applications and Section 6.7 reports on a technical evaluation of the suitability of different liquids and that changes in capacitance readings can be reliably mapped to tilting and motion. To conclude, Section 6.8 discusses the limitations of Liquido.

6.1 RELATED WORK

The following section shortly presents relevant research that employs liquids for HCI and discusses them regarding LIQUIDO. Section 2.1.3 discusses the majority of related work.

6.1.1 *Liquid-Based Interaction*

Liquids have been used in HCI for input and output before. They are often used for tactile or haptic feedback by varying the amount of liquid in an object [CWB13], splashing onto users fingers [RMS13], or through controlling the viscosity [Jan10]. Moreover, researchers investigate interactions in a liquid [SPH12], sensing touch through liquid displacement [HKI08], and detection of liquid levels without wires [DLY02].

The use of liquids to sense tilting builds upon a known principle called **liquid capacitive inclinometers**, i.e., the tilt is derived from varying coverages of liquid on one or multiple capacitive sensors. Whereas Takemura et al. propose a liquid rate gyroscope that uses a dielectric liquid to sense tilt [Tak+09], they require a high voltage power supply and a special liquid.

LIQUIDO proposes to use tap water combined with off-the-shelf 3D printing and tinkering equipment (e.g., an Arduino). Moreover, many methods require electronic components that need to be produced and assembled. LIQUIDO is applicable in different parts inside of many volumetric objects out-of-the-box with little effort. It is light-weight, easy-to-apply and operates on standard off-the-shelf 3D printers and does not require embedding components after printing.

6.2 FABRICATION AND SENSING APPROACH

Multi-material fabrication is often limited to either solid or deformable materials. As a consequence, the fabrication of moving mechanical parts inside an object is difficult to achieve. Therefore, this chapter proposes to embed liquids into 3D-printed objects **while printing** to easily sensing a variety of tilting and motion interaction. Unlike moving mechanical parts that must be assembled after printing, this approach does not require conventional as-

sembly but allows the fluid to be embedded seamlessly during the printing process without requiring post-treatment.

6.2.1 *Fabrication of Liquid-Filled Objects*

As depicted in Figure 6.1, LIQUIDO involves a three-step printing process for liquid-filled interactive 3D objects:

1. Hybrid objects are designed and 3D-printed with an empty cavity.

2. During printing, the 3D printer stops and a liquid is filled into the cavity.

3. The 3D printer continues to seal the cavity.

During printing, the 3D printer needs to be stopped once to fill in the liquid. This step may be automated using a liquid pump mechanism that can be integrated or attached to the printer (cf. [Zeh+17]) or a liquid deposition modeling system (cf. [Wan+16]).

6.2.2 *Sensing Principle*

In order to sense the movement of liquid inside of the cavity, conductive electrodes are distributed at the wall of the cavity inside the 3D object. Liquid levels are then measured at various locations inside the cavity using capacitive sensing. From these liquid levels, LIQUIDO determines the location and motion of the liquid and infers the movement of the 3D object.

Figure 6.1: Fabrication process: (a) Start 3D printing, (b) stop & add liquid, (c) continue printing to seal object & sense tilting or motion.

A 3D object can contain multiple liquid-based **movement sensors**. To that end, a LIQUIDO object can be designed using a similar graphical application and interaction techniques as described in Section 3.3. First, the user loads a volumetric 3D model that is shown in a 3D view of the application. Second, the user may add various movement sensors to the model by using a two-step interaction technique:

1. She selects a movement sensor from a sidebar.

2. She adds the sensor to the object via dragging and dropping it onto a part of the 3D model.

After adding movement sensors, the application automatically creates required conductive sensing structures and routes all necessary wires. Finally, the user can export printer-ready 3D models.

Since liquids tend to level out horizontally, they can be used to determine motion or tilting regarding gravity. Therefore, this section investigates **liquid-based movement sensors**, that build upon a design space that consists of the following two dimensions:

1. The **resolution of movement**, i.e., a sensor may infer a binary movement, multiple levels of movement, or a continuous movement.

2. The **number of detectable directions** of movement, i.e., a sensor may detect the movement of a liquid in one, two, or three dimensions.

This section explores the design space by proposing concepts for two liquid-based movement sensors, that build upon the same principle as **liquid capacitive inclinometers**. That is, the tilt is derived from varying coverages of liquid on one or multiple capacitive sensors. Based on this underlying principle, a sensor either detects **one-dimensional continuous**, or **two-dimensional multi-level** liquid movements. They can be 3D-printed without printer modifications and provide enough room for the liquid to flow. Moreover, this section discusses the set of tilt and motion interactions enabled by both sensors.
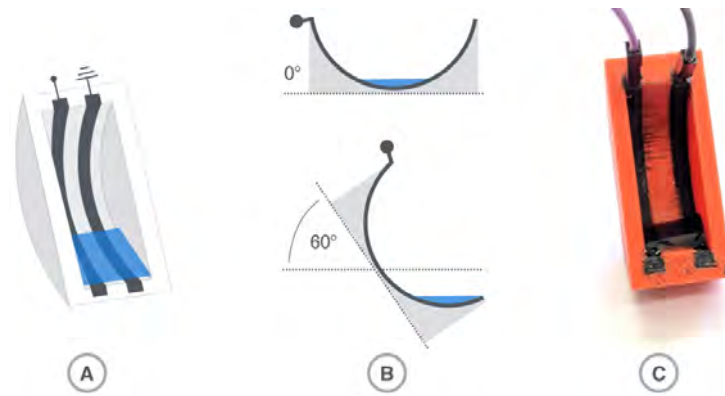
Figure 6.2: The halfpipe sensor filled with liquid as a schematic in 3D (A) and 2D (B). C illustrates a prototype.

6.4.1 *Halfpipe Sensor*

The **halfpipe sensor** can detect continuous one-dimensional tilts in combination with minimal wiring. It consists of a chamber that is formed like a halved cylinder to achieve the same liquid level at any tilt (see Figure 6.2). Two equally sized (curved) conductive electrodes are printed parallel to each other alongside the cylindrical surface. A small amount of liquid equally covers both electrodes.

The following phenomenon is exploited to measure tilting with the first electrode: The closer a dielectric liquid gets towards a capacitive sensor, the higher the capacitance. That is, if an electrode is covered by liquid at its end, less capacitance is measured at its start (see Figure 6.2b). To that end, the dielectric liquid has to be connected to the same ground as the sensor. Thus, the second electrode is used for grounding. In general, this sensor requires two distinct wires of which one is connected to a capacitive sensor and the other to ground. To further reduce the number of wires, the human body can also be used as ground (for this, a user has to touch the second electrode). LIQUIDO uses linear regression to map raw capacitance to a tilt angle. For calibration of the linear regression function, raw data for one extreme tilt (i.e., the maximal tilt in one direction) and the horizontal tilt (i.e., the non-tilted rest position of the liquid that equals 0°) needs to be recorded.

Figure 6.2 shows a prototype that is constructed to keep liquid up to ±60° and, thus, detects continuous tilts from -60° to +60°. In general, due to the cylindrical design, this sensor can cover a broader range of tilts by extending the electrodes.
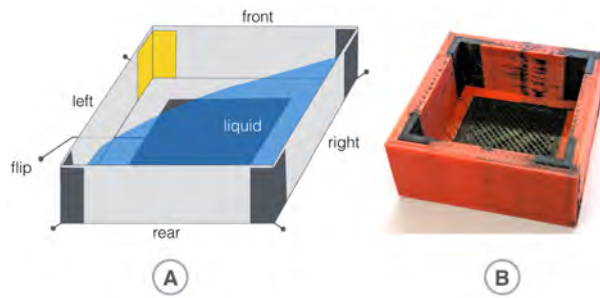
Figure 6.3: A tilted cubic sensor: One electrode is triggered due to a lack of liquid (A). B illustrates a prototype.

# of grounded electrodes	tilt
four	balanced
three	to one vertex (4x)
two	to one edge (4x)
zero	flipped over

Table 6.1: Possible tilt states when using the cubic sensor.

6.4.2 *Cubic Sensor*

While the halfpipe sensor allows measuring continuous tilts in one dimension, the **cubic sensor** measures discrete tilts in two dimensions. It consists of a rectangular chamber with four distinct electrodes in each vertex (see Figure 6.3). In a balanced position, all four electrodes ground each other due to the dielectric liquid. When tilting or moving an object, one or more electrodes are no longer grounded. This effect can be used to infer motion or tilt (e.g., towards left) and intermediate states (e.g., towards the front left). Also, horizontal balance (i.e., all electrodes ground each other) and flipping the object over (i.e., no electrode is grounded) can be detected by the number of electrodes that ground each other (see Figure 6.1). For this sensor, no calibration is required.

A cubic sensor with these four electrodes would determine inverted values when used flipped over. Therefore, the concept is extended by adding a single central electrode in the middle of the chamber. If liquid does not cover any electrode, the sensor has been flipped over, and the tilts must be reported inverted.

6.4.3 *Combining and Integrating Sensors*

While both sensors by themselves already determine one- or two-dimensional tilts, they can also be combined inside of a 3D object, resulting in various configurations that provide greater interactive possibilities (see Table 6.2). For example, two or three halfpipe sensors, orthogonal to each other, could detect continuous tilts in two or three dimensions. Similarly, position-

		Directions		
		One	**Two**	**Three**
Resolution	**Multi-Level**	-	1 cubic sensor	2 orthogonal cubic sensors
	Continuous	1 halfpipe sensor	2 orthogonal half-pipe sensors	3 orthogonal half-pipe sensors

Table 6.2: Classification of the halfpipe and cubic sensors with respect to the design space of liquid-based movement sensors.

ing a cubic sensor on each lying surface of a 3D object would enable sensing of the orientation of the object as well as two-dimensional tilts regardless of the orientation.

In order to achieve proper integration, all electrodes need to be routed to the outside of the 3D object. This process can be automatized using the routing approach presented in Section 3.4. However, sufficient spacing between conductors is required. A spacing of 5 mm between electrodes and wires was satisfactory to ensure independent sensing performance.

In conclusion, a 3D object can contain multiple sensors. Their measurements can be read out independently and simultaneously by the capacitive sensor.

6.4.4   *Interactions*

Using the previously described sensors, a variety of motion and tilt interactions are detectable (see Figure 6.4).

TILT INTERACTIONS

The most basic interaction is **tilting** in various directions. Using the cubic sensor, tilts towards left, right, front and rear and intermediate states (e.g., front left) can be detected. Moreover, **flipping** an object over upside down to trigger an action can be very lightweight (e.g., like turning a die). Balanced and flipped states are distinguishable with the cubic sensor.
Based on the halfpipe sensor, **rotating** interactions can be supported that require more precise input than discrete tilts. For instance, the sensor can be directly embedded into rotation-aware 3D-printed objects. In complex
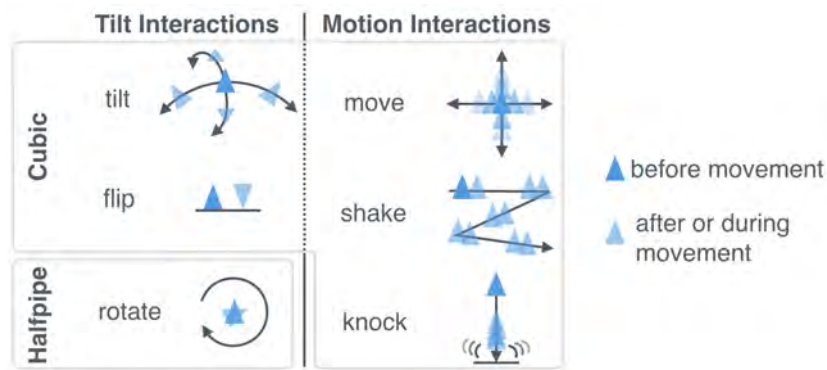
Figure 6.4: Illustration of various tilt and motion interactions supported by the cubic or halfpipe sensor.

objects, this can also be used to implement 3D-printed tangible controls (e.g., a tactile rotary knob containing a halfpipe sensor).

MOTION INTERACTIONS

By quickly **moving** an object, the liquid is pushed into different regions of an object. This effect can be used to sense the direction of motion with the cubic sensor. Based on this, **shaking** in different directions (e.g., left to right or front to rear) can be distinguished by analyzing movements over time. Moreover, repeatedly **knocking** an object (with a cubic sensor) onto a solid surface can be detected by analyzing balanced and flipped states over time.

6.5 IMPLEMENTATION

6.5.1 *Sensing*

The controller board used for evaluation consists of an Arduino Mega 2560 (tethered to a PC) and an MPR121 capacitive sensor (12 sensing pins at a sample rate of 29 Hz). Raw capacitance data is reported as ADC count ($C = const./ADC$) [Fre10]. The sensing pins are connected to the printed objects with breadboard jumper cables.

After testing different generally available liquids (see Section 6.7.2), the most suitable liquid was tap water because it showed the most linear correlation between tilt and capacitive raw data. That is, the full range of tilts is covered
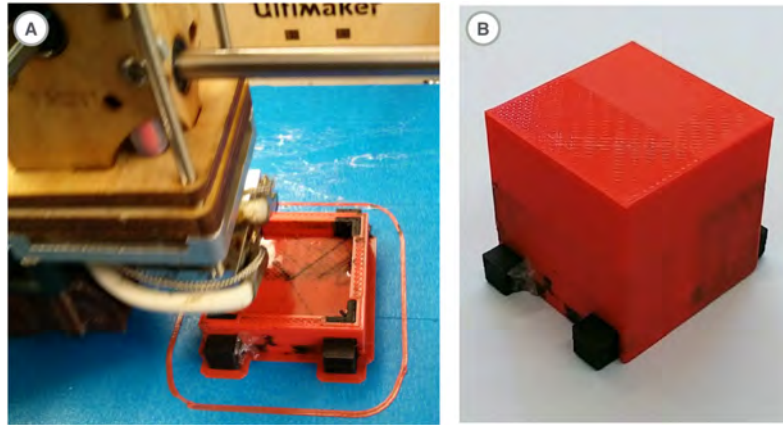
Figure 6.5: A cubic sensor is 3D-printed with liquid already filled in (A). The finished prototype is closed watertight (B).

at nearly the same resolution. Moreover, it is most readily available and can be used without safety precautions.

6.5.2 *Fabrication*

For the implementation of LIQUIDO, an Ultimaker Original 3D printer with Dual Extrusion Kit (ca. 1300 €), ordinary PLA (ca. 30 €/kg) and a commercially available conductive PLA by Proto-pasta (ca. 140 €/kg), which has an average resistivity of $30 - 115\,\Omega * \text{cm}$, was used. The extrusion temperature was $220\,^\circ\text{C}$, the nozzle diameter 0.8 mm, and the cooling fan was turned on.

The fabrication process uses an existing 3D model and is as follows:

1. The 3D model is equipped with one or multiple sensors using the design tool.

2. Then, a standard dual-extrusion 3D printer creates the 3D object (see Figure 6.5).

3. During printing, the printer is stopped to fill in the liquid.

4. After this intermediate step, the printing process resumes.

The prototypes were manually designed using Blender and reusable Open-SCAD scripts that allow generating sensing structures depending on adjustable parameters, such as the size or the thickness of conductors. These scripts also generate the wires that connect a sensor to the outside. How-
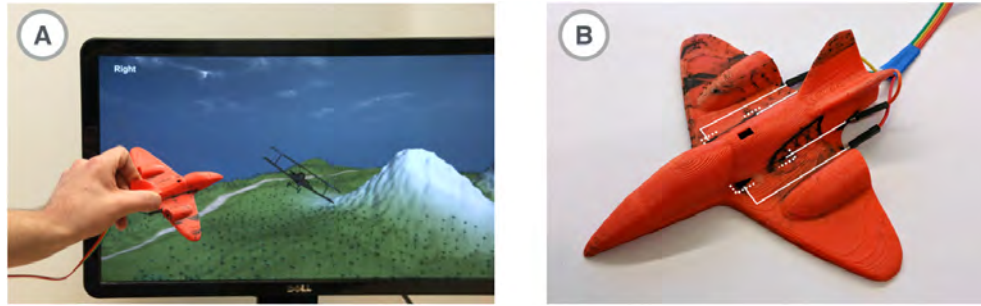
Figure 6.6: Controlling a flying simulation with a 3D-printed airplane (B) that consists of an embedded cubic sensor (location and wires are highlighted in white).

ever, this process can be further automated using routing algorithms (see Section 3.4) and a design tool (see Section 6.3).

Moreover, depending on the size of the sensor, the amount of liquid varies. Empirical tests found that the smallest amount of liquid that adequately covers all electrodes is best for operation.

6.6 EXAMPLE APPLICATIONS

This section presents three example applications based on either the halfpipe or cubic sensor.

6.6.1 *Tangible Airplane Game (cubic)*

The first example application is a 3D-printed airplane with an embedded cubic sensor (2×2 cm^2) connected to a capacitive sensor via four distinct wires (see Figure 6.6). In combination with a flight simulator, the physical object can be used to fly through a territory by tilting the plane to different directions (e.g., tilt to the front to dive). Shaking the airplane restarts the simulation.

6.6.2 *Tangible Ship Game (halfpipe)*

A simple sailing ship featuring an embedded halfpipe sensor was printed (see Figure 6.7). By tilting the ship up or down, a user controls the direction
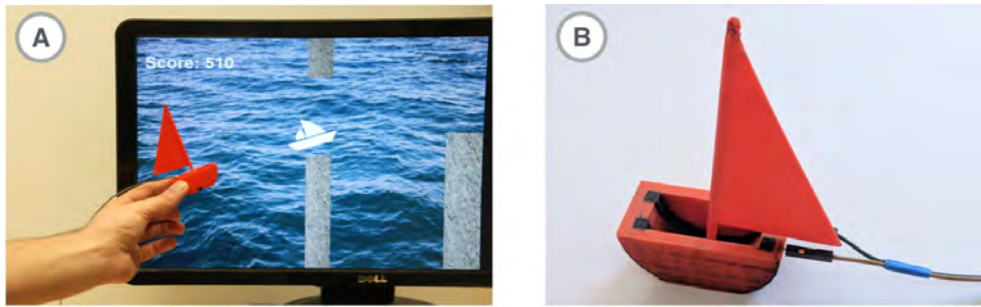
Figure 6.7: Avoiding obstacles with a 3D-printed ship (A) with an embedded half-pipe sensor (B).
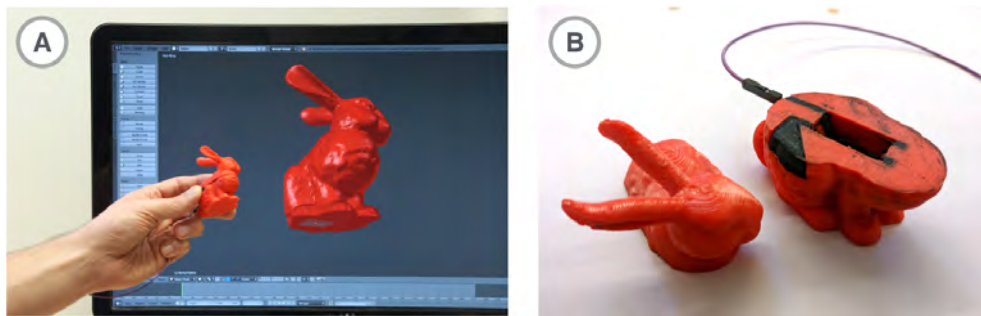
Figure 6.8: A physical object is rotated for 3D navigation.

in which the ship is swimming, thereby guiding the virtual ship safely past varying obstacles.

6.6.3   *Tangible 3D Navigation (halfpipe)*

For CAD experts, rotating a 3D view of a digital model is easy. However, for novice users, the following application can be used to quickly explore digital 3D models of objects by rotating their 3D-printed counterparts. To illustrate this scenario, the well-known Stanford Bunny ($54 \times 54 \times 45$ mm^3) [TL94] with a halfpipe sensor inside was printed (see Figure 6.8). The object can be used to inspect different views of the 3D model around one axis (in case of the Bunny the lateral axis) by manipulation its physical proxy object. By including multiple halfpipe sensors, further axes can be controlled. The second electrode is connected to a touch electrode at the side of the bunny.

6.7 EVALUATION

6.7.1 *Setup and Measurements*

Data was recorded on a PC connected to an Arduino Mega 2560. Capacitive data was measured by an MPR121 chip (sample rate 29 Hz) which was connected to one electrode (3.5 mm thick) of a halfpipe sensor (40 18 (height of 15 18)mm). The second electrode was connected to the ground of the Arduino. As the ground-truth reference, an MPU 6050 tilt sensor was used. The tilt sensor and the halfpipe sensor were both mounted on a rod to enforce equal tilt.

For each test cycle, 1 ml of liquid is dispensed into the halfpipe sensor. The rod is turned several times to either side (range from -60° to 60°). After a test cycle, the liquid is removed, and the sensor is cleaned and dried.

6.7.2 *Comparison of Different Liquids*

To investigate which liquids are most suited to be embedded into 3D-printed objects while printing and to sense one-dimensional tilt via the halfpipe sensor, four liquids based on water were tested, as they are readily available and cheap: Salt solution (0.05 g/ml), vinegar solution (0.1 g/ml), dish soap solution (0.001 g/ml), and pure tap water.

Each liquid according to the procedure described above. The results show that tap water has the broadest range of data (172 counts) and vinegar the least range (50 counts). Salt (124 counts) and dish soap (117 counts) have nearly the same range.

Figure 6.9 illustrates the polynomial trend lines (second degree) of all liquids for different tilts. The trend line for tap water shows that mean values arranging around an almost linear trend line ($f(x) = 0.0016\,x^2 + 1.0411\,x + 393.26$). In contrast, the trend lines for salt, vinegar, and dish soap solution level off or even bend down for larger tilts. Especially for salt and vinegar, ADC values drop beyond about 130 for tilts greater than 50°. As an invertible function is required to compute tilt from raw data unambiguously, these liquids are unsuitable. Also, the range of vinegar is low. Thus, a precise interpretation of vinegar values is more difficult. As a consequence, tap water was used for the accuracy evaluation, because of its invertible and linear trend line. De-
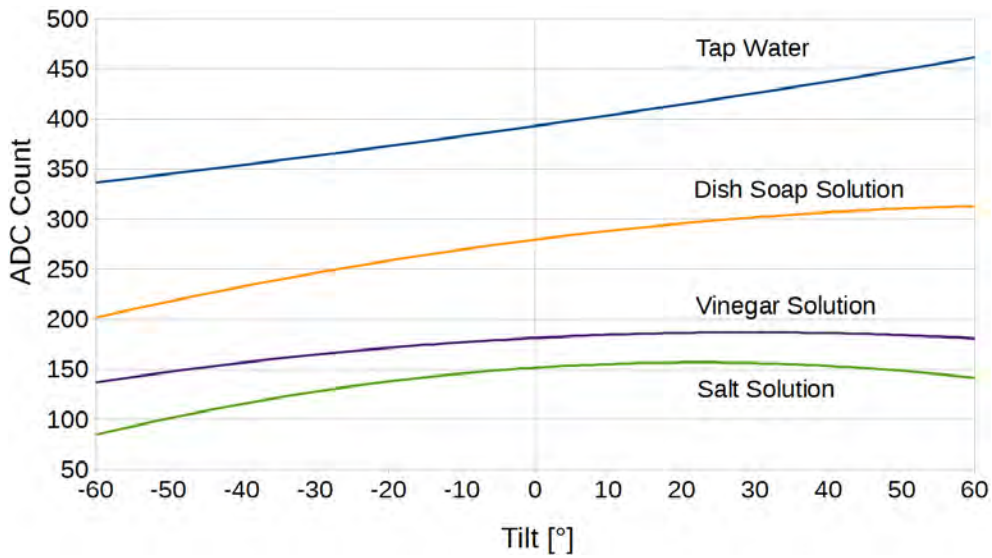
Figure 6.9: Trend lines for tap water, dish soap solution, vinegar solution, and salt solution showing the dependency between the ground-truth tilt and measured counts for the halfpipe sensor.

spite its invertible trend line, dish soap solution leaks through the container (probably due to reduced surface tension).

6.7.3   *Accuracy of Tilting*

The ground-truth tilts were compared with the measurements from the halfpipe sensor (containing 1 ml tap water). As illustrated in Figure 6.10, there is an offset that is often towards the last extreme (±60°). That is, the halfpipe sensor tends towards that particular side if the tilt is extreme. One reason may be that liquid remains on some electrode parts and connects them unintentionally.
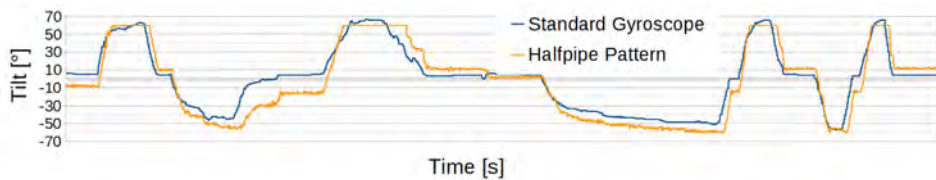
Figure 6.10: Comparison between tilts reported by the halfpipe sensor (orange) versus an MPU 6050 tilt sensor (blue) over a timeframe of 184s.

6.8 DISCUSSION AND LIMITATIONS

This chapter presents results on 3D-printed liquid-based movement sensors. However, it currently has limitations that must be considered during fabrication and sensing.

6.8.1 *Adhesion and Sensibility*

While LIQUIDO focuses on coarse-grained tilting and motion interactions which are adequate in many application scenarios (e.g., rapid prototyping or tangible games), the sensing principle is less precise compared to traditional sensors. First, adhesion effects can occur which cause some liquid to remain on the electrodes and, thus, influence the measurement results. Second, liquid-based sensors are sensitive to interference from vibration or shock which may result in false measurements.

6.8.2 *Temperature Dependency*

All prototypes were evaluated at room temperature. Since the volume of liquids depends on the temperature, using the sensors at other temperatures may require either a different amount of liquid or recalibration. Also, the sensors are not suitable for extreme temperatures that cause the liquid to freeze or enter the gas phase.

6.8.3 *Geometry and Scalability*

The approach requires a volumetric object inside which a sensor can be inserted, and conductors can be routed. Geometries with thin structures, high curvatures, or cavities remain challenging.

Moreover, scalability is an important issue, as the size of a sensor inside a 3D object may vary from small to very large. The minimal size of a sensor and the minimal cross-sectional size of a conductor are limited by the resolution and nozzle diameter of today's commodity 3D printers. These restrictions are likely to be eliminated by future printers. The second limit to miniatur-

izing sensors relates to the volume of a chamber. If shrunk too much, it may not hold enough liquid to measure a movement reliably.

6.9 CONCLUSION

This chapter presented LIQUIDO, a method to capacitively sense a variety of tilting and motion interactions based on embedding liquids into 3D-printed objects. In summary, the main contributions of this chapter are:

1. Liquid-based sensors to capacitively measure tilt and motion via liquids in various volumetric 3D objects.

2. A printing process using a standard dual-extrusion 3D printer and commercially available materials.

3. Three interactive example applications demonstrate that many 3D-printable objects can embed both sensors.

4. Technical evaluations on (i) the suitability of different liquids and (ii) the accuracy of liquid-based sensors that found that LIQUIDO operates best with tap water and can reliably determine tilt compared to a ground-truth measurement.

Figure 6.11: The classification of LIQUIDO regarding the design space of 3D-printed interaction.

As illustrated in Figure 6.11, LIQUIDO contributes liquid-based sensors that consist of solid materials with embedded conductive and liquid sensing structures. They may be embedded in closed-volumetric 3D-printable objects to enable constant measurement of continuous one-dimensional or multi-level two-dimensional tilts or motions. On top of these interactions, more complex motions such as flipping, shaking, and knocking objects are supported.

The next chapter continues the exploration of liquid-filled 3D-printed objects by extending LIQUIDO so that interactions with an object can be memorized in its internal structure.

7

OFF-LINE SENSING: 3D-PRINTED MEMORIZING OF
INTERACTIONS

The last chapter introduced the LIQUIDO approach that combines capacitive sensing with embedded liquids inside a 3D-printed object to detect various tilting and motion interactions. On this basis, this chapter extends this approach by contributing OFF-LINE SENSORS, that detect one-time interactions performed with objects without requiring any active electronics nor power during the interaction. OFF-LINE SENSORS memorize stimuli such as pressure, squeeze, acceleration, tilt, flip, heat, and freeze. Users may extract whether a sensor was exposed to the interaction by using a capacitive touchscreen.

The remainder of this chapter is structured as follows. Section 7.1 discusses related work. Section 7.2 introduces the OFF-LINE SENSING fabrication pipeline and the sensing principle. Section 7.3 then details on the generation and design of objects. On this basis, Section 7.4 presents a set of sensors for capturing mechanical forces, physical manipulations and environmental conditions. This section is followed by Section 7.5 that details on the implementation of sensing and fabrication. Then, Section 7.6 presents results on a technical evaluation of all sensors. To conclude, Section 7.7 discusses the limitations of OFF-LINE SENSING.

7.1 RELATED WORK

The following section shortly presents relevant research concerning interactive metamaterials and discusses them regarding LIQUIDO. Section 2.1.3 discusses the majority of related work.

7.1.1 *Interactive Metamaterials*

Metamaterials, i.e., structures engineered to yield new properties, are investigated in material science to indicate, for instance, tilting or shock (cf. [Uli18]). An emerging stream of research is investigating how to digitally fabricate objects containing metamaterials[1] Such metamaterials convey digital information employing terahertz imaging [WSM13], magnetic storage [ICG17], or air pockets [Li+17]. Moreover, they enrich fabricated objects with mechanical functionality [Ion+16], logical operations [Ion+17], dynamic textures [Ion+18], or self-folding [Sun+17b].

By adding to this stream of research, OFF-LINE SENSORS allow objects to memorize one-time interactions that can be integrated into 3D-printed objects and digitally read-out with a standard capacitive touchscreen. They are 3D-printed in a single pass without requiring additional assembly of electronics

7.2 FABRICATION AND SENSING APPROACH

This section introduces the OFF-LINE SENSING principle underlying all OFF-LINE SENSORS and the fabrication pipeline to easily create them, starting from the specification of a sensor to extracting whether it was exposed to an interaction.
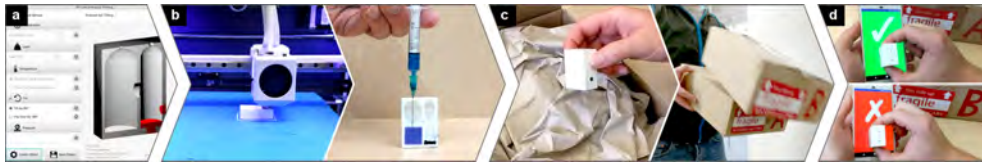
Figure 7.1: An OFF-LINE SENSOR may monitor whether a fragile parcel was improperly tilted: After the sender specifies the sensor in a specification tool (a), two identical sensors are 3D-printed and filled with a conductive liquid (b). After placing each sensor into parcels A and B, both are shipped (c). The recipient checks whether the sensor was exposed to tilting by placing it on her capacitive touchscreen (d).

7.2.1 *Fabrication Pipeline*

SPECIFICATION

A specification tool enables users to choose from a list of OFF-LINE SENSORS and export printer-ready fabrication file (see Figure 7.1a). Section 7.3 describes this concept of graphical specification in more detail.

PRINTING AND POST-PROCESSING

The user slices the 3D-printable files with printer-specific settings and hands it over to the 3D printer (see Figure 7.1b). After 3D printing, the sensor must be further prepared for deployment by following the generated instructions. For most sensors, only filling with a conductive medium (e.g., tap water) is required which may be automated using the process described in Section 6.2. Some sensors require further post-processing, such as freezing of the embedded liquid or cutting off specific parts.

DEPLOYMENT AND INTERACTION

After post-processing, the user deploys the sensor in the desired interaction context (see Figure 7.1c). If the sensor was exposed to the pre-defined interaction, its state is permanently altered. Otherwise, it remains in its initial state.

---

1 This stream, called **no-assembly 3D printing** throughout this thesis, is discussed in more detail in Section 2.1.3.
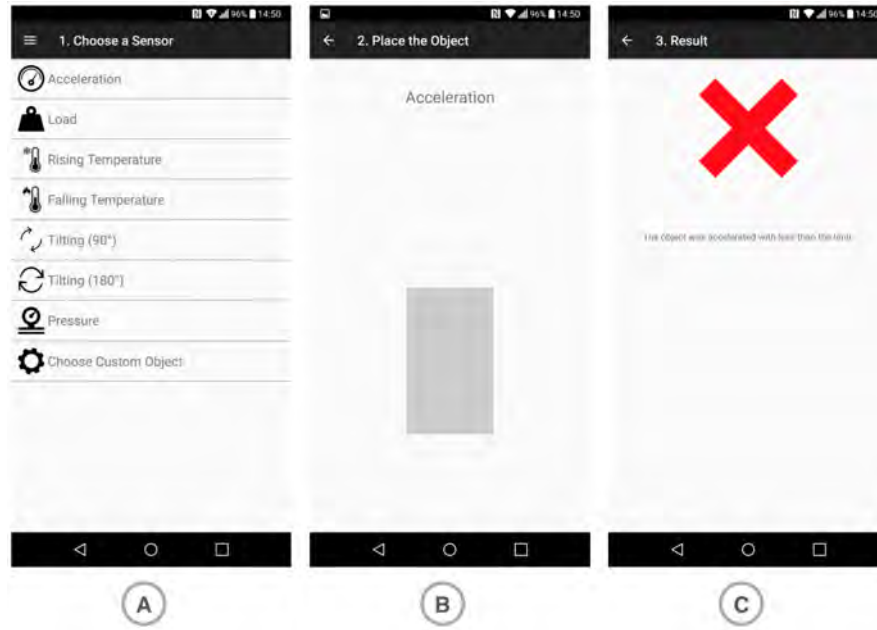
Figure 7.2: The process to extract the internal state of an OFF-LINE SENSOR: After se-
lecting a sensor (A), the user places the OFF-LINE SENSOR on a pre-defined
area on the capacitive touchscreen. After the application determines the
internal state, it is displayed to the user (C).

COLLECTION AND EXTRACTION

For the user to check whether an interaction occurred, she may use an ap-
plication that utilizes the capacitive touchscreen of her mobile device (see
Figure 7.1d). The extraction process (see Figure 7.2):

- First, the user chooses the type of sensor in an application.

- Second, the user places the sensor on a highlighted area on the touch-
  screen, while connecting her finger to the user electrode. Then, the
  application on the mobile device determines whether the interaction
  occurred by analyzing if a touch point exists at a pre-defined location,
  saved together with the sensor type in the definition file during speci-
  fication.

- Third, the application display the status of the OFF-LINE SENSOR to the
  user.
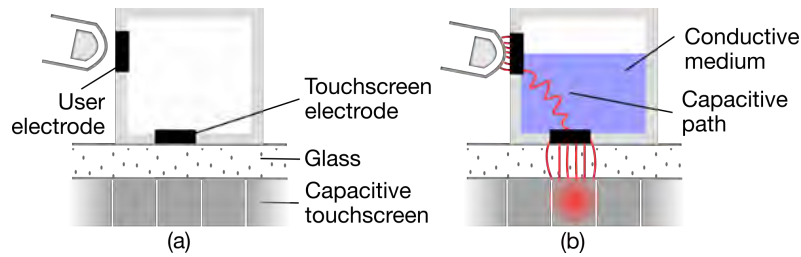
Figure 7.3: Sensing principle: Depending on the state of the sensor, a conductive
path between the user and the touchscreen is formed (b) or not (a).

7.2.2 *Sensing Principle*

OFF-LINE SENSORS consist of conductive electrodes, insulating material and
hollow volumes, called **chambers**, filled with a conductive medium (e.g., tap
water). As illustrated in Figure 7.3a, they employ two types of forwarding
electrodes (in short **forwarders**):

- The **user electrode** connects the finger of the user to the sensor and
  thus grounds it concerning the touchscreen.

- The **touchscreen electrode** connects the sensor to the underlying capac-
  itive touchscreen and enables it to determine the state of the sensor.

As depicted in Figure 7.3b, the internal state of the sensor is determined via
the touchscreen electrode as follows: Once a conductive medium alters the
electrical properties of the sensor, a capacitive path from the finger of the
user throughout the sensor onto the touchscreen is formed. This capacitive
path results in a measurable change in capacitance at the touchscreen.

7.3 DESIGN

This section proposes the concept of a **graphical specification tool** to inter-
actively generate 3D-printable objects according to user-defined properties.
In the context of OFF-LINE SENSORS, an interactive specification tool enables
users to choose and configure sensors from a list (see Figure 7.4). After the
3D model of the sensor is created, the tool offers the user a 3D preview and
export of:

- 3D-printable files for conductive and insulating materials,

- instructions on how to post-process the sensor, and
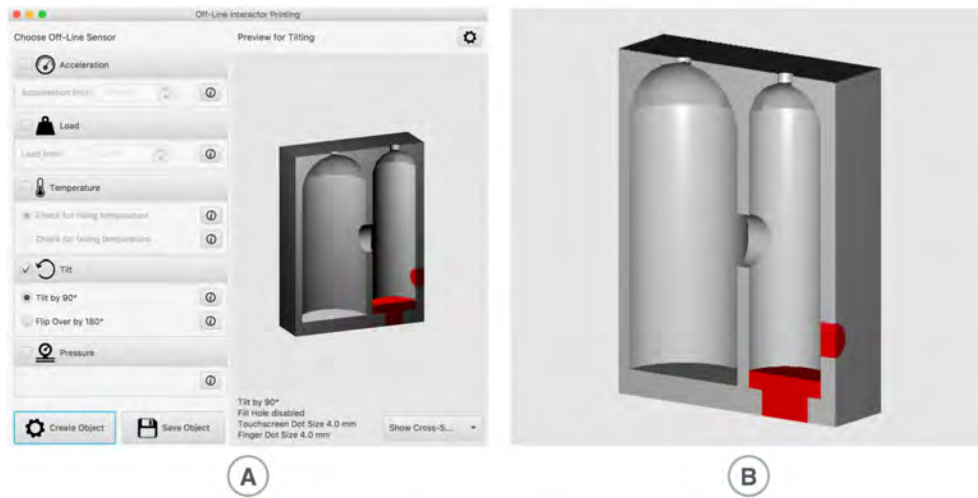
Figure 7.4: Illustration of the specification tool (A) and a close-up view of the generated sensor (B).

- a definition file stating the location of electrodes, a capacitive marker for identification, and the properties of the sensor.

This concept eases the creation of 3D-printed sensors by removing the need for users to be an expert in CAD. It provides information on each sensor and allows the user to adjust high-level properties depending on

- the sensor (e,g., the pressure to be sensed),

- the 3D printer (e.g., the thickness of wires), and

- the touchscreen (e.g., the size of an electrode, an important factor depending on the precision of the printer and the touchscreen used for reading the sensing results).

7.4 OFF-LINE SENSORS

This section presents first results on OFF-LINE SENSORS, 3D-printed structures that employ OFF-LINE SENSING, and addresses fundamental conceptual and technical challenges. To that end, this chapter focuses on a basic, yet widely used set of interactions that serve as a foundation for more advanced interactions:

- The **pressure** and **squeeze** sensors detect a **mechanical force** applied to a 3D object.
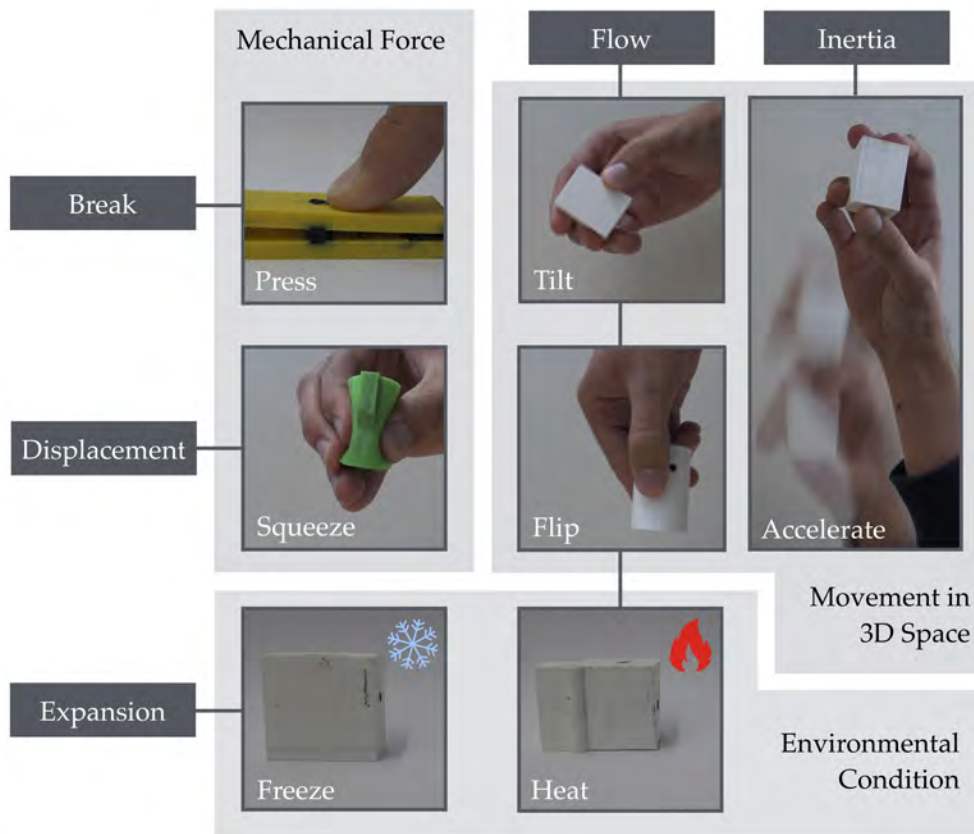
Figure 7.5: Overview of OFF-LINE SENSORS that detect pressure, squeeze, acceleration, tilt, flip, heat, and freeze.

- The **acceleration**, **tilt**, and **flip** sensors detect a specific **movement in 3D space**.

- The **heat** and **freeze** sensors react to varying **environmental conditions** around a 3D object.

Figure 7.5 illustrates the explored set of sensors that are based on the physical property of liquids and solids (cf. [Var87]). The underlying principle of the press sensor is a structural break when a certain level of force is exceeded. The other sensors employ properties of liquids, i.e., that liquids flow regarding gravity, are displaced when constricted, exhibit inertia, or change its volume when frozen. The following sections present the concept of each sensor in detail and discuss practical challenges.
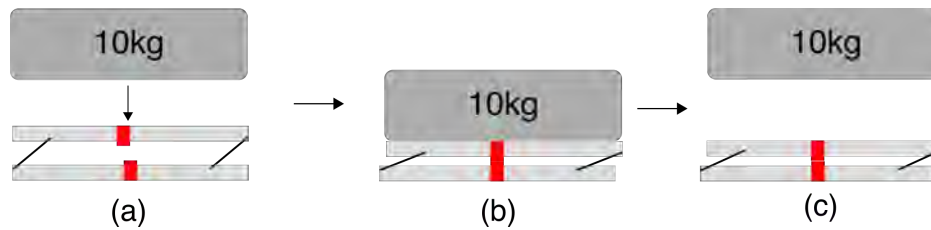
Figure 7.6: Once a force is applied (b), the previously unconnected electrodes (a) connect (c). Both electrodes are shown in red.

7.4.1 *Pressure Sensor*

This sensor reacts to an evenly distributed pressure caused, for instance, by applying a certain weight. It consists of two plates on top of each other, connected by two to six thin pillars (see Figure 7.6). The pillars have an angle of 45° to facilitate a controlled buckling. Both plates also contain a user electrode on top and a touchscreen electrode at the bottom. If the force limit has not yet been exceeded, the two electrodes are a few millimeters apart. If more than the maximal force is evenly applied, the pillars break. As a result, the user and the touchscreen electrode connect, which creates a direct connection between the finger and the touchscreen during the read-out process. Since a slight displacement of the upper plate occurs during the buckling, both electrodes are slightly offset to each other to improve the connection between both electrodes after buckling.

PRACTICAL CHALLENGES

After printing, the sensor must be checked for unwanted connections between the electrodes. These can be caused by oozing effects of the printing material, which falsifies the response. During deployment, the internal state of the sensor only changes when the applied force is perpendicular to the plates, as the pillars are designed only to break that way. In other cases, the state of the sensor will not change. To simultaneously check for pressures applied in other directions, multiple copies of this sensors may be printed and oriented as such.

For the read-out, the bottom plate of the sensor is placed on the touchscreen. Depending on the printer, the electrode should be slightly displaced outwards to improve the connection to the touchscreen. This displacement is not required for the user electrode because the softer finger better connects
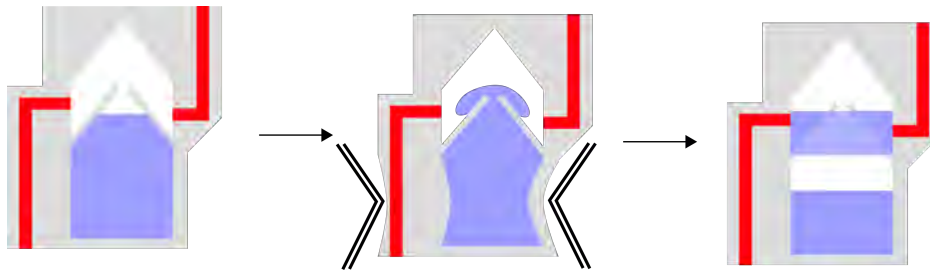
Figure 7.7: By applying a two-sided pressure, the deformable material is compressed, and the liquid is poured out of the upper hole.

to the electrode. Also, a slight force on the sensor should be exerted to counteract a possible spring effect of the pillars.

7.4.2 *Squeeze Sensor*

The internal state of the sensor changes when squeezed from two sides with a distinct force. The sensor consists of two superimposed cone-shaped chambers (see Figure 7.7): The lower chamber is filled with liquid. The upper chamber contains both electrodes. A small hole at the top of the cone of the lower chamber connects both chambers. If the sensor is squeezed, the lower chamber is compressed, and the liquid is pressed through the hole, separating both chambers. The liquid is collected in the upper chamber and connects the two electrodes.

PRACTICAL CHALLENGES

This sensor should be printed with deformable material to allow for compression. Moreover, a liquid needs to be filled only into the lower chamber. If too much liquid is used, the lower chamber will overflow, which falsifies the response of the sensor. Therefore, either a syringe with a needle should be used to avoid filling the outer chamber or the process may be automatized using the process described in Section 6.2.

7.4.3 *Acceleration Sensor*

The acceleration sensor reacts to accelerations that exceed a pre-defined level. It consists of two chambers (see Figure 7.8). The larger one is filled with a conductive liquid (e.g., tap water). A wall that is variable in height separates
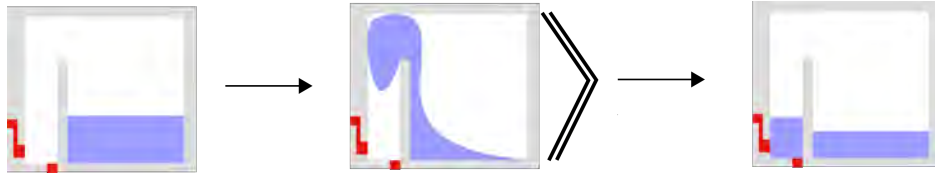
Figure 7.8: By accelerating, liquid spills over into the second chamber.

both chambers. If the sensor is accelerated in the opposite direction of the smaller chamber, the liquid inside the chamber is forced into the direction of the smaller chamber because of the inertia. If the acceleration is large enough, the liquid spills over the parting wall. As a result, it is caught in the smaller chamber. For the read-out, the smaller chamber contains a user electrode and a touchscreen electrode, only connected by a liquid in case of acceleration. For instance, the amount of liquid and the height of the wall can be varied to alter the acceleration level.

PRACTICAL CHALLENGES

The larger chamber must be filled with a liquid either after or automatically during printing (see the process described in Section 6.2). During deployment, users must ensure that the sensor is not tilted. A small angular change can already significantly alter the acceleration limit. Ideally, the sensor is oriented horizontally without tilt. For the read-out, the sensor is placed on the touchscreen and touched with a finger. During this phase, small tilts are irrelevant, while greater tilts can lead to a falsification of the state.

7.4.4   *Tilt Sensor*

Using this sensor, tilts around 90°, depending on the volume of the liquid, can be detected. The sensor consists of two chambers (see Figure 7.9): The left chamber contains a liquid. If the sensor is tilted (i.e., the left chamber is
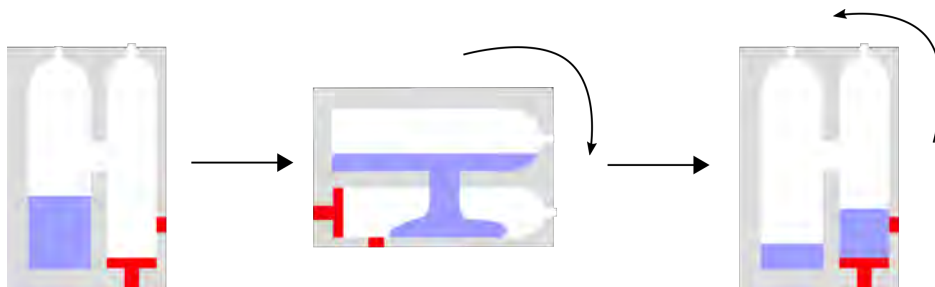
Figure 7.9: By tilting, the liquid gets to the second chamber.
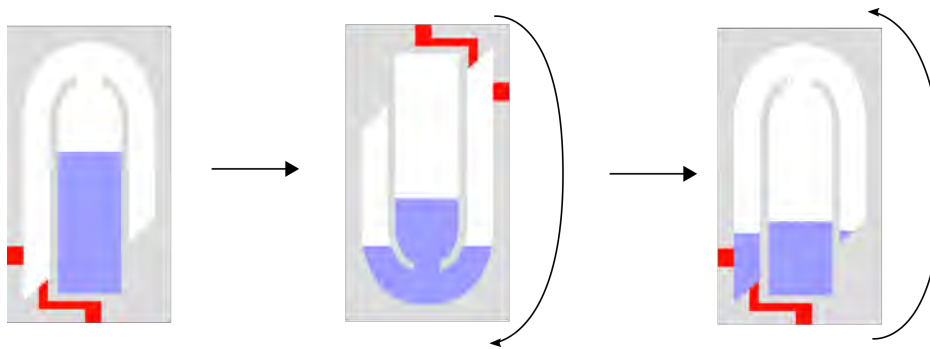
Figure 7.10: When the sensor is flipped over, the liquid is disposed into the second chamber.

above the right), the liquid flows through the hole down and connects the electrodes.

PRACTICAL CHALLENGES

If the volume of the chamber is too small compared to the connecting hole, problems with air displacement are likely to occur. As a countermeasure, both chambers either require a hole for air leakage or the size of the connecting hole need to be increased. The tilt angle can be influenced best by varying the amount of liquid. With less liquid, the tilt angle ranges around 90°. With more liquid, even smaller tilt angles are recognized.

7.4.5   *Flip Sensor*

The flipping over sensor consists of two interlocked chambers (see Figure 7.10). The inner chamber is filled with liquid. If the sensor is flipped over, the liquid flows from the inner into the outer chamber. When rotated by only 90°, the liquid remains through the dome-shaped cover in the inner chamber.

PRACTICAL CHALLENGES

After printing, a liquid needs to be filled only into the inner chamber. If too much liquid is used, the inner chamber will overflow, which falsifies the response of the sensor. A syringe with a needle should be used to avoid filling the outer chamber. As described for the previous sensors, this may be easily automatized using the process described in Section 6.2.
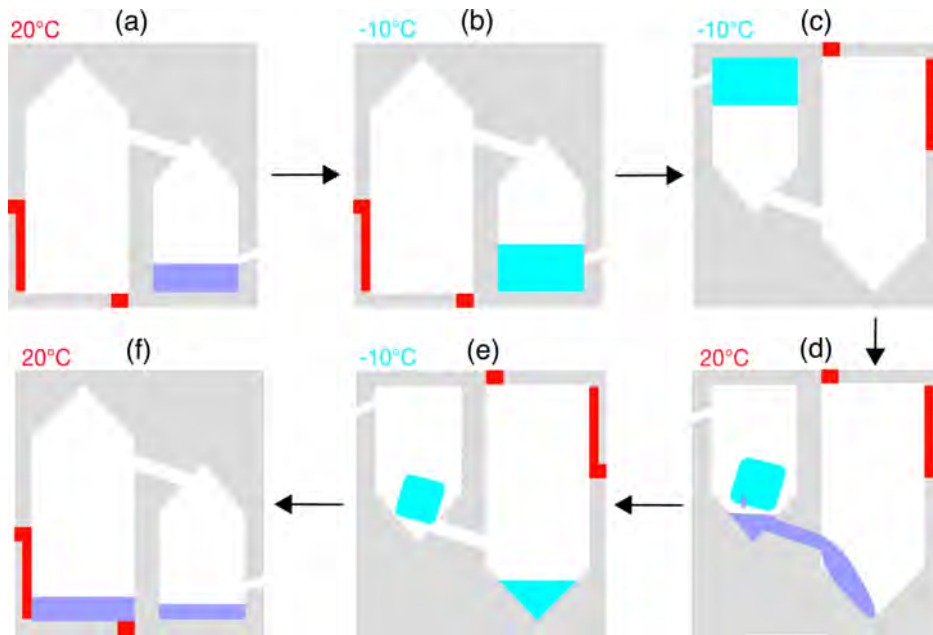
Figure 7.11: After filled (a) and frozen (b), the frozen liquid remains in the smaller chamber as long as the temperature is under a certain threshold (c). If the temperature rises, it is disposed into the bigger chamber (d/e) for later read-out (f).

7.4.6 *Heat Sensor*

This sensor detects temperature changes that heat-up above a certain limit through thermal conduction (cf. Fourier's law). If the sensor is kept below a certain temperature during deployment, the state will not change. However, if the temperature is increased above the limit, the state change will occur. The status change is also memorized when the temperature temporarily exceeds the threshold.

As illustrated in Figure 7.11, the sensor is subdivided into two chambers. The smaller chamber is filled with a liquid (a). The two electrodes for the detection of the state are printed in the bigger chamber. If the sensor is stored under the melting point of the liquid during deployment (b), the frozen liquid will remain in its form, and no liquid will enter the bigger chamber (c). However, if the sensor is stored above the melting point, the frozen liquid starts to melt, causing liquid to accumulate at the bottom of the smaller chamber (d). From there, it flows through a small tube into the adjacent bigger chamber, where it is then recognized by the presence of a connection between the electrodes. If the sensor is stored again under the melting point before the read-out (e), the liquid freezes in the bigger chamber. However, as

Figure 7.12: Due to the increased volume of a frozen liquid (middle), a thin wall breaks, resulting in the deposition of liquid into the left chamber.

the liquid remains in this chamber until the read-out, the state change can still be detected by heating the sensor (f).

PRACTICAL CHALLENGES

Before deployment, the liquid is either inserted automatically (see Section 6.2) or filled through a small hole after printing. To that end, the sensor must be placed upside down (see Figure 7.11a), because otherwise the liquid immediately flows into the next chamber. After this step, the object (i.e., the liquid) is frozen and then turned around again for deployment.

A challenge for the practical use of this sensor is the setting of the desired reaction temperature. The temperature depends on the melting point of the selected liquid, which can be varied through melting-point depression or by using a liquid with another melting point.

If the state is to be read-out after deployment, the sensor must be rotated upside down again, so that the touchscreen electrode points downwards. In this orientation, the rotation prevents the ice, which is still present in the chamber, from flowing into the other chamber. Since ice is not electrically conductive, it must be melted before the read-out.

7.4.7   *Freeze Sensor*

The internal state of the freeze sensor changes when stored for a particular time under a temperature limit. The sensor consists of two chambers (see Figure 7.12). The larger of the two chambers is wholly filled with a conductive liquid with negative thermal expansion (i.e., it increases in volume when cooled). The smaller one contains both electrodes. Both chambers are liquid-tightly separated from each other by a thin wall. When the liquid freezes, it increases in volume and breaks through the thin wall. As a result, the wall is no longer leak proof. If the frozen liquid is heated again, it leaks through the crack into the second chamber and connects the electrodes.

PRACTICAL CHALLENGES

As this sensor requires a liquid with negative thermal expansion, tap water is used (it expands in volume approx. 9%). After printing, the larger chamber must be wholly filled with liquid. The sensor can be read-out if not frozen, as then enough liquid can connect the electrodes.

A challenge for the practical use of this sensor is the setting of the desired reaction temperature. The temperature depends on the freezing point of the selected liquid, which can be varied through freezing-point depression (e.g., the freezing point of water can be lowered by adding salt). Liquids with an increased freezing point can be used to obtain a sensor with a higher reaction temperature.

7.4.8 *Conclusion*

As depicted in Table 7.1, the set of OFF-LINE SENSORS can be classified according to schematic and conceptual properties. Sensors consist of a certain number of chambers and tunnels between chambers. While the presented sensors use often use two chambers connected via one tunnel, the number of chambers and tunnels is, in principle, not limited and can be used to detect, for instance, sequential interactions. Moreover, several compositions of materials show that the principle could be used as the basis for a large number of new sensors.

In order to strengthen practicability, OFF-LINE SENSORS focus on detecting binary or multiple levels (specified during design time) of an interaction.

	Mechanical Force		Movement in 3D Space			Environmental Condition	
	Press	Squeeze	Accelerate	Tilt	Flip	Freeze	Heat
Schematic Properties							
Number of Chambers	0	2	2	2	2	2	2
Number of Tunnels	0	1	1	1	1	0–1	1
Number of Forwarders	2	2	2	2	2	2	2
Material Composite							
Conceptual Properties							
Irreversibility	structural	funneled	none	funneled	funneled	structural	funneled
Resolution	multi-level (pre-defined)	multi-level (pre-defined)	multi-level (pre-defined)	binary	binary	multi-level (pre-defined)	multi-level (pre-defined)

Table 7.1: Classification of each OFF-LINE SENSOR with respect to schematic and conceptual properties.

However, the principle may be extended to continuous levels of interaction by measuring liquid levels via capacitive raw data with extended sensor electrodes that function as a coaxial cylindrical capacitor. Also, sensors are intentionally designed to resist (accidental or malicious) attempts to reverse their internal state by irreversibly destroying structures or employing conic funnels and small tunnels.

7.5   IMPLEMENTATION

The specification tool utilizes OpenSCAD scripts to create OFF-LINE SENSORS. As a consequence, sensors can be easily changed or added by providing a new OpenSCAD script. The software used for read-out on a capacitive touchscreen is implemented for Android.

The implementation of OFF-LINE SENSORS utilizes the dual extrusion printer BCN3D Sigma to print conductive and insulating materials simultaneously. The accompanying software BCN3D Cura was used for slicing. The conductive electrodes consist of carbon-doped Proto-pasta Conductive PLA (cPLA) with a volume resistivity of $30 - 115\,\Omega * \text{cm}$ (printing temperature of $220\,°\text{C}$ at the cost of $140\,€/\text{kg}$). For insulating parts, Verbatim PLA was used (printing temperature of $212\,°\text{C}$ at the cost of $30\,€/\text{kg}$). For the pressure sensor, NinjaFlex TPU was used (printing temperature of $225\,°\text{C}$ at the cost of $90\,€/\text{kg}$).

Since in most cases the sensor can only be used once, less importance was placed on the printing quality. The thickness of the layers was set to 0.2 mm to keep the printing duration low. Retraction of the filament was enabled to prevent unwanted connections between the conductive parts. For all sensors, an infill density of 20% was chosen, which is adequate for sensors using normal PLA. Also, this density allows for sufficient flexibility in sensors made of deformable TPU. The printing speed was set to 40 mm/s for most sensors. Only for deformable TPU, the printing speed was reduced at the beginning of the print to ensure a better cohesion between the first few layers. Since sensors are filled with liquid in many cases, they were printed with a material flow of 110% for solid parts and 125% for deformable parts to avoid leaking.

7.6 EVALUATION

Technical experiments were conducted to evaluate the prototypes of all OFF-LINE SENSORS. The following section reports on the findings and provides guidelines for designing and printing OFF-LINE SENSORS.

7.6.1 *Pressing*

The prototype of the pressure sensor has dimensions of $6.1 \times 2 \times 1.4 \text{ cm}^3$. After triggering, the height of the sensor is reduced to 1.1 cm. The maximal force before collapse depends on several factors which may be varied by designers:

- the number and thickness of the pillars

- the material strength and angle of the pillars

- the printing direction and inter-layer adhesion strength

As the sensor is designed for evenly distributed forces, the effect of the distribution of the pillars on the maximal force is almost negligible. However, varying levels of force can still be recognized by controlling the number of pillars. Thus, the pressure sensor was evaluated with 2, 4, and 6 pillars (thickness 0.5 mm). The weight was increased until it responded. As a result, three levels of forces can be reliably distinguished: The sensor reacts for 2 pillars at 5.2 kg ($\sigma = 0.13$ kg), for 4 pillars at 10.5 kg ($\sigma = 0.21$ kg), and for 6 pillars at 16.4 kg ($\sigma = 0.11$ kg). Using more pillars is easily possible but requires a bigger size of the overall sensor. Moreover, pillars printed with normal PLA were tested. However, due to the elastic material properties of PLA, the electrodes rebound despite the sensor was triggered. Applying more pressure from the finger during read-out can counteract this problem. However, the amount required was unpleasant, both for the finger and for the stability of the touchscreen. Thus, cPLA should be used for the pillars, as it is more brittle than normal PLA. As a result, the sensor does no longer rebound. Both plates should be printed in a sideways direction to improve the quality of the pillars and to reduce the risk that the sensor peels off the printing plate during printing. To that end, the base area also has been enlarged.

7.6.2   *Squeezing*

The prototype of the squeeze sensor has a diameter of 3.5 cm (height of 2.6 cm). The reaction of the sensor depends on several factors which may be varied by designers:

- the volume of the liquid

- the infill density of the insulating material

The results show that 5 ml of tap water yield a reliable detection of squeezing. The amount of force required can be fine-tuned by varying the infill density or by changing the amount of liquid. Also, the printing quality is an important factor, as otherwise, the deformable TPU leaks liquid. Sensors should be printed with a slower printing speed of 30 mm/s and an increased material flow of 125%.

7.6.3   *Accelerating*

The prototype of the accelerating sensor has dimensions of $4 \times 2.4 \times 4$ cm^3. The reaction of the sensor depends on several factors which may be varied by designers:

- the wall height and dimension of the chamber

- the viscosity and volume of the liquid

- the angle of acceleration

It was measured at which acceleration the state changed for varying wall heights and 3 ml of tap water. To that end, the sensor was mounted to a smartphone. Then, the measurements of the accelerometer of the smartphone were compared to the response of the sensor. By repeating different levels of acceleration (between 1-15 m/s^2) 20 times, the results suggest that at least two accelerations can be reliably distinguished:

- For a wall height of 10 mm, $5\,\text{m/s}^2$ ($\sigma = 1\,\text{m/s}^2$) acceleration was detected (e.g., equals a starting car).

- For a wall height of 18 mm, $12\,\text{m/s}^2$ ($\sigma = 1\,\text{m/s}^2$) acceleration was detected (e.g., equals an emergency stop in a car).

By further varying factors (e.g., viscosity), more levels of acceleration could be distinguished.

7.6.4 *Tilting*

The prototype of the tilting sensor has dimensions of $2.8 \times 1.8 \times 4$ cm^3. The reaction of the sensor depends on several factors which may be varied by designers:

- the viscosity of the liquid

- the amount of liquid

2 ml of tap water is sufficient to operate this sensor. However, the primary challenge is that chambers should not be airtightly closed because otherwise, the remaining air in both chambers blocks the liquid from flowing into the second chamber. Thus, the sensor employs two air-holes at its top to allow for sufficient air circulation.

7.6.5 *Flipping Over*

The prototype of the flipping over sensor has a diameter of 3.4 cm (height of 5.1 cm). The reaction of the sensor depends on the same factors as for tilting. Also, similar to tilting, air circulation is a challenge if the sensor is airtightly closed. As an air-hole at the top would result in leaking liquid in the case of flipping over, the size of the hole connecting both chambers is increased. Thereby, air and liquid can be exchanged between chambers more easily.

7.6.6 *Heating*

The prototype of the heat sensor has dimensions of $4.4 \times 2 \times 3$ cm^3. This sensor was evaluated with pure tap water (melting point approx. $0\,^\circ$C) and 2 mm PLA walls (with rather low thermal conductivity). After being frozen for several hours, the internal state of the prototype changed after approx. 10 minutes at $23\,^\circ$C room temperature.

In general, the defrosting time depends on several factors which may be varied by designers:

- the temperature difference between inside and outside

- the time of exposure to the temperature difference

- the thermal conductivity and thickness of the insulating material

By varying the factors of Fourier's law (e.g., other materials or liquids with other melting points), the defrosting time (i.e., the temperature at which the sensor reacts) can be controlled.

7.6.7 *Freezing*

The prototype for the freeze sensor has dimensions of $4.3 \times 2.2 \times 3.2$ cm^3. After being exposed to $23\,°C$ room temperature for several hours, the internal state of the prototype changed after approx. 15 minutes at $0\,°C$.

Besides the factors for the heat sensor, the freezing time depends on these factors:

- the material strength and thickness of the inner wall

- the initial volume of the liquid

As this sensor builds upon a fracture in its internal structure, it highly depends on the material properties of the inner wall. If the printing quality is too high, it will not break. Thus, as for the pressure sensor, the brittler cPLA is used. Repeatably freezing the sensor 20 times showed that an inner wall thickness of 0.5 mm results in a reliable fracture to trigger the state change. Similar to the previous sensor, the reaction temperature can be controlled by using liquids with varying freezing points or changing the freezing temperature of tap water by adding salt.

7.7 DISCUSSION AND LIMITATIONS

This chapter presents first results on OFF-LINE SENSORS that memorize interactions by leveraging capacitive coupling. However, the approach has limitations that must be considered during design, printing, and sensing.

7.7.1 *Manual Post-Processing*

Currently, OFF-LINE SENSORS need to be manually post-processed to remove support and add a conductive medium (e.g., using a syringe). The latter can be circumstanced by depositing liquids into sensors during 3D printing as described in Section 6.2.

Besides for pressing, all OFF-LINE SENSORS are intentionally designed to be printable without support material. With the emergence of multi-extruder printers, support may be printed with water-soluble PVA and washed out after printing.

7.7.2 *Reversibility and Reusability*

OFF-LINE SENSORS operate only once for a pre-defined interaction. They are intentionally designed to withstand accidental or malicious attempts to reverse their state (e.g., by using conic funnels or small holes) That is, the reversion of a sensor is hard because only small residues of liquid are sufficient to trigger a sensor.

In principle, sensors that use a liquid may be thoroughly dried and refilled several times for reuse because the solid structures are unmodified. If the sensor is no longer intended for use, it can be either disposed of, as it mostly consists of biodegradable PLA, or recycled as 3D printing filament (e.g., via a filament extruder [fil18]).

7.7.3 *Continuity*

Although OFF-LINE SENSORS respond well to one discrete interaction, they are unable to sense an interaction performed multiple times. Moreover, OFF-LINE SENSORS focus on binary measurements with standard touchscreens to strengthen practicability. While different discrete levels can be detected simultaneously by printing multiple sensors with varying properties, future work could advance the detection towards continuous levels of interaction in one single sensor by correlating liquid levels inside a chamber with capacitive raw data provided by the touchscreen.

7.7.4 *Scalability*

Scalability is an important issue, as the size of a sensor and the capacitive touchscreen may vary from small to very large. The electrodes of a sensor are optimized for the size of a fingertip (16–20 mm [DRS03]). Also, the approach requires a volumetric object inside which a sensor can be inserted, and conductors can be routed. Thus, geometries with thin structures, high curvatures, or cavities remain challenging.

The resolution and the nozzle diameter of today's commodity 3D printers limit the minimal size of a sensor. The minimal cross-sectional size of a conductor is 3×3 mm^2. The second limit to miniaturizing sensors relates to the volume of a chamber. If shrunk too much, they may not be sufficient to hold enough liquid. Similarly, the diameter of the connection between the chambers limits the size of a sensor. Therefore, considering fluid dynamics, a small diameter can increase the adhesion of the liquid to its walls to a level where no more liquid is transported between the chambers.

7.7.5 *Combination of Sensors*

Off-line sensors may be combined into one 3D-printed object by merging and printing multiple sensors together. However, sensors based on different conductive media may not be compatible (e.g., frozen vs. liquid media). Also, environmental conditions need to be considered. For instance, using a liquid to detect flipping over in a refrigerated car remains challenging as the freezing point of the liquid needs to be sufficiently low.

7.8   conclusion

This chapter presented concepts and approaches for off-line sensing, including a set of sensors that memorize pre-defined interaction via embedded 3D-printed structures filled with a conductive medium. In summary, the main contributions of this chapter are:

1. A consumer-level fabrication pipeline to easily create, 3D-print and capacitively read-out off-line sensors.

2. OFF-LINE SENSORS that memorize the stimuli pressure, squeeze, acceleration, tilt, flip, heat, and freeze.

3. A proof-of-concept evaluation shows their feasibility.

OFF-LINE SENSORS are close-volumetric objects that are read-out on-screen (see Figure 7.13). OFF-LINE SENSING is not a competing but complementing approach compared to traditional sensing, suited for off-line capture without supervision, possibly over a long timespan. To that end, this chapter aims to take a first step in exploring OFF-LINE SENSING for HCI by addressing fundamental conceptual and technical challenges. Therefore, it focuses on a basic, yet widely used set of one-time binary interactions that serve as a foundation for more advanced interactions.

Although inspired by logistics (see Figure 7.1), OFF-LINE SENSING is applicable in other domains, where it is beneficial to deploy sensors without supervision, possibly over a long timespan. For instance, an OFF-LINE SENSOR may be (1) attached to existing objects to monitor their status (e.g., to check if a rented tool was appropriately handled), or (2) integrated into fabricated objects to ensure that environmental conditions were met (e.g., an outdoor plant pot equipped with a freeze sensor signals that frost occurred at least once).

The next chapter summarizes and integrates the contributions of this thesis regarding the previously established design space (see Section 2.4).
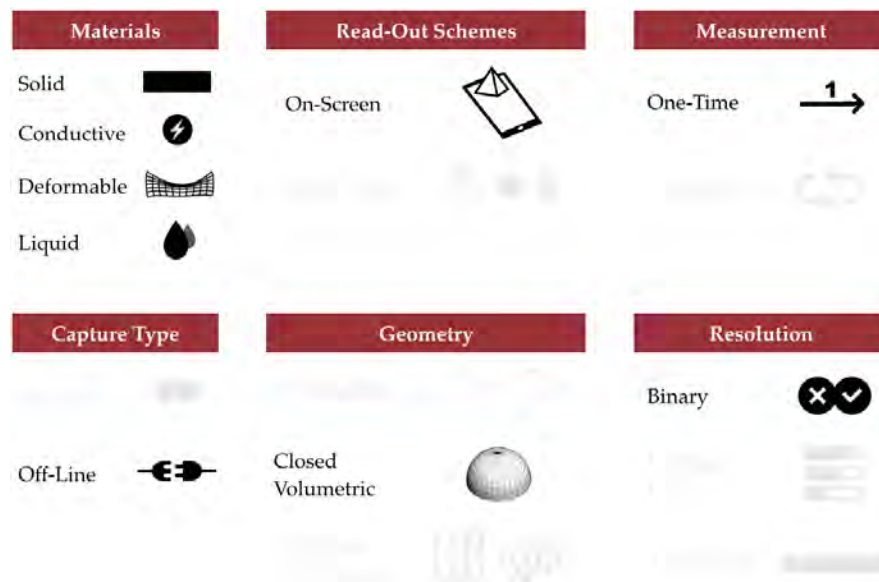
Figure 7.13: The classification of OFF-LINE SENSING regarding the design space of 3D-printed interaction.

Part V

INTEGRATION & CONCLUSIONS

CONCLUSIONS

8.1 SUMMARY

This thesis has argued that the trends for increasingly customized interactive devices can be fused with the emergence of 3D printing. In consequence, this fusion would allow users to design, generate and print an interactive device according to their personal needs or a specialized use case. Based on a design space for 3D-printed custom-made interactive devices, this thesis has explored how to fabricate 3D-printed objects that detect touch, deformation, or environmental stimuli.

TOUCH INTERACTION

In this research direction, CAPRICATE contributed a fabrication pipeline that enables users to easily design and 3D print highly customized objects that feature embedded capacitive multi-touch sensing. Objects are printed in a single pass using a commodity multi-material 3D printer, making CAPRICATE accessible to a wide audience of researchers, application developers, and end users. To enable touch input on a wide variety of 3D-printable surfaces, CAPRICATE proposes two techniques for designing and printing embedded sensors of a custom shape. It was technically and practically validated by a series of experiments and example applications, which demonstrate the broad applicability of CAPRICATE. By investigating 3D-printed capacitive sensing, this contribution forms the basis for all subsequent contributions.

DEFORMATION INTERACTION

In this research direction, the contributions of this thesis were two-fold:

First, this thesis contributed TRILATERATE, a fabrication pipeline to 3D-print customizable objects that detect the 3D position of a finger hovering, touching, or pressing them via capacitive trilateration. By combining capacitance

measurements of multiple electrodes placed inside the object, a 3D position is trilaterated in 3D space. TRILATERATE automatically places electrodes and operates on consumer-level 3D printers. The evaluation showed that the 3D position of a finger and multiple stages of pressure input can be reliably distinguished.

Second, this thesis contributes FLEXIBLES, 3D-printed flexible tangibles that are deformation-aware and operate on capacitive touchscreens. This approach added expressive deformation input to interaction with on-screen tangibles. Based on different types of deformation mapping, it contributed a set of 3D-printable sensors that capture pressing, squeezing, and bending input with multiple levels of intensities. Further, the posture of a FLEXIBLE is recognized on a capacitive touchscreen through a point pattern in which points additionally are encoded through varying intensity of capacitance. These concepts can be integrated into many 3D-printed objects with custom geometries and in different locations. A FLEXIBLE is printed in a single pass on a consumer-level 3D printer without requiring further assembly. A series of interactive prototypes, example applications, and a technical evaluation showed the feasibility and broad applicability of FLEXIBLES.

ENVIRONMENTAL INTERACTION

In this research direction, the contributions of this thesis were two-fold:

First, LIQUIDO proposed to embed liquids into 3D-printed objects to sense various tilting and motion interactions via capacitive sensing. It requires less assembly effort after printing and is a low-cost and easy-to-apply way of extending the input capabilities of 3D-printed objects. LIQUIDO contributed two liquid sensing patterns and a practical printing process using a standard dual-extrusion 3D printer and commercially available materials. A series of evaluations and a set of interactive example applications showed its feasibility.

Second, OFF-LINE SENSING extended the concept of liquid-filled 3D-printed objects in order to detect one-time interactions, such as accelerating or flipping. OFF-LINE SENSORS memorize a pre-defined interaction via an embedded structure filled with a conductive medium (e.g., a liquid). Whether a sensor was exposed to the interaction, can be read-out via a capacitive touchscreen. This approach does neither require active electronics nor power at the time of the interaction. Sensors are printed in a single pass on a consumer-level 3D printer. A series of experiments showed the feasibility of OFF-LINE SENSING.

INTEGRATION

Section 2.4 introduced a design space for 3D-printed interactive objects that allow all contributions to be classified according to its dimensions:

Multi-material 3D printing enables to create new composites of printable materials and complex, non-developable 3D objects. Therefore, this thesis investigated **material composites** with rising complexity, ranging from composites of two to four materials. It explores the general possibilities that multi-material 3D printing in combination with functional materials offers. With the advent of 3D printers that can print more and more materials simultaneously, it will be most likely possible to create 3D objects consisting of solid, deformable, conductive and liquid parts. Moreover, the contributed sensing concepts mostly operate on closed-volumetric **complex geometries**, required for routing of traces inside the object. While a vast variety of objects are closed-volumetric, TRILATERATE extends hover, touch, and pressure sensing to operate on small-scale netted and fine-grained geometries.

While the presented contributions of this thesis each feature a unique set of interaction sensing with different **resolution**, they are all based on the
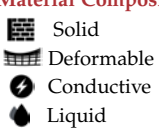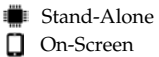
	Enabling Touch	Adding Deformation		Adding Environment	
	CAPRICATE (Chapter 3)	TRILATERATE (Chapter 4)	FLEXIBLES (Chapter 5)	LIQUIDO (Chapter 6)	OFF-LINE (Chapter 7)
Material Composite Solid, Deformable, Conductive, Liquid					
Most Complex Geometry	Closed Volumetric	Netted & Fine-Grained	Closed Volumetric	Closed Volumetric	Closed Volumetric
Measurement	Constantly	Constantly	Constantly	Constantly	One-Time
Capture Type	On-Line	On-Line	On-Line	On-Line	Off-Line
Resolution	Binary, Multi-Level	Continuous	Binary, Multi-Level, Continuous	Multi-Level, Continuous	Binary
Read-Out Scheme Stand-Alone, On-Screen					

Table 8.1: Contributions of each chapter concerning the design space presented in Section 2.4.

underlying principle of capacitive sensing. Therefore, all sensors can be, in principle, combined in a single 3D-printed object. For instance, sensor concepts for constant or one-time **measurements**, and on- or off-line **capture** do not inherently conflict. Also, approaches that operate with an on-screen **read-out** are directly transferable to a stand-alone use case. However, the transfer from stand-alone to on-screen approaches (such as TRILATERATE) does not apply without exception and requires further efforts.

8.2   DIRECTIONS FOR FUTURE RESEARCH

This thesis contributed towards the goal of end-user accessible, entirely 3D-printable customizable interactive devices. It yields interesting open challenges that research may be address in the future.

SUPPORT FOR FURTHER INTERACTIONS

While this thesis explored many sensor concepts that target touch, deformation, and environmental interactions, additional challenges remain in each direction: Regarding touch input, multi-touch on netted and fine-grained objects is still challenging because current approaches either require too much space for electrodes or need to route too many traces per area. Therefore, future research shall address how to reduce the number of wires and also support multi-touch at high resolution. Moreover, the deformation of an object, in general, refers to any change in the shape or size of a 3D object. While this thesis investigates press, squeeze, and bend deformations, many deformations, such as twisting or stretching, remain unexplored in the context of 3D-printed interaction. Similarly, OFF-LINE SENSING presents first results on the memorization of interactions through capacitive coupling. It lays the foundation for a new kind of sensing, which, in contrast to traditional sensing, does not require energy during sensing and only operates by coding internal states in a suitable meta-structure. As a consequence, many kinds of meta-structure may be envisioned by research that, for instance, improve over binary resolution, support additional interactions, or detect sequences of interactions.

In general, the set of in- and output modalities is much broader than the scope of a single thesis. For instance, it ranges from input via stacking, combining, or splitting 3D objects to output such as tactile haptics, mechanical actuation, or visual 3D output. In consequence, future research shall explore

additional interactions to strengthen the expressiveness of 3D-printed interactive objects further.

3D-PRINTED METAMATERIAL

With advances in 3D printing technologies, a striving research trend is to integrate functionality directly in the material itself instead of adding additional components. While research in the field of Computer Graphics is already investigating how to design material properties computationally (cf. [Bic+10; Sko+13; Zeh+17]), these findings need to be transferred to the domain of HCI and extended to sense input or provide output actively.

The properties of such computationally designed materials can extend upon the current possibilities of combining different types of materials (e.g., deformable vs. solid) by allowing an interpolation in-between material types to create objects with new properties. In consequence, future research shall further focus on the generation of input and output capabilities by controlling microscopic material properties.

EMBEDDED 3D-PRINTED ELECTRONICS

While the ultimate goal of 3D-printed interactive devices is the complete and integrated printing of electronics and an enclosing object, the fabrication processed of standard electrical components is far from being shifted to 3D printing. In order to mitigate this issue, research investigates automatic pick-and-place printing technologies, that not only print conductive traces and enclosure but also automatically place and connect electrical components (cf. [Was+16]).

Towards this goal, it is necessary to design 3D models that not only consist of enclosing material and conductive traces but also encode the appropriate sub-millimeter dimensions of electrical components. This task is currently carried out manually by experts, which is very time-consuming and prone to errors. Future research shall investigate methods to automate the placement of components or the routing of conductive traces in order to minimize the effort required by users to create a customized interactive object.

GENERALIZATION OF INTERACTION CONCEPTS

The specification of complex 3D-printed user interfaces based on abstract interaction concepts, possible for a sequence of interactions or multiple 3D

objects, is an open research challenge. Based on this thesis, research shall explore suitable sets of interaction concepts, which allow the broadest possible range of 3D-printed user interfaces (e.g., a handful of touch-based interaction concepts enable a broad range of interactions on today's smartphones). It remains open how such a set of interaction concepts for 3D-printed objects would look like and, further, whether a set of interaction concepts for 3D-printed interaction that is independent of the specific object geometry exists at all.

DECOUPLING OF INTERACTION AND TECHNOLOGY

Digital fabrication technologies gave rise to a multitude of different 3D modeling file format. While practical and valid, they focus on the specification of (multiple) materials for the printing process (cf. the 3D Manufacturing Format [kei18]). However, as research is moving towards the automatic creation of custom interactive devices, the specification of the locations of interactive components, their interaction with each other and also the communication with other objects or systems is becoming more and more critical. As a consequence, research shall further focus on contributing and unifying methods to specify the interactive behavior of an object in itself and with its surroundings. That is, users may define interactions without requiring knowledge about the particular printing process, the material properties, or geometrical details. Due to this decoupling of interaction description from technology-specific properties, algorithms may apply and possibly transform a conceptual interaction description to the requirements of users, different 3D geometries, or printing technologies.

8.2.1   *Concluding Remarks*

This thesis contributed to the vision of interactive devices that are individually designed and printed all at once rather than being mass-produced and assembled (cf. [Wil+12]). The presented concepts and approaches aim to become a valuable asset to researchers, application developers, and end user to 3D-print custom-made interactive devices.

LIST OF FIGURES

LIST OF TABLES

LISTINGS

BIBLIOGRAPHY

[3D-18]   3D-Matter. *Meet Testman! – 3D Matter*. 2018. URL: `https://my3dmatter.com/meet-testman/` (visited on Aug. 7, 2018).

[3DH18a]   3DHubs. *Additive Manufacturing Technologies: An Overview*. 2018. URL: `https://www.3dhubs.com/knowledge-base/additive-manufacturing-technologies-overview` (visited on Aug. 7, 2018).

[3DH18b]   3DHubs. *FDM 3D Printing Materials Compared*. 2018. URL: `https://www.3dhubs.com/knowledge-base/fdm-3d-printing-materials-compared` (visited on Aug. 7, 2018).

[AWB11]   F. Aezinia, Y. Wang, and B. Bahreyni. 'Touchless Capacitive Sensor for Hand Gesture Detection.' In: *2011 IEEE SENSORS*. 2011 IEEE SENSORS. Oct. 2011, pp. 546–549. DOI: `10.1109/ICSENS.2011.6127321`.

[AWB12]   F. Aezinia, Y. Wang, and B. Bahreyni. 'Three Dimensional Touchless Tracking of Objects Using Integrated Capacitive Sensors.' In: *IEEE Transactions on Consumer Electronics* 58.3 (Aug. 2012), pp. 886–890. ISSN: 0098-3063. DOI: `10.1109/TCE.2012.6311332`.

[Ahm13]   Majid Ahmadloo. 'Design and Fabrication of Geometrically Complicated Multiband Microwave Devices Using a Novel Integrated 3D Printing Technique.' In: *2013 IEEE 22nd Conference on Electrical Performance of Electronic Packaging and Systems* (Oct. 2013), pp. 29–32. DOI: `10.1109/EPEPS.2013.6703460`.

[AGV10]   Eric Akaoka, Tim Ginn, and Roel Vertegaal. 'DisplayObjects: Prototyping Functional Physical Interfaces on 3D Styrofoam, Paper or Cardboard Models.' In: *Proceedings of the Fourth International Conference on Tangible, Embedded, and Embodied Interaction*. TEI '10. New York, NY, USA: ACM, 2010, pp. 49–56. ISBN: 978-1-60558-841-4. DOI: `10.1145/1709886.1709897`.

[An+18]   Byoungkwon An et al. 'Thermorph: Democratizing 4D Printing of Self-Folding Materials and Interfaces.' In: *Proceedings of the 2018 CHI Conference on Human Factors in Computing Systems.*

CHI '18. New York, NY, USA: ACM, 2018, 260:1–260:12. ISBN: 978-1-4503-5620-6. DOI: 10.1145/3173574.3173834.

[And12]   Chris Anderson. *Makers: The New Industrial Revolution*. Random House, 2012. ISBN: 978-1-84794-067-4.

[Bäc+16]   Moritz Bächer, Benjamin Hepp, Fabrizio Pece, Paul G. Kry, Bernd Bickel, Bernhard Thomaszewski, and Otmar Hilliges. 'DefSense: Computational Design of Customized Deformable Input Devices.' In: *Proceedings of the 2016 CHI Conference on Human Factors in Computing Systems*. CHI '16. New York, NY, USA: ACM, 2016, pp. 3806–3816. ISBN: 978-1-4503-3362-7. DOI: 10.1145/2858036.2858354.

[Bal+99]   Ravin Balakrishnan, George Fitzmaurice, Gordon Kurtenbach, Karan Singh, and King Street East. 'Exploring Interactive Curve and Surface Manipulation Using a Bend and Twist Sensitive Input Strip.' In: *Proceedings of the 1999 symposium on Interactive 3D graphics* (1999), pp. 111–118. DOI: 10.1145/300523.300536.

[BGL18]   Rafael Ballagas, Sarthak Ghosh, and James Landay. 'The Design Space of 3D Printable Interactivity.' In: *Proc. ACM Interact. Mob. Wearable Ubiquitous Technol.* 2.2 (July 2018), 61:1–61:21. ISSN: 2474-9567. DOI: 10.1145/3214264.

[BBR10]   Patrick Baudisch, Torsten Becker, and Frederik Rudeck. 'Lumino: Tangible Blocks for Tabletop Computers Based on Glass Fiber Bundles.' In: *Proceedings of the 28th International Conference on Human Factors in Computing Systems - CHI '10*. New York, New York, USA: ACM Press, 2010, p. 1165. ISBN: 978-1-60558-929-9. DOI: 10.1145/1753326.1753500.

[Bax96]   L K Baxter. *Capacitive Sensors: Design and Applications, Vol. 1 of IEEE Press Series on Electronics Technology*. 1996.

[Ben+01]   Eran Ben-Joseph, Hiroshi Ishii, John Underkoffler, Ben Piper, and Luke Yeung. 'Urban Simulation and the Luminous Planning Table: Bridging the Gap between the Digital and the Tangible.' In: *Journal of Planning Education and Research* 21.2 (Dec. 1, 2001), pp. 196–196. ISSN: 0739456X. DOI: 10.1177/073945601128993166.

[Bic+10]   Bernd Bickel, Moritz Bächer, Miguel a. Otaduy, Hyunho Richard Lee, Hanspeter Pfister, Markus Gross, and Wojciech Matusik. 'Design and Fabrication of Materials with Desired Deformation Behavior.' In: *ACM Transactions on Graphics* 29.4

(July 26, 2010), p. 1. ISSN: 07300301. DOI: 10 . 1145 / 1833351 . 1778800.

[BP08] Mark Billinghurst and Ivan Poupyrev. 'Tangible Augmented Reality.' In: *SIGGRAPH Asia '08*. New York, New York, USA: ACM Press, 2008, pp. 1–10.

[BPH13] Eric Brockmeyer, Ivan Poupyrev, and Scott Hudson. 'PAPILLON: Designing Curved Display Surfaces with Printed Optics.' In: *Proceedings of the 26th Annual ACM Symposium on User Interface Software and Technology - UIST '13*. New York, New York, USA: ACM Press, 2013, pp. 457–462. ISBN: 978-1-4503-2268-3. DOI: 10.1145/2501988.2502027.

[Bur+15] Jesse Burstyn, Nicholas Fellion, Paul Strohmeier, and Roel Vertegaal. *PrintPut: Resistive and Capacitive Input Widgets for Interactive 3D Prints*. Ed. by Julio Abascal, Simone Barbosa, Mirko Fetter, Tom Gross, Philippe Palanque, and Marco Winckler. Vol. 9296. Series Title: Lecture Notes in Computer Science Publication Title: INTERACT 2015. Cham: Springer International Publishing, 2015. 332-339. ISBN: 978-3-319-22700-9. DOI: 10.1007/978-3-319-22701-6.

[CW15] Varun Perumal C and Daniel Wigdor. 'Printem: Instant Printed Circuit Boards with Standard Office Printers & Inks.' In: *Proceedings of the 28th Annual ACM Symposium on User Interface Software & Technology*. UIST '15. New York, NY, USA: ACM, 2015, pp. 243–251. ISBN: 978-1-4503-3779-3. DOI: 10 . 1145 / 2807442 . 2807511.

[Cha+12] Liwei Chan, Stefanie Müller, Anne Roudaut, and Patrick Baudisch. 'CapStones and ZebraWidgets: Sensing Stacks of Building Blocks, Dials and Sliders on Capacitive Touch Screens.' In: *Proceedings of the 2012 ACM Annual Conference on Human Factors in Computing Systems - CHI '12*. New York, New York, USA: ACM Press, 2012, p. 2189. ISBN: 978-1-4503-1015-4. DOI: 10.1145/2207676.2208371.

[Cha+06] W. Chang, K. E. Kim, H. Lee, J. K. Cho, B. S. Soh, J. H. Shim, G. Yang, S. Cho, and J. Park. 'Recognition of Grip-Patterns by Using Capacitive Touch Sensors.' In: *2006 IEEE International Symposium on Industrial Electronics*. 2006 IEEE International Symposium on Industrial Electronics. Vol. 4. July 2006, pp. 2936–2941. DOI: 10.1109/ISIE.2006.296083.

[Chi+15]   Chin-yu Chien, Rong-Hao Liang, Long-Fei Lin, Liwei Chan, and Bing-Yu Chen. 'FlexiBend : Enabling Interactivity of Multi-Part , Deformable Fabrications Using Single Shape-Sensing Strip.' In: *Proceedings of the 28th Annual ACM Symposium on User Interface Software & Technology - UIST '15*. New York, New York, USA: ACM Press, 2015, pp. 659–663. ISBN: 978-1-4503-3779-3. DOI: 10.1145/2807442.2807456.

[Coh88]   Jacob Cohen. *Statistical Power Analysis for the Behavioral Sciences*. Routledge, 1988. ISBN: 978-1-134-74270-7. DOI: 10.4324/9780203771587.

[Col+99]   James P. Coleman, Anne T. Lynch, Puttanachetty Madhukar, and John H. Wagenknecht. 'Printed, Flexible Electrochromic Displays Using Interdigitated Electrodes.' In: *Solar Energy Materials and Solar Cells* 56.3 (Jan. 30, 1999), pp. 395–418. ISSN: 0927-0248. DOI: 10.1016/S0927-0248(98)00144-5.

[Cor+13]   Christian Corsten, Ignacio Avellino, Max Möllers, and Jan Borchers. 'Instant User Interfaces: Repurposing Everyday Objects As Input Devices.' In: *Proceedings of the 2013 ACM International Conference on Interactive Tabletops and Surfaces*. ITS '13. New York, NY, USA: ACM, 2013, pp. 71–80. ISBN: 978-1-4503-2271-3. DOI: 10.1145/2512349.2512799.

[CWB13]   Christian Corsten, Chat Wacharamanotham, and Jan Borchers. 'Fillables: Everyday Vessels As Tangible Controllers with Adjustable Haptics.' In: *CHI '13 Extended Abstracts on Human Factors in Computing Systems on - CHI EA '13*. 2013, pp. 2129–2138. ISBN: 9781450319522. DOI: 10.1145/2468356.2468732.

[DRS03]   Kiran Dandekar, Balasundar I Raju, and Mandayam a Srinivasan. '3-D Finite-Element Models of Human and Monkey Fingertips to Investigate the Mechanics of Tactile Sense.' In: *Journal of Biomechanical Engineering* 125.5 (2003), p. 682. ISSN: 01480731. DOI: 10.1115/1.1613673. PMID: 14618927.

[DKY16]   Claudia Daudén Roquet, Jeeeun Kim, and Tom Yeh. '3D Folded PrintGami: Transforming Passive 3D Printed Objects to Interactive by Inserted Paper Origami Circuits.' In: *Proceedings of the 2016 ACM Conference on Designing Interactive Systems*. DIS '16. New York, NY, USA: ACM, 2016, pp. 187–191. ISBN: 978-1-4503-4031-1. DOI: 10.1145/2901790.2901891.

[DKP15]   Artem Dementyev, Hsin-Liu (Cindy) Kao, and Joseph a. Paradiso. 'SensorTape: Modular and Programmable 3D-Aware Dense Sensor Network on a Tape.' In: *Proceedings of the 28th Annual ACM Symposium on User Interface Software & Technology*. UIST '15. New York, New York, USA: ACM Press, Nov. 5, 2015, pp. 649–658. ISBN: 978-1-4503-3779-3. DOI: `10.1145/2807442.2807507`.

[DMC18]   Ruta Desai, James McCann, and Stelian Coros. 'Assembly-Aware Design of Printable Electromechanical Devices.' In: *Proceedings of the 31st Annual ACM Symposium on User Interface Software and Technology*. UIST '18. New York, NY, USA: ACM, 2018, pp. 457–472. ISBN: 978-1-4503-5948-1. DOI: `10.1145/3242587.3242655`.

[DLY02]   Paul H. Dietz, Darren Leigh, and William S. Yerazunis. 'Wireless Liquid Level Sensing for Restaurant Applications.' In: *Proceedings of IEEE Sensors* 1 (MAY 2002 2002), pp. 715–720. DOI: `10.1109/ICSENS.2002.1037191`.

[DKA14]   M. Q. Duong, Y. Kawahara, and T. Asami. 'Design of Touch-Sensitive Surface with Arbitrary Shape Based on Time-Domain Reflectometry Using Injket Printing.' In: *2014 IEEE Radio and Wireless Symposium (RWS)*. 2014 IEEE Radio and Wireless Symposium (RWS). Jan. 2014, pp. 16–18. DOI: `10.1109/RWS.2014.6830134`.

[ESM11]   Christoph Endres, Tim Schwartz, and Christian A. Müller. '"Geremin": 2D Microgestures for Drivers Based on Electric Field Sensing.' In: *Proceedings of the 16th International Conference on Intelligent User Interfaces*. IUI '11. New York, NY, USA: ACM, 2011, pp. 327–330. ISBN: 978-1-4503-0419-1. DOI: `10.1145/1943403.1943457`.

[Esp+14]   David Espalin, Danny W. Muse, Eric MacDonald, and Ryan B. Wicker. '3D Printing Multifunctionality: Structures with Electronics.' In: *The International Journal of Advanced Manufacturing Technology* 72.5-8 (Mar. 4, 2014), pp. 963–978. ISSN: 0268-3768. DOI: `10.1007/s00170-014-5717-7`.

[fil18]   filabot. *Filament Maker - Recycle Filament for Any 3D Printer – Filabot*. 2018. URL: `https://www.filabot.com/` (visited on Aug. 7, 2018).

[Fre10]   Semiconductor Freescale. *Proximity Capacitive Touch Sensor Controller MPR121*. 2010. URL: https://www.sparkfun.com/datasheets/Components/MPR121.pdf (visited on Aug. 7, 2018).

[FKS14]   Markus Funk, Oliver Korn, and Albrecht Schmidt. 'An Augmented Workplace for Enabling User-Defined Tangibles.' In: *CHI '14 Extended Abstracts on Human Factors in Computing Systems*. CHI EA '14. New York, NY, USA: ACM, 2014, pp. 1285–1290. ISBN: 978-1-4503-2474-8. DOI: 10.1145/2559206.2581142.

[Geb16]   Andreas Gebhardt. *Additive Fertigungsverfahren: additive Manufacturing und 3D-Drucken für Prototyping - Tooling - Produktion*. 5., neu bearbeitete und erweiterte Auflage. OCLC: 960805666. München: Hanser, 2016. 711 pp. ISBN: 978-3-446-44401-0.

[Go+12]   Kentaro Go, Katsutoshi Nonaka, Koji Mitsuke, and Masayuki Morisawa. 'Object Shape and Touch Sensing on Interactive Tables with Optical Fiber Sensors.' In: *Proceedings of the Sixth International Conference on Tangible, Embedded and Embodied Interaction - TEI '12*. New York, New York, USA: ACM Press, 2012, p. 123. ISBN: 978-1-4503-1174-8. DOI: 10.1145/2148131.2148158.

[GHP11]   Nan-Wei Gong, Steve Hodges, and Joseph A. Paradiso. 'Leveraging Conductive Inkjet Technology to Build a Scalable and Versatile Surface for Ubiquitous Sensing.' In: *Proceedings of the 13th International Conference on Ubiquitous Computing*. UbiComp '11. New York, NY, USA: ACM, 2011, pp. 45–54. ISBN: 978-1-4503-0630-0. DOI: 10.1145/2030112.2030120.

[Gon+14]   Nan-wei Gong, Jürgen Steimle, Simon Olberding, Steve Hodges, Nicholas Edward Gillian, Yoshihiro Kawahara, and Joseph A. Paradiso. 'PrintSense: A Versatile Sensing Technique to Support Multimodal Flexible Surface Interaction.' In: *Proceedings of the 32nd Annual ACM Conference on Human Factors in Computing Systems - CHI '14*. New York, New York, USA: ACM Press, Apr. 26, 2014, pp. 1407–1410. ISBN: 978-1-4503-2473-1. DOI: 10.1145/2556288.2557173.

[GWP12]   Nan-Wei Gong, Chiu-Yen Wang, and Joseph A. Paradiso. 'Low-Cost Sensor Tape for Environmental Sensing Based on Roll-to-Roll Manufacturing Process.' In: *2012 IEEE Sensors*. IEEE, Oct. 2012, pp. 1–4. ISBN: 978-1-4577-1767-3. DOI: 10.1109/ICSENS.2012.6411347.

[GA16]   Timo Götzelmann and Christopher Althaus. 'TouchSurface-Models: Capacitive Sensing Objects Through 3D Printers.' In: *Proceedings of the 9th ACM International Conference on PErvasive Technologies Related to Assistive Environments*. PETRA '16. New York, NY, USA: ACM, 2016, 22:1–22:8. ISBN: 978-1-4503-4337-4. DOI: 10.1145/2910674.2910690.

[GS16]   Timo Götzelmann and Daniel Schneider. 'CapCodes: Capacitive 3D Printable Identification and On-Screen Tracking for Tangible Interaction.' In: *Proceedings of the 9th Nordic Conference on Human-Computer Interaction - NordiCHI '16*. New York, New York, USA: ACM Press, 2016, pp. 1–4. ISBN: 978-1-4503-4763-1. DOI: 10.1145/2971485.2971518.

[GF01]   Saul Greenberg and Chester Fitchett. 'Phidgets: Easy Development of Physical Interfaces Through Physical Widgets.' In: *Proceedings of the 14th Annual ACM Symposium on User Interface Software and Technology*. UIST '01. New York, NY, USA: ACM, 2001, pp. 209–218. ISBN: 978-1-58113-438-4. DOI: 10.1145/502348.502388.

[GS18]   Daniel Groeger and Jürgen Steimle. 'ObjectSkin: Augmenting Everyday Objects with Hydroprinted Touch Sensors and Displays.' In: *Proceedings of the ACM on Interactive, Mobile, Wearable and Ubiquitous Technologies* 1.4 (Jan. 2018), 134:1–134:23. ISSN: 2474-9567. DOI: 10.1145/3161165.

[GCS16]   Daniel Gröger, Elena Chong Loo, and Jürgen Steimle. 'HotFlex: Post-Print Customization of 3D Prints Using Embedded State Change.' In: *Proceedings of the 2016 CHI Conference on Human Factors in Computing Systems*. CHI '16. New York, NY, USA: ACM, 2016, pp. 420–432. ISBN: 978-1-4503-3362-7. DOI: 10.1145/2858036.2858191.

[Gro15]   Tobias Alexander Große-Puppendahl. 'Capacitive Sensing and Communication for Ubiquitous Interaction and Environmental Perception.' Darmstadt: Technische Universität Darmstadt, 2015. URL: http://tuprints.ulb.tu-darmstadt.de/4568/.

[Gro+13] Tobias Grosse-Puppendahl, Andreas Braun, Felix Kamieth, and Arjan Kuijper. 'Swiss-Cheese Extended: An Object Recognition Method for Ubiquitous Interfaces Based on Capacitive Proximity Sensing.' In: *Proceedings of the SIGCHI Conference on Human Factors in Computing Systems*. CHI '13. New York, NY, USA:

ACM, 2013, pp. 1401–1410. ISBN: 978-1-4503-1899-0. DOI: `10 . 1145/2470654.2466186`.

[Gro+14]   Tobias Grosse-Puppendahl, Sebastian Herber, Raphael Wimmer, Frank Englert, Sebastian Beck, Julian von Wilmsdorff, Reiner Wichert, and Arjan Kuijper. 'Capacitive Near-Field Communication for Ubiquitous Interaction and Perception.' In: *Proceedings of the 2014 ACM International Joint Conference on Pervasive and Ubiquitous Computing*. UbiComp '14. New York, NY, USA: ACM, 2014, pp. 231–242. ISBN: 978-1-4503-2968-2. DOI: `10 . 1145/2632048.2632053`.

[Gro+17]   Tobias Grosse-Puppendahl, Christian Holz, Gabe Cohn, Raphael Wimmer, Oskar Bechtold, Steve Hodges, Matthew S. Reynolds, and Joshua R. Smith. 'Finding Common Ground: A Survey of Capacitive Sensing in Human-Computer Interaction.' In: *Proceedings of the 2017 CHI Conference on Human Factors in Computing Systems*. CHI '17. New York, NY, USA: ACM, 2017, pp. 3293–3315. ISBN: 978-1-4503-4655-9. DOI: `10.1145/3025453. 3025808`.

[Gün+17]   Sebastian Günther, Martin Schmitz, Florian Müller, Jan Riemann, and Max Mühlhäuser. 'BYO*: Utilizing 3D Printed Tangible Tools for Interaction on Interactive Surfaces.' In: *Proceedings of the 2017 ACM Workshop on Interacting with Smart Objects - SmartObject '17*. New York, New York, USA: ACM Press, 2017, pp. 21–26. ISBN: 978-1-4503-4902-4. DOI: `10.1145/3038450. 3038456`.

[Guo+17]   Shuang Zhuang Guo, Kaiyan Qiu, Fanben Meng, Sung Hyun Park, and Michael C. McAlpine. '3D Printed Stretchable Tactile Sensors.' In: *Advanced Materials* 29.27 (2017), pp. 1–8. DOI: `10 . 1002/adma.201701218`. pmid: 28474793.

[HIS17]   Kazune Hagino, Daisuke Iwai, and Kosuke Sato. 'Place Management of Electrodes for Embedding Capacitive Multi-Touch Sensor on 3D Printed Surfaces.' In: *Proceedings of the 1st Annual ACM Symposium on Computational Fabrication - SCF '17*. 2017, pp. 1–2. ISBN: 978-1-4503-4999-4. DOI: `10 . 1145 / 3083157 . 3092889`.

[Han+06]   M.S. Hancock, Sheelagh Carpendale, F.D. Vernier, Daniel Wigdor, and Chia Shen. 'Rotation and Translation Mechanisms for Tabletop Interaction.' In: *First IEEE International Workshop on Horizontal Interactive Human-Computer Systems (TABLETOP '06).*

Vol. 2006. IEEE, 2006, pp. 79–88. ISBN: 0-7695-2494-X. DOI: `10 . 1109/TABLETOP.2006.26`.

[HBW11]   Chris Harrison, Hrvoje Benko, and Andrew D. Wilson. 'OmniTouch: Wearable Multitouch Interaction Everywhere.' In: *Proceedings of the 24th Annual ACM Symposium on User Interface Software and Technology*. UIST '11. New York, NY, USA: ACM, 2011, pp. 441–450. ISBN: 978-1-4503-0716-1. DOI: `10 . 1145 / 2047196 . 2047255`.

[HNR68]   P. E. Hart, N. J. Nilsson, and B. Raphael. 'A Formal Basis for the Heuristic Determination of Minimum Cost Paths.' In: *IEEE Transactions on Systems Science and Cybernetics* 4.2 (July 1968), pp. 100–107. ISSN: 0536-1567. DOI: `10.1109/TSSC.1968.300136`.

[He+17]   Liang He, Gierad Laput, Eric Brockmeyer, and Jon E Froehlich. 'SqueezaPulse : Adding Interactive Input to Fabricated Objects Using Corrugated Tubes and Air Pulses.' In: *Proceedings of the Tenth International Conference on Tangible, Embedded, and Embodied Interaction - TEI '17*. New York, New York, USA: ACM Press, 2017, pp. 341–350. ISBN: 978-1-4503-4676-4. DOI: `10.1145/ 3024969.3024976`.

[HBB11]   Fabian Hennecke, Franz Berwein, and Andreas Butz. 'Optical Pressure Sensing for Tangible User Interfaces.' In: *Proceedings of the ACM International Conference on Interactive Tabletops and Surfaces - ITS '11*. New York, New York, USA: ACM Press, Nov. 13, 2011, p. 45. ISBN: 978-1-4503-0871-7. DOI: `10 . 1145 / 2076354 . 2076362`.

[HKI08]   O. Hilliges, D. Kim, and S. Izadi. 'Creating Malleable Interactive Surfaces Using Liquid Displacement Sensing.' In: *2008 3rd IEEE International Workshop on Horizontal Interactive Human Computer Systems*. 2008 3rd IEEE International Workshop on Horizontal Interactive Human Computer Systems. Oct. 2008, pp. 157–160. DOI: `10.1109/TABLETOP.2008.4660199`.

[Hin+16]   Ken Hinckley, Seongkook Heo, Michel Pahud, Christian Holz, Hrvoje Benko, Abigail Sellen, Richard Banks, Kenton O'Hara, Gavin Smyth, and William Buxton. 'Pre-Touch Sensing for Mobile Interaction.' In: *Proceedings of the 2016 CHI Conference on Human Factors in Computing Systems*. CHI '16. New York, NY, USA: ACM, 2016, pp. 2869–2881. ISBN: 978-1-4503-3362-7. DOI: `10.1145/2858036.2858095`.

[Hod+13]   Steve Hodges, Stuart Taylor, Nicolas Villar, James Scott, and John Helmes. 'Exploring Physical Prototyping Techniques for Functional Devices Using .NET Gadgeteer.' In: *Proceedings of the 7th International Conference on Tangible, Embedded and Embodied Interaction*. TEI '13. Place: New York, New York, USA. 2013, p. 271. ISBN: 9781450318983. DOI: 10.1145/2460625.2460670.

[HV11]   David Holman and Roel Vertegaal. 'TactileTape : Low-Cost Touch Sensing on Curved Surfaces.' In: *Proceedings of the 24th Annual ACM Symposium Adjunct on User Interface Software and Technology*. 2011, pp. 17–18. ISBN: 978-1-4503-1014-7. DOI: 10.1145/2046396.2046406.

[HBK15]   Christian Holz, Senaka Buthpitiya, and Marius Knaust. 'Bodyprint: Biometric User Identification on Mobile Devices Using the Capacitive Touchscreen to Scan Body Parts.' In: *Proceedings of the ACM CHI'15 Conference on Human Factors in Computing Systems* 1 (2015), pp. 3011–3014. DOI: 10.1145/2702123.2702518.

[Hoo+14]   Jonathan Hook, Thomas Nappey, Steve Hodges, Peter Wright, and Patrick Olivier. 'Making 3D Printed Objects Interactive Using Wireless Accelerometers.' In: *Proceedings of the Extended Abstracts of the 32Nd Annual ACM Conference on Human Factors in Computing Systems*. CHI EA '14. New York, NY, USA: ACM, 2014, pp. 1435–1440. ISBN: 978-1-4503-2474-8. DOI: 10.1145/2559206.2581137.

[Hua+98]   Jian Huang, Roni Yagel, Vassily Filippov, and Yair Kurzion. 'An Accurate Method for Voxelizing Polygon Meshes.' In: *Proceedings of the 1998 IEEE Symposium on Volume Visualization*. Series Title: VVS '98. New York, NY, USA: ACM, 1998, pp. 119–126. ISBN: 1-58113-105-4. DOI: 10.1145/288126.288181.

[Hub+12]   Jochen Huber, Jürgen Steimle, Chunyuan Liao, Qiong Liu, and Max Mühlhäuser. 'LightBeam: Interacting with Augmented Real-World Objects in Pico Projections.' In: *Proceedings of the 11th International Conference on Mobile and Ubiquitous Multimedia*. MUM '12. New York, NY, USA: ACM, 2012, 16:1–16:10. ISBN: 978-1-4503-1815-0. DOI: 10.1145/2406367.2406388.

[HPS16]   Charles Hudin, Sabrina Panëels, and Steven Strachan. 'INTACT : Instant Interaction with 3D Printed Objects.' In: *Proceedings of the 2016 CHI Conference Extended Abstracts on Human Factors in Computing Systems - CHI EA '16*. New York, New York, USA:

ACM Press, 2016, pp. 2719–2725. ISBN: 978-1-4503-4082-3. DOI: `10.1145/2851581.2892351`.

[Hud14]   Scott E. Hudson. 'Printing Teddy Bears: A Technique for 3D Printing of Soft Interactive Objects.' In: *Proceedings of the 32nd Annual ACM Conference on Human Factors in Computing Systems - CHI '14*. New York, New York, USA: ACM Press, 2014, pp. 459–468. ISBN: 978-1-4503-2473-1. DOI: `10.1145/2556288.2557338`.

[HM06]   Scott E. Hudson and Jennifer Mankoff. 'Rapid Construction of Functioning Physical Interfaces from Cardboard, Thumbtacks, Tin Foil and Masking Tape.' In: *Proceedings of the 19th Annual ACM Symposium on User Interface Software and Technology*. UIST '06. New York, NY, USA: ACM, 2006, pp. 289–298. ISBN: 978-1-59593-313-3. DOI: `10.1145/1166253.1166299`.

[Ion+16]   Alexandra Ion, Johannes Frohnhofen, Ludwig Wall, Robert Kovacs, Mirela Alistar, Jack Lindsay, Pedro Lopes, Hsiang-ting Chen, and Patrick Baudisch. 'Metamaterial Mechanisms.' In: *Proceedings of the 29th Annual Symposium on User Interface Software and Technology - UIST '16*. New York, New York, USA: ACM Press, 2016, pp. 529–539. ISBN: 978-1-4503-4189-9. DOI: `10.1145/2984511.2984540`.

[Ion+18]   Alexandra Ion, Robert Kovacs, Oliver S. Schneider, Pedro Lopes, and Patrick Baudisch. 'Metamaterial Textures.' In: *Proceedings of the 2018 CHI Conference on Human Factors in Computing Systems*. CHI '18. New York, NY, USA: ACM, 2018, 336:1–336:12. ISBN: 978-1-4503-5620-6. DOI: `10.1145/3173574.3173910`.

[Ion+17]   Alexandra Ion, Ludwig Wall, Robert Kovacs, and Patrick Baudisch. 'Digital Mechanical Metamaterials.' In: *Proceedings of the 2017 CHI Conference on Human Factors in Computing Systems*. CHI '17. New York, NY, USA: ACM, 2017, pp. 977–988. ISBN: 978-1-4503-4655-9. DOI: `10.1145/3025453.3025624`.

[IP14]   Yoshio Ishiguro and Ivan Poupyrev. '3D Printed Interactive Speakers.' In: *Proceedings of the 32nd Annual ACM Conference on Human Factors in Computing Systems - CHI '14*. New York, New York, USA: ACM Press, 2014, pp. 1733–1742. ISBN: 978-1-4503-2473-1. DOI: `10.1145/2556288.2557046`.

[IU97]   Hiroshi Ishii and Brygg Ullmer. 'Tangible Bits: Towards Seamless Interfaces Between People, Bits and Atoms.' In: *Proceedings of the SIGCHI Conference on Human Factors in Computing Systems*

- *CHI '97*. Vol. 39. New York, New York, USA: ACM Press, 1997, pp. 234–241. ISBN: 0-89791-802-9. DOI: 10.1145/258549.258715. pmid: 80.

[ICG17]   Vikram Iyer, Justin Chan, and Shyamnath Gollakota. '3D Printing Wireless Connected Objects.' In: *ACM Transactions on Graphics* 36.6 (Nov. 20, 2017), pp. 1–13. ISSN: 07300301. DOI: 10.1145/3130800.3130822.

[Jan10]   Yvonne Jansen. 'Mudpad : Fluid Haptics for Multitouch Surfaces.' In: *Human Factors* (2010), pp. 4351–4356. DOI: 10.1145/1753846.1754152.

[Kar+13]   Mustafa Emre Karagozler, Ivan Poupyrev, Gary K. Fedder, and Yuri Suzuki. 'Paper Generators: Harvesting Energy from Touching, Rubbing and Sliding.' In: *Proceedings of the 26th Annual ACM Symposium on User Interface Software and Technology*. UIST '13. New York, NY, USA: ACM, 2013, pp. 23–30. ISBN: 978-1-4503-2268-3. DOI: 10.1145/2501988.2502054.

[KG15]   Çağdaş Karataş and Marco Gruteser. 'Printing Multi-Key Touch Interfaces.' In: *Proceedings of the 2015 ACM International Joint Conference on Pervasive and Ubiquitous Computing*. UbiComp '15. New York, NY, USA: ACM, 2015, pp. 169–179. ISBN: 978-1-4503-3574-4. DOI: 10.1145/2750858.2804285.

[KM14]   Kunihiro Kato and Homei Miyashita. 'Extension Sticker: A Method for Transferring External Touch Input Using a Striped Pattern Sticker.' In: *Proceedings of the Adjunct Publication of the 27th Annual ACM Symposium on User Interface Software and Technology*. UIST'14 Adjunct. New York, NY, USA: ACM, 2014, pp. 59–60. ISBN: 978-1-4503-3068-8. DOI: 10.1145/2658779.2668032.

[KM15]   Kunihiro Kato and Homei Miyashita. 'ExtensionSticker: A Proposal for a Striped Pattern Sticker to Extend Touch Interfaces and Its Assessment.' In: *Proceedings of the 33rd Annual ACM Conference on Human Factors in Computing Systems - CHI '15*. Vol. 1. New York, New York, USA: ACM Press, 2015, pp. 1851–1854. ISBN: 978-1-4503-3145-6. DOI: 10.1145/2702123.2702500.

[KM16]   Kunihiro Kato and Homei Miyashita. '3D Printed Physical Interfaces That Can Extend Touch Devices.' In: *Proceedings of the 29th Annual Symposium on User Interface Software and Technology - UIST '16 Adjunct*. New York, New York, USA: ACM Press,

2016, pp. 47–49. ISBN: 978-1-4503-4531-6. DOI: `10.1145/2984751.2985700`.

[KTI13]   Yuichiro Katsumoto, Satoru Tokuhisa, and Masa Inakage. 'Ninja Track: Design of Electronic Toy Variable in Shape and Flexibility.' In: *Proceedings of the 7th International Conference on Tangible, Embedded and Embodied Interaction*. TEI '13. New York, NY, USA: ACM, 2013, pp. 17–24. ISBN: 978-1-4503-1898-3. DOI: `10.1145/2460625.2460628`.

[Kaw+13] Yoshihiro Kawahara, Steve Hodges, Benjamin S. Cook, Cheng Zhang, and Gregory D. Abowd. 'Instant Inkjet Circuits: Lab-Based Inkjet Printing to Support Rapid Prototyping of Ubi-Comp Devices.' In: *Proceedings of the 2013 ACM International Joint Conference on Pervasive and Ubiquitous Computing*. Ubi-Comp '13. New York, NY, USA: ACM, 2013, pp. 363–372. ISBN: 978-1-4503-1770-2. DOI: `10.1145/2493432.2493486`.

[KLT12]   Yoshihiro Kawahara, Hoseon Lee, and Manos Tentzeris. 'Sen-Sprout: Inkjet-Printed Soil Moisture and Leaf Wetness Sensor.' In: *Proceedings of the 2012 ACM Conference on Ubiquitous Computing*. 2012, p. 4503. ISBN: 978-1-4503-1224-0.

[kei18]   keinhaus. *3MF Specification*. 2018. URL: `https://3mf.io/specification/` (visited on Aug. 7, 2018).

[Kha+12] Mohammadreza Khalilbeigi, Roman Lissermann, Wolfgang Kleine, and Jürgen Steimle. 'FoldMe: Interacting with Double-Sided Foldable Displays.' In: *Proceedings of the Sixth International Conference on Tangible, Embedded and Embodied Interaction*. TEI '12. New York, NY, USA: ACM, 2012, pp. 33–40. ISBN: 978-1-4503-1174-8. DOI: `10.1145/2148131.2148142`.

[Kha+11] Mohammadreza Khalilbeigi, Roman Lissermann, Max Mühlhäuser, and Jürgen Steimle. 'Xpaaand: Interaction Techniques for Rollable Displays.' In: *Proceedings of the SIGCHI Conference on Human Factors in Computing Systems*. CHI '11. New York, NY, USA: ACM, 2011, pp. 2729–2732. ISBN: 978-1-4503-0228-9. DOI: `10.1145/1978942.1979344`.

[Kho15]   Kholoudabdolqader. *FDM Filament Driver Diagram*. Dec. 21, 2015. URL: `https://commons.wikimedia.org/wiki/File:Filament_Driver_diagram.jpg` (visited on Aug. 7, 2018).

[Kim+17] Kyuyoung Kim, Jaeho Park, Ji hoon Suh, Minseong Kim, Yongrok Jeong, and Inkyu Park. '3D Printing of Multiaxial Force Sensors Using Carbon Nanotube (CNT)/Thermoplastic

Polyurethane (TPU) Filaments.' In: *Sensors and Actuators, A: Physical* 263 (2017), pp. 493–500. ISSN: 09244247. DOI: `10.1016/j.sna.2017.07.020`.

[Kle+04]   Scott R. Klemmer, Jack Li, James Lin, and James A. Landay. 'Papier-Mâché: Toolkit Support for Tangible Input.' In: *Proceedings of the SIGCHI Conference on Human Factors in Computing Systems*. CHI '04. New York, NY, USA: ACM, 2004, pp. 399–406. ISBN: 978-1-58113-702-6. DOI: `10.1145/985692.985743`.

[Kra+11]   Sven Kratz, Tilo Westermann, Michael Rohs, and Georg Essl. 'CapWidgets: Tangible Widgets versus Multi-Touch Controls on Mobile Devices.' In: *Proceedings of the 2011 Annual Conference Extended Abstracts on Human Factors in Computing Systems - CHI EA '11*. New York, New York, USA: ACM Press, 2011, p. 1351. ISBN: 978-1-4503-0268-5. DOI: `10.1145/1979742.1979773`.

[Lap+15]   Gierad Laput, Eric Brockmeyer, Scott E. Hudson, and Chris Harrison. 'Acoustruments: Passive, Acoustically-Driven, Interactive Controls for Handheld Devices.' In: *Proceedings of the 33rd Annual ACM Conference on Human Factors in Computing Systems - CHI '15*. New York, New York, USA: ACM Press, 2015, pp. 2161–2170. ISBN: 978-1-4503-3145-6. DOI: `10.1145/2702123.2702414`.

[LCH15]   Gierad Laput, Xiang 'Anthony' Chen, and Chris Harrison. '3D Printed Hair: Fused Deposition Modeling of Soft Strands, Fibers, and Bristles.' In: *Proceedings of the 28th Annual ACM Symposium on User Interface Software & Technology*. UIST '15. New York, NY, USA: ACM, 2015, pp. 593–597. ISBN: 978-1-4503-3779-3. DOI: `10.1145/2807442.2807484`.

[Le +14]   Mathieu Le Goc, Stuart Taylor, Shahram Izadi, and Cem Keskin. 'A Low-Cost Transparent Electric Field Sensor for 3D Interaction on Mobile Devices.' In: *Proceedings of the SIGCHI Conference on Human Factors in Computing Systems*. CHI '14. New York, NY, USA: ACM, 2014, pp. 3167–3170. ISBN: 978-1-4503-2473-1. DOI: `10.1145/2556288.2557331`.

[Led+17]   David Ledo, Fraser Anderson, Ryan Schmidt, Lora Oehlberg, Saul Greenberg, and Tovi Grossman. 'Pineal: Bringing Passive Objects to Life with Embedded Mobile Devices.' In: *Proceedings of the 2017 CHI Conference on Human Factors in Computing Systems*. CHI '17. New York, NY, USA: ACM, 2017, pp. 2583–2593. ISBN: 978-1-4503-4655-9. DOI: `10.1145/3025453.3025652`.

[LS04]   Chia-Hsun Lee and Ted Selker. 'iSphere: A Proximity-Based 3D Input Device.' In: *ACM SIGGRAPH 2004 Posters*. SIGGRAPH '04. New York, NY, USA: ACM, 2004, pp. 72–. ISBN: 978-1-58113-896-2. DOI: 10.1145/1186415.1186499.

[Lei+12]   Simon J Leigh, Robert J Bradley, Christopher P Purssell, Duncan R Billson, and David a Hutchins. 'A Simple, Low-Cost Conductive Composite Material for 3D Printing of Electronic Sensors.' In: *PLoS ONE* 7.11 (Nov. 21, 2012). Ed. by Jeongmin Hong, e49365. ISSN: 1932-6203. DOI: 10.1371/journal.pone.0049365. PMID: 23185319.

[Li+17]   Dingzeyu Li, Avinash S Nair, Shree K Nayar, and Changxi Zheng. 'AirCode: Unobtrusive Physical Tags for Digital Fabrication.' In: *Proceedings of the 30th Annual ACM Symposium on User Interface Software and Technology - UIST '17*. New York, New York, USA: ACM Press, 2017, pp. 449–460. ISBN: 978-1-4503-4981-9. DOI: 10.1145/3126594.3126635. arXiv: 1707.05754.

[Li+16]   Hanchuan Li, Eric Brockmeyer, Elizabeth J. Carter, Josh Fromm, Scott E. Hudson, Shwetak N. Patel, and Alanson Sample. 'PaperID: A Technique for Drawing Functional Battery-Free Wireless Interfaces on Paper.' In: *Proceedings of the 2016 CHI Conference on Human Factors in Computing Systems*. CHI '16. New York, NY, USA: ACM, 2016, pp. 5885–5896. ISBN: 978-1-4503-3362-7. DOI: 10.1145/2858036.2858249.

[Lia+14]   Rong-Hao Liang, Liwei Chan, Hung-Yu Tseng, Han-Chih Kuo, Da-Yuan Huang, De-Nian Yang, and Bing-Yu Chen. 'Gauss-Bricks: Magnetic Building Blocks for Constructive Tangible Interactions on Portable Displays.' In: *Proceedings of the 32nd Annual ACM Conference on Human Factors in Computing Systems - CHI '14*. New York, New York, USA: ACM Press, 2014, pp. 3153–3162. ISBN: 978-1-4503-2473-1. DOI: 10.1145/2556288.2557105.

[Lia+13]   Rung-Huei Rong-Hao Liang et al. 'GaussBits: Magnetic Tangible Bits for Portable and Occlusion-Free Near-Surface Interactions.' In: *Proceedings of the SIGCHI Conference on Human Factors in Computing Systems - CHI '13*. New York, New York, USA: ACM Press, 2013, p. 1391. ISBN: 978-1-4503-1899-0. DOI: 10.1145/2470654.2466185.

[Lis+12]   Roman Lissermann, Simon Olberding, Benjamin Petry, Max Mühlhäuser, and Jürgen Steimle. 'PaperVideo: Interacting with

Videos on Multiple Paper-like Displays.' In: *Proceedings of the 20th ACM International Conference on Multimedia*. MM '12. New York, NY, USA: ACM, 2012, pp. 129–138. ISBN: 978-1-4503-1089-5. DOI: 10.1145/2393347.2393372.

[LMW12]   Amit Joe Lopes, Eric MacDonald, and Ryan B. Wicker. 'Integrating Stereolithography and Direct Print Technologies for 3D Structural Electronics Fabrication.' In: *Rapid Prototyping Journal* 18.2 (2012), pp. 129–143. ISSN: 1355-2546. DOI: 10.1108/13552541211212113.

[Mac+15] Robert MacCurdy, Robert Katzschmann, Youbin Kim, and Daniela Rus. 'Printable Hydraulics: A Method for Fabricating Robots by 3D Co-Printing Solids and Liquids.' In: *arXiv preprint arXiv:1512.03744* (Dec. 11, 2015). arXiv: 1512.03744.

[Man18]   Mosaic Manufacturing. *Multi-Color 3D Printing: Palette+*. 2018. URL: https://www.mosaicmanufacturing.com/ (visited on Aug. 7, 2018).

[Maz+12] Aaron D. Mazzeo, William B. Kalb, Lawrence Chan, Matthew G. Killian, Jean-Francis Bloch, Brian A. Mazzeo, and George M. Whitesides. 'Paper-Based, Capacitive Touch Pads.' In: *Advanced Materials* 24.21 (June 5, 2012), pp. 2850–2856. ISSN: 1521-4095. DOI: 10.1002/adma.201200137.

[Mel14]   D. A. Mellis. 'Do-It-Yourself Fabrication of Electronic Devices.' In: *IEEE Pervasive Computing* 13.3 (July 2014), pp. 22–29. ISSN: 1536-1268. DOI: 10.1109/MPRV.2014.45.

[MI07]   David A Mellis and Tom Igoe. 'Arduino : An Open Electronics Prototyping Platform.' In: *Proceedings of the 2007 Annual Conference on Human Factors in Computing Systems - CHI '07*. 2007, pp. 1–11.

[Mel+13] David A Mellis, Sam Jacoby, Leah Buechley, Hannah Perner-wilson, and Jie Qi. 'Microcontrollers as Material: Crafting Circuits with Paper, Conductive Ink, Electronic Components, and an Untoolkit.' In: *Proceedings of the 7th International Conference on Tangible, Embedded and Embodied Interaction*. 2013, pp. 83–90. ISBN: 978-1-4503-1898-3.

[MM09]   Pranav Mistry and Pattie Maes. 'SixthSense: A Wearable Gestural Interface.' In: *ACM SIGGRAPH ASIA 2009 Sketches*. SIG-GRAPH ASIA '09. New York, NY, USA: ACM, 2009, 11:1–11:1. DOI: 10.1145/1667146.1667160.

[MMC09]   Pranav Mistry, Pattie Maes, and Liyan Chang. 'WUW - Wear Ur World: A Wearable Gestural Interface.' In: *CHI '09 Extended Abstracts on Human Factors in Computing Systems.* CHI EA '09. New York, NY, USA: ACM, 2009, pp. 4111–4116. ISBN: 978-1-60558-247-4. DOI: 10.1145/1520340.1520626.

[MGF13]   David Molyneaux, Hans Gellersen, and Joe Finney. 'Cooperative Augmentation of Mobile Smart Objects with Projected Displays.' In: *ACM Transactions on Interactive Intelligent Systems* 3.2 (Aug. 2013), 7:1–7:35. ISSN: 2160-6455. DOI: 10.1145/2499474.2499476.

[Mos+16] S. Moscato, R. Bahr, T. Le, M. Pasian, M. Bozzi, L. Perregrini, and M. M. Tentzeris. 'Infill-Dependent 3-D-Printed Material Based on NinjaFlex Filament for Antenna Applications.' In: *IEEE Antennas and Wireless Propagation Letters* 15 (2016), pp. 1506–1509. ISSN: 1536-1225. DOI: 10.1109/LAWP.2016.2516101.

[MN94]   Tamotsu Murakami and Naomasa Nakajima. 'Direct and Intuitive Input Device for 3-D Shape Deformation.' In: *Conference Companion on Human Factors in Computing Systems - CHI '94.* New York, New York, USA: ACM Press, 1994, pp. 233–236. ISBN: 0-89791-651-4. DOI: 10.1145/259963.260449.

[Mur+08] Roderick Murray-Smith, John Williamson, Stephen Hughes, Torben Quaade, and Steven Strachan. 'Rub the Stane.' In: *CHI '08 Extended Abstracts on Human Factors in Computing Systems.* CHI EA '08. New York, NY, USA: ACM, 2008, pp. 2355–2360. ISBN: 978-1-60558-012-8. DOI: 10.1145/1358628.1358683.

[Nag+18] Steven Nagels, Raf Ramakers, Kris Luyten, and Wim Deferme. 'Silicone Devices: A Scalable DIY Approach for Fabricating Self-Contained Multi-Layered Soft Circuits Using Microfluidics.' In: *Proceedings of the 2018 CHI Conference on Human Factors in Computing Systems.* CHI '18. New York, NY, USA: ACM, 2018, 188:1–188:13. ISBN: 978-1-4503-5620-6. DOI: 10.1145/3173574.3173762.

[Nak+17] Satoshi Nakamaru, Ryosuke Nakayama, Ryuma Niiyama, and Yasuaki Kakehi. 'FoamSense: Design of Three Dimensional Soft Sensors with Porous Materials.' In: *Proceedings of the 30th Annual ACM Symposium on User Interface Software and Technology - UIST '17.* New York, New York, USA: ACM Press, 2017, pp. 437–447. ISBN: 978-1-4503-4981-9. DOI: 10.1145/3126594.3126666.

[NHK15]   Koya Narumi, Steve Hodges, and Yoshihiro Kawahara. 'ConductAR: An Augmented Reality Based Tool for Iterative Design of Conductive Ink Circuits.' In: *Proceedings of the 2015 ACM International Joint Conference on Pervasive and Ubiquitous Computing* (2015), pp. 791–800. DOI: 10.1145/2750858.2804267.

[Ngu+15]   Vinh Nguyen, Pramod Kumar, Sang Ho Yoon, Ansh Verma, and Karthik Ramani. 'SOFTii: Soft Tangible Interface for Continuous Control of Virtual Objects with Pressure-Based Input.' In: *Proceedings of the Ninth International Conference on Tangible, Embedded, and Embodied Interaction - TEI '14*. New York, New York, USA: ACM Press, 2015, pp. 539–544. ISBN: 978-1-4503-3305-4. DOI: 10.1145/2677199.2687898.

[Nit+18]   Aditya Shekhar Nittala, Anusha Withana, Narjes Pourjafarian, and Jürgen Steimle. 'Multi-Touch Skin: A Thin and Flexible Multi-Touch Sensor for On-Skin Input.' In: *Proceedings of the 2018 CHI Conference on Human Factors in Computing Systems*. CHI '18. New York, NY, USA: ACM, 2018, 33:1–33:12. ISBN: 978-1-4503-5620-6. DOI: 10.1145/3173574.3173607.

[OM11]   Željko Obrenovic and Jean-Bernard Martens. 'Sketching Interactive Systems with Sketchify.' In: *ACM Transactions on Computer-Human Interaction* 18.1 (May 2011), 4:1–4:38. ISSN: 1073-0516. DOI: 10.1145/1959022.1959026.

[Oh+18]   Hyunjoo Oh, Tung D. Ta, Ryo Suzuki, Mark D. Gross, Yoshihiro Kawahara, and Lining Yao. 'PEP (3D Printed Electronic Papercrafts): An Integrated Approach for 3D Sculpting Paper-Based Electronic Devices.' In: *Proceedings of the 2018 CHI Conference on Human Factors in Computing Systems*. CHI '18. New York, NY, USA: ACM, 2018, 441:1–441:12. ISBN: 978-1-4503-5620-6. DOI: 10.1145/3173574.3174015.

[Olb+13]   Simon Olberding, Nan-Wei Gong, John Tiab, Joseph A. Paradiso, and Jürgen Steimle. 'A Cuttable Multi-Touch Sensor.' In: *Proceedings of the 26th Annual ACM Symposium on User Interface Software and Technology*. UIST '13. New York, NY, USA: ACM, 2013, pp. 245–254. ISBN: 978-1-4503-2268-3. DOI: 10.1145/2501988.2502048.

[Olb+15]   Simon Olberding, Sergio Soto Ortega, Klaus Hildebrandt, and Jürgen Steimle. 'Foldio: Digital Fabrication of Interactive and Shape-Changing Objects With Foldable Printed Electronics.' In: *Proceedings of the 28th Annual ACM Symposium on User Interface*

Software & Technology - UIST '15. New York, New York, USA: ACM Press, 2015, pp. 223–232. ISBN: 978-1-4503-3779-3. DOI: `10.1145/2807442.2807494`.

[OWS14]   Simon Olberding, Michael Wessely, and Jürgen Steimle. 'PrintScreen: Fabricating Highly Customizable Thin-Film Touch-Displays.' In: *Proceedings of the 27th Annual ACM Symposium on User Interface Software and Technology*. UIST '14. New York, NY, USA: ACM, 2014, pp. 281–290. ISBN: 978-1-4503-3069-5. DOI: `10.1145/2642918.2647413`.

[OST13]   Makoto Ono, Buntarou Shizuki, and Jiro Tanaka. 'Touch & Activate: Adding Interactivity to Existing Objects Using Active Acoustic Sensing.' In: *Proceedings of the 26th Annual ACM Symposium on User Interface Software and Technology - UIST '13*. New York, New York, USA: ACM Press, 2013, pp. 31–40. ISBN: 978-1-4503-2268-3. DOI: `10.1145/2501988.2501989`.

[OST15]   Makoto Ono, Buntarou Shizuki, and Jiro Tanaka. 'Sensing Touch Force Using Active Acoustic Sensing.' In: *Proceedings of the Ninth International Conference on Tangible, Embedded, and Embodied Interaction - TEI '15*. New York, New York, USA: ACM Press, 2015, pp. 355–358. ISBN: 978-1-4503-3305-4. DOI: `10.1145/2677199.2680585`.

[Ou+16]   Jifei Ou, Gershon Dublon, Chin-yi Cheng, Felix Heibeck, Karl Willis, and Hiroshi Ishii. 'Cilllia: 3D Printed Micro-Pillar Structures for Surface Texture, Actuation and Sensing.' In: *Proceedings of the 2016 CHI Conference on Human Factors in Computing Systems* c (2016), pp. 5753–5764. DOI: `10.1145/2858036.2858257`.

[PCH14]   M Pakanen, A Colley, and J Häkkilä. 'Squeezy Bracelet - Designing a Wearable Communication Device for Tactile Interaction.' In: *Proceedings of the 8th Nordic Conference on Human-Computer Interaction Fun, Fast, Foundational - NordiCHI '14*. New York, New York, USA: ACM Press, Oct. 26, 2014, pp. 305–314. ISBN: 978-1-4503-2542-4. DOI: `10.1145/2639189.2639238`.

[Pan+15]   Julian Panetta, Qingnan Zhou, Luigi Malomo, Nico Pietroni, Paolo Cignoni, and Denis Zorin. 'Elastic Textures for Additive Fabrication.' In: *ACM Transactions on Graphics* 34.4 (2015), 135:1–135:12. ISSN: 07300301. DOI: `10.1145/2766937`.

[Par+16]   Patrick Parzer, Kathrin Probst, Teo Babic, Christian Rendl, Anita Vogl, Alex Olwal, and Michael Haller. 'FlexTiles: A Flexible, Stretchable, Formable, Pressure-Sensitive, Tactile Input Sensor.' In: *Proceedings of the 2016 CHI Conference Extended Abstracts on Human Factors in Computing Systems - CHI EA '16*. New York, New York, USA: ACM Press, 2016, pp. 3754–3757. ISBN: 978-1-4503-4082-3. DOI: 10.1145/2851581.2890253.

[Par+17]   Patrick Parzer, Adwait Sharma, Anita Vogl, Jürgen Steimle, Alex Olwal, and Michael Haller. 'SmartSleeve: Real-Time Sensing of Surface and Deformation Gestures on Flexible, Interactive Textiles, Using a Hybrid Gesture Detection Pipeline Patrick.' In: *Proceedings of the 30th Annual ACM Symposium on User Interface Software and Technology - UIST '17*. New York, New York, USA: ACM Press, 2017, pp. 565–577. ISBN: 978-1-4503-4981-9. DOI: 10.1145/3126594.3126652.

[Pen+15]   Huaishu Peng, Jennifer Mankoff, Scott E Hudson, and James McCann. 'A Layered Fabric 3D Printer for Soft Interactive Objects.' In: *Proceedings of the 33rd Annual ACM Conference on Human Factors in Computing Systems - CHI '15*. Vol. 1. New York, New York, USA: ACM Press, 2015, pp. 1789–1798. ISBN: 978-1-4503-3145-6. DOI: 10.1145/2702123.2702327.

[PRM14]   Thiago Pereira, Szymon Rusinkiewicz, and Wojciech Matusik. 'Computational Light Routing: 3D Printed Optical Fibers for Sensing and Display.' In: *ACM Trans. Graph.* 33.3 (June 2014), 24:1–24:13. ISSN: 0730-0301. DOI: 10.1145/2602140.

[Pér+15]   Jesús Pérez, Bernhard Thomaszewski, Stelian Coros, Bernd Bickel, José A. Canabal, Robert Sumner, and Miguel A. Otaduy. 'Design and Fabrication of Flexible Rod Meshes.' In: *ACM Transactions on Graphics* 34.4 (July 2015), 138:1–138:12. ISSN: 0730-0301. DOI: 10.1145/2766998.

[PML07]   Daniel Periard, Evan Malone, and Hod Lipson. 'Printing Embedded Circuits.' In: *Proceedings of the 18th Solid Freeform Fabrication Symposium, Austin TX*. 2007, pp. 503–512.

[Pru18]   Prusa. *Original Prusa I3 MK3 Multi Material 2.0*. 2018. URL: https://shop.prusa3d.com/en/printer-upgrades/183-original-prusa-i3-mk3-multi-material-upgrade-kit.html (visited on Aug. 7, 2018).

[PIS13]   Parinya Punpongsanon, Daisuke Iwai, and Kosuke Sato. 'De-forMe: Projection-Based Visualization of Deformable Surfaces Using Invisible Textures.' In: *SIGGRAPH Asia 2013 Emerging Technologies on - SA '13*. New York, New York, USA: ACM Press, Nov. 19, 2013, pp. 1–3. ISBN: 978-1-4503-2632-2. DOI: `10.1145/2542284.2542292`.

[PIS15]   Parinya Punpongsanon, Daisuke Iwai, and Kosuke Sato. 'Projection-Based Visualization of Tangential Deformation of Nonrigid Surface by Deformation Estimation Using Infrared Texture.' In: *Virtual Reality* 19.1 (Mar. 2015), pp. 45–56. ISSN: 1359-4338. DOI: `10.1007/s10055-014-0256-y`.

[QB10]   Jie Qi and Leah Buechley. 'Electronic Popables : Exploring Paper-Based Computing through an Interactive Pop-Up Book.' In: *Proc. TEI'10*. ACM, 2010, pp. 121–128. ISBN: 978-1-60558-841-4.

[QB12]   Jie Qi and Leah Buechley. 'Animating Paper Using Shape Memory Alloys.' In: *Proceedings of the 2012 ACM annual conference on Human Factors in Computing Systems - CHI '12* (2012). Place: New York, New York, USA, p. 749. DOI: `10.1145/2207676.2207783`.

[QB14]   Jie Qi and Leah Buechley. 'Sketching in Circuits : Designing and Building Electronics on Paper.' In: (2014), pp. 1713–1721.

[RSL14]   Raf Ramakers, Johannes Schöning, and Kris Luyten. 'Paddle: Highly Deformable Mobile Devices with Physical Controls.' In: *Proceedings of the 32nd Annual ACM Conference on Human Factors in Computing Systems*. CHI '14. 2014, pp. 2569–2578. ISBN: 978-1-4503-2473-1. DOI: `10.1145/2556288.2557340`.

[RTL15]   Raf Ramakers, Kashyap Todi, and Kris Luyten. 'PaperPulse: An Integrated Approach for Embedding Electronics in Paper Designs.' In: *Proceedings of the 33rd Annual ACM Conference on Human Factors in Computing Systems*. CHI '15. New York, NY, USA: ACM, 2015, pp. 2457–2466. ISBN: 978-1-4503-3145-6. DOI: `10.1145/2702123.2702487`.

[Rek02]   Jun Rekimoto. 'SmartSkin: An Infrastructure for Freehand Manipulation on Interactive Surfaces.' In: *Proceedings of the SIGCHI Conference on Human Factors in Computing Systems Changing Our World, Changing Ourselves - CHI '02*. New York, New York, USA: ACM Press, 2002, p. 113. ISBN: 1-58113-453-3. DOI: `10.1145/503376.503397`.

[Ren+12]   Christian Rendl, Patrick Greindl, Michael Haller, Martin Zirkl, Barbara Stadlober, and Paul Hartmann. 'PyzoFlex: Printed Piezoelectric Pressure Sensing Foil.' In: *Proceedings of the 25th Annual ACM Symposium on User Interface Software and Technology - UIST '12*. New York, New York, USA: ACM Press, 2012, p. 509. ISBN: 978-1-4503-1580-7. DOI: 10.1145/2380116.2380180.

[Ren+14]   Christian Rendl et al. 'FlexSense: A Transparent Self-Sensing Deformable Surface.' In: *Proceedings of the 27th Annual ACM Symposium on User Interface Software and Technology - UIST '14*. New York, New York, USA: ACM Press, 2014, pp. 129–138. ISBN: 978-1-4503-3069-5. DOI: 10.1145/2642918.2647405.

[RMS13]   Hendrik Richter, Felix Manke, and Moriel Seror. 'LiquiTouch: Liquid As a Medium for Versatile Tactile Feedback on Touch Surfaces.' In: *Proceedings of the 7th International Conference on Tangible, Embedded and Embodied Interaction - TEI '13*. New York, New York, USA: ACM Press, 2013, p. 315. ISBN: 978-1-4503-1898-3. DOI: 10.1145/2460625.2460678.

[Rie+18]   Jan Riemann, Martin Schmitz, Alexander Hendrich, and Max Mühlhäuser. 'FlowPut: Environment-Aware Interactivity for Tangible 3D Objects.' In: *Proceedings of the ACM on Interactive, Mobile, Wearable and Ubiquitous Technologies* 2.1 (Mar. 26, 2018). cites:Weigel2013, pp. 1–23. ISSN: 24749567. DOI: 10.1145/3191763.

[San+09]   Rajesh Sankaran, Brygg Ullmer, Jagannathan Ramanujam, Karun Kallakuri, Srikanth Jandhyala, Cornelius Toole, and Christopher Laan. 'Decoupling Interaction Hardware Design Using Libraries of Reusable Electronics.' In: *Proceedings of the 3rd International Conference on Tangible and Embedded Interaction*. TEI '09. Place: New York, New York, USA. 2009, p. 331. ISBN: 9781605584935. DOI: 10.1145/1517664.1517732.

[Sar+17]   Harpreet Sareen, Udayan Umapathi, Patrick Shin, Yasuaki Kakehi, Jifei Ou, Hiroshi Ishii, and Pattie Maes. 'Printflatables: Printing Human-Scale, Functional and Dynamic Inflatable Objects.' In: *Proceedings of the 2017 CHI Conference on Human Factors in Computing Systems*. CHI '17. New York, NY, USA: ACM, 2017, pp. 3669–3680. ISBN: 978-1-4503-4655-9. DOI: 10.1145/3025453.3025898.

[Sar+12]   John Sarik, Alex Butler, Nicolas Villar, James Scott, and Steve Hodges. 'Combining 3D Printing and Printable Electronics.' In:

Proceedings of the 6th International Conference on Tangible, Embedded and Embodied Interaction (TEI '12). 2012, pp. 1–5. ISBN: 978-1-4503-1174-8.

[SPH12]   Munehiko Sato, Ivan Poupyrev, and Chris Harrison. 'Touché: Enhancing Touch Interaction on Humans, Screens, Liquids, and Everyday Objects.' In: *Proceedings of the 2012 ACM Annual Conference on Human Factors in Computing Systems - CHI '12*. New York, New York, USA: ACM Press, 2012, p. 483. ISBN: 978-1-4503-1015-4. DOI: 10.1145/2207676.2207743.

[Sav16]   Valkyrie Savage. '3-D Printing Interactive Objects.' In: *XRDS: Crossroads, The ACM Magazine for Students* 22.3 (2016), pp. 44–48. ISSN: 15284972. DOI: 10.1145/2893495.

[SCH13]   Valkyrie Savage, Colin Chang, and Björn Hartmann. 'Sauron: Embedded Single-Camera Sensing of Printed Physical User Interfaces.' In: *Proceedings of the 26th Annual ACM Symposium on User Interface Software and Technology*. UIST '13. New York, New York, USA: ACM Press, 2013, pp. 447–456. ISBN: 978-1-4503-2268-3. DOI: 10.1145/2501988.2501992.

[Sav+15]   Valkyrie Savage, Sean Follmer, Jingyi Li, and Björn Hartmann. 'Makers' Marks: Physical Markup for Designing and Fabricating Functional Objects.' In: *Proceedings of the 28th Annual ACM Symposium on User Interface Software & Technology*. UIST '15. New York, New York, USA: ACM Press, Nov. 5, 2015, pp. 103–108. ISBN: 978-1-4503-3779-3. DOI: 10.1145/2807442.2807508.

[Sav+14]   Valkyrie Savage, Ryan Schmidt, Tovi Grossman, George Fitzmaurice, and Björn Hartmann. 'A Series of Tubes: Adding Interactivity to 3D Prints Using Internal Pipes.' In: *Proceedings of the 27th Annual ACM Symposium on User Interface Software and Technology*. UIST '14. New York, New York, USA: ACM Press, 2014, pp. 3–12. ISBN: 978-1-4503-3069-5. DOI: 10.1145/2642918.2647374.

[SZH12]   Valkyrie Savage, Xiaohan Zhang, and B Hartmann. 'Midas: Fabricating Custom Capacitive Touch Sensors to Prototype Interactive Objects.' In: *Proceedings of the 25th Annual ACM Symposium on User Interface Software and Technology*. 2012, pp. 579–588. ISBN: 978-1-4503-1580-7.

[Sch16]   Martin Schmitz. 'Exploring 3D Printed Interaction.' In: *Proceedings of the TEI '16: Tenth International Conference on Tangible, Embedded, and Embodied Interaction*. TEI '16. New York, New York,

USA: ACM Press, 2016, pp. 705–708. ISBN: 978-1-4503-3582-9. DOI: 10.1145/2839462.2854105.

[Sch+18]   Martin Schmitz, Martin Herbers, Niloofar Dezfuli, Sebastian Günther, and Max Mühlhäuser. 'Off-Line Sensing: Memorizing Interactions in Passive 3D-Printed Objects.' In: *Proceedings of the 2018 CHI Conference on Human Factors in Computing Systems*. CHI '18. New York, NY, USA: ACM, 2018, 182:1–182:8. ISBN: 978-1-4503-5620-6. DOI: 10.1145/3173574.3173756.

[Sch+15a]   Martin Schmitz, Mohammadreza Khalilbeigi, Matthias Balwierz, Roman Lissermann, Max Mühlhäuser, and Jürgen Steimle. 'Capricate: A Fabrication Pipeline to Design and 3D Print Capacitive Touch Sensors for Interactive Objects.' In: *Proceedings of the 28th Annual ACM Symposium on User Interface Software & Technology*. UIST '15. New York, New York, USA: ACM Press, Nov. 5, 2015, pp. 253–258. ISBN: 978-1-4503-3779-3. DOI: 10.1145/2807442.2807503.

[Sch+16]   Martin Schmitz, Andreas Leister, Niloofar Dezfuli, Jan Riemann, Florian Müller, and Max Mühlhäuser. 'Liquido: Embedding Liquids into 3D Printed Objects to Sense Tilting and Motion.' In: *Proceedings of the 2016 CHI Conference Extended Abstracts on Human Factors in Computing Systems*. CHI EA '16. New York, New York, USA: ACM Press, 2016, pp. 2688–2696. ISBN: 978-1-4503-4082-3. DOI: 10.1145/2851581.2892275.

[Sch+17]   Martin Schmitz, Jürgen Steimle, Jochen Huber, Niloofar Dezfuli, and Max Mühlhäuser. 'Flexibles: Deformation-Aware 3D-Printed Tangibles for Capacitive Touchscreens.' In: *Proceedings of the 2017 CHI Conference on Human Factors in Computing Systems*. CHI '17. New York, NY, USA: ACM, 2017, pp. 1001–1014. ISBN: 978-1-4503-4655-9. DOI: 10.1145/3025453.3025663.

[Sch+19]   Martin Schmitz, Martin Stitz, Florian Müller, Markus Funk, and Max Mühlhäuser. './Trilaterate: Sensing Hover, Touch, and Force on 3D-Printed Objects via Capacitive Trilateration.' In: *Proceedings of the 2019 CHI Conference on Human Factors in Computing Systems*. CHI '19. New York, NY, USA: ACM, 2019. ISBN: 978-1-4503-5970-2. DOI: 10.1145/3290605.3300684.

[Sch+12]   Bertrand Schneider, Megan Strait, Laurence Muller, Sarah Elfenbein, Orit Shaer, and Chia Shen. 'Phylo-Genie: Engaging Students in Collaborative 'Tree- Thinking' through Tabletop Techniques.' In: *Proceedings of the 2012 ACM Annual Conference*

on Human Factors in Computing Systems - CHI '12. New York, New York, USA: ACM Press, 2012, pp. 3071–3080. ISBN: 978-1-4503-1015-4. DOI: `10.1145/2207676.2208720`.

[Sch+15b] Christian Schumacher, Bernd Bickel, Jan Rys, Steve Marschner, Chiara Daraio, and Markus Gross. 'Microstructures to Control Elasticity in 3D Printing.' In: *ACM Transactions on Graphics* 34.4 (July 27, 2015), 136:1–136:13. ISSN: 07300301. DOI: `10.1145/2766926`.

[She+13] C Shemelya, F Cedillos, E Aguilera, E Maestas, J Ramos, D Espalin, D Muse, R Wicker, and E MacDonald. '3D Printed Capacitive Sensors.' In: *2013 Ieee Sensors*. Ieee, Nov. 2013, pp. 1–4. ISBN: 978-1-4673-4642-9. DOI: `10.1109/ICSENS.2013.6688247`.

[SBS06] Jia Sheng, Ravin Balakrishnan, and Karan Singh. 'An Interface for Virtual 3D Sculpting via Physical Proxy.' In: *Proceedings of the 4th International Conference on Computer Graphics and Interactive Techniques in Australasia and Southeast Asia*. GRAPHITE '06. New York, NY, USA: ACM, 2006, pp. 213–220. ISBN: 978-1-59593-564-9. DOI: `10.1145/1174429.1174467`.

[SRM14] Michael Shorter, Jon Rogers, and John McGhee. 'Enhancing Everyday Paper Interactions with Paper Circuits.' In: *Proceedings of the 2014 conference on Designing interactive systems - DIS '14* (2014). Place: New York, New York, USA, pp. 39–42. DOI: `10.1145/2598510.2598584`.

[SN07] Beat Signer and Moira C Norrie. 'PaperPoint : A Paper-Based Presentation and Interactive Paper Prototyping Tool.' In: (2007), pp. 15–17.

[Sko+13] Mélina Skouras, Bernhard Thomaszewski, Stelian Coros, Bernd Bickel, and Markus Gross. 'Computational Design of Actuated Deformable Characters.' In: *ACM Transactions on Graphics* 32.4 (2013), p. 1. ISSN: 07300301. DOI: `10.1145/2461912.2461979`.

[SH12] R. Slyper and J. Hodgins. 'Prototyping Robot Appearance, Movement, and Interactions Using Flexible 3D Printing and Air Pressure Sensors.' In: *2012 IEEE RO-MAN: The 21st IEEE International Symposium on Robot and Human Interactive Communication*. 2012 IEEE RO-MAN: The 21st IEEE International Symposium on Robot and Human Interactive Communication. Sept. 2012, pp. 6–11. DOI: `10.1109/ROMAN.2012.6343723`.

[Sly12] Ronit Slyper. 'Sensing Through Structure.' 2012.

[SPH11]   Ronit Slyper, Ivan Poupyrev, and Jessica Hodgins. 'Sensing Through Structure: Designing Soft Silicone Sensors.' In: *Proceedings of the Fifth International Conference on Tangible, Embedded, and Embodied Interaction - TEI '11*. New York, New York, USA: ACM Press, 2011, pp. 213–220. ISBN: 978-1-4503-0478-8. DOI: `10.1145/1935701.1935744`.

[Smi+98]   J. Smith, T. White, C. Dodge, J. Paradiso, N. Gershenfeld, and D. Allport. 'Electric Field Sensing for Graphical Interfaces.' In: *IEEE Computer Graphics and Applications* 18.3 (May 1998), pp. 54–60. ISSN: 0272-1716. DOI: `10.1109/38.674972`.

[Smi96]   J. R. Smith. 'Field Mice: Extracting Hand Geometry from Electric Field Measurements.' In: *IBM Systems Journal* 35.3.4 (1996), pp. 587–608. ISSN: 0018-8670. DOI: `10.1147/sj.353.0587`.

[Smi99]   Joshua Reynolds Smith. 'Electric Field Imaging.' PhD Thesis. Massachusetts Institute of Technology, 1999.

[Sny87]   John Snyder. *Map Projections: A Working Manual*. Vol. 1395. US Government Printing Office, 1987.

[Son+15]   Peng Song, Zhongqi Fu, Ligang Liu, and Chi-Wing Fu. 'Printing 3D Objects with Interlocking Parts.' In: *Computer Aided Geometric Design*. Geometric Modeling and Processing 2015 35-36 (May 1, 2015), pp. 137–148. ISSN: 0167-8396. DOI: `10.1016/j.cagd.2015.03.020`.

[Spi+16]   Andrew Spielberg, Alanson Sample, Scott E. Hudson, Jennifer Mankoff, and James McCann. 'RapID: A Framework for Fabricating Low-Latency Interactive Objects with RFID Tags.' In: *Proceedings of the 2016 CHI Conference on Human Factors in Computing Systems*. CHI '16. New York, NY, USA: ACM, 2016, pp. 5897–5908. ISBN: 978-1-4503-3362-7. DOI: `10.1145/2858036.2858243`.

[Spi+13]   Martin Spindler, Wolfgang Büschel, Charlotte Winkler, and Raimund Dachselt. 'Tangible Displays for the Masses: Spatial Interaction with Handheld Displays by Using Consumer Depth Cameras.' In: *Personal and Ubiquitous Computing* 18.5 (Nov. 21, 2013), pp. 1213–1225. ISSN: 1617-4909. DOI: `10.1007/s00779-013-0730-7`.

[SJM13]   Jürgen Steimle, Andreas Jordt, and Pattie Maes. 'Flexpad: Highly Flexible Bending Interactions for Projected Handheld Displays.' In: *Proceedings of the SIGCHI Conference on Human Factors in Computing Systems - CHI '13*. New York, New York,

USA: ACM Press, 2013, pp. 237–246. ISBN: 978-1-4503-1899-0.
DOI: 10.1145/2470654.2470688.

[SII12]   Yuta Sugiura, Masahiko Inami, and Takeo Igarashi. 'A Thin
             Stretchable Interface for Tangential Force Measurement.' In:
             *Proceedings of the 25th Annual ACM Symposium on User Inter-
             face Software and Technology - UIST '12*. New York, New York,
             USA: ACM Press, 2012, p. 529. ISBN: 978-1-4503-1580-7. DOI:
             10.1145/2380116.2380182.

[Sug+11]   Yuta Sugiura, Gota Kakehi, Anusha Withana, Calista Lee,
             Daisuke Sakamoto, Maki Sugimoto, Masahiko Inami, and
             Takeo Igarashi. 'Detecting Shape Deformation of Soft Objects
             Using Directional Photoreflectivity Measurement.' In: *Proceed-
             ings of the 24th Annual ACM Symposium on User Interface Soft-
             ware and Technology - UIST '11*. New York, New York, USA:
             ACM Press, 2011, p. 509. ISBN: 978-1-4503-0716-1. DOI: 10.1145/
             2047196.2047263.

[Sun+15]   X. Sun, S. M. Felton, R. J. Wood, and S. Kim. 'Printing An-
             gle Sensors for Foldable Robots.' In: *2015 IEEE/RSJ Interna-
             tional Conference on Intelligent Robots and Systems (IROS)*. 2015
             IEEE/RSJ International Conference on Intelligent Robots and
             Systems (IROS). Sept. 2015, pp. 1725–1731. DOI: 10.1109/IROS.
             2015.7353600.

[Sun+17a]   Subramanian Sundaram, Ziwen Jiang, Pitchaya Sitthi-Amorn,
             David S. Kim, Marc A. Baldo, and Wojciech Matusik. '3D-
             Printed Autonomous Sensory Composites.' In: *Advanced Materi-
             als Technologies* 2.3 (Mar. 2017), p. 1600257. ISSN: 2365709X. DOI:
             10.1002/admt.201600257.

[Sun+17b]   Subramanian Sundaram, David S Kim, Marc A Baldo, Ryan
             C Hayward, and Wojciech Matusik. '3D-Printed Self-Folding
             Electronics.' In: *ACS Applied Materials & Interfaces* 9.37 (Sept. 20,
             2017), pp. 32290–32298. ISSN: 1944-8244. DOI: 10.1021/acsami.
             7b10443.

[Tak+09]   Kenjiro Takemura, Shinichi Yokota, Mamoru Suzuki, Kazuya
             Edamura, Hideo Kumagai, and Tsunehiko Imamura. 'A Liquid
             Rate Gyroscope Using Electro-Conjugate Fluid.' In: *Sensors and
             Actuators A: Physical* 149.2 (2009), pp. 173–179. ISSN: 09244247.
             DOI: 10.1016/j.sna.2008.12.004.

[Tan+15]   Dominique Tan, Maciej Kumorek, Andres A. Garcia, Adam Mooney, Derek Bekoe, and United Kingdom. 'Projectagami: A Foldable Mobile Device with Shape Interactive Applications.' In: *Proceedings of the 33rd Annual ACM Conference Extended Abstracts on Human Factors in Computing Systems - CHI EA '15*. New York, New York, USA: ACM Press, Apr. 18, 2015, pp. 1555–1560. ISBN: 978-1-4503-3146-3. DOI: 10.1145/2702613.2732801.

[TÖ11]   Daniel Tobjörk and Ronald Österbacka. 'Paper Electronics.' In: *Advanced materials (Deerfield Beach, Fla.)* 23.17 (May 3, 2011), pp. 1935–61. ISSN: 1521-4095. DOI: 10.1002/adma.201004692. pmid: 21433116.

[Tor+15]   Cesar Torres, Tim Campbell, Neil Kumar, and Eric Paulos. 'HapticPrint: Designing Feel Aesthetics for 3D Printing.' In: *UIST '15 Proceedings of the 28th Annual ACM Symposium on User Interface Software & Technology* (2015), pp. 583–591. DOI: 10.1145/2807442.2807492.

[TPH15]   Giovanni Maria Troiano, Esben Warming Pedersen, and Kasper Hornbæk. 'Deformable Interfaces for Performing Music.' In: *Proceedings of the 33rd Annual ACM Conference on Human Factors in Computing Systems - CHI '15*. New York, New York, USA: ACM Press, 2015, pp. 377–386. ISBN: 978-1-4503-3145-6. DOI: 10.1145/2702123.2702492.

[Tru+18]   Ryan L. Truby, Michael Wehner, Abigail K. Grosskopf, Daniel M. Vogt, Sebastien G. M. Uzel, Robert J. Wood, and Jennifer A. Lewis. 'Soft Somatosensitive Actuators via Embedded 3D Printing.' In: *Submitted* 1706383 (2018), pp. 1–8. ISSN: 09359648. DOI: 10.1002/adma.201706383.

[TL94]   Greg Turk and Marc Levoy. 'Zippered Polygon Meshes from Range Images.' In: *Proceedings of the 21st Annual Conference on Computer Graphics and Interactive Techniques*. SIGGRAPH '94. New York, NY, USA: ACM, 1994, pp. 311–318. ISBN: 978-0-89791-667-7. DOI: 10.1145/192161.192241.

[UKM16]   Saraha Ueno, Kunihiro Kato, and Homei Miyashita. 'A Tangible Interface to Realize Touch Operations on the Face of a Physical Object.' In: *Proceedings of the 29th Annual Symposium on User Interface Software and Technology - UIST '16 Adjunct*. New York, New York, USA: ACM Press, 2016, pp. 81–83. ISBN: 978-1-4503-4531-6. DOI: 10.1145/2984751.2985711.

[Uli18]   Uline. *Damage Indicators, Shock Sensors in Stock - ULINE*. 2018. URL: https://www.uline.com/Cls_10/Damage-Indicators (visited on Aug. 7, 2018).

[Ull+08]   Brygg Ullmer et al. 'Tangible Menus and Interaction Trays: Core Tangibles for Common Physical/Digital Activities.' In: *Proceedings of the 2nd International Conference on Tangible and Embedded Interaction*. TEI '08. New York, NY, USA: ACM, 2008, pp. 209–212. ISBN: 978-1-60558-004-3. DOI: 10.1145/1347390.1347436.

[US16]   Nobuyuki Umetani and Ryan Schmidt. 'SurfCuit: Surface Mounted Circuits on 3D Prints.' In: *Ieee Cg&a* (2016). ISSN: 02721716. DOI: 10.1109/MCG.2017.40. arXiv: 1606.09540.

[VS17]   Nirzaree Vadgama and Jürgen Steimle. 'Flexy: Shape-Customizable, Single-Layer, Inkjet Printable Patterns for 1D and 2D Flex Sensing.' In: *Proceedings of the Eleventh International Conference on Tangible, Embedded, and Embodied Interaction*. TEI '17. New York, NY, USA: ACM, 2017, pp. 153–162. ISBN: 978-1-4503-4676-4. DOI: 10.1145/3024969.3024989.

[Van+13]   Karen Vanderloock, Vero Vanden Abeele, Johan A.K. Suykens, and Luc Geurts. 'The Skweezee System: Enabling the Design and the Programming of Squeeze Interactions.' In: *Proceedings of the 26th Annual ACM Symposium on User Interface Software and Technology - UIST '13*. New York, New York, USA: ACM Press, 2013, pp. 521–530. ISBN: 978-1-4503-2268-3. DOI: 10.1145/2501988.2502033.

[vOsc+08]   Thijs H.J. J. van Osch, Jolke Perelaer, Antonius W.M. M. De Laat, and Ulrich S. Schubert. 'Inkjet Printing of Narrow Conductive Tracks on Untreated Polymeric Substrates.' In: *Advanced Materials* 20.2 (Jan. 18, 2008), pp. 343–345. ISSN: 09359648. DOI: 10.1002/adma.200701876.

[Var87]   Natan B Vargaftik. *Handbook of Physical Properties of Liquids and Gases-Pure Substances and Mixtures*. 2. ed. Hemisphere Publishing Corporation, New York, NY, 1987. ISBN: 3540169725.

[Váz+15]   Marynel Vázquez, Eric Brockmeyer, Ruta Desai, Chris Harrison, and Scott E. Hudson. '3D Printing Pneumatic Device Controls with Variable Activation Force Capabilities.' In: *Proceedings of the 33rd Annual ACM Conference on Human Factors in Computing Systems - CHI '15*. New York, New York, USA: ACM Press, 2015, pp. 1295–1304. ISBN: 978-1-4503-3145-6. DOI: 10.1145/2702123.2702569.

[VSH11]   Nicolas Villar, James Scott, and Steve Hodges. 'Prototyping with Microsoft .NET Gadgeteer.' In: *Proceedings of the Fifth International Conference on Tangible, Embedded, and Embodied Interaction - TEI '11*. New York, New York, USA: ACM Press, 2011, p. 377. ISBN: 978-1-4503-0478-8. DOI: 10.1145/1935701.1935790.

[Voe+15]   Simon Voelker, Christian Cherek, Jan Thar, Thorsten Karrer, Christian Thoresen, Kjell Ivar Øvergård, and Jan Borchers. 'PERCs: Persistently Trackable Tangibles on Capacitive Multi-Touch Displays.' In: *Proceedings of the 28th Annual ACM Symposium on User Interface Software and Technology - UIST '15*. New York, New York, USA: ACM Press, 2015, pp. 351–356. ISBN: 978-1-4503-3779-3. DOI: 10.1145/2807442.2807466.

[Voe+13]   Simon Voelker, Kosuke Nakajima, Christian Thoresen, Yuichi Itoh, Kjell Ivar Øvergård, and Jan Borchers. 'PUCs: Detecting Transparent, Passive Untouched Capacitive Widgets on Unmodified Multi-Touch Displays.' In: *Proceedings of the 2013 ACM International Conference on Interactive Tabletops and Surfaces - ITS '13*. New York, New York, USA: ACM Press, 2013, pp. 101–104. ISBN: 978-1-4503-2271-3. DOI: 10.1145/2512349.2512791.

[16]   *Voxel8 Developer's Kit*. 2016. URL: https://support.voxel8.co (visited on Oct. 17, 2018).

[Wan+18a] Guanyun Wang, Humphrey Yang, Zeyu Yan, Nurcan Gecer Ulu, Ye Tao, Jianzhe Gu, Levent Burak Kara, and Lining Yao. '4DMesh: 4D Printing Morphing Non-Developable Mesh Surfaces.' In: *Proceedings of the 31st Annual ACM Symposium on User Interface Software and Technology*. UIST '18. New York, NY, USA: ACM, 2018, pp. 623–635. ISBN: 978-1-4503-5948-1. DOI: 10.1145/3242587.3242625.

[Wan+16]   Guanyun Wang, Lining Yao, Wen Wang, Jifei Ou, Chin-yi Cheng, and Ishii Hiroshi. 'xPrint : A Modularized Liquid Printer for Smart Materials Deposition.' In: *Proc. of CHI 2012* (2016).

[Wan+11]   Johnty Wang, Nicolas Alessandro, Sidney Fels, and Bob Pritchard. 'SQUEEZY: Extending a Multi-Touch Screen with Force Sensing Objects for Controlling Articulatory Synthesis.' In: *Proceedings of the International Conference on New Interfaces for Musical Expression*. Oslo, Norway, 2011, pp. 531–532.

[Wan+18b] Tianyi Wang, Ke Huo, Pratik Chawla, Guiming Chen, Siddharth Banerjee, and Karthik Ramani. 'Plain2Fun: Augmenting Ordinary Objects with Interactive Functions by Auto-Fabricating Surface Painted Circuits.' In: *Proceedings of the 2018 Designing Interactive Systems Conference*. DIS '18. New York, NY, USA: ACM, 2018, pp. 1095–1106. ISBN: 978-1-4503-5198-0. DOI: 10.1145/3196709.3196791.

[Was+16] Florens Wasserfall, Daniel Ahlers, Norman Hendrich, and Jianwei Zhang. '3D-Printable Electronics-Integration of SMD Placement and Wiring into the Slicing Process for FDM Fabrication.' In: *Proceedings of the 27th Annual International Solid Freeform Fabrication*. Austin, Texas, 2016, pp. 1826–1837.

[Wat+14] Chihiro Watanabe, Alvaro Cassinelli, Yoshihiro Watanabe, and Masatoshi Ishikawa. 'Generic Method for Crafting Deformable Interfaces to Physically Augment Smartphones.' In: *Proceedings of the Extended Abstracts of the 32nd Annual ACM Conference on Human Factors in Computing Systems - CHI EA '14*. New York, New York, USA: ACM Press, Apr. 26, 2014, pp. 1309–1314. ISBN: 978-1-4503-2474-8. DOI: 10.1145/2559206.2581307.

[WLG13] Christian Weichel, Manfred Lau, and Hans Gellersen. 'Enclosed: A Component-Centric Interface for Designing Prototype Enclosures.' In: *Proceedings of the 7th International Conference on Tangible, Embedded and Embodied Interaction*. TEI '13. New York, NY, USA: ACM, 2013, pp. 215–218. ISBN: 978-1-4503-1898-3. DOI: 10.1145/2460625.2460659.

[Wei+15] Martin Weigel, Tong Lu, Gilles Bailly, Antti Oulasvirta, Carmel Majidi, and Jürgen Steimle. 'iSkin: Flexible, Stretchable and Visually Customizable On-Body Touch Sensors for Mobile Computing.' In: *Proceedings of the 33rd Annual ACM Conference on Human Factors in Computing Systems*. CHI '15. New York, NY, USA: ACM, 2015, pp. 2991–3000. ISBN: 978-1-4503-3145-6. DOI: 10.1145/2702123.2702391.

[Wei+17] Martin Weigel, Aditya Shekhar Nittala, Alex Olwal, and Jürgen Steimle. 'SkinMarks: Enabling Interactions on Body Landmarks Using Conformal Skin Electronics.' In: *Proceedings of the 2017 CHI Conference on Human Factors in Computing Systems*. CHI '17. New York, NY, USA: ACM, 2017, pp. 3095–3105. ISBN: 978-1-4503-4655-9. DOI: 10.1145/3025453.3025704.

[WS17]   Martin Weigel and Jürgen Steimle. 'DeformWear: Deformation Input on Tiny Wearable Devices.' In: *Proceedings of the ACM on Interactive, Mobile, Wearable and Ubiquitous Technologies* 1.2 (June 30, 2017), pp. 1–23. ISSN: 24749567. DOI: 10.1145/3090093.

[Wei91]   Mark Weiser. 'The Computer for the 21st Century.' In: *Scientific American* 265.3 (1991), pp. 94–105. ISSN: 0036-8733.

[Wei+09]   Malte Weiss, Julie Wagner, Yvonne Jansen, Roger Jennings, Ramsin Khoshabeh, James D. Hollan, and Jan Borchers. 'SLAP Widgets: Bridging the Gap Between Virtual and Physical Controls on Tabletops.' In: *Proceedings of the 27th International Conference on Human Factors in Computing Systems - CHI 09*. New York, New York, USA: ACM Press, Apr. 4, 2009, p. 481. ISBN: 978-1-60558-246-7. DOI: 10.1145/1518701.1518779.

[WTM16]   Michael Wessely, Theophanis Tsandilas, and Wendy E. Mackay. 'Stretchis: Fabricating Highly Stretchable User Interfaces.' In: *Proceedings of the 29th Annual Symposium on User Interface Software and Technology*. UIST '16. New York, NY, USA: ACM, 2016, pp. 697–704. ISBN: 978-1-4503-4189-9. DOI: 10.1145/2984511.2984521.

[Wie+12]   Alexander Wiethoff, Hanna Schneider, Michael Rohs, Andreas Butz, and Saul Greenberg. 'Sketch - a - TUI : Low Cost Prototyping of Tangible Interactions Using Cardboard and Conductive Ink.' In: *Proceedings of the Sixth International Conference on Tangible, Embedded and Embodied Interaction* (2012), pp. 309–312.

[Wil+11a] Cary Williams, Xing Dong Yang, Grant Partridge, Joshua Millar-Usiskin, Arkady Major, and Pourang Irani. 'TZee: Exploiting the Lighting Properties of Multi-Touch Tabletops for Tangible 3D Interactions.' In: *Proceedings of the 2011 Annual Conference on Human Factors in Computing Systems - CHI '11*. New York, New York, USA: ACM Press, 2011, p. 1363. ISBN: 978-1-4503-0228-9. DOI: 10.1145/1978942.1979143.

[Wil+12]   Karl Willis, Eric Brockmeyer, Scott Hudson, and Ivan Poupyrev. 'Printed Optics: 3D Printing of Embedded Optical Elements for Interactive Devices.' In: *Proceedings of the 25th Annual ACM Symposium on User Interface Software and Technology - UIST '12*. New York, New York, USA: ACM Press, 2012, p. 589. ISBN: 978-1-4503-1580-7. DOI: 10.1145/2380116.2380190.

[WSM13]   Karl D. D. Willis, Takaaki Shiratori, and Moshe Mahler. 'Hide-Out: Mobile Projector Interaction with Tangible Objects and Surfaces.' In: *Proceedings of the 7th International Conference on Tangible, Embedded and Embodied Interaction*. TEI '13. New York, NY, USA: ACM, 2013, pp. 331–338. ISBN: 978-1-4503-1898-3. DOI: `10.1145/2460625.2460682`.

[WW13]   Karl D. D. Willis and Andrew D. Wilson. 'InfraStructs: Fabricating Information Inside Physical Objects for Imaging in the Terahertz Region.' In: *ACM Transactions on Graphics* 32.4 (July 1, 2013), 138:1–138:10. ISSN: 07300301. DOI: `10.1145/2461912.2461936`.

[Wil+11b] Karl D.D. Willis, Ivan Poupyrev, Scott E. Hudson, and Moshe Mahler. 'SideBySide: Ad-Hoc Multi-User Interaction with Handheld Projectors.' In: *Proceedings of the 24th Annual ACM Symposium on User Interface Software and Technology*. UIST '11. New York, NY, USA: ACM, 2011, pp. 431–440. ISBN: 978-1-4503-0716-1. DOI: `10.1145/2047196.2047254`.

[WPS11]   Karl D.D. Willis, Ivan Poupyrev, and Takaaki Shiratori. 'Motionbeam: A Metaphor for Character Interaction with Handheld Projectors.' In: *Proceedings of the SIGCHI Conference on Human Factors in Computing Systems*. CHI '11. New York, NY, USA: ACM, 2011, pp. 1031–1040. ISBN: 978-1-4503-0228-9. DOI: `10.1145/1978942.1979096`.

[Wil10]   Andrew D. Wilson. 'Using a Depth Camera As a Touch Sensor.' In: *ACM International Conference on Interactive Tabletops and Surfaces*. ITS '10. New York, NY, USA: ACM, 2010, pp. 69–72. ISBN: 978-1-4503-0399-6. DOI: `10.1145/1936652.1936665`.

[WB11]   Raphael Wimmer and Patrick Baudisch. 'Modular and Deformable Touch-Sensitive Surfaces Based on Time Domain Reflectometry.' In: *Proceedings of the 24th Annual ACM Symposium on User Interface Software and Technology - UIST '11*. New York, New York, USA: ACM Press, 2011, pp. 517–526. ISBN: 978-1-4503-0716-1. DOI: `10.1145/2047196.2047264`.

[WGS18]   Anusha Withana, Daniel Groeger, and Jürgen Steimle. 'Tacttoo: A Thin and Feel-Through Tattoo for On-Skin Tactile Output.' In: *The 31st Annual ACM Symposium on User Interface Software and Technology*. UIST '18. New York, NY, USA: ACM, 2018, pp. 365–378. ISBN: 978-1-4503-5948-1. DOI: `10.1145/3242587.3242645`.

[Xu+15]   Hongyi Xu, Yijing Li, Yong Chen, Jernej Barb, and Jernej Barbič. 'Interactive Material Design Using Model Reduction.' In: *ACM Transactions on Graphics* 34.18 (2015). DOI: 10.1145/2699648.

[Yao+13]   Lining Yao, Ryuma Niiyama, Jifei Ou, Sean Follmer, Clark Della Silva, and Hiroshi Ishii. 'PneUI: Pneumatically Actuated Soft Composite Materials for Shape Changing Interfaces.' In: *Proceedings of the 26th Annual ACM Symposium on User Interface Software and Technology*. UIST '13. New York, NY, USA: ACM, 2013, pp. 13–22. ISBN: 978-1-4503-2268-3. DOI: 10.1145/2501988. 2502037.

[Yoo+17]   Sang Ho Yoon, Ke Huo, Yunbo Zhang, Guiming Chen, Luis Paredes, Subramanian Chidambaram, and Karthik Ramani. 'iSoft : A Customizable Soft Sensor with Real-Time Continuous Contact and Stretching Sensing.' In: *Proceedings of the 30th Annual ACM Symposium on User Interface Software and Technology - UIST '17*. New York, New York, USA: ACM Press, 2017, pp. 665–678. ISBN: 978-1-4503-4981-9. DOI: 10.1145/3126594. 3126654.

[Yoo+18]   Sang Ho Yoon, Luis Paredes, Ke Huo, and Karthik Ramani. 'MultiSoft: Soft Sensor Enabling Real-Time Multimodal Sensing with Contact Localization and Deformation Classification.' In: *Proc. ACM Interact. Mob. Wearable Ubiquitous Technol.* 2.3 (Sept. 2018), 145:1–145:21. ISSN: 2474-9567. DOI: 10.1145/3264955.

[YST15]   Arika Yoshida, Buntarou Shizuki, and Jiro Tanaka. 'Capacitive Blocks: A Block System That Connects the Physical with the Virtual Using Changes of Capacitance.' In: *Proceedings of the 28th Annual ACM Symposium on User Interface Software & Technology - UIST '15 Adjunct*. New York, New York, USA: ACM Press, Nov. 6, 2015, pp. 85–86. ISBN: 978-1-4503-3780-9. DOI: 10.1145/ 2815585.2815731.

[Yu+11]   Neng-Hao Yu et al. 'TUIC: Enabling Tangible Interaction on Capacitive Multi-Touch Display.' In: *Proceedings of the 2011 Annual Conference on Human Factors in Computing Systems - CHI '11*. New York, New York, USA: ACM Press, 2011, p. 2995. ISBN: 978-1-4503-0228-9. DOI: 10.1145/1978942.1979386.

[Zeh+17]   Jonas Zehnder, Espen Knoop, Moritz Bächer, and Bernhard Thomaszewski. 'MetaSilicone: Design and Fabrication of Composite Silicone with Desired Mechanical Properties.' In: *ACM*

Transactions on Graphics 36.6 (Nov. 20, 2017), pp. 1–13. ISSN: 07300301. DOI: 10.1145/3130800.3130881.

[Zha+16]   Xiaoting Zhang, Xinyi Le, Zihao Wu, Emily Whiting, and Charlie C L Wang. 'Data-Driven Bending Elasticity Design by Shell Thickness.' In: *Eurographics Symposium on Geometry Processing* 35.5 (2016). DOI: 10.1111/cgf.12972.

[ZLH17]   Yang Zhang, Gierad Laput, and Chris Harrison. 'Electrick: Low-Cost Touch Sensing Using Electric Field Tomography.' In: *Proceedings of the 2017 CHI Conference on Human Factors in Computing Systems*. CHI '17. New York, NY, USA: ACM, 2017, pp. 1–14. ISBN: 978-1-4503-4655-9. DOI: 10.1145/3025453.3025842.

[Zha+11]   Yizhong Zhang, Chunji Yin, Changxi Zheng, and Kun Zhou. 'Computational Hydrographic Printing.' In: *Acm Tog* 34.4 (2011), pp. 1–11.

[Zha+15]   Haisen Zhao, Lin Lu, Yuan Wei, Dani Lischinski, Andrei Sharf, Daniel Cohen-Or, and Baoquan Chen. 'Printed Perforated Lampshades for Continuous Projective Images.' In: *arXiv* VV (2015). arXiv: 1510.03023.

[Zho+16]   Yi Zhou, Shuangjiu Xiao, Ning Tang, Zhiyong Wei, and Xu Chen. 'Pmomo: Projection Mapping on Movable 3D Object.' In: *Proceedings of the 2016 CHI Conference on Human Factors in Computing Systems*. CHI '16. New York, NY, USA: ACM, 2016, pp. 781–790. ISBN: 978-1-4503-3362-7. DOI: 10.1145/2858036.2858329.

[Zim+95]   Thomas G. Zimmerman, Joshua R. Smith, Joseph a. Paradiso, David Allport, and Neil Gershenfeld. 'Applying Electric Field Sensing to Human-Computer Interfaces.' In: *Proceedings of the SIGCHI Conference on Human Factors in Computing Systems - CHI '95*. New York, New York, USA: ACM Press, 1995, pp. 280–287. ISBN: 0-201-84705-1. DOI: 10.1145/223904.223940. pmid: 2006.

[Zir+11]   Martin Zirkl et al. 'An All-Printed Ferroelectric Active Matrix Sensor Network Based on Only Five Functional Materials Forming a Touchless Control Interface.' In: *Advanced materials (Deerfield Beach, Fla.)* 23.18 (May 10, 2011), pp. 2069–74. ISSN: 1521-4095. DOI: 10.1002/adma.201100054. pmid: 21438036.